Aus der

Universitäts-Hautklinik Tübingen

Efficacy of the MEK inhibitor trametinib in combination with disulfiram in BRAF-wild type melanoma cells

Thesis submitted as requirement to fulfill the degree „Doctor of Philosophy" in *Experimental Medicine* (PhD)

at the
Faculty of Medicine
Eberhard Karls Universität
Tübingen

by

Meraz Torres, Francisco

2022

Dean: Professor Dr. B. Pichler

First reviewer: Professor Dr. C. Garbe
Second reviewer: Professor Dr. B. Macek

Date of oral examination: 16.12.2022

Dedication

A mi padre. †

Espero que donde quiera que estés, estés orgulloso de tu hijo. Esto es para ti Papá.

A mi madre.

A quien le debo todo lo que soy o espero ser. Por qué tu amor fue el combustible que hizo que no me rindiera.

A mi esposa, Astrid.

Por nunca soltar mi mano en los momentos más complejos, por tu inagotable amor, compartir tu vida conmigo y hacerme creer en mí.

Y a mi hija Valentina.

Por demostrarme el amor incondicional. Para un siempre "*Nena con su Papi, Papi con su Nena*". Que la vida me permita seguir disfrutando tu eterna sonrisa.

List of Abbreviations

Aa	amino acid
AP	alkaline phosphatase
AJCC	American Joint Committee on Cancer
AKT	protein Kinase B (PKB)
AML	Acute Myeloid Leukemia
AMP	adenosine monophosphate
ATF4	activating transcription factor 4
ATM	ataxia telangiectasia mutant
ATP	adenosine triphosphate
ATPase	adenosine triphosphatase
ATOX1	antioxidant 1 copper chaperone
BAD	BCL-2-associated death promoter
BCL-2	B-cell lymphoma protein 2
BCL-XL	B-cell lymphoma extra-large
BIM	BCL -2 interacting mediator of cell death
BIM-EL	BCL -2 interacting mediator of cell death extra-long
BiP	Binding immunoglobin protein
BRAF	V-Raf Murine Sarcoma Viral Oncogene Homolog B
BRAFi	BRAF inhibitor
BRAF-WT	BRAF wild type
cAMP	cyclic adenosine monophosphate
cDNA	complementary DNA
CCS	copper chaperone for superoxide dismutase
CDK	cyclin-dependent kinase
CHOP	CCAAT-enhancer-binding protein homologous protein
CI	confidence interval
cKIT	proto-oncogene receptor tyrosine kinase (CD117/SCF receptor)
CREB	cAMP response element-binding protein
CTD	C-terminal domain
CTKD	C-terminal kinase domain
COX17	Cytochrome c oxidase copper chaperone
CTL-4	Cytotoxic T-lymphocyte-associated Protein 4
CTR1	copper transporter 1

Cu^{+}	copper(I) ion
Cu^{2+}	copper(II) ion
DAPK1	death-associated protein kinase 1
del	deletion
DNA	deoxyribonucleic acid
DMEM	Dulbecco's Modified Eagle Medium
dNTP	deoxynucleotide
DSB	double-strand break
DSF	disulfiram
DUSP	dual specificity phosphatase
ECM	extracellular matrix
EGFR	epidermal growth factor receptor
ER	endoplasmic reticulum
ERK1/2	extracellular signal-regulated protein kinase 1/2
EV	empty vector
FACS	fluorescence activated cell sorting
FCS	Fetal Calf Serum
FDA	Food and Drug Administration
FFPE	Formalin fixed and paraffin embedded
FOXO	forkhead box protein O1
G1 phase	Gap 1 phase
G2 phase	Gap 2 phase
GAPDH	glyceraldehyde-3-phosphate dehydrogenase
GDP	guanosindiphosphat
GF	growth factor
GPCR	G-protein coupled receptor
GPx	Glutathionperoxidase
GRB2	growth factor receptor-bound protein 2
GRP78	glucose regulated protein 78
GSK3β	glycogen synthase kinase 3β
GTP	Guanosintriphosphat
HBSS	Hank's Balanced Salt Solution
HIF-1α	Hypoxia induced factor 1α
HRP	horse radish peroxidase

IC50	half maximal inhibitory concentrations
JAK	Janus kinase
JNKi	JNK inhibitor
KIM	kinase interaction motif
LDH	lactate dehydrogenase
M phase	mitosis phase
MAPK	mitogen-activated protein kinase
MAPKi	MAPK pathway inhibitor
MEK	Mitogen-activated protein kinase (MAPKK/MAP2K)
Mcl1	induced myeloid leukemia cell differentiation protein 1
MDCK	Madin-Darby canine kidney epithelial cells
MEK1/2	MAP kinase / ERK kinase 1/2
MITF	Microphthalmia-associated transcription factor
mRNA	messenger ribonucleic acid
MUH	4-methylumbelliferyl heptanoate (MUH)
mTOR	mechanistic target of rapamycin
NADPH	Nicotinamide adenine dinucleotide phosphate
NFκB	nuclear factor kappa-light-chain-enhancer of activated B cells
NF-1	neurofibromin 1
NTKD	N-terminal kinase domain
NPL4	Nuclear protein localization protein 4
OD	optical density
O_2^-	superoxide anion
PBS	phosphate buffered saline
PDK1	3'-phosphoinositide-dependent kinase-1
PDX	patient derived xenograft
PI3K	phosphoinositide 3-kinase
PMSF	phenylmethanesulphonyl fluoride
PVDF	polyvinylidene difluoride
P8/NUPR1	nuclear protein 1
PTEN	phosphate and tensin homolog
qPCR	quantitative polymerase chain reaction
RAF	rapidly accelerated fibrosarcoma
RAS	rat sarcoma

RGP	radial growth phase
RNA	ribonucleic acid
ROS	Reactive oxygen species
rRNA	ribosomal ribonucleic acid
siRNA	short interfering RNA
RSK	p90 ribosomal S6 kinase
RTK	receptor tyrosine kinase
S	serine
S phase	synthesis phase
SD	standard deviation
SEM	standard error of the mean
sgRNA	single guide RNA
SHP2	Src homology region 2 domain-containing phosphatase-2
shRNA	short hairpin RNA
siRNA	small interfering RNA
SOD1	Superoxide dismutase 1
SOS	son of sevenless
SPRY	Sprouty
SRF	serum-response factor
STAT	signal transducer and activator of transcription
S6	ribosomal protein S6
T (amino acid)	threonine
TCGA	The Cancer Genome Atlas
TERT	Telomerase reverse transcriptase
UPR	unfolded protein response
UV	ultraviolet
VGP	vertical growth phase
WT	wild-type
Y	tyrosine

List of Contents

1 Introduction

1.1 Malignant melanoma

Melanoma is the fifth most prevalent cancer in the United States of America, associated with an incidence of 80,000 new cases per year and higher than 10,000 deaths per year [1]. Its incidence continues to growth at an accelerated rate. Melanoma prevalence has doubled in the last 30 years, with a worldwide incidence of 300,000 new melanoma cases in 2018 [2]. Melanoma is an aggressive skin cancer, with unusual complexity to treat and high mortality, being responsible for 55.9-65.9% of all the skin cancer related deaths [3]. Melanoma can develop by a neoplastic transformation of the pigment-forming melanocytes or their precursors [4, 5] . It can develop either from a nevus or directly from non-lesional skin on all parts of the body, e.g. head, trunk, eye, anorectal or vulva region or mucous membranes [6, 7].

The stage of melanoma has a considerable influence on the course of the disease, prognosis and treatment [8]. According to the 9th edition of the American Joint Committee on Cancer (AJCC), melanoma is classified in five stages starting from stage 0, melanoma in situ, to stage IV where the melanoma has spread to distant skin, lymph nodes, lungs or any distant organ [7]. The 5-year survival rate for stage I melanoma is high meaning 99% for stage IA, and 97% for stage IB, according to evaluations of the AJCC melanoma staging database[9]. However, once metastasis has begun, survival rates decrease severely. For instance, in the metastatic stage IV, the 5-year survival rate is only about 16%, with remarkably poor median overall survival (6 to 9 months) [5, 6]. Notwithstanding, due to current therapies the median overall survival could be extended to 14-35 months for melanoma patients in stage IV [10]. Regardless of cumulative evidence and developed of new therapies during the last years, the five-year survival rate for distant stages is still low at 16% [11, 12] .

1.1 Genomic classification of cutaneous melanoma

The discovery of the BRAFV600E mutation in 2002 by Davies, *et al*. [13] and the next generation of sequencing technologies opened the door for mapping the genomic landscape of melanoma subgroups [14]. The main mutations in cutaneous melanoma occur in the mitogen activated protein kinase (MAPK) pathway. Through the analysis of DNA, RNA and proteins of more than 333 cutaneous melanomas (including both primary and metastatic), revealed the description of the most common genomic alterations. As a result, a framework for genomic

classification into one of the four subtypes was established based on the pattern of the most prevalent significantly mutated genes: BRAF mutant, NRAS mutant, NF1 mutant and Triple-WT (wild type), as is illustrated in Table 1 [15].

Table 1. Classification by subgroups of cutaneous melanoma. Description and prevalence of mutations in cutaneous melanoma according to the genomic classification of cutaneous melanoma **[15].**

PREVALENCE OF MUTATIONS IN CUTANEOUS MELANOMA DIVIDED BY SUBGROUPS		
BRAF subtype	**47%**	Activating mutations in BRAF, $BRAF^{Mut}$ *(V600E, V600K, V600R)*
RAS subtype	**29%**	Activating mutations in RAS isoforms NRAS, HRAS and KRAS, RAS^{Mut}
NF-1 subtype	**9%**	Loss-of-function mutations of NF1 (*LoF*)
Triple-WT subtype	**15%**	Absence of NF-1, BRAF or RAS mutations

The largest genomic melanoma group (about 47%) is defined by the presence of BRAF hot spot mutations. Among, them 85% comprise the prominent V600 amino acid residue mutations (V600E, V600K and V600R). With 29% of cases, RAS hot-spot mutations (predominantly in NRAS) define the second most common category, which in conjunction with the high prevalence of mutations in BRAF has led to the search for and development of highly selective kinase inhibitors that target the MAPK pathway [16].

The third most frequent subgroup (9%) includes melanomas with aberrations in the gene NF1. Most mutations are "Loss-of-Function" (*LoF*) events. Since NF1 is a GTPase-activating protein known to down-regulate RAS activity through its intrinsic GTPase activity, NF1-*LoF* mutations are an alternative way to activate the canonical MAPK pathway [16]. Consequently, activation is critical for the RAS/MAPK pathway in melanoma [17]. Approximately 60% of NF1 mutant melanomas harbor co-mutations in known RASopathy genes, which mainly affect the RAS-MAPK signaling [18]. The last genomic group is the Triple-wild type (Triple-WT), which is a heterogeneous subgroup, described by the lack of mutations in the BRAF, N/H/K-RAS, or NF1 hot spots. The prevalence of the Triple-WT melanoma subgroup is about 15% of all melanomas [14]. Nevertheless, all of the melanoma subgroups that do not hold a BRAF mutation are grouped together as the BRAF wild-type (BRAF-WT) melanoma subgroup (53%). This group encompasses as a single group the subgroups of $NRAS^{mut}$ melanoma, NF1- *LoF* melanoma and Triple-WT melanoma [18].

1.2 Signaling pathways in melanoma

1.2.1 MAPK pathway

The mitogen-activated protein kinase (MAPK) signaling pathway, also known as RAS/ RAF/ MEK/ ERK pathway, holds a critical and important role in melanocyte biology and metabolism, as it positively regulates proliferation and melanogenesis [19]. Consequently, the MAPK signaling cascade is hyperactivated in about 80% of skin melanomas. Eventually this hyper-activation represents a critical factor in increasing the rate of progression, cell migration, differentiation and invasion of cutaneous melanoma [20]. As a result, active mutations in RAS and BRAF or loss of function mutations in NF-1 melanoma result in significant activation of the MAPK signal cascade, which is independent of growth factors binding to the upstream receptor tyrosine kinases, as is illustrated in Figure 1 [21].

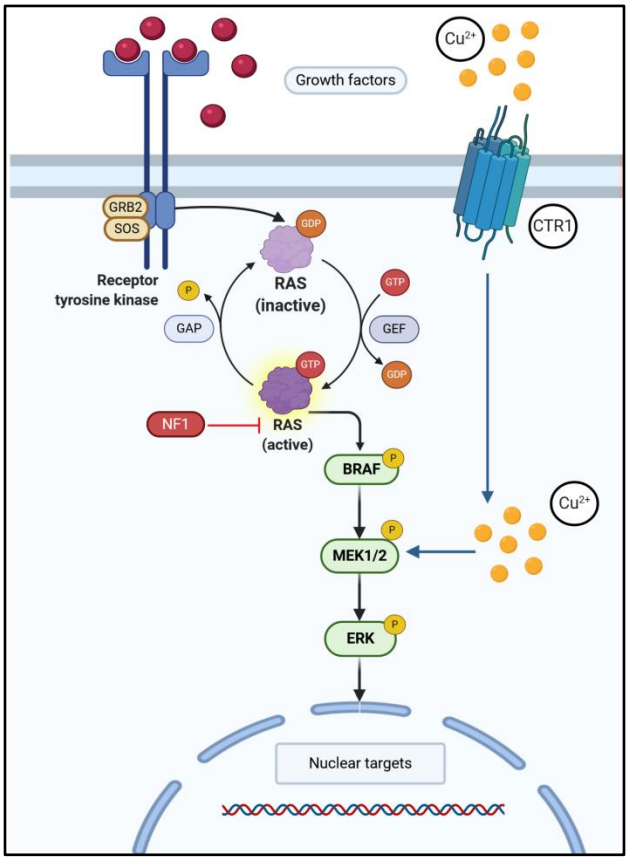

Figure 1: The MAPK signaling pathway –Mechanisms of MAPK hyperactivation in malignant melanoma, which is highly critical in the melanoma progress.

Different extracellular stimuli activate the MAPK signaling pathway through a membrane receptor as receptor tyrosine kinases (RTKs). These stimuli are cytokines and growth factors. The RAS protein is the first element of the MAPK signaling pathway. This small G-protein is activated through binding of GTP. The cleavage division of GTP into GDP further inactivates the protein. This cycle continues permanently, working like a molecular

switch. There are 3 different RAS proteins (HRAS, KRAS and NRAS). NRAS protein has the highest mutation rate of RAS proteins, being found in 29% of cutaneous melanoma. Once the RAS protein has been activated, the hierarchical activation of the canonical MAPK signaling pathway is initiated. The MAPK kinase is located and integrated from ARAF, BRAF and CRAF/RAF1[22]. As important as the RAS proteins is BRAF. BRAF protein is one of the most relevant proteins for the development of target therapy because about 50% of cutaneous melanomas have a mutation in this protein, which the most predominant mutation is $BRAF^{V600E}$. Further down the pathway, RAS phosphorylates MEK1 and MEK2. The MEK1/2 proteins have a great advantage, it is capable of phosphorylating Thr202 and Tyr204 from MAPK due to a double specificity. In order to perform the precise phosphorylation of the MEK1 and MEK2 proteins, the presence of copper (Cu^{2+}) is essential [2, 23].

Cu^{2+} is also crucial for the main activity of MEK. The phosphorylation of ERK1/2 by MEK1 is enhanced by the binding of 2 copper ions to the MEK molecule [2]. In addition, MEK1 activity is decreased if the intracellular Cu^{2+} levels decline. This Cu^{2+} dependent phenomenon occurs even in $BRAF^{mut}$ melanomas. Furthermore, it has been shown that lower ERK1/2 phosphorylation levels are found in melanoma cells when the intracellular Cu^{2+} ions are substantially low-slung [24]. The above highlights that Cu^{2+} is an essential co-factor in the phosphorylation of MEK in malignant melanoma [25]. Lastly, ERK1 and ERK2 move after double phosphorylation into the nucleus to activate various nuclear transcription factors [26].

Through the Cancer Genome Atlas (CGAA) program, which is a multidimensional and systematic program to achieve the description of a panel of cutaneous melanomas at the DNA, RNA and protein level was achieved. This panel shows a very specific and extensive association of the MAPK signaling pathway with cutaneous melanoma, which is grounded on the high prevalence and often mutual exclusiveness of specific mutations in different genes [27]. This evidence provides a strong basis for considering that hyperactivation of MAPK pathway signaling plays one of the most significant roles in cutaneous malignant melanoma. Besides the frequent mutations of BRAF, RAS isoforms or NF-1, the hyperactivation of the MAPK signaling pathway is performed by several additional mechanisms. One of the most relevant mechanisms that play an important role in the hyperactivation of the MAPK signaling pathway are the G-protein-associated guanine nucleotide binding proteins (GPCR), the expression and aberrant activity of receptor tyrosine kinases and the interaction with several acting growth factors such as autocrine and paracrine growth factors [28].

1.2.2 PI3K/ AKT signaling pathway

The PI3K/AKT pathway is one of the most relevant and important signaling networks in cancer and melanoma. There is increasing evidence that the PI3K/AKT pathway plays a critical role in melanoma proliferation and metabolism. This important participation of the PI3K/AKT pathway in melanoma proliferation is strongly linked to the simultaneous and parallel activation of RAS-RAF-MEK-ERK signaling, as illustrated in Figure 2. The activation or reactivation of the PI3K/AKT signaling pathway is linked to the initiation, development and even therapeutic resistance of cutaneous melanoma[29]. As a consequence, it is significant to mention that the activation of PI3K/AKT signaling plays an important role in the progression of cutaneous melanoma. [30].

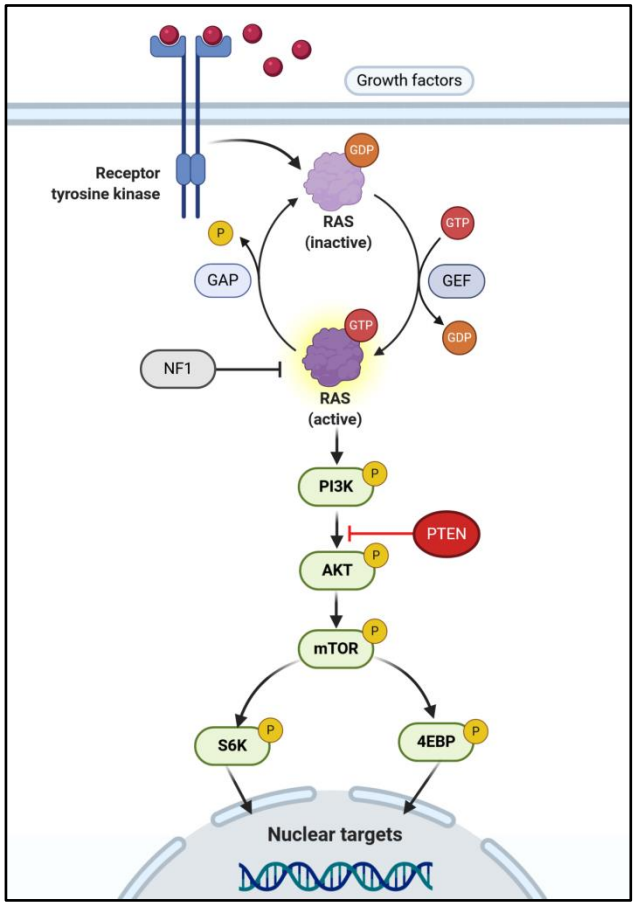

Figure 2: The PI3K/AKT signaling pathway – This signaling pathway is critical for regulating cell-cycle, proliferation and longevity. PI3K activation phosphorylates and activates AKT and subsequently mTOR and S6K, concluding the activation of nuclear targets. The PI3K/AKT signaling and the MAPK pathway are not independent pathway, and a further modification, inhibition or activation of one of the members concludes with a further modification of another pathway, illustrating that both signaling pathways holds a constant interaction.

The PI3K/ AKT signaling pathway acts as a regulator of various intracellular processes which are critical for the proper functioning of melanoma cells. This process is crucial for cell proliferation, protein synthesis and apoptosis. In addition, the PI3K/ AKT signaling pathway is activated through signals such as binding to various nutrients, hormones and specific growth factors. The activation of RTK receptors through growth factors induces the recruitment of the PI3K to the plasma membrane. This recruitment of PI3K to the plasma membrane is also conducted via activation of RAS proteins via GTP binding. Currently eight different mammalian isoforms of PI3K are known and particularly class 1-PI3K executes important functions in cellular processes [31]. Upon completion of PI3K activation, the phosphorylation of phosphatidylinositol group 3'-OH occurs. This results in phosphatidylinositol-(3,4)-P2 (PIP2) being transferred to phosphatidylinositol-(3,4,5)-P3 (PIP3). Through the interaction of PIP3 with AKT's pleckstrin homological domain, AKT phosphorylation is induced. This phosphorylation of AKT is mainly carried out in Thr^{308} and Ser473 by PDK1 and mTORC2, respectively. By activation of the AKT several proteins are regulated among them the mTOR complex [32]. Contrary to PI3K, lipid phosphatases dephosphorylate PIP3 back to PIP2 and therefore are counter-regulators of PI3K. One of the clearest examples and one that plays an important role in melanoma is the PTEN protein. Therefore, PTEN loss or inactivating are associated with the overactivation of the PI3K pathway [33, 34].

1.2.3 Crosstalk between the MAPK and the PI3K/ AKT signaling pathway

The MAPK pathway plays an essential role in the development, growth and therapy of malignant melanoma. Principally, to carry out cell growth and differentiation, the MAPK signaling pathway connects to and interacts with other signaling pathways, especially the PI3K signaling pathway. As a result, the constant interaction between these signaling pathways is highly associated with tumor growth and cell migration. Although not all the crossing points of the MAPK and PI3K tracks are fully known, it has been described that both tracks not only have several interference sites, but also share triggers [35, 36]. Further, in recent years it has been observed that the PI3K/ AKT signaling pathway consists of 802 proteins and the MAPK cascade needs more than 2,000 proteins to transfer the signals successfully. From overlapping proteins, it is clear that both signaling pathways influence each other. Both signaling pathways are activated by several extra and intracellular stimuli. Initially, PI3K as well as MAPK are activated by G-protein coupled receptors (GPCR), tyrosine kinase receptors (RTK) or activated RAS proteins. Both pathways regulate cell metabolism, proliferation and survival of the

melanoma cells. Accordingly, the MAPK and the PI3/ATK signaling pathway are not considered as two independent ways, as is illustrated in Figure 3 [33].

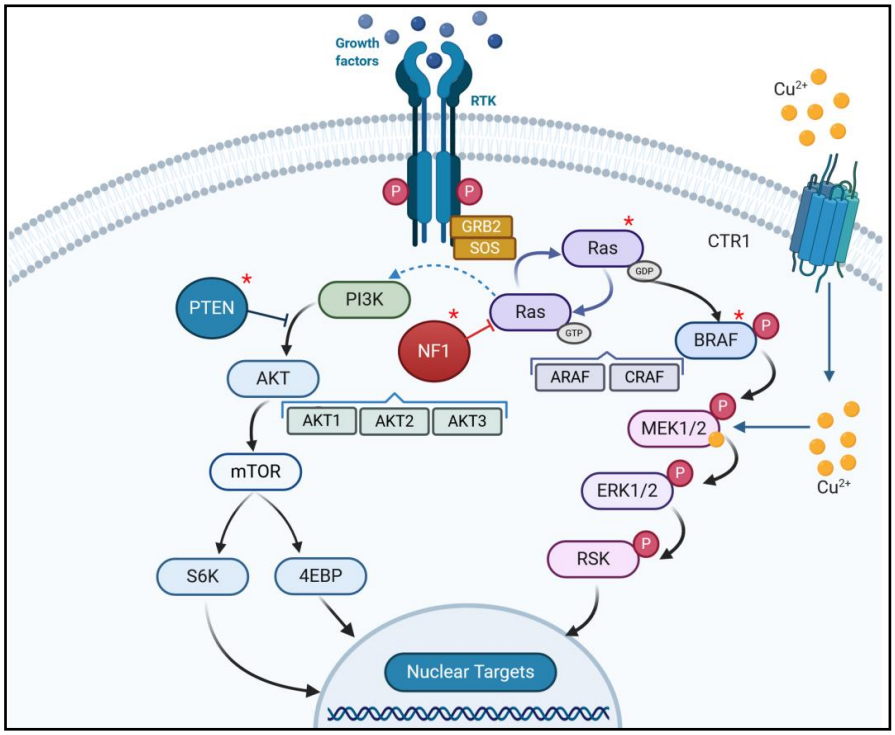

Figure 3: The MAPK and PI3K/ AKT signaling pathway – Common mechanisms of hyperactivation in malignant melanoma. This image shows on the one hand that hyperactivation of the MAPK pathway plays a critical role in the development, progression and survival of melanoma. In addition, it specifically shows that copper plays a fundamental role as a cofactor for the activation and phosphorylation of MEK1/2 and therefore the consequent activation of MAPK signaling leading to the activation of nuclear factors. It also shows that the transport of copper into the intracellular space is mediated by an important copper transporter called CTR1, which is permanently activated upon intracellular copper demand and is not dependent on the copper gradient. On the other hand, it shows the PI3K/ AKT signaling pathway and the interaction that the 2 signaling pathways constantly have. Therefore, they cannot be considered as totally independent pathways. Finally, it shows with red asterisks the main mutations found both in the MAPK signaling pathway (such as BRAF, RAS, NF1) as well as in the PI3K/ AKT signaling pathway (such as PTEN).

The MAPK- and PI3K/AKT signaling pathways influence each other in several ways, so inhibiting one of them can result in altering the function of the reciprocal pathway. Especially, the MAPK route is positively influenced by the PI3K/AKT, which concludes in an enhanced activation of the ERK [23]. In contrast, the activation of ERK has a negative effect on the PI3K/AKT signaling pathway [37]. To achieve full MAPK inhibition and avoid the development of resistance mechanisms, a combined inhibition of the MAPK pathway and the PI3K/AKT pathway should always be considered. Therefore, this mechanism concretely proves that both pathways are intimately connected and that their activation is not completely independent [32]. In addition, the MAPK signaling pathway actively participates in the inhibition of apoptosis and interacts with several other pathways besides the PI3K signaling pathway, such as the NFκB and JAK-STAT signaling pathway [10, 37]. The NFκB and JAK-STAT signaling pathway actively participate in the regulation of many processes of cellular

equilibrium, such as the immune response, the cell-cycle, proliferation and oncogenesis. However, abnormal regulation of these pathways induces the opposite effect. For instance, in response to chemotherapy with doxorubicin, transient activation of both PI3K/AKT and p38 MAPK has been observed, following sustained activation of ERK1/2 and JNK. Inactivation of PI3K/AKT and p38 MAK enhanced chemotherapy-induced apoptosis. Further activation of ERK1/2 apparently exerted a positive effect on apoptosis. In summary, regulation of the PI3K/AKT and MAPK signaling pathway plays a relevant role in melanoma survival [38, 39].

1.3 Current therapies for melanoma

Melanoma therapy involves different treatment options according to the clinical stage [19]. By the American Cancer Society, the melanoma in situ (stage 0) is treated by a wide excision surgery with a 5mm margin of normal skin around it. For stage 0 melanoma in delicate areas on the face, might be performed Mohs surgery or use a topic immune response modifier (Imiquimod). Stage I-II is treated by wide excision surgery as the standard treatment; however, the size of the margin depends on the depth and position of the melanoma [40-43]. Subsequent sentinel lymph node biopsy (SLNB) is always recommended. If an SLNB does not present any melanoma cell, no further treatment is recommended, however, if SLNB is positive for melanoma cells, additional treatments with targeted therapies (for melanoma with BRAF gene mutations) or immune checkpoint inhibitors are recommended [7, 9, 43] .

Once melanoma has spread to lymph nodes (Stage III), adjuvant treatment with targeted therapy or immune checkpoint inhibitor in addition to the standard therapy, which is a wide excision of the primary tumor and extensive lymph node dissection is advised. Lastly, when melanoma has already spread to distant lymph nodes or distant organs (Stage IV), surgery is only indicated to remove skin tumors or enlarged lymph nodes which cause symptoms. In this melanoma stage, target therapy drugs and checkpoint inhibitors are indicated as first-line therapy. Therapy of stage III/IV melanomas has changed during the last years with the new forms of target therapy and immunotherapy, which have mostly replaced chemotherapy (standard treatment for metastatic melanoma until 2011) [7, 9, 43-45]. The acutely approved target therapies for melanoma are illustrated in Table 2, emphasizing the year of discovery and the subgroup to which they are indicated.

Table 2. Approved target therapy for metastatic melanoma [46, 47].

APPROVED TARGET THERAPY FOR METASTATIC MELANOMA					
Therapy	**Year of discovery**	**ORR (%)**	**PSF (Months)**	**OR (Months)**	**Melanoma subgroup target**
Vemurafenib	2011	50	7.3	17.8	$BRAF^{mut}$
Dabrafenib	2013	53	8.8	18.7	$BRAF^{mut}$
Trametinib	2013	54	4.8	15.6	$BRAF^{mut}$
Dabrafenib+ Trametinib	2014	69	11	25.1	$BRAF^{mut}$
Vemurafenib+ Cobimetinib	2015	70	12.3	22.3	$BRAF^{mut}$
Enconafenib+ Binimetinib	2016	63	14.9	NR	$BRAF^{mut}$

NR: nor reported, **ORR:** overall response rate, **OS:** overall survival, **PFS**: progression-free survival.

In addition, several immune checkpoint inhibitors such as anti-PD1 and anti-CTLA-4 have been developed, exposing a good efficacy against cutaneous melanoma. However, at present there are still patients (up to 50%) who do not benefit from immunotherapy. Therefore, further research is needed to provide a wider range of options for the effective treatment of cutaneous melanoma[48, 49]. The immunotherapies approved for the treatment of metastatic melanoma are illustrated in Table 3, highlighting the year of discovery, response and the subgroup for which they are indicated.

Table 3. Approved immunotherapy therapy for metastatic melanoma [50].

APPROVED IMMUNOTHERAPY FOR METASTATIC MELANOMA					
Therapy	**Year of discovery**	**ORR (%)**	**PSF (Months)**	**OR (Months)**	**Melanoma subgroup target**
Ipilimumab	2011	11-19	2.8	11.5-19.9	All subgroups
Pembrolizumab	2014	36-37	8.3	32.3	All subgroups
Nivolumab	2014	40-44	5.4-6.9	37.6	All subgroups
Ipilimumab + Nivolumab	2015	58	11.5	Not reached	All subgroups

NR: nor reported, **ORR:** overall response rate**, OS:** overall survival**, PFS:** progression-free survival.

1.3.1 Pharmacological inhibition of the MAPK signaling pathway

The discovery of the constitutive activation of the MAPK signaling pathway a majority of malignant melanomas exposing this signaling pathway as an excellent therapeutic target, firmly marked the beginning of a new era in melanoma therapy [51]. During the past few years, different pharmacological inhibitors specifically targeting to individual proteins of the MAPK

pathway, such as the mutated BRAF (e.g. dabrafenib, vemurafenib, encorafenib) or MEK (e.g. trametinib, cobimetinib, binimetinib), have been developed, and were brought to clinical application. Patients with $BRAF^{V600}$ mutant melanomas have shown improved on progression free survival and prolonged overall survival rates. However, the development of potent targeted therapies for RAS, NF1-*LoF* and Triple WT melanoma subtypes still represents a significant unmet medical need [52-54].

1.3.1.1 MEK inhibitors

MAPK signaling pathways involve a family of protein kinases that play a key role in the regulation of various cellular signals in melanoma, including differentiation, proliferation, and cell survival. MAPK pathways transduce several stimuli, mediating specific intracellular effects [55]. As a result, inhibition of MEK proteins (mitogen activated protein kinase or MAP2K or MAPKK) leads to interference in cell development, progression and differentiation [24, 26, 51, 55].

1.3.1.2 Trametinib (GSK1120212)

Trametinib (Mekinist®), also known as GSK1120212 or JTP-74057, is a small molecule, which belongs to the second generation of MEK kinase inhibitors. Trametinib was published as new MEK inhibitor by Novartis in the year 2013 and approved by the FDA on May 29, 2013. The IUPAC name of trametinib is acetamide, N-(3-(3-Cyclopropyl-5-) [(2-fluoro-4-iodophenyl) amino]-6,8-dimethyl-2,4,7-trioxo-3,4,6,7tetrahydro-pyrido[4,3-d] pyri-midi-ne-1(2H)-yl) phenyl). Trametinib has a molecular weight of 615.39 g/mol and its corresponding molecular formula is $C_{26}H_{23}FIN_5O_4$ [56]. Trametinib is an orally bioavailable drug, which precisely binds to MEK1 and MEK2, resulting in mitogen-activated protein kinase (MAPK) inhibition and subsequent inhibition of melanoma cell growth and proliferation. The chemical structure of trametinib is represented in the Figure 4 [56, 57].

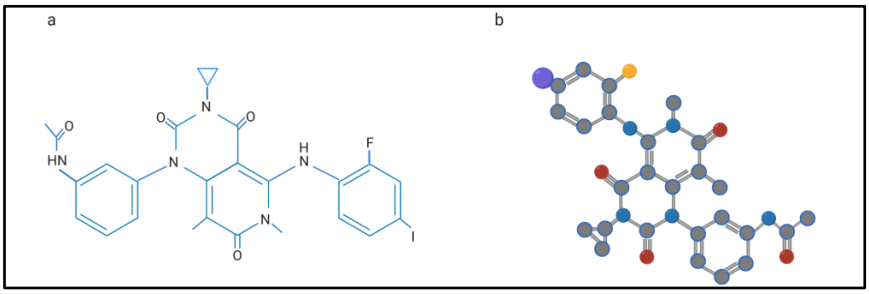

Figure 4: The image shows schematically the chemical structure of the MEK inhibitor trametinib ($C_{26}H_{23}FIN_5O_4$); a) Conventional skeletal formula, **b)** stylized representation[56].

It is characterized as a reversible, selective allosteric ATP inhibitor with a strong activity against MEK 1 and MEK 2 kinases (as is represented in Figure 5), with over 50-fold selectivity for cancer cells. Its half-maximum inhibitory concentration (IC_{50}) for MEK1/2 is between 0.7–0.9 nmol. But further screening revealed that at concentration between 1.0-2.5nmol, trametinib efficiently inhibits the phosphorylation of ERK, blocks Ki67, induces G1 cell-cycle arrest and decreases tumor progression in $BRAF^{V600E}$ melanoma xenograft models [56-58]. In mouse models, trametinib failed to cross the blood-brain barrier. The advantage of this effect is that it significantly reduces the probability of generating brain toxicity [57]. The mechanisms of action of trametinib are illustrated in Figure 5.

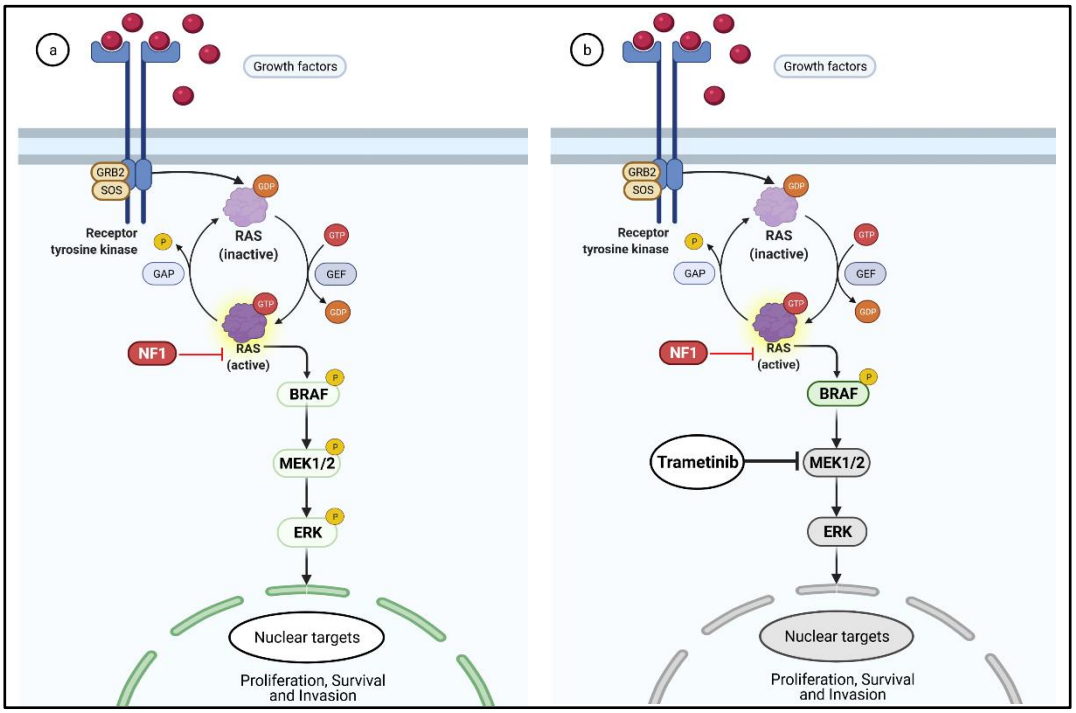

Figure 5: Mechanism of action of the trametinib. a) The image shown depicts the hyperactivation of the MAPK pathway, which is critical in the development, proliferation and survival of melanoma. MAPK hyperactivation concludes with the consequent activation of nuclear targets. b) The image shows specifically the intracellular site where trametinib performs its action (trametinib target site). The target inhibition of the MEK1/2 concludes with the inhibition of the phosphorylation of MEK1/2 and the further mitigation of the MAPK pathway activity.

Trametinib is orally bioavailable. It is easily absorbed through the upper gastrointestinal tract, and once in the bloodstream, 97.4% of trametinib binds to plasma proteins. Its half-life is between 3.9 and 4.8 days and its clearance rate are 4.9 L/h; therefore, these conditions provide a constant inhibition of the MAPK pathway, as is illustrated in Figure 5. Its visible volume distribution (*Vc/F*) is 214 L [59]. After one and a half h of administration, trametinib reaches its maximum plasma concentration. After 1.5 h of oral administration of 2 mg, its plasma concentration is 22.2 ng/mL. 80% of the doses administered are excreted through the feces, and less than 20% of the dose is excreted through the urine. Interestingly, <0.1% of the excretion rate is performed in the parent compound form [57, 60, 61].

A number of MEK1/2 inhibitors had previously been studied as alternative therapies for MAPK-dependent tumors, but trametinib was the first MEK inhibitor to be introduced into clinical practice. Trametinib was approved by the FDA to treat BRAF-mutant metastatic melanoma in patients not previously treated with a BRAF inhibitor, as a monotherapy or in combination with Dabrafenib (BRAF inhibitor). Trials with the combination of trametinib and dabrafenib have shown significant improvements in response rates and progression-free survival in patients with $BRAF^{mut}$ melanoma compared with chemotherapy (dacarbazine 1000 mg/m^2 or paclitaxel 175 mg/m^2) [56, 62].

1.3.1.3 Combination of trametinib with other therapies

Trametinib as monotherapy was approved for the treatment of malignant melanoma with BRAF V600E or V600K mutations ($BRAF^{V600mut}$) in 2013 by the FDA. Subsequently, through GlaxoSmithKline, it was developed for the combination therapy with the BRAF inhibitor dabrafenib, specific for $BRAF^{V600mut}$ melanoma. In 2014, From this moment, the combination therapy of trametinib with dabrafenib was approved by the FDA and accepted worldwide for the treatment of the $BRAF^{V600mut}$ melanoma. Several phase I and phase II trials were initiated to assess the effectivity of MEK inhibitor trametinib in combination with some other therapies for the treatment of $BRAF^{V600mut}$ melanoma. However, there are currently no studies looking at effectivity due combination therapy of the MEK inhibitor trametinib with other drugs for the treatment of BRAF-WT melanoma [63].

1.4 Cellular copper uptake

1.4.1 Human copper transport protein 1 (hCTR1)

In melanoma cells melanocytic cells, the main Cu^{2+} acquisition is achieved by the human transmembrane protein CTR1 (hCTR1), a high-affinity Cu^{2+} transport protein. The hCTR1 is encoded by the gene SLC31A1 and has a high-affinity to copper with a $K_m \approx 2\ \mu M$, and this condition is particularly specific for Cu^{2+}. The hCTR1 is an extremely well-maintained high-affinity Cu^{2+} uptake protein. The only identified substitute substrate is the isoelectric Ag^{+} [64, 65]. hCTR1 is a fairly small polypeptide consisting of 190 amino acid residues. The hCTR1 consists of three transmembrane segments, an extracellular amino and an intracellular carboxy-terminal end [66]. Homotrimer CTR1 forms a central conical pore in association across the plasma membrane, which maintains an extracellular access with 8 Å in diameter that communicates with an intracellular access with 22 Å in diameter [67, 68]. The extracellular part of the canonical pore holds a ring of six methionine residues, which provide the binding and permeating spot for Cu^{2+} [2, 69]. Intracellularly, the carboxylic terminus of 14 amino acids concludes with a trimer of H-C-H, which represent the intracellular Cu-binding site, which is the exit of the pore in the cytosol, as is illustrated in Figure 6 [65, 70, 71].

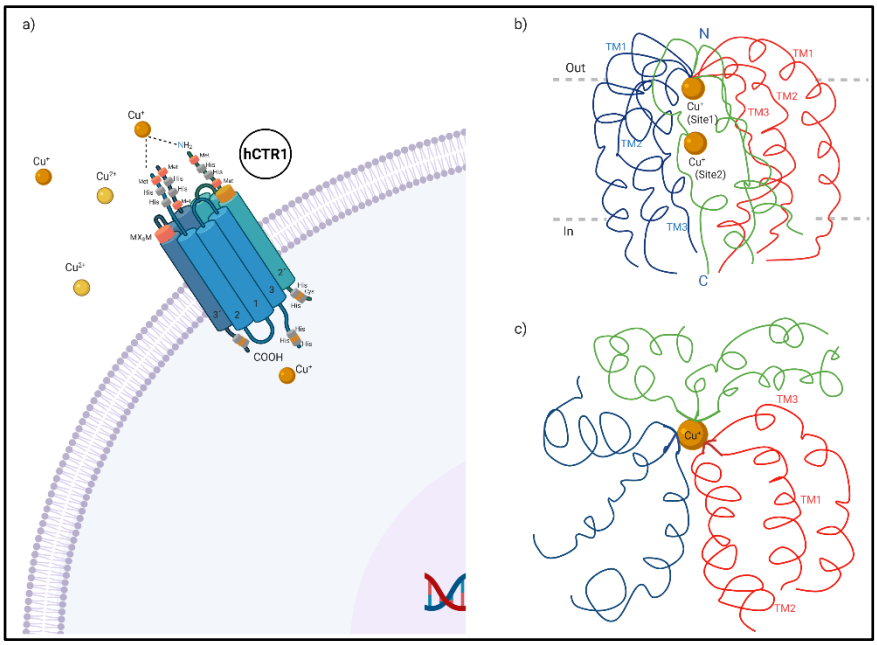

Figure 6: Function and structure of the hCTR1. **a)** This figure shows the transmembrane location of the CTR1 and its function of transferring copper ions from the extracellular space to the intracellular space. Similarly, it is shown that it can uptake Cu^{2+} ions, but has greater affinity to Cu^{+} ions. The final destination of copper is the intracellular space, specifically the cytosol. **b)** Side view of the corresponding symmetric trimer of the hCTR1 molecule, showing each unit with a different color. The gray lines at the top and bottom show the approximate limit of the membrane that delimits the outer extracellular and intracellular space of the cell membrane. In addition, the N and C terminals are shown, as well as the transmembrane helixes are marked. **c)** Top view of the CTR1, from the extracellular side [72].

The architecture of the hCTR1 protein is mainly composed by a systemic trimer which each subunit contains an extracellular N1 terminal, three transmembrane helixes and finally an intracellular C terminal. The transmembrane helixes are called TM1, TM2 and TM3 [72]. In normal conditions, the TM1 and TM2 are inclined over the cell membrane, unlike the TM3, which runs approximately perpendicular to the cell membrane and could come into contact with the TM2 from the next subunit. On the extracellular side, TM2 delimits the narrow section of the pore that follows the extracellular flank. Opposite to, on the intracellular side of the cell, the narrow region of the pore is defined by TM1 [72, 73]. This distribution along the alignment of intracellular and extracellular pores, jointly with the central three-fold symmetry subunits axis is the classical architecture of the CTR1 protein, which allows a copper conduction capacity, as illustrated in Figure 7 [72-74].

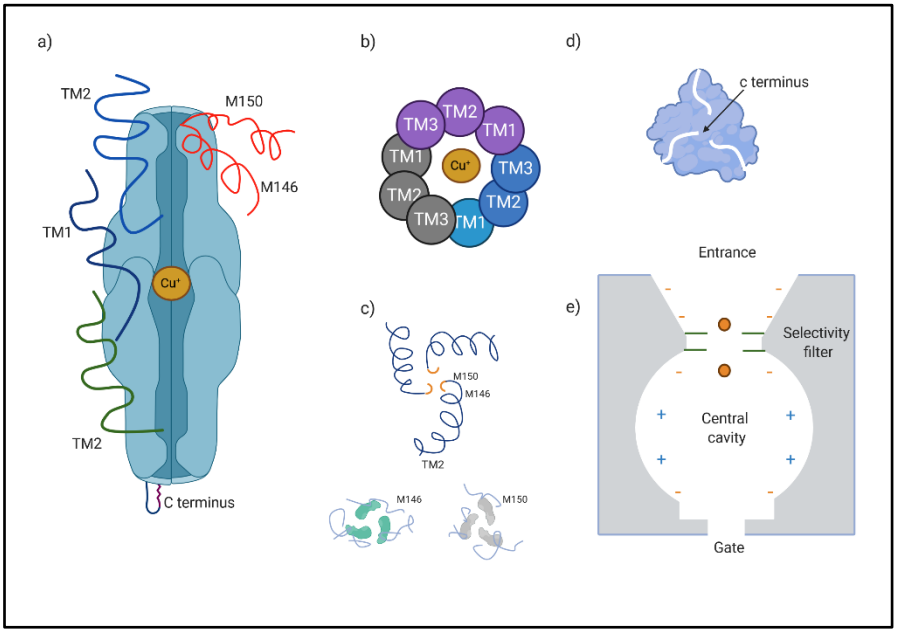

Figure 7: hCTR1 ion (Cu) conduction pore. **a)** The central ion conduction pore of sCtr1 is presented, showing a central enlargement, as well as the two methionine rings (M146 and M150) b) Top view of the distribution of the CTR1 helixes. **c)** The two corresponding methionine rings in TM2 (M146 and M150) attached to the extracellular segment make up the selectivity filter. The associated 2Fo-Fc electron density for each of the methionine side chains (contoured at 1.7 σ) is shown as a blue or green meshes figure (depending on M146 or M150) at the bottom. **d)** CTR1 intracellular Cu gate. It can be seen that the C-terminal tail following TM3 spreads to the central pore alignment, which forms the intracellular gate for Cu. **e)** Suggested mechanism of Cu selection and Permeation. Two subunits are displayed. The 2 important methionine rings coordinate two Cu^{+} ions. The CTR1 electrostatic potential throughout the ion pore is shown [72].

Thus, hCTR1 plays an important role in controlling the intracellular metabolism of copper in melanoma cells because it mediates a constant transport of Cu^{2+}, which under normal circumstances reaches between 5 and 10 Cu^{2+} ions per trimer per second into the cytoplasm. Given the dependence of intracellular Cu^{2+} uptake on hCTR1, the essential requirements for intracellular Cu^{2+} in melanoma cells is the expression of hCTR1 [75]. In mammals, copper can exist in two different oxidation states, which are Cu(I) or Cu^{+} and Cu(II) or Cu^{2+}. Several

authors have shown that hCTR1 is significantly more selective for Cu^{+} than for Cu^{2+}. The resulting redox activity is used by Cu-dependent enzymes to produce catalysis [66, 69, 70, 72].

Based on the structure, the trimeric ion channel model of hCTR1 and the energy-independent Cu^{2+} transport over the cell membranes, CTR1 could theoretically function as an ion channel. However, Ren F. *et al.*, showed that the rate of transmission of Cu^{2+} ions (~10 ions per second per trimer) is lower than that commonly archived by ion channels [72, 76]. Therefore, the Cu^{2+} mechanism of CTR1 has been widely studied. It has been described that, in order to obtain an appropriate Cu^{2+} uptake activity, the integration of several specific Cu^{2+} ion permeation mechanisms must be available. These mechanisms depend on the pore's dimensions along the Cu^{2+} ion pathway. Thus, two well maintained methionine residues, associated in a MX3M sequence motif by TM2 (M150 and M146), arrange the first and second layer of methionine triads, which cause a high selectivity in the extracellular Cu^{2+} input [72]. Therefore these 2 layers of methionine in association with the sulfur atoms of the side chain of each triad generate each a binding site for Cu^{2+} through the central core. Due to the inclination of TM2's propellers, the ion conduction pore becomes narrower below the selectivity filter, resulting in a central cavity with greater space, which allows the continuous passage of Cu^{2+}. In the meantime, TM1 slopes towards the central pore axis and makes a slight edge around the pore near the intracellular side. Through this internal modification of the segments of the CTR1, it is possible to compensate the opening of the pore through TM2 by the inclination of TM1 and therefore to restrict the internal diameter of the pore [72, 73, 76]. Finally, next to the TM3, the intracellular C-terminus has a highly conserved HCH motif that forms an additional Cu-binding site, which plays a very relevant role because it transports Cu^{2+} to cytoplasmic Cu-chaperones [77].

1.4.2 Divalent metal transporter 1 (DMT1)

Melanoma cells have a second copper importer, which is capable of carrying Cu^{2+} from the extracellular to the intracellular compartment. These secondary Cu^{2+} transporter is called divalent metal transporter 1 (DMT1) but also well known as divalent cation transporter 1. DMT1 is ubiquitously, even in cancer cells, but mainly in the apical membrane of enterocytes along the duodenum [78]. DMT1 is a membrane protein which is composed of a single subunit and classified as type III from the integral membrane protein classification [79]. It is composed of a transmembrane domain of 12 α-helices and subsequently two sites for N-core glycosylation, which are located in the extracellular segment between two α- helices. The

molecular structure of DMT1 shows that both N- and C- terminal ends are oriented towards the cytoplasm, unlike in hCTR1, where N- terminal is oriented towards the extracellular space and C-terminal is oriented towards the cytoplasm. The C-terminal domain of DMT1 has no homology to the C-terminal domain of CTR1 and therefore is not capable of transporting copper to the enzymes that are associated with Cu-transporters. Consequently, the C-terminal of DMT1 does not play a relevant role in the release of intracellular Cu. Furthermore, it is not known which co-transporters, substances or proteins take over copper from DMT1 [80, 81].

DMT1 acts as a proton-coupled pump, which use the cell membrane potential to create an active Cu^{2+} transport. DMT1 shows the same affinity for both Cu oxidation states. When the CTR1 gene is turned off and there is an intracellular Cu deficiency, DMT1 compensates for that. Although DMT1 has an adequate function in the transport of copper, it is not a Cu specific transporter. DMT1 transports also other ions like Fe^{2+}, Zn^{2+}, Ni^{2+}, Cd^{2+}, Co^{2+}, Pb^{2+} and Mn^{2+} [50]. Taken together, DMT1 has the copper shutting capacity, as is illustrated in Figure 8 [82].

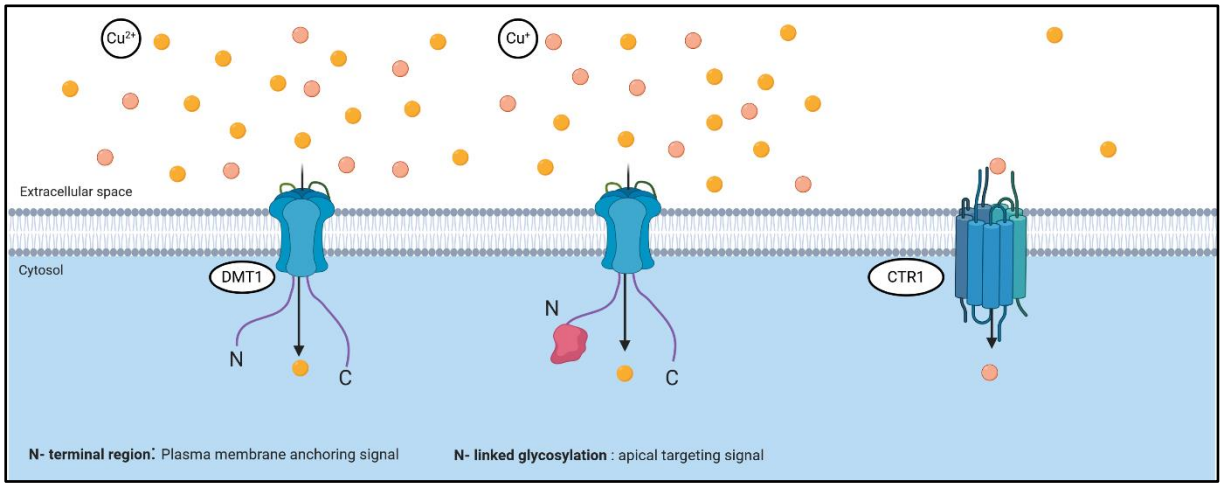

Figure 8: DMT1 and hCTR1 transporters. The image shows how transport from the extracellular space to the intracellular space is mediated mainly by hCTR1, which is not gradient-dependent. DMT1 plays an important role in the complementary transport of copper into the intracellular space. The figure shows that the main copper transporter hCTR1 transports either Cu^{2+} or Cu^{+} in a highly specific and selective manner. Copper transport through hCTR1 does not depend on copper density in the extracellular space, i.e. even if there is no high concentration of copper ions in the extracellular space, the transporter is highly selective and will be able to transport the copper that is available. In contrast, DMT1 is a complementary copper transporter. DMT1 is not a copper-specific transporter, and has a high affinity for other metals. However, it is capable of carrying out complementary copper transport. Copper transport by DMT1 is gradient-dependent, i.e. there must be more copper in the extracellular space in order to be able to transport copper into the intracellular space.

1.5 Intracellular Cu distribution

1.5.1 Intracellular Cu-chaperones

The Cu-chaperones have been widely studied and evolutionarily preserved. The intracellular transport of copper is carried out by its specialized system through Cu-chaperones, which comprise the proteins ATOX1, CCS and COX17 [67]. These Cu-chaperones facilitate Cu^{+}/Cu^{2+} delivery to the cuproenzymes found in the cytosol trans-Golgi or mitochondrial network in an efficient and effective manner, as is illustrated in the Figure 9. Simultaneously to the intracellular distribution of copper, glutathione (GSH), which is found in large quantities in the cytosol, as well as metallothionein proteins limit the cellular toxicity of free Cu^{+} ions [69, 81, 83].

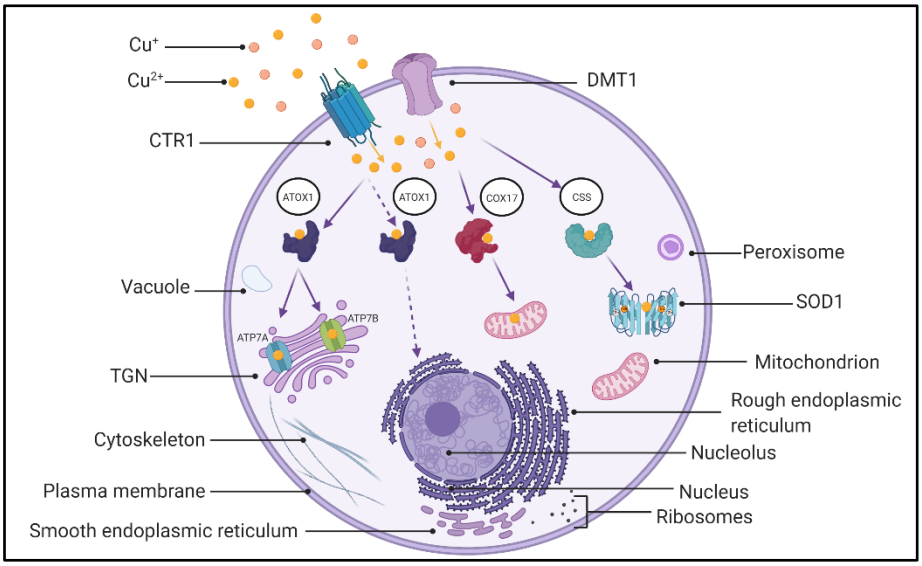

Figure 9: The role of the cytoplasmic copper chaperones. The image shows the main role of the copper chaperones ATOX1, CCS and COX17 and the target site of copper transport. It also adds the postulated copper transport by ATOX1 to the nucleus, which has been previously described by several authors [67].

Specifically, the redox-sensitive antioxidant 1 Cu-chaperone (ATOX1) is responsible for mobilizing and delivering Cu^{2+} to the Copper-dependent P-type ATP7A or ATP7B ATPases, according to the metabolic and dynamic needs of the cell, described in Figure 9 [65, 67, 81]. Once the Cu^{2+} is located at the corresponding ATPase, it will facilitate the mobilization of Cu^{2+} to the lumen of the trans-Golgi network where the Cu^{2+} load of the highly Cu-dependent enzymes, such as ceruloplasmin, tyrosinase and lysis oxidase, occurs [84]. The Cu-chaperone ATOX1 is an exceptionally small protein (8kDa) that contains a central metal blinding site, which is the responsible for the displacement of Cu^{2+} [85]. As a result, ATOX1 plays an essential role in the intracellular Cu^{2+} metabolism and any overexpression or down-regulation significantly disturbs the copper metabolism similar to Menkes disease caused by ATP7A

mutation or Wilson disease with an ATP7B mutation [81, 86, 87]. At the end of the carrying route, ATOX1 interacts with the N-terminal domain of ATP7A/B. These N- terminal domains comprises 6 metal binding domains (MBDs) which are small protein domains (7 kDa) joined by linkers. From those, the MBD4 mediates the release of Cu^{2+} from the ATOX1 binding site and carries it to the ATP7B. As a result, the Cu^{2+} extrusion passageway is facilitated by ATOX1 [81]. The interface between ATOX1 and MBD4 of ATP7B is mediated by protein to protein interactions, as is illustrated in Figure 10.

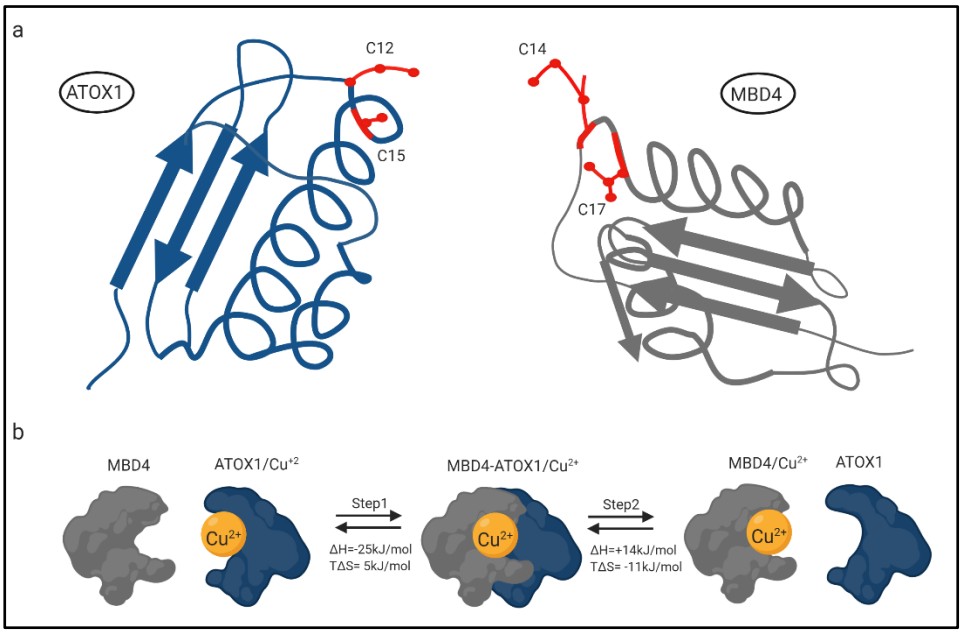

Figure 10: Cu transport from ATOX1 to MBD4. (a) ATOX1 and MBD4 structural model which showed in red the highlighting Cys residues which are able to bind Cu^{2+} **(b)**. Suggested 2-step transport mechanism of the Cu^{2+} from ATOX1 to MBD4 thought with thermodynamic (ΔH and TΔS) corresponding values for all the process [88, 89].

Once the Cu^{2+} acquisition by the melanoma cells is achieved, the copper chaperones COX17 and CSS facilitate the effective delivery of Cu to cuproenzymes located in the mitochondria or cytosol. Simultaneously, huge quantities of molecules like metallothionein and GSH protect the melanoma cell from cellular toxicity from copper ions [88]. In the cytosol, CCS triggers Cu, Zn-superoxide dismutase (SOD1) by straight insertion of the Cu cofactor, which is essential for catalyzing the disproportionation of superoxide to hydrogen peroxide and dioxygen [90]. Lastly, COX17 transports Cu inside the inner membrane area of the mitochondria and employs two accessory molecules, SCO1 and COX11, to metallize the CuA and CuB spots of cytochrome c oxidase. While the physiological significance of all Cu chaperones has been explained in the studies of Menkes and Wilson disease, the influence of dedicated Cu delivery structures in the context of supplementary pathophysiology such as cancer remains to be explored [91].

1.6 The role of copper chaperones in cancer

Initiation, growth and progression of melanoma and other cancers like endometrial, brain and breast are associated with high serum Cu^{2+} levels for a long time (years) their diagnosis [92-95]. There are also data where it is described that high levels of Cu^{2+} are associated with higher mortality in different types of cancer as the superoxide dismutase (CCS) with the breast cancer or ATOX1 with osteosarcoma [96, 97]. This association is not clearly established for melanoma; however, there are many studies that are currently being developed in order to establish the biological importance of Cu^{2+} in the development of melanoma. Interestingly, the expression levels of Cu-chaperones CCS, COX17 and ATOX1 are considerably elevated in non-small cell lung carcinoma (NSCLC) when they are directly compared to normal lung tissue. Nevertheless, ATOX1 might play a stronger role in tumorigenesis, growth, and cancer progression than other Cu-chaperones. However, high expression levels of Cu-chaperones have not been observed in melanoma. During the last few years several functional studies have been carried out, whose results showed that the knock down of the Cu-chaperone ATOX1 decreased the growth of NSCLC cell lines *in vitro*. These results support the theory that the ATOX1 plays a substantial role in tumorigenesis in NSCLC. Similarly, several studies in breast cancer patients revealed that the Cu-chaperone ATOX1 is found to be overexpressed at the mRNA and protein level. In addition, a specific inhibitor (DCAC50) of ATOX1 and CCS was developed and tested on lung cancer cell lines by Wang *et al*. The aim of this inhibitor was to interrupt intracellular Cu^{2+} transport and subsequently block the Cu^{2+} transport to its corresponding target. Accordingly, DCAC50 decreased cell viability in human breast and lung cancer cell lines, thought abrupt induction of redox stress and reduction of ATP levels. These results showed that ATOX1 holds an essential role in tumorigenesis and contributes to the biology of the cancer cells [65, 81, 84, 86].

1.6.1 The impact of ATOX1 in the development of melanoma

The study and analysis of the expression of every Cu-chaperon in melanoma was performed, but with special interest in ATOX1. The analysis was carried out through the database of the Human Protein Atlas (HPA) and the Gene Expression through Normal and Tumoral Tissues (GENT). In the databases, it was observed that the expression of ATOX1-mRNA was substantially higher in several types of cancer, mainly breast and melanoma, when compared to their respective normal tissues. Additionally, the mRNA expression was significantly higher in some melanoma cell lines (e.g. WM115 and SKMEL30) when were

compared with several another cancer cell lines, as is illustrated in Figure 11. Further analysis of expression in the HPA, GENT and the Cancer Cell Line Encyclopedia (CCLE) revealed that ATOX1 is exceedingly expressed in several melanoma cell lines (SKMEL30 and WM115) more than other cancer cell lines (such cancer cells from brain, kidney, eye, lung and gastrointestinal tract). Similarly, it was previously described that Cu plays a relevant role in $BRAF^{V600E}$-driven MAPK signaling in melanoma cell lines and in melanoma-genesis. Ye-Jin Kim *et al.* in 2019 described that down-regulation of ATOX1 reduced BRAFV600E-dependent growth and MAPK signaling in melanoma cell lines. DCAC50, an inhibitor of ATOX1, exhibited a reduction of ERK1/2 phosphorylation in $BRAF^{mut}$ Melanoma, concluding with a further inhibition of cell growth in a dose-dependent manner [81]. Taken together, ATOX1 expression plays an important role in melanoma development and progression.

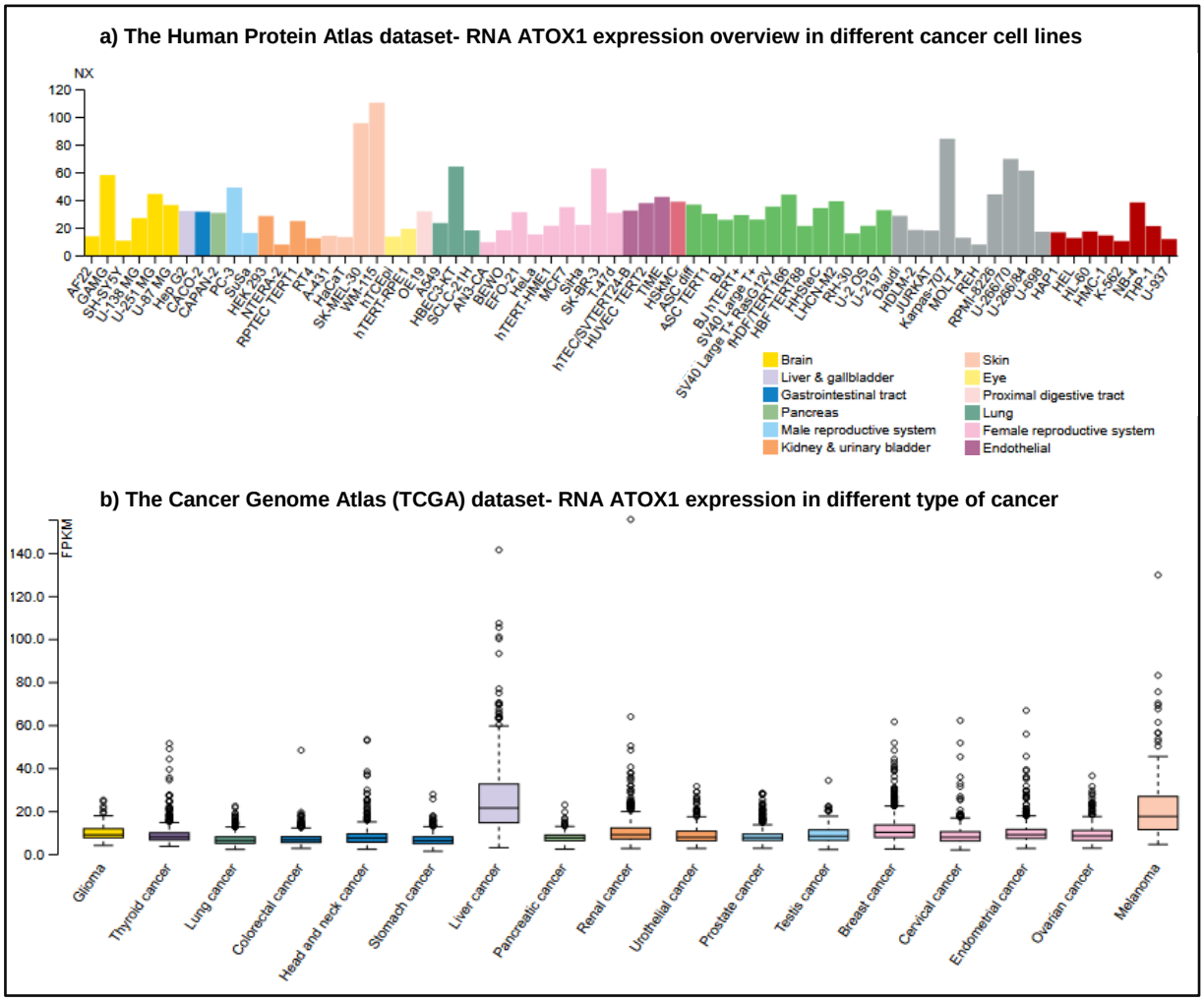

Figure 11: ATOX1 expression in several cancer cells. ATOX1 is significantly higher expressed in melanoma than another cell cancer cells. The analysis was carried out through the database of the Human Protein Atlas (a) and the Gene Expression through Normal and Tumoral Tissues, GENT (b).

ATOX1 transcript levels in non-melanoma cells lines and melanoma cell lines (e.g. A375 and WM88) were tested by the Broad Institute Cancer Cell Line Encyclopedia (CCLE) database and it showed that the ATOX1 was highly expressed in all the melanoma cell lines, as is illustrated in Figure 12. This detailed data base offers a broad gene expression exploration for more than 1,000 cancer cell lines. Interestingly, the levels of DNA methylation and mRNA of ATOX1 were significantly higher in melanoma cell lines than in other cancer cell lines, including multiple myeloma, which also holds high expression of ATOX1, as is also illustrated in Figure 12. Moreover, ATOX1-mRNA and ATOX1-DNA levels were not only significantly higher in melanoma cell lines compared to all other cancer cell lines, as was described by Ye-Jin Kim *et al*. in 2019 [65, 81]. Taken together, The ATOX1 gene is shown to be persistently upregulated in melanoma and is comparably higher than in other cancers, opening a door to explore whether modification of ATOX1 expression influences the biology of melanoma cells. These data are illustrated in Figure 12.

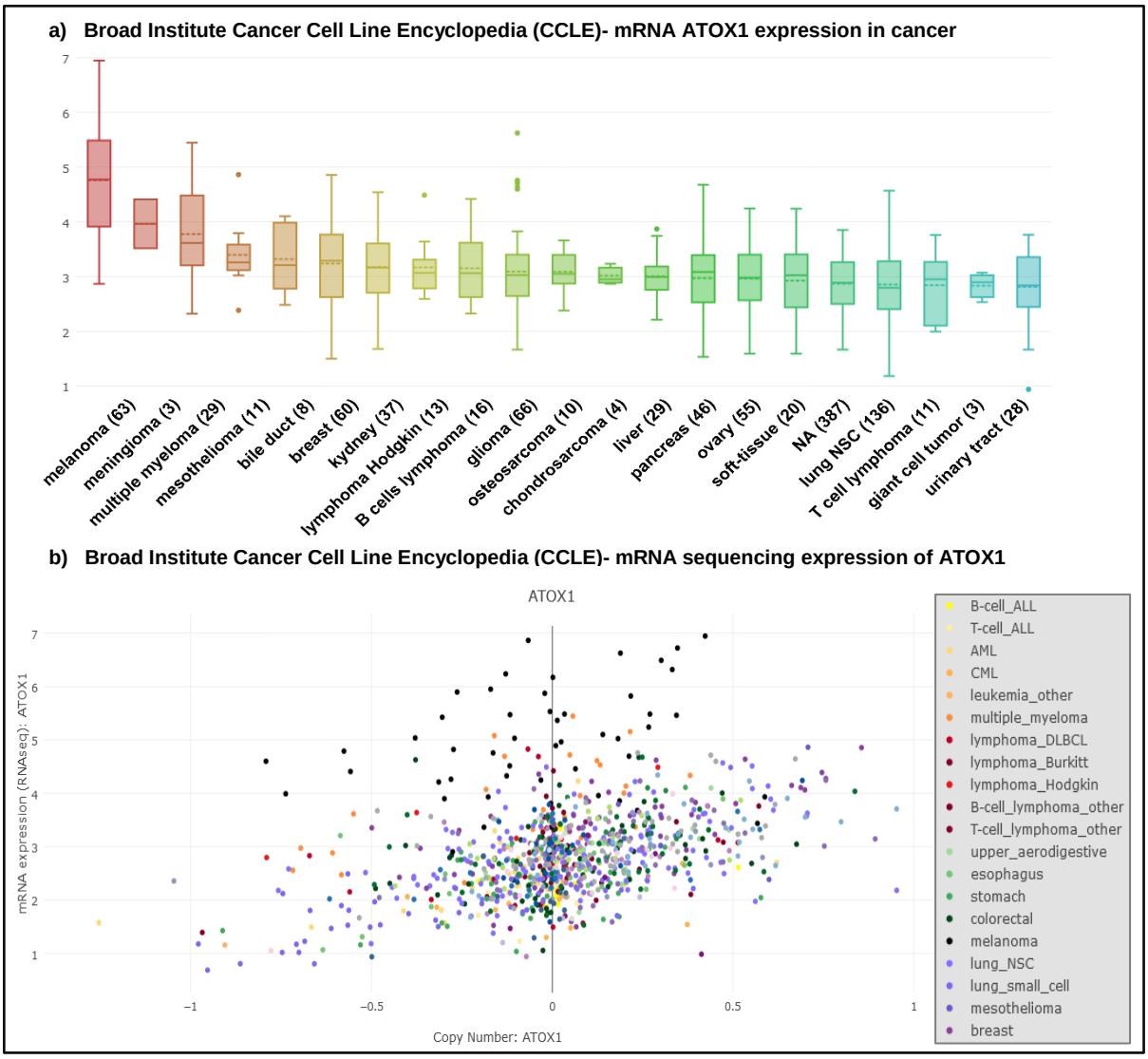

Figure 12. ATOX1 expression in several cancer cells. ATOX1 is significantly higher expressed in melanoma than another cell cancer cells. The analysis was conducted through the database of the Broad Institute Cancer Cell Line Encyclopedia (CCLE).

Considering that ATOX1 expression levels on melanoma were high in in all HPA, GENT and CCLE databases, a further analysis of the correlation between altered ATOX1-mRNA expressions in cutaneous melanoma patients was conducted. Patient samples which expressed higher levels of ATOX1-mRNA expression were correlated with a shorter median survival via The Cancer Genome Atlas (TCGA), R2 genomics analysis and the Human Protein Atlas (HPA) programs. Previously presented data suggest the postulated theory that there is an association between the ATOX1 expression and tumorigeneses, growth and progression of melanoma. By the R2 genomic analysis database, it was confirmed that ATOX1 gene is expressed in melanoma higher than another cancer cell lines, such is breast, prostate and lung cancer cells.

A genomic analysis database was performed through R2 genomic analysis on the expression profiles of 214 primary melanoma (n=16) and metastatic melanoma (n=198) MMC tumor tissues. Patients included were stage III and stage IV metastatic melanoma patients. The cohort was patients with $BRAF^{mut}$ metastatic melanoma and were treated with BRAF inhibitors as monotherapy or in a combination of BRAF inhibitor dabrafenib and the MEK inhibitor trametinib (n=158). To complete the cutoff, 56 patients who had been treated with the immunotherapeutic with melanoma-associated antigen 3 vaccination (MAGE-A3) [98]. In this cohort was found that samples with extremely high ATOX 1 expression have shorter median overall survival and poor clinical progress than the samples with low ATOX 1 expression, as illustrated in Figure 13.

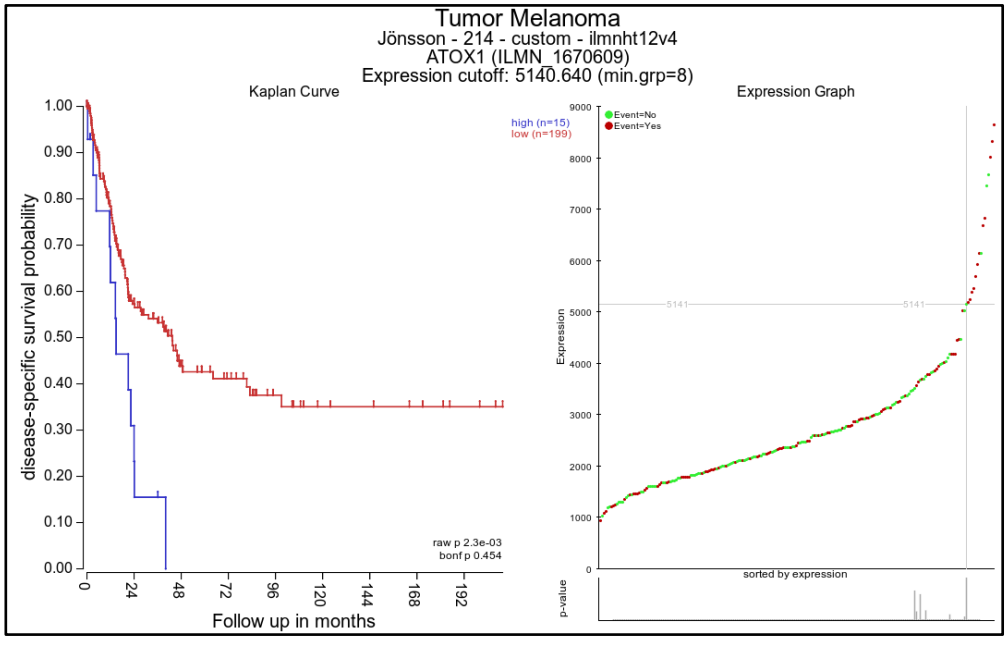

Figure 13. Melanoma with ATOX1-overexpression is associated with poor clinical prognosis. Patient samples with expressed higher levels of ATOX1-mRNA expression were correlated with a shorter median overall survival via R2 genomics analysis.

Taken together, it is concluded that the ATOX1 gene plays a highly relevant role in the development and prognosis of melanoma and over makes a reference that its monitoring and targeting of its effect become one of the main targets for the treatment of the Nobel melanoma treatments of the future. Moreover, targeting ATOX1 in combination with different therapies is one of the most outstanding alternatives for the treatment of metastatic melanoma, which remains a completely unexplored area in current oncology.

1.6.2 ATOX1 as a target therapy target in melanoma

Several authors described that Cu^{2+} act as an essential cofactor for MEK1/2 phosphorylation and subsequent hyper-activation of MAPK signaling in melanoma. It was demonstrated that Cu^{2+} is absolutely essential for $BRAF^{V600E}$-driven MAPK signaling and melanomagenesis [25, 81]. Consequently, the inhibition of Cu^{2+} transport and MEK-Cu^{2+} dependent phosphorylation could be a target for therapy in melanoma. The therapeutic inhibition of the Cu^{2+} transporter ATOX1 by DCAC50 (specific inhibitor of ATOX1 and CCS) has been tested with remarkable results [81, 99]. DCAC50 significantly decreased ERK1/2 phosphorylation on $BRAF^{mut}$ melanoma and its subsequent cell growth in a dose-dependent manner. At this point, these results propose that targeting ATOX1 and the intracellular metabolism of Cu^{2+} are an alternative and novel approach for melanoma [86].

1.7 Modification of Cu^{2+} metabolism as a cancer treatment

As described above, trace metals as Cu^{2+} afford critical nutrient support to melanoma cells, where acts as a specific cofactor for the appropriate MEK1 phosphorylation of ERK1/2 through a Cu-MEK1 interface [2, 25] . Thus, Cu^{2+} plays a relevant role in the growth, development and proliferation of melanoma. Because of this, the use of metal chelators in cancer treatment has generated renewed interest. During the last year this included the exploration of specific Cu^{2+} chelating compounds, such as disulfiram (DSF). DSF is a thiuram derivative which has shown strong antitumor activity in recent years. In addition, it was described that DSF induces antitumor effects in a Cu^{2+}-dependent manner in diverse cancers, such as: colon, breast and prostate cancer [100-102]. Thus, DSF appears as an anticancer therapeutic option for melanoma, also because of the essential trace metal function of the Cu^{2+}

in melanoma. To sum up, DSF attracted some interest as candidate for "repurposing" as alternative melanoma therapy.

1.7.1 Disulfiram (DSF)

DSF (Antabuse® or Antabus®) is an FDA-approved (1952) alcoholism therapy that has been used for about 60 years in the United States due to its specific ability to inhibit the aldehyde dehydrogenase (ALDH1/2) [103, 104]. Further inhibition of cytosolic and mitochondrial ALDH isoforms, which are responsible for acetaldehyde accumulation and unpleasant effects when alcohol is consumed such as hot flushes, vomiting and shortness of breath to severe symptoms as cardiovascular collapse, respiratory depression, seizures and even death, has been identified [105, 106]. DSF is a tetraethyl derivate that contains dimethyl-dithiocarbamate (tetraethyl thiuram disulfide) and its stoichiometric formula is $C_{10}H_{20}N_2S_4$. It´s molecular weight is 296.5g/mol. DSF is an inexpensive, safe (lethal dose [8,6gr/kg]) and well-tolerated drug.

Once DSF is absorbed, it is reduced to its main metabolite, bis-diethyldithiocarbamate (bis-ET) by the glutathione reductase. The molecular weight of monovalent ET is 148.3g/mol and its stoichiometric formula is $C_5H_{10}NS_2$. ET is a highly polar, hydrophilic compound that is effortlessly decomposed into diethylamine (DEA) and carbon disulfide and subsequently eliminated from the organism. In contrast to DSF, ET has two intact thiol groups, which gives it a high affinity to divalent ion-metals such as copper (Cu^{2+}) and zinc (Zn^{2+}). Thus, ET chelates strongly available metal ions, such as, copper (Cu^{2+}) generating the bis-(diethyldithiocarbamate)-Cu^{2+}) complex (CuET), as is illustrated in Figure 14. Lastly, CuET is an acid-stable, neutrally charged and hydrophobic complex. Although the anticancer mechanism of DSF are not yet fully understood, published data show that the cytotoxicity of DSF is mediated by the formation of the CuET complex [100, 104, 107-109].

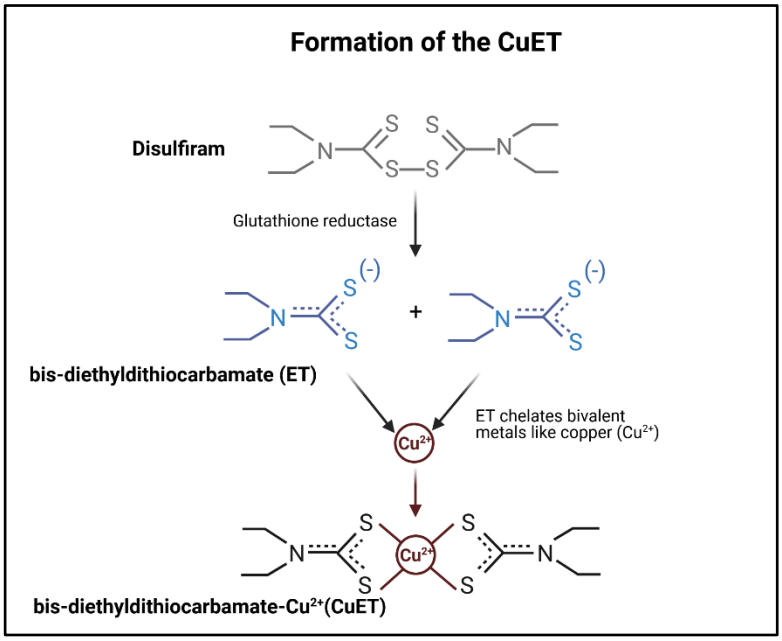

Figure 14: Metabolism of DSF and its principal metabolite diethyldithiocarbamate (ET). DSF is rapidly reduced into two molecules of its principal active metabolite diethyldithiocarbamate (ET) that hold high ability to chelate bivalent metal ions like Cu^{2+} due to its intact thiol groups. This irreversibly process is mediated by the glutathione reductase from the erythrocytes, once the DSF is already in the blood system. The reduction of the DSF to bis-ET is started in around 4 min after it is in the circulatory system. Due to the intact thiol groups in ET it can intensely chelate Cu^{2+}. The final complex of the ET and Cu^{2+} (CuET) has already been described as the functional molecule that carries out the anticancer activity. Figure modified from Meraz-Torres, et.al., 2020 [104].

DSF has an exceptional good oral bioavailability and a high absorption rate along the entire length of the upper gastrointestinal tract (85–90%). The unabsorbed DSF is eliminated by the feces (10–15%). In the blood, 99% of the DSF is quickly and irreversibly reduced into its corresponding thiol bis-diethyldithiocarbamate (bis-ET) monomers by the action of the erythrocytes glutathione reductase system, as was already described [100, 104, 105]. ET monomers are a highly polar and hydrophilic compound that is easily decomposed in an acidic environment into DEA and carbon disulfide (CS2), which are the main DSF´s elimination route. DEA follows the renal breakdown and its renal elimination pathway. Contrary, CS2 is further oxidized to carbonyl sulfide (COS), decomposed into sulfur radicals and lastly eliminated by the respiratory cycle. In addition to the DSF decomposition path, the rest of the ET is discomposed to ET-glucuronide and thus eliminated via renal elimination; which complements the total elimination of the DSF as illustrated in the Figure 15. Taken together, once the ET has formed, an efficient system of reduction, decomposition and elimination of DSF is activated. This system concludes with a high rate of elimination of DSF via pulmonary and renal routes, as previously described. This system is highly effective, giving it a plasma half-life of 10 hours (h) [101]. This emphasizes the safety of DSF, which is reflected in an extremely high lethal dose in humans [oral LD_{50} 8.6g/kg] [104]. The main routes of DSF elimination are illustrated in Figure 15.

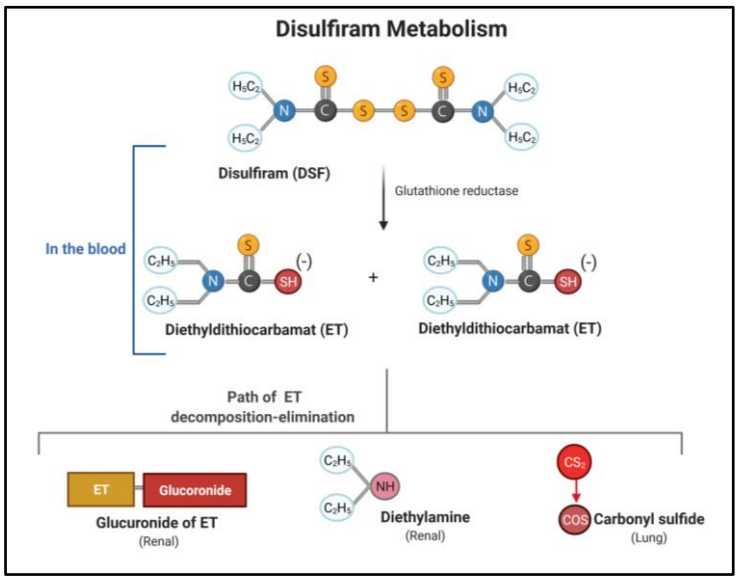

Figure 15. Metabolism of disulfiram (DSF) and its principal metabolite diethyldithiocarbamate (ET). DSF is rapidly reduced into two molecules of its principal active metabolite ET that hold high ability to chelate bivalent metal ions like Cu^{2+}. When monomeric ET molecules fail to bind to a protein (mainly albumin or ceruloplasmin) or to a divalent metal (such as Cu^{2+}, Zn^{2+}, Ag^{2+}), it loses its stability and therefore proceeds to a pathway of breakdown and subsequent its elimination. The principal pathways of the decomposition and final elimination of the DSF are either renal (as Glucuronide of ET or DEA) or lung pathway (as a Carbonyl sulfide). Figure modified from Meraz-Torres, et.al., 2020 [104, 106].

1.7.2 Mode of action Disulfiram as an anticancer drug

Current data postulate that the cytotoxicity of DSF is mediated by the presence of divalent metal ions as copper. As previously described, the main metabolite of DSF, ET, strongly chelates copper ions to form a CuET complex [110]. Several authors have described different mechanisms associated with CuET, such as, induction of reactive oxygen species (ROS), inhibition of the proteasome, and blocking of the degradation of IκB and thereby inhibition of the nuclear translocation of NFκB. To encompass these aspects, cellular uptake of CuET induces high intracellular free Cu^{+} accumulation, which generates a massive ROS induction having a huge range of consequences like DNA damage induction [101, 111]. In addition, the above-mentioned copper accumulation induces an NPL4 immobilization in focal cytoplasmatic clusters, although the P97 ATP activity remains unchanged. NPL4 in addition to P97 and UFD1 are segregases or chaperones of proteins, which are targeted for proteasomal degradation [100]. At the same time, CuET induces P53 and activates stress-activated related protein kinases as JNK and several death pathways [101, 112], as is illustrated in Figure 16. Also, many *in vitro* experimental studies, DSF and its metabolite ET have been shown to induce intracellular anticancer mechanisms, concluding in an effective inhibition of tumor cell proliferation and subsequent induction of tumor cell death [113-115]. Taken together, DSF

exerts a number of diverse intracellular effects leading to the ultimate activation of death mechanisms such as DNA breakage and apoptosis[101, 104, 116].

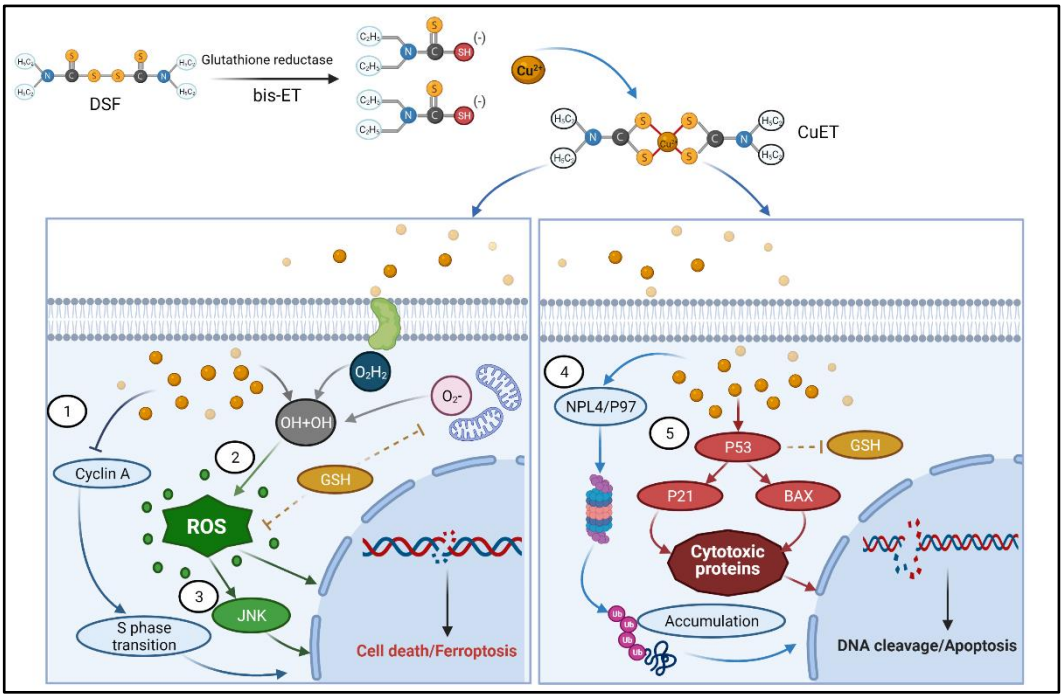

Figure 16. Mode of action of CuET on cancer cells. Cellular uptake of CuET causes an intracellular accumulation of free copper pool (Cu^{+}) which induces massive production of Reactive Oxygen Species (ROS), which holds a huge range of effects, as the further activation of the JNK pathway that concludes in the induction of DNA damage and Ferroptosis. Glutathione (GSH) is a major ROS scavenger that reduces intracellular ROS to provide balance and inhibit cell damage. In addition, the intracellular Cu^{+} accumulation mediated by DSF inhibits the Cyclin A, which is a significant factor to the S phase transition of the cell-cycle. (**left**) Simultaneously, the Cu^{+} accumulation induces P53/P21 signaling activation and inhibition of proteasome activity due to the immobilization of the NPL4/P97 molecule. These pathways conclude in a further accumulation of poly-ubiquitinylated proteins and further induction of death pathways, such as apoptosis **(right).** Figure modified from Meraz-Torres, et.al., 2020 [104].

1.7.3 Mode of action of Disulfiram on melanoma cells

There are reports that the copper complex CuET has anti-proliferative and pro-apoptotic effects in a CASPASE dependent manner in melanoma. These effects were observed in both, superficial spreading melanomas and nodular melanomas [102]. In addition, metastatic melanoma cell lines such as C8161, C8146A, C832C and A375 showed higher sensitivity to CuET than cells derived from primary melanomas. Redox state imbalance, induction of ferroptosis or activation of the intrinsic apoptotic pathway were some of the main mechanisms in which DSF-mediated melanoma cell death was described. Moreover, melanoma has been one of the main models in which Cu^{2+} significantly potentiated the antitumor effect of DSF. Also, the cell growth of benign skin cell as melanocytes and keratinocytes was almost not affected by CuET [117, 118]. The effects of CuET in the context of genomic melanoma subgroups like BRAF-WT melanoma cells, has not been examined.

1.7.4 Future perspectives of Disulfiram on melanoma

Although the specific mechanisms of DSF in melanoma have not yet been fully described, the results of different pre-clinical trials support the putative theory that DSF has a strong anticancer effect [104, 119]. The observed anticancer effects of DSF are mediated by copper, which reinforces the postulated theory on the significant role of copper in melanoma. Of note, CuET might enhance the application of target therapy in melanoma. On normal conditions, the body regulates the intracellular Cu^{2+} metabolism [2]. Consequently, to achieve therapeutic copper concentrations, copper supplements need to administered, which do not confer significant adverse events. Although DSF has exhibited strong anticancer activity in different cancer models, far-reaching melanoma research still remains.

In the meantime, some clinical trials have been performed in order to explore the clinical effectivity of DSF as anti-cancer therapy in melanoma. Clinical effectivity of the DSF in Stage IV melanoma have been explored as a single therapy (Phase II, NCT00256230), in combination with arsenic trioxide in patients with metastatic melanoma with at least one previous systemic therapy (phase I, NCT00571116) and finally in combination with chelated zinc after diagnosis of disseminated metastatic melanoma which failed during its first line therapy (phase II, NCT02101008) [104, 106]. The main outcome of the trials with published results was satisfactory tolerability (grade 1 and 2 toxicities) with only gastrointestinal discomfort and discreate elevation of the liver transaminases. In addition, clinical improvement, such as disease stabilization or improved overall or progression-free survival, was evident some in the DSF treatment groups [120-123]. To sum up, there are currently no published data in which DSF has been combined with targeted therapy or oncologic immune therapies such as immune-checkpoints.

2 Aim of the Thesis

Beyond the $BRAF^{V600}$ mutations, which cause hyperactivation of the MAPK pathway in about 40% of all cutaneous melanomas, other mutations in genes such as NRAS and NF1 (BRAF-WT melanoma subgroup) cause constitutive firing of MEK1/2 and ERK1/2 in another 30-35% of the cases. Therefore, a therapy with clinically available MEK inhibitors like trametinib seems to be a logic consequence for BRAF-WT melanomas with activated MAPK signaling. The clinical efficacy and safety of MEK inhibitors as monotherapy have already been investigated in clinical trials. The phase 3 clinical trial NEMO investigated the MEK inhibitor binimetinib as a monotherapy in comparison to dacarbazine in patients with advanced NRAS mutated melanoma [124]. The median progression-free survival (PFS) was 2.8 months in the MEK inhibitor group and 1.5 months in the dacarbazine group. Median overall survival (OS) reached 11.0 months with the MEK inhibitor and was 10.1 months with the chemotherapy. The overall response rate of the binimetinib monotherapy was poor, only 15%, but still higher than the 7% reported in the dacarbazine group. Despite positive, this result was disappointing and significantly worse than the results obtained with BRAF inhibitors (BRAFi) monotherapy used to treat $BRAF^{V600E/K}$ mutant melanomas. Based on that, the hoped-for approval of MEK inhibitors for the treatment of $NRAS^{mut}$ metastatic melanoma by the FDA and EMA failed to materialize. Therefore, combinations with other drugs, able to induce high response rates in BRAF-WT melanoma are needed.

DSF has proven to be a promising candidate in the search for a clinically available compound that has a melanoma-inhibiting effect by itself and in combination with MEK inhibitors, has a putative additional therapeutic effect. DSF showed tumor cell killing activity in several preclinical tumor models, including melanoma [100, 104]. In accordance with its antitumor effects in preclinical models, DSF was also clinically tested. DSF in combination with chemotherapy showed an improvement in tumor-specific survival on the one hand in an adjuvant setting for high-risk breast cancer patients and on the other hand in non-small cell lung cancer [114, 125]. Additionally, a reduced cancer-specific mortality associated with the use of DSF as an anti-alcoholism drug could be identified for colon, prostate and breast cancer patients between 2000-2013 [100, 126]. These results supported the hypothesis that disulfiram (DSF) has an anti-cancer effect on melanoma cells, and that its combination with the MEK inhibitor trametinib could represent a promising cancer therapy for patients with metastatic BRAF-WT melanomas (BRAF-WT).

Therefore, we performed the preclinical study on DSF in its active metabolized, copper-bound form Cu^{2+}/di-ethyldithiocarbamate (CuET) in combination with the MEK inhibitor trametinib for the treatment of melanoma BRAF-WT cell lines and patient-derived short-term culture models (NRAS melanoma models). As a consequence, the tumor-specific cytotoxicity of trametinib, CuET and the combination of trametinib with CuET were tested in 2D and 3D melanoma models, as well as *in vivo* patient derivate xenograft mouse models.

3 Materials and methods

3.1 Material

3.1.1 Chemicals and solutions

Chemicals/Solutions	Supplier/Company
4-Methylumbelliferylheptanoate (MUH substrate)	Sigma Life Science, J&K Scientific
4% Paraformaldehyde	Histology department
Adenosine 5´triphosphate (ATP) disodium salt hydrate	Sigma-Aldrich, AppliChem
Agar Noble	BD Difco
Agar Noble, Ultrapure	Alfa Aesar (Thermo Fisher Scientific)
Agarose	Lonza
Alarm Blue®	Life technologies
Ammonium diethyldithiocarbamat (TCA)	Sigma-Aldrich
Ammonium persulfate (APS, (NH4)2S2O8)	Roth
Amphotericin B (Fungizone, 250 µg/mL amphotericin B, 205µg/mL sodium deoxycholate)	Gibco by Life Technologies
Ampicillin	Sigma-Aldrich
Aprotinin	Sigma-Aldrich
β-mercaptoethanol	Merck, Roth
Bambanker	Nippon Genetics Europe
Biofreeze	Biochrome
Boric acid	Roth
Bradford	Bio-Rad
Bromophenol blue	Roth
Bovine Serum Albumin	Sigma-Aldrich, Roth
Calcein-AM (#56496,20x 50µg)	Sigma Life Science
Carboxymethylcellulose sodium	Sigma-Aldrich
CHAPS	Merck
CnT-40 Melanocyte Medium	CELLnTEC
CnT- Basal Medium (CnT-PR-BM.1)	CELLnTEC
CnT- Prime Fibroblast (CnT-PR-F)	CELLnTEC
Collagenase	Genaxxo Bioscience
Coenterazine	Sigma-Aldrich
Collagen G1 (0.5% Collagen Solution in 0.01 N HCL)	Matrix Bioscience
Collagen Type 1 (rat tail, 100mg)	Corning
Complete Protease Inhibitor cocktail	Roche
Coomassie Brillant BlueR-250 staining solution	Bio-Rad
Copper gluconate	Sigma-Aldrich

Copper sulfate	Sigma-Aldrich
Corning Matrigel Basal Membrane Matrix	VWR
CremophorEL	Merck Millipore
Crystal Violet Solution (HT90132, 2.3% Crystal Violet, 0.1% Ammonium oxalate and 20% ethyl alcohol)	Sigma-Aldrich
D-Luceferin	Lifeline Cell Technology
DermaLife Basal Medium	Lifeline Cell Technology
Developer and Replenisher	GBX Carestream Dental
Dimethyl sulfoxide (DMSO), cell culture grade	AppliChem
di-Sodium Hydrogene phosphate (Na_2HPO_4)	VWE, Millipore
Dipotassium Phosphate (K_2HPO_4)	Merck
Dispase	Gibco by Life Technologies
Dithiothreitol (DTT)	Merck
Doxycycline hyclate	AppliChem
dNTP-mix	Pharmacia Biotech
Dulbecco´s Modified Eagle Medium (DMEM), high Glucose (D6429, 4500 mg/L glucose, L-glutamine, sodium pyruvate, and sodium bicarbonate)	Sigma Life Science
Dulbecco´s Phosphate Buffered Saline (PBS) (D8537, Without calcium chloride and magnesium chloride)	Sigma Life Science
Ethylenediaminetetraacetic acid (EDTA, Titriplex II)	Merck
Fetal Calf Serum (FCS)	Sigma Life Science
Fetal Calf Serum (FCS), Tetracacline-free	Biochrome
Fixer and Replenisher	GBX Carestream Dental
Fuji medical X-Ray film	Fujifilm Corporations
Gentamycin (50mg/mL)	Sigma
Glycerol	Sigma
Glycine	Roth
Hank´s Balanced Salt Solution (HBSS)(H6648, with sodium Bicarbonate, without phenol red, calcium chloride and Magnesium sulfate)	Sigma Life Science
Hematoxylin	Dako
HEPES	AppliChem
Hyaluronidase	Sigma-Aldrich
Hydrogen peroxide (H_2O_2 50% wt. in H_2O)	Sigma-Aldrich
Hydrochloric acid	Sigma-Aldrich
Isofluran CP	CP-Pharma
Isopropanol	VWR Chemical
Kaiser´s glycerol gelatin	Sigma-Aldrich
LD buffer for DNA marker (6x)	Thermo Scientific
Leupeptin	Sigma-Aldrich

Levofloxacin	Sigma-Aldrich
Lipofectamin RNAiMAX	Thermo Fisher Scientific
Lipofectamine 3000 transfection reagent	Thermo Fisher Scientific
L-dihydroascorbate (DHA)	Sigma-Aldrich
Magnesium sulfate ($MgSO_4$)	Merck
Magnesium chloride hexahydrate ($MgCl_2$-6 H_2O)	Merck
Methanol	VWR Chemical
Mowiol	Sigma-Aldrich
NcleoSpin® RNA-Kit	Macherey-Nagel
N,N,N´, N´-Tetramethylethylenediamin	Merck
Non-fat dry milk powder	Cell Signaling Technology
NP-40	Caibiochem
PageRuler Plus Prestained Protein Ladder	Thermo Fisher Scientific
Passive Buffer (5x)	Promega
PMSF	Roche
Penicillin/Streptomycin (10 000 U/mL Penicillin, 10mg/mL Streptomycin)	Gibco by Life Technologies
Pepstatin A	Roth
Perform	Schülke & Mayr
Phenyimethylsulfonyl fluoride (PMSF)	Sigma Life Science
Pierce ECL Western blot substrate	Thermo Fisher Scientific
PhosSTOP™	Roche
Polyacrylamide	Roth
Polybrene	Sigma-Aldrich
Potassium chloride (KCL)	AppliChem
Potassium dihydrogen phosphate (KH_2PO_4)	Merck
Propidium Iodide	Sigma Life Science
Potassium pyrophosphate	Merck
RPMI 1640 (+L-Glutamine, +25 mM HEPES)	Gibco by Life Technologies
Random Hexamer primer	Bioline
Resazurin sodium salt	Sigma
Rotophorese Gel40 (19:1) (40% Acrylamide-Bisacrylamide-stock solution)	Roth
RNAse	Thermo Scientific
Sodium azide	Merck
Sodium citrate trisodium salt dehydrate	Roth
Sodium chloride (NaCl)	Merk, AppliChem
Sodium deoxycholate	AppliChem
Sodium dodecyl sulfate (SDS)	Roth
Sodium fluoride (NaF)	Merck
Sodium hydrogen Carbonat ($NaHCO_3$)	Merck

Sodium hydroxide (NaOH)	Merck
Sodium orthovanadate	Sigma Life Science
Sodium Pyrophosphate	Sigma Life Science
StemPro Accutase	Gibco
ScreenFect® A transfection reagent	GENAXXON bioscience
Superscript II reverse transcriptase kit	Invitrogen
SuperSignal West Dura extended duration substrate	Thermo Fisher Scientific
N_3 N_3 N_3, N_3 –Tetramethylethylenediamine (TEMED)	Roth
Trans-Blot® Turbo™ PVDF Membrane	Bio-Rad
Trans-Blot® Turbo™ Filter Paper	Bio-Rad
Trans-Blot® Turbo™ Transfer buffer	Bio-Rad
Tetraethylthiuram disulfide	Sigma-Aldrich
Triethylendiamin	Bio-Rad
Tris	Roth, AppliChem
Tricine	Sigma-Aldrich
Tris-HCL	Sigma Life Science
Triton X-100 Detergent	Calbiochem, AppliChem
0.05% Trypsin/EDTA	Gibco by Technologies
Tween20	AppliChem
Tween40	AppliChem
Visio Blot Standard 1	Serva

Table 4: Chemicals and solutions

3.1.2 General buffers and solutions

Composition	Concentration	Stock	Volume/Amount	ad
Tris-HCL pH 7.6	1M	Tris-HCL (MW 157.6 g/mol)	78.8 g	500 mL ddH_2O pH 7.6 (NaOH)
Tris base pH 8.8	1.5M	Tris base=Tris (hydroxymethyl) aminomethan (MW 121.14 g/mol)	90.86 g	500 mL ddH_2O pH 8.8(NaOH)
Tris base pH 6.8	1 M	Tris base=Tris (hydroxymethyl) aminomethan (MW 121.14 g/mol)	12.11 g	100 mL ddH_2O pH 6.8 (HCL)
APS	10% (w/v)	Ammonium persulfate (MW 228.37 g/mol)	1 g	10 mL ddH_2O
SDS	10% (w/v)	Sodium dodecylsulfate (MW 288.37 g/mol)	10 g	100 mL ddH_2O
EDTA pH 8.0	0.5 M	Ethylenediaminetetra-acetic acid= Titriplex II (MW 292.24 g/mol)	73.06 g	500 mL ddH_2O pH 8.0 (NaOH)
HEPES ph 8.0	1 M	4-(2-hydroxyrthyl)-1-piperazineethanesulfonic acid (MW 238.30 g/mol)	2.383 g	10 mL ddH_2O sterile filtered

HEPES ph 8.0	0.01	1 M HEPES pH 8.0	100 µL	10 mL ddH_2O
NaCl	4 M	Sodium Chloride	23.376 g	100 mL ddH_2O
$CaCl_2$	100nM	Calcium Chloride (MW 147.02 g/mol)	14.702 g	1 L ddH_2O autoclave
LiCL	4M	Lithium Chloride (MW 42.39 g/mol)	16.956 g	100 ml ddH_2O sterile filtered
Glycine	1.25 M	Glycine (MW 75.07 g/mol)	4.7 g	50 mL PBS
ATP	0.5 M	Adenosine-5'- Triphosphoric acid disodium salt (MW 551.1 g/mol)	5 g	18 mL ddH_2O sterile filtered
Sodium citrate-trisodium salt dehydrate	10 mM	Sodium citrate buffer (1X) pH 6.0	2.94 g	1 L ddH_2O

Table 5: General buffers and solutions

3.1.3 Buffers and solutions for Western blot analysis

Phosphatase inhibitors

Stock	Concentration	Molecular weight	Volume/Amount	ad
Sodium Fluoride	0.5 M	41.99 g/mol	1.05 g	50 mL ddH_2O
Sodium Orthovanadate	0.1 M	183.91 g/mol pH10 (NaOH, orange)	0.91975 g	50 mL ddH_2O boil until clear (10 min) to RT
Sodium Pyrophosphate Decahydrate	0.1 M	446.06 g/mol	2.23 g	50 mL ddH_2O

Table 6: Phosphatase inhibitors

Protease inhibitors

Stock	Concentration	Molecular weight	Volume/Amount	ad
Pepstatin A	1 mg/mL/1.46 mM	685.9 g/mol	5 mg	5mL EtOH (99%)
Leupeptin A	10 mg/mL/ 21.03 mM	475.6 g/mol	1 mg	100 µL ddH_2O
Aprotinin	10 mg/mL/ 1.54 nM	6511.5 g/mol	1 mg	100 µL HEPES 0.01M, pH 8.0
PMSF	100 mM	174.2 g/mol	1 g	57 mL C_3H_8O

Table 7: Protease inhibitors

RIPA lysis buffer

Composition	Concentration	Stock	Volume/Amount
Tris-HCL ph 7.6	25nM	1 M Tris-HCL ph 7.6	2.5 mL
NaCl	150 mM	2 M NaCl	7.5 mL
NP-40	1% (v/v)	100% (v/v) NP-40	1 mL
Sodium deoxycholate	1% (w/v)	Sodium deoxycholate	1 g
SDS	0.1 % (w/v)	10% (w/v) SDS	1 mL
RIPA buffer (10 mL) ad			
+ Phosphatase inhibitors			
Sodium Fluoride (NaF)	20 mM	0.5 M	4 mL
Sodium Orthovanadate	1 mM	0.1 M	1 mL
Sodium Pyrophosphate	1 mM	0.1 M	1 mL
ddH_2O			*ad.100 mL*
+ Protease inhibitors			
Pepstatin A	10 µM	1 mg/mL/ 1.46 mM	68.4 µL
Leupeptin	49.21 µM	1 mg/mL/ 21.03 mM	23.4 µL
Aprotinin	3.85 µM	10 mg/mL/ 1.54 mM	25 µL
PMSF	100 µM	100 mM	10 µL

Note: 10 mL aliquots of RIPA buffer with phosphatase inhibitors are stored at -20°C and supplemented with protease inhibitors before to use.

Table 8: RIPA lysis buffer

Laemmli buffer (6X)

Composition	Concentration	Stock	Volume/Amount
Tris Base pH 6.8	0.3 M	1 M Tris base pH 6.8	30 mL
SDS	12% (w/v)	Sodium dodecyl sulfate (MW 288.37 g/mol)	12 g
Glycerol	30% (v/v)	100% (v/v) Glycerol	30 mL
β-Mercaptoethanol	30% (v/v)	100% (v/v) β-Mercaptoethanol	30 mL
Bromophenol blue	1.5 mg/mL	Bromophenol blue (MW 669.96 g/mol)	0.15 g
ddH_2O			**ad 100 mL**

Table 9: Laemmli buffer (6X)

Stripping buffer

Composition	Concentration	Molecular weight	Volume/Amount
SDS	2% (w/v)	10% (w/v) SDS	20 mL
Tris-HCl pH 6.8	65 mM	1 M Tris-HCl pH 6.8	6.5 mL
β-Mercaptoethanol	100 mM	β-Mercaptoethanol	720 µL
ddH_2O			ad 100 mL

Table 10: Stripping buffer

SDS PAGE running buffer (10X)

Composition	Concentration	Molecular weight	Volume/Amount
Tris Base	247.6 mM	121.14 g/mol	30 g
Glycine	1.918 M	75.07 g/mol	144 g
SDS	34.7 mM	288.37 g/mol	10 g
ddH_2O			**ad 1 L**

Note: The SDS PAGE running buffer (10X) is diluted in ddH_2O at 1:10 immediately before use to obtain SDS PAGE running buffer (1X).

Table 11: SDS PAGE running buffer (10X)

Western blot transfer buffer (10X)

Composition	Concentration	Molecular weight	Volume/Amount
Tris Base	478.8 mM	121.14 g/mol	30 g
Glycine	386.3 mM	75.07 g/mol	29 g
SDS	12.83 mM	288.37 g/mol	3.7 g
ddH_2O			ad 1 L

Note: The Western blot transfer buffer (10X) is diluted in H_2O and methanol at 1:7:2 immediately before use to obtain Western blot transfer buffer (1X).

Table 12: Western blot transfer buffer (10X)

Phosphate buffered saline (10X)

Composition	Concentration	Molecular weight	Volume/Amount
NaCl	1.37 M	58.44 g/mol	80 g
KCl	26.8 mM	74.55 g/mol	2 g
Na_2HPO	101.4 mM	141.96 g/mol	14.4 g
KH_2PO_2	17.6 mM	136.09 g/mol	2.4 g
ddH_2O			ad 1 L (pH 7.4)

Note: The Phosphate buffered saline (10X) is sterilized by autoclaving and diluted in ddH_2O at 1:10 immediately before use to obtain phosphate buffered saline (1X).

Table 13: Phosphate buffered saline (10X)

Equilibration buffer for CSP start

Composition	Concentration	Molecular weight	Volume/Amount
Tris-HCl	76.1 mM	157.6 g/mol	19.2 g
NaCL	102.7 mM	58.44 g/mol	9.6 g
$MgCl_2$-6 H_2O	49.2 mM	203.3 g/mol	16 g
ddH_2O			ad 1.6 L (pH 9.5)

Table 14: Equilibration buffer for CSP Start

3.1.4 Cell culture media and solutions

Composition of cell culture media and their application

Basis	Supplements	Cells
RPMI 1640 with L-Glutamine and 25 mM HEPES(Gibco,Thermo Fisher Scientific	10% FCS (Sigma Life Science), 1% Penicillin/Streptomycin (Gibco,Thermo Fisher Scientific)	Cancer cells
Opti-MEM™ I Reduced Serum Medium	Gibco,Thermo Scientific Fisher Scientific	Cancer cells
DMEM, high glucose (Sigma Life Science)	10% FCS (Sigma Life Science) 1% Penicillin/Streptomycin (Gibco,Thermo Fisher Scientific)	Fibroblasts
CnT-Prime Fibroblast (CELLnTEC)	Not	Fibroblast
CnT-Basal Medium (CELLnTEC)	CnT-07 Supplement Pack for CnT-07 culture	Keratinocytes
CnT-40 Melanocyte Medium (CELLnTEC)	Not	Melanocytes
DermaLife Basal Medium (Lifeline Cell Technology)	DermaLife M LifeFactors Kit for DermaLife M Melanocyte Medium	Melanocytes

Table 15: Composition of cell culture media and their application

Composition of cryo medium and its application.

Basis	Supplements	Cells
FCS (Sigma Aldrich)	10% DMSO (Sigma Aldrich)	Cancer cells, Fibroblasts, Melanocytes
Bambanker (Nippon Genetics Europe)	-	Cancer cells
Biofreeze (Biochrome)	-	Cancer cells
CnT Basal Medium (CELLnTEC)	10% Glycerol	Keratinocytes

Table 16: Composition of cryo medium and its application.

Nevi solution

Composition	Concentration	Stock	Volume/Amount
Collagenase	0.05%	Collagenase (240 U/mg)	50 mg
Hyaluronidase	0.1%	Hyaluronidase (646.3 U/mg)	100 mg
Dispase	0.15% (~1.25 U/mL)	Dispase (0.89 U/mg)	150 mg
HBSS (w/o Ca^{2+} and Mg^{2+})			ad 100 mL

Table 17: Nevi solution

Transport medium for tissue

Basis	Supplements	Cells
HBSS (Sigma Life Science)	0.2% Gentamycin (Sigma) 1% Penicillin / Streptomycin (Gibco, Thermo Fisher Scientific) and addition of 1% Amphotericin B (Fungizone) (Gibco by LifeTechnologies)	Tissue transport

Table 18: Transport medium for tissue

3.1.5 Signaling pathway inhibitors, activators and cytostatic agents

Signaling pathway inhibitors, activators and cytostatic agents

Inhibitor	Target	Molecular weight	Stock Concentration	Solvent	Supplier
Ammonium tetrathiomolybdate (TTM)	99.97% trace metals basis	471.5 g/mol	10mM	DMSO	Sigma Aldrich
Ammonium Diethyldithio-Carbamate (ET)	Inhibitor of the enzyme ALDH	166.31 g/mol	1µM	DMSO	Sigma Aldrich
Bathocuproine-disulfonic acid disodium	Cu^{+} chelator	564.54 g/mol	1mM	DMSO	Sigma Aldrich
Cisplatin	chemotherapy	301.0 g/mol	100mM	infusion Solution	Hexal AG
Copper(II)-Gluconate 98%	chemical metal, atomic number 29	453.84 g/mol	1µM	PBS	Sigma Aldrich
Copper(II)-sulfate 98%	chemical metal, atomic number 29	159.61 g/mol	1µM	PBS	Sigma Aldrich
Dabrafenib	$BRAF^{V600E/K}$	519.56 g/mol	1mM	DMSO	GlaxoSmithKine
N-Acetyl-L-cysteine (NAC)	Antioxidant Precursor to γ-glutamyl-cysteinylglycine	163.19 g/mol	1mM	RPMI medium	Sigma Aldrich
L- Reduce Glutathione	Antioxidant **(**tripeptide**)**	307.32 g/mol	2.5mM	RPMI medium	Signal Aldrich
Puromycin	antibiotic protein	471.5 g/mol	10mg/mL	H_2O	InvivoGen
SP600125 (JNKi)	JNK inhibitor	202.2 g/mol	100mM	DMSO	InvivoGen

Trametinib *(GSK1120212)*	MEK1/2	615.39 g/mol	1mM	DMSO	Novartis
Tetraethylthiuram disulfide (DSF)	Inhibitor of the enzyme ALDH	296.54.5 g/mol	1µM	DMSO	Sigma Aldrich
Vemurafenib *(PLX4032)*	$BRAF^{V600E/K}$	489.92 g/mol	50 mM	DMSO	LC Laboratories
Z-VAD-FMK	Pan-CASPASE Inhibitor	467.92 g/mol	20µM	DMSO	InvivoGen

Table 19: Signaling Pathway inhibitors, activators and cytostatic agents

Vehicle for the in vivo experiments

Composition	**Concentration**	**Dilution**	**Volume/Amount** add Cremophor EL (20%) saline solution 0.9% (75%) (Ratio 0.5:2:7,5)
Disulfiram (DSF)	50µg/g	1mg/5µL DMSO	100µL/20g mice
Trametinib	0,3 mg/kg	6µg/5µL DMSO	100µL/20g mice
Vehicle control	-	5µL DMSO	100µL/20g mice

Table 20: Vehicle

3.1.6 Kits

Kit	**Supplier**
Alamar Blue® Cell viability assay	Life Technologies
Amersham ECL Prime Western blotting detection reagent	GE Healthcare
CDP-Star	Roche
First strand cDNA synthesis kit	Thermo Fisher Scientific
GoTaq qPCR MasterMix	Promega
Lab Vision™ UltraVision™ LP detection system: AP Polymer	Thermo Scientific
Lab Vision™ Liquid Fast-Red substrate system	Thermo Scientific
LDH Cytotoxicity detection kit	Clontech
Lipofectamine RNAimax reagent	Invitrogen By Life Technologies
Maxima first strand cDNA synthesis kit	Thermo Scientific
NE-PER™ Nuclear and Cytoplasmic extraction reagents	Thermo Fisher Scientific
NucleoSpin® RNA-kit	Machinerey&Nagel
Pierce™ BCA Protein assay kit	Thermo Fisher Scientific
Pierce™ ECL Western blotting substrate	Thermo Scientific
ScreenFect® Transfection kits	Genaxxon Bioscience GmbH
Superscript II Reverse transcriptase kit	Invitrogen

Table 21: Kits

3.1.7 Enzymes

Enzyme	Supplier
Collagenase (240 U/mg)	Millipore
Dispase II (0.89 U/mg)	Gibco
Hyaluronidase (grade I, 646.3 U/mg)	AppliChem
RNAse A (105.3 U/mg)	AppliChem

Table 22: Enzymes

3.1.8 Primers

Target	Direction	Sequence (5' → 3')	Annealing temperature	Supplier
β-ACTIN	forward	ttgttacaggaagtcccttgcc	55°C	biomers.net
	reverse	atgctatcacctcccctgtgtg	55°C	biomers.net
ATF4	forward	tggggaaaggggaagaggttgtaa	60°C	biomers.net
	reverse	agtcgggtttgggggctgaag	61°C	biomers.net
ATOX1	forward	ttgttacaggaagtcccttgcc	55°C	biomers.net
	reverse	tctggaagccagcgggaggat	61°C	biomers.net
CCS	forward	cagaatggaggatgagcagctg	56°C	biomers.net
	reverse	gagcgtgcaatgatgccacagg	62°C	biomers.net
CHOP	forward	aaggcactgagcgtatcatgt	51°C	biomers.net
	reverse	tgaagatacacttccttcttgaacac	52°C	biomers.net
COX 17	forward	ttgcccggagaccaagaaggc	62°C	biomers.net
	reverse	attatttattcacacagcagaccac	52°C	biomers.net
CTR1	forward	ccaggaccaaatggaaccatcc	59°C	biomers.net
	reverse	accacctggatgatgtgcagca	60°C	biomers.net
DMT1	forward	agctccaccatgacaggaacct	57°C	biomers.net
	reverse	tggcaatagagcgagtcagaacc	58°C	biomers.net
P8	forward	ccattcctacctcgggcctctcatc	63°C	biomers.net
	reverse	tcttggtgcgacctttccggc	62°C	biomers.net
TBP	forward	tgcacaggagccaagagtgaa	60°C	biomers.net
	reverse	cacatcacagctccccacca	62°C	biomers.net

Table 23: Primers.

3.1.9 Antibodies

Target	Source	Dilution	Supplier	Product number
β-ACTIN	mouse	(1:1000)	Cell Signaling Technology	#3700
AKT 1 (C73H10)	rabbit	(1:1000)	Cell Signaling Technology	#2938
Anti-P8	rabbit	(1:250)	abcam	#ab6028
ATF-4 (D4B8)	rabbit	(1:500)	Cell Signaling Technology	#11815
ATOX1	mouse	(1:250)	Santa Cruz Biotechnology, INC.	#sc-398742
BAD	rabbit	(1:1000)	Cell Signaling Technology	#9292
BAX (Clone:6A7)	mouse	(1:250)	BD Biosciences	#556467
BCL-2	mouse	(1:250)	Santa Cruz Biotechnology, INC.	#sc-509
BIM (C34C5)	rabbit	(1:1000)	Cell Signaling Technology	#2933
CASPASE-3	rabbit	(1:1000)	Cell Signaling Technology	#9662
CHOP (L63F7)	mouse	(1:500)	Cell Signaling Technology	#2895
Cleaved CASPASE-3^{Asp175}	rabbit	(1:1000)	Cell Signaling Technology	#9664
Cleaved PARP-3^{Asp214}	rabbit	(1:1000)	Cell Signaling Technology	#5625
c-JUN	rabbit	(1:1000)	Cell Signaling Technology	#9165
CYTOCHROME C	rabbit	(1:1000)	Cell Signaling Technology	#4272
ERK1/2	mouse	(1:1000)	Cell Signaling Technology	#4696
ERK1/2 (p44/42 MAP)	rabbit	(1:1000)	Cell Signaling Technology	#9102
LAMIN B1 (c-20)	goat	(1:200)	Santa Cruz Biotechnology, INC.	# sc-6216
NF-1	rabbit	(1:1000)	Cell Signaling Technology	#14623
PARP	rabbit	(1:1000)	Cell Signaling Technology	#9532
Phospho-S6$^{(Ser235/236)}$	rabbit	(1:1000)	Cell Signaling Technology	#2211
PJNK	mouse	(1:250)	Santa Cruz Biotechnology, INC.	#sc-6254
P$^{T202/Y204}$**-ERK1/2**	rabbit	(1:1000)	Cell Signaling Technology	#4370
P$^{T202/Y204}$**-ERK1/2**	mouse	(1:1000)	Cell Signaling Technology	#9106
P^{T359}**-RSK**	rabbit	(1:1000)	Cell Signaling Technology	#8753
P$^{T359/S363}$**-RSK**	rabbit	(1:1000)	Cell Signaling Technology	#9344
p-AKT^{S473} **(587F11)**	mouse	(1:1000)	Cell Signaling Technology	#4051
pγH2AX^{S139} **(JBW301)**	mouse	(1:200)	Merck	#05-636
P21 Waf1/Cip1	mouse	(1:1000)	Cell Signaling Technology	#2946
P53 (DO-1)	mouse	(1:500)	Santa Cruz Biotechnology, INC.	#sc-126
RSK$^{1/2/3}$	rabbit	(1:1000)	Cell Signaling Technology	#9355
SAPK/JNK	rabbit	(1:1000)	Cell Signaling Technology	#9252
S6 (5G10)	rabbit	(1:1000)	Cell Signaling Technology	#2217

Table 24: Antibodies

3.1.9.1 Secondary antibodies

Target	Source	Dilution	Supplier	Product number
anti-Rabbit IgG HRP-Linked	mouse	(1:3000)	Cell Signaling Technology	#7074
anti-Rabbit IgG AP-Linked	mouse	(1:3000)	Cell Signaling Technology	#7054
anti-Mouse IgG HRP-Linked	rabbit	(1:3000)	Cell Signaling Technology	#7076
anti-Mouse IgG AP-Linked	rabbit	(1:3000)	Cell Signaling Technology	#7056
anti-Goat IgG HRP-Linked	rabbit	(1:2500)	Novus bio	#7073
anti-Goat IgG AP-Linked	mouse	(1:2500)	Cell Signaling Technology	#7056S

Table 25: Secondary antibodies

3.1.10 siRNA

Gene ID	Gene Sequence 5`-3`	Nucleotides	Supplier
SLC11A2	*Guide* UAAUAGUGSUGSGSSSGCCCCC	22nt	Riboxx
	Guide UAGAAAUAGACUUUGGACCCCC	22nt	
	Guide AGAAAGUCAUUCAUCCCUGCCCCC	24nt	
	Passenger GGGGGCUUUCUCAUCACUAUUA	22nt	
	Passenger GGGGGUCCAAAGUCUAUUUCUA	22nt	
	Passenger GGGGGCAGGGAUGAAUGACUUUCU	24nt	
SLC31A1(1317)	*Guide* AUAUUUAAACUGGCACCCACCCCC	23nt	Riboxx
	Guide UAUUUAGUCUCAAACCACCCCC	22nt	
	Guide AUUAUCACAAUCCAAGAGCCCCC	23nt	
	Passenger GGGGGUGGGUGCCAGUUAAAUAU	23nt	
	Passenger GGGGGUGGUUUGAGACUAAAUA	22nt	
	Passenger GGGGGCUCUUGGAUUGUGAUAAU	23nt	
ATOX1 (475)	*Guide* AUGUCAUACUUAACUCCUCCCCC	23nt	Riboxx
	Guide AUACUUAACUCCUCCAAGCCCCC	23nt	
	Guide UGUCAUACUUAACUCCUCCCCC	22nt	
	Passenger GGGGGAGGAGUUAAGUAUGACAU	23nt	
	Passenger GGGGGCUUGGAGGAGUUAAGUAU	23nt	
	Passenger GGGGGAGGAGUUAAGUAUGACA	22nt	
Sox10	*Guide* CCGUAUGCAGCACAAGAAA-dTdT	23 nt	Riboxx
	Passenger UUUCUUGUGCUGCAUACGG-dTdT	23 nt	
nonsil	*Guide* AAUUCUCCGAACGUGUCAGU-dTdT	23 nt	Riboxx
	Passenger ACGUGACACGUUCGGAGAAUU-dTdT	23nt	

Table 26: siRNAs

3.1.11 Cell lines

Eukaryotic cell lines with origin and mutational status

Cell line	Origin	NRAS mutation	NF1 mutation	BRAF mutation	Acquired resistance
SKMEL23	Melanoma	-	-	-	-
WM1366	VGP Melanoma	Q61L	-	-	-
SKMEL30	Metastatic Melanoma (cutaneous)	Q61K	-	-	-
WM1346	Metastatic Melanoma (cutaneous)	+	-	-	-
MelJuso	Metastatic Melanoma	Q61L	L1779P*	-	-
SKMEL113	Melanoma	-	deletion	-	-
WM3918	Metastatic Melanoma (parotid)	-	deletion	-	-
MeWo	Metastatic Melanoma (lymph node)	-	Q1336* /del	-	-
LOX-IMVI	Metastatic Melanoma (lymph node)	-	Q1174*	V600E	-
451LU S	Metastatic Melanoma (lung, xenograft)	-	-	V600E	-
A375 S	Metastatic Melanoma	-	K1290	V600E	-
Me1617 S	Metastatic Melanoma (lung)	-	-	V600E	-
SKMEL19 S	Metastatic Melanoma	-	-	V600E	-
SKMEL28 S	Metastatic Melanoma	-	-	V600E	-
451LU R	451LU S			V600E	Vemurafenib
A375 R	A375 S	-	K1290	V600E	Vemurafenib
Mel1617 R	Mel1617 S	-	-	V600E	Vemurafenib
SKMEL 19 R	SKMEL9 S	-	-	V600E	Vemurafenib
SKMEL 28 R	SKMEL28 S	-	-	V600E	Vemurafenib
A375 RR	A375 S	-	K1290	V600E	Vemurafenib + Trametinib
Mel1617 RR	Mel1617 S	-	-	V600E	Vemurafenib + Trametinib

Table 27: Cell lines

Melanoma Patient-Derived Short-Term cultures with the respective mutational status

Cell line	Origin	NRAS	NF1	BRAF

		mutation	mutation	mutation
TÜMEL1	lymph node	-	n.d.	BRAF V600E
TÜMEL61	lymph node	-	n.d.	BRAF V600E
TÜMEL62-1	brain metastasis	NRAS Q61R	n.d.	-
TÜMEL78	skin metastasis	-	n.d.	BRAF V600E
TÜMEL96	brain metastasis	-	n.d.	BRAF V600E
TÜMEL110	Endolumenal met.	G436A	n.d.	-
TÜMEL115	lymph node	-	n.d.	BRAF V600E
TÜMEL119	lymph node	-	n.d.	BRAF V600E
TÜMEL123-1	skin metastasis	NRAS Q61R	n.d.	-
TÜMEL173	adrenal gland met.	NRAS G12V	n.d.	-
TÜMEL176	skin metastasis	-	n.d.	-

Table 28: Melanoma Patient-Derived Short-Term cultures with the respective mutational status

3.1.12 Consumables

Consumable	Supplier
T175 tissue culture flask	Cellstar® Greiner Bio-One
T75 tissue culture flask	Sarstedt
T25 tissue culture flask	Cellstar® Greiner Bio-One
6-well tissue culture plate	Sarstedt
12-well tissue culture plate	Costar Corning
24-well tissue culture plate	Costar Corning
48-well tissue culture plate	Costar Corning
96-well tissue culture plate	Sarstedt
100 mm x 20 mm cell culture dishes (PS; with vent)	Cellstar® Greiner Bio-One
94 mm x 16 mm Petri dishes (with vent)	Greiner Bio-One
50 mL polypropylene tube	Cellstar® Greiner Bio-One / Falcon
15 mL polypropylene tube	Cellstar® Greiner Bio-One
5 mL round-bottom polystyrene tube	Sarstedt
2 mL cryo tube (round bottom, external thread)	Greiner Bio-One
2 mL tube	Eppendorf
1.5 mL tube	Eppendorf
0.5 mL tube	Biozym
BD Plastipak (1 mL) Luer slip syringe without needle	BD
BD Plastipak SubQ 26G1/2 with needle	BD
Cell scraper	Corning
Cell Strainer "Easy Strainer" (100 µm)	Greiner Bio-One
Corning BioCoat Collagen I Cell Culture Flasks	Corning
Lightcycler 480 Multiwellplate 96	Roche
FiltrEX™ 96-well white filter plates with 0.2 µm PVDF Membrane	Corning
Pasteur capillary pipettes	Wu Mainz
Pipette tips	Greiner Bio-One; Mettler Toledo

SurPhob filtered pipette tips	Biozym
Serological pipettes	Costar Corning
PVDF Membrane	Roche
Whatman Filter Paper	Whatman, GE Healthcare
Fuji medical X-Ray film	Fujifilm Corporations
X250 Plastic feeding tubes 20GAX38MM (FTP-20-38)	Instech Laboratories, Fisher Scientific

Table 29: Consumables

3.1.13 Laboratory equipment

Equipment	Supplier
Pipetus	Hirschmann; PeqLab (VWR)
Pipettes	Eppendorf; Gilson
Multi-channel pipette	Rainin; Brand
Forceps	Fine Science Tools
Mr. Frosty™ freezing container	Thermo Scientific
Cool Cell	Biocision
Centrifuge Mikro 200	Hettich Zentrifugen
Centrifuge 5414	Eppendorf
Heraeus® fresco 17 centrifuges	Thermo Scientific
Heraeus® Multifuge X3 FR	Thermo Scientific
Varifuge 3.0 R	Heraeus Sepatech
Vortex-Genie 2	Scientific Industries
Phase-contrast CK40 culture microscope (Light Microscope)	Olympus
Leica TCS SP8 (Confocal Laser Microscope)	Leica
Axiovert inverse fluorescence microscope	Zeiss
FACS LSR II	BD Biosciences
Mini-PROTEAN vertical electrophoresis cell	Bio-Rad
Spacer and short plates	Bio-Rad
Trans-Blot® cell	Bio-Rad
Trans-Blot® Semi-Dry transfer cell	Bio-Rad
Trans-Blot® turbo	Bio-Rad
Lightcycler® 96	Roche
PTC-200 Peltier thermal cycler	MJ Research
Nanodrop nanophotometer	Implen™
TriStar LB 941 luminometer	Berthold Technologies
EpiChemi3 darkroom imaging system	UVP Bioimaging Systems
Epson Perfection V850 Pro Scanner	Epson

Table 30: Laboratory equipment

3.1.14 Software

Application	Software (Supplier)
Statistical Analysis and Graphic	GraphPad Prism 8.3.1
Image Analysis and Editing	ImageJ, GIMP 2.10.8
Digitalization of X-ray films with Perfection V850 Pro Scanner	Epson
Digitalization of Colony Formation Assays and Gel Documentation with EpiChemi3 Darkroom Imaging System	LabWorks (Lablogics Inc.)
Flow Cytometric Analyses	FACSDiva Software (BD),
Measurement of fluorescence, luminescence and absorption with TriStar LB 941 Luminometer	MikroWin2000
Analysis of Drug Combination Effects	COMPOSYN

Table 31: Software

4 Methods

4.1 Cell biological methods

4.1.1 Cultivation of eukaryotic cells

All cells were maintained at 37°C and 5% CO_2 in a humidified atmosphere. Cancer cell lines (Table 26) as well as patient-derived cells (Table 27) and melanoma xenograft-derived cell lines (Table 27) were cultured in RPMI 1640 medium with L-Glutamine and HEPES supplemented with 10% FCS and 1% penicillin/streptomycin. Primary skin cells were cultured in the appropriate culture media (Table 14). For passaging and cell seeding, cells were detached using Trypsin/EDTA, the reaction stopped by addition of FCS-containing culture medium and cell pellets formed by centrifugation at 800 x g for 4 min. An appropriate number of cells was re-seeded for further cultivation and expansion or used in an experiment. For cryo-conservation, cell pellets were resuspended in the respective cryo medium (Table 15) at $1x10^6$ to $2x10^6$cells/mL and 1mL/cryotube frozen with the help of Cool Cell or Mr. Frosty™ freezing containers at -80°C for short-term storage. The cryotubes were transferred to a liquid nitrogen tank for long-term storage.

4.1.2 Generation of resistant cell lines

Melanoma cell lines with acquired resistance towards the BRAFV600E inhibitor vemurafenib as a monotherapy or in combination with different MEK1/2 inhibitors (trametinib, cobimetinib) were generated by chronic treatment with increasing concentrations of the respective inhibitors for several months, culminating in a final concentration of 2µM for vemurafenib, 50nM for trametinib and 200nM for cobimetinib in the cell culture medium. In addition to, the melanoma cell lines 451 Lu, SKMEL30, WM266-4 and WM3918 with acquired resistance towards the CuET were generated by chronic treatment with increasing concentrations of CuET for several months, concluding in a final concentration of 400nM for CuET in the cell culture medium. Medium was added freshly at least two times a week. Inhibitor/therapy-free cell culture medium was used 24 h before the resistant cells were subjected to experiments.

4.1.3 Isolation of melanoma cells from tumor tissue

Melanoma cells were isolated from excised melanoma xenografts from immunocompromised mice to establish therapy-conditioned sub cell lines (Table 26) as well as from tumor tissue from melanoma patients to obtain patient-derived cells (Table 26). To this end, the tissue was cut into small pieces using a scalpel and incubated in 1-2 mL nevi solution in a 6-well plate (Table 16) at 37°C for 1 h to 2 h. The digestion process was stopped by addition of 3 mL culture medium (RPMI1640 with 10% FCS and 1% penicillin / streptomycin). Cells were dissociated from the tissue by thoroughly pipetting up and down (10-15X) using a 10 mL serological pipette and filtering through a 100µm cell strainer. After centrifugation at 1500 x g for 5 min, the resulting cell pellet is either resuspended 30 Material and Methods in culture medium and seeded into appropriately sized tissue culture flasks for cultivation (5.2.1.3) or directly resuspended in cryo medium and stored at -80°C. The use of patient tissue samples was approved by the local medical ethical committee (340/2018B02) and performed in accordance with the Declaration of Helsinki Principles. Informed consent was provided by all patients.

4.1.4 Cell viability assays

4.1.4.1 MUH assay

Viability of the melanoma cells was assessed using the 4-methylumbelliferyl heptanoate (MUH) assay. Briefly, 2.5×10^3 cells were seeded into cavities of a 96- well plate. After 24 h cells were treated in hexaplicates for 72 h with increasing concentrations of signaling pathway inhibitors (e.g. MEK inhibitor, trametinib, (up to 2µM) or CuET (up to 1µM)) either as single or combinational treatments. To analyze viability, cells were washed with PBS, subsequently incubated with 100µg/mL 4-methylumbelliferyl heptanoate diluted in PBS (1:100 dilution of 10 mg/mL stock) for 1h at 37 °C. In viable cells, 4-methylumbelliferyl heptanoate is hydrolyzed by intracellular esterase's and lipases producing the highly fluorescent 4-methylumbelliferone. The arising fluorescence (λex 355 nm, λem 460 nm) is detected with a Tristar fluorescence microplate reader (Berthold Technologies). The intensity of fluorescence is indicative of the number of viable cells and based on that, the relative viable cell number remaining after treatment was calculated relative to the respective control cells.

4.1.4.2 Alamar Blue assay

An Alamar Blue assay was used in order to analyze the viability of melanoma cells following treatment with signaling pathway inhibitors. In two-dimensional culture conditions, 2.5×10^3 melanoma cells were seeded in cavities of a 6-well, 12-well or 96-well plate, respectively, and 24 h later treated with the indicated concentrations and combinations of signaling pathway inhibitors for 3 days (2mL/cavity,1mL/cavity or 100µL/cavity). After pre-diluting a 1 mg/mL resazurin (Sigma) stock solution at 1:10 in culture medium, 200µL, 100µL or 10µL of this solution was added to the 2mL, 1mL or 100µL culture medium in each 6-well, 12-well or 96-well cavity and incubated for 1 h at 37 °C. During that time, resazurin is metabolized to fluorescent resorufin by mitochondrial reductases in viable cells. To assess the relative number of viable cells following treatment in tissue slices, at the end of the treatment, 200µL / 100µL of pre-diluted resazurin (1:10 dilution of 1mg/mL stock in culture medium) is added to the supernatant in the 12-well or 24-well cavities, respectively and incubated for 1 h to 12 h at 37 °C until there was a clear color change from blue to pink in the wells of the untreated control cells indicative for a successful turnover of the resazurin. Subsequently, 50µL of culture medium is transferred to a 96-well plate in quadruplicates to detect the resulting fluorescence by a Tristar fluorescence microplate reader (Berthold Technologies) with λex of 540nm and λem of 640nm. If cells were already cultured on 96-well plates, the plates could be directly measured in the microplate reader. The relative viable cell number remaining after inhibitor treatment was determined relative to the respective control cells.

4.1.5 Cell-cycle analysis

For the cell-cycle analysis, 2.5×10^5 cells were seeded into cavities of a 6-well plate and incubated for 24 h. Subsequently, the cells were treated with indicated concentrations and combinations of trametinib (MEK inhibitor) and CuET for 3 days. For the experiments using co-treated with NAC, 2.5×10^5 cells were seeded and pre-treated with NAC 1mM during 24 h before to perform the appropriate treatment. As a result, the appropriate treatment was started 48 h after the seeding. Treatment was carried out in triplicates and DMSO (0.02%) was used as a solvent control. To analyze the cell-cycle distribution, floating and adherent cells were harvested, permeabilized with 70% ice cold ethanol overnight, washed with PBS twice and resuspended in PBS with 50µg/mL propidium iodide (Sigma-Aldrich) and 100µg/mL RNAse A (AppliChem). After staining for 30 min (m) in the dark, the distribution of the cells in the different cell-cycle phases was detected with a BD^{TM}LSR II flow cytometer (BD Biosciences) using the FACSDiva^{TM} software (BD Biosciences).

4.1.6 Clonogenic assays

Clonogenic assays were used to evaluate the effects of long-term drug therapy on melanoma cell growth. Briefly, cells were coated at low density into a 12-well plate with 500 cells/cavity. After 24 h, cells were treated in triplicates with MEK inhibitors (trametinib) as a monotherapy or in combination with CuET at the indicated concentrations and combinations (trametinib 10nM, CuET 125nM). Twice a week, the culture medium was exchanged and simultaneously fresh inhibitors added. After 14 d, cells were fixed with 4% paraformaldehyde for 10 m, washed with PBS and stained with a 0.1% Coomassie Brilliant Blue solution (Bio-Rad) containing 30% methanol and 10% acetic acid. Pictures of the stained plates were taken with the EpiChemi3 Darkroom Imaging System (UVP Bioimaging Systems) and the LabWorks software (Lablogics Inc.).

4.1.7 Three-dimensional spheroid culture

For the correct generation of melanoma cell spheroids, the hanging drop method was performed. To this end, droplets of 25µL culture medium containing 250 melanoma cells each were dappled onto the lid of PBS filled Petri dishes (30 drops/ dish). Due to gravity, cells within one drop are forced into a cellular aggregate. After incubation for 6 d, the produced spheroids were directly harvested to perform a spheroid growth assay (4.1.7.1).

4.1.7.1 Spheroid growth assay

After 6 d of culturing melanoma cells in hanging drops (250 cells per 25µL drop) leading to spheroid development, spheroids were collected and implanted either in culture medium with 1.2 mg/mL collagen I. To this end, cavities of a 12-well plate were embedded in culture medium containing 1.2 mg/mL collagen I and after gelation 8 to 10 spheroids in 300µL added to each 12-well plate cavity. After 6 h, 500µL of culture medium was applied on top with MEK inhibitors (trametinib at 10nM) as monotherapy or added in in combination with CuET (125nM) as the indicated concentrations and every treatment regimen set up in triplicates. Growth medium containing the corresponding treatment was exchanged twice a week and light microscopic pictures taken every 24 h. At the 6^{th} d was performed a staining with Calcein-AM 2µM/ PI 8µM and fluorescent microscope pictures were taken. Quantification of the spheroid sizes (diameter of spheroid cross sections) was performed with ImageJ.

4.2 Molecular biological methods

4.2.1 Isolation of total RNA from eukaryotic cells

Cells were harvested with Trypsin/EDTA. A cell pellet was produced by centrifugation at 3,000 rpm for 5 m, washed twice with cold PBS and either stored at -20°C or directly used for RNA isolation. Total RNA extraction was performed with the NucleoSpin RNA kit (Machery-Nagel) according to the manufacturer's instructions. The RNA was eluted in 60µL of RNAse-free H_2O and stored at -80°C.

4.2.2 Determination of RNA concentration

The RNA concentration of respectively sample was determined photometrically through the use of the Nanodrop NanoPhotometer (Implen^{TM}) with the correct program and settings for RNA measurement.

4.2.3 Reverse transcription

Reverse transcription of 1µg RNA into cDNA was done with the help of the first strand cDNA synthesis kit (Thermo Fisher Scientific) using random hexamer primers.

Ingredient	**Amount**	**Volume**
RNA sample		
RNA	1µg	
RNA-free H_2O	XµL	
Total	*10*µL	**Denaturation:** 70°C for 10 min
Master-Mix	**Per sample**	
5X RT Buffer	4 µL	
Random Hexamer Primer [100 µM]	1 µL	
RiboLock RNAse Inhibitor [20 U/µL]	1 µL	
dNTP Mix [10 mM]	2 µL	
M-MuLV Reverse Transcriptase [20 U/µL]	2 µL	
Total	10 µL	**Add** Master-Mix to RNA sample **Incubation**: 25°C for 10 min **cDNA Synthesis:**50°C for 45 min **Termination:** 85°C for 5 min

Table 32: cDNA synthesis with the first strand cDNA synthesis kit.

4.2.4 Quantitative real-time PCR

Quantitative real-time PCR (RT-PCR) analysis was achieved with the LightCycler® 96 System (Roche) using GoTaq qPCR MasterMix (Promega) to analyses 1µL of cDNA with the suitable oligonucleotide primer pair listed in Table 22. 100µM stocks of oligonucleotide primers are pre-diluted 1:10 in ddH_2O to obtain 10µM working stocks.

Solutions quantitative real-time PCR

Ingredient	Volume
Master-Mix Per sample	
GoTaq® qPCR Master Mix (2X)	5 µL
ddH_2O	3.6 µL
Primer (forward) [10 µM]	0.2 µL
Primer (reverse) [10 µM]	0.2 µL
cDNA	1 µL

Table 33: Quantitative real-time PCR with GoTaq qPCR master mix (Promega)

Lightcycler 96 Program

Step	Sub-Step	Temperature	Time	Ramp	Acquisition
Pre-Incubation	-	95°C	3 min	4.4°C/s	-
Amplification	Denaturation	95°C	10 s	4.4°C/s	-
(40 cycles)	Annealing	56°C – 60°C	10 s	2.2°C/s	-
	Elongation	72°C	10 s	4.4°C/s	single
Melting Curve	Denaturation	95°C	10 s	4.4°C/s	-
	Re-Annealing	65°C	1 min	2.2°C/s	-
	Melting	97°C	1 s	0.2°C/s	continuous
Cooling	-	37°C	30 s	2.2°C/s	-

Table 34: Lightcycler 96 Program

Subsequently was performed the quantification of target gene expression relative to a control (Housekeeper) sample according to Pfaffl (2001) and using *TBP* or *β-actin* as reference gene. Consequently, the efficiency of the real-time PCR was designed for the different oligonucleotide primer pairs with the assistance a cDNA dilution row with following calculation of a standard curve and its grade or slope. The above is defined in the following formula:

$$\textbf{Efficiency}_{target/reference} = 2^{(-1/slope)}$$

Constructed on the precise efficiencies for reference genes and target gene, relative mRNA expression can be calculated according to:

$$\textit{Relative mRNA expression (target)} = \frac{\textit{Efficiency(target)}^{\Delta CP\,target(control\text{-}sample)}}{\textit{Efficiency(reference)}^{\Delta CP\,reference(control\text{-}sample)}}$$

All the experiments were done in triplicates and PCR product punctually confirmed by melting curve analysis.

4.2.5 siRNA transfection

To explore if any of the transmembrane Cu^{2+} transporters or intracellular chaperones played a relevant role in the transport of Cu^{2+} to the cell nucleus, the transfection of different siRNAs was performed. The goal of this transfection was to induce a specific gene knock down and explore the role of this in the translocation the Cu^{2+} into the nucleus. The *ATOX1* gene, the *SLC31A1* gene, which encodes *CTR1* and the *SLC11A2* gene, which encodes *DMT1*, in addition to other Cu^{2+} related genes, were knocked down with the corresponding siRNA. A non-silencing siRNA was used as a control.

The cells were transfected using the Lipofectamin RNAiMAX reagent. The cells were transfected in three different settings, in 96-well plates, for performing viability assay to determinate the cytotoxicity of the different treatments on transfected cells, in 6-well plates to explore the protein level effect and by qPCR analysis, to confirm the knockdown and finally in T75 flask to explore if these genes are related to the Cu^{2+} -uptake by the melanoma cells.

Cell number	OptiMem Media	Lipofectamin RNAiMAX	siRNA
Protocol to 96-well plate			
2500 in 100µL media	20µL	0.05µL	0.6 pmol
Protocol to 6-well plate			
2500 in 2mL media	500µL	2.5µL	15 pmol
Protocol to T75			
2 x 10^6 in 10mL media	2mL	12.5µL	90 pmol

Table 35: siRNA transfection protocol.

4.3 Protein biochemical methods

4.3.1 Western blot analysis

4.3.1.1 Whole cell protein extracts (lysates)

Melanoma cells were harvested with Trypsin/EDTA as the normal process. A cell pellet was generated by centrifugation, washed twice with cold PBS and either stored at -20°C or directly lysed with RIPA lysis buffer supplemented with protease inhibitors and phosphatase

inhibitors (Table 7). To this end, the cell pellet was meticulously re-suspended in the RIPA lysis buffer (approx. 100 µL / $1x10^6$ cells) and incubated on ice for 30 min. During the incubation time, the cell suspension was vortexed every 10 min (3 vortexed times). To clear the cell lysate from cell debris and DNA, a 20 min centrifugation step at 13 000 rpm followed. The resulting supernatant was transferred into a new 1.5 mL tube and straight used for following analyses or stored at -20°C.

4.3.1.2 Determination of protein concentration

Protein concentrations of the samples were determined using the Pierce™ BCA protein assay kit (Thermo Fisher Scientific) according to the manual.

4.3.1.3 SDS-Polyacrylamide Gel-electrophoresis

20µg – 30µg of whole cell lysate protein samples were separated by electrophoresis on SDS-polyacrylamide gels. Hence, precise volumes of the lysates were supplemented with 6X Laemmli buffer and the samples heated for 3 min at 100°C. Generally, 1.5 mm SDS-polyacrylamide gels with a stacking gel and a 10% acrylamide concentration in the running gel were used. The detection of proteins with a size exceeding 90 kDa (e.g. NF1) or below 30 kDa (e.g. ATOX1 or P21) was performed on 8% and 12% resolving gels, respectively. The samples along with a pre-stained protein ladder serving as a molecular weight standard were loaded onto the gel. Separation was performed at 130 V and monitored with the assistance of the protein marker.

1.5mm SDS-Polyacrylamide Gel						
Running gel	**2 gels**			**5 gels**		
	8%	*10%*	*12%*	*8%*	*10%*	*12%*
40% Acrylamide	4 mL	5 mL	6 mL	10 mL	12.5 mL	15 mL
1.5 M Tris base pH8.8		5 mL			12.5 mL	
10% SDS		0.2 mL			0.5 mL	
Millipore H_2O, autoclaved	10.6 mL	9.6 mL	8.6 mL	26.5 mL	24 mL	21.5mL
10% APS		0.2 mL			0.5 mL	
TEMED		8 µL			20 µL	
		-> 2x 10 ml			-> 5x 10 ml	
		8-12% Acrylamide			8-12% Acrylamide	
Stacking gel	**2 gels**			**10 gels**		
40% Acrylamide	0.75 mL			3.75 mL		
1.0 M Tris base pH6.8	0.75 mL			3.75 mL		
10% SDS	0.06 mL			0.3 mL		
Millipore H_2O, autoclaved	4.4 mL			22 mL		
10% APS	0.06 mL			0.3 mL		
TEMED	6 µL			30 µL		
	> 2x 3 mL,			> 10x 3 mL,		
	5% Acrylamide			5% Acrylamide		

Table 36: Conformation of SDS-Polyacrylamide gels.

4.3.1.4 Western blot

All the analyzed proteins were transferred from the respective gel onto a polyvinylidene difluoride (PVDF) membrane by either a semi-dry Trans-Blot Turbo System (Bio-Rad) or a tank Blotting System (Bio-Rad). To this end, the PVDF or LF PVDF membrane was previously activated with ethanol/methanol, pre-equilibrated with 5mL of 1X Transfer Buffer, positioned on a transfer buffer-soaked filter paper in the Tank Blot cassette or on a two transfer stacks on the Semi-dry Tank Blot; subsequently capped with the gel and another Transfer buffer-soaked Whatman filter paper/ transfer stacks in the respective case. The cassette was inserted into the transfer buffer-filled tank with the membrane fronting the anode in both cases. Protein transfer was conducted at 2.5 A constant, up to 25 V for 10 min on the Semi-dry blot and 400 mA for 3 h for the Wet-blot.

4.3.1.5 Immunodetection

After a wash step with PBS with 0.1% Tween-20 (PBS-T) and later on blocking for 1 h with 5% dry milk in PBS-T, the blots were prodded overnight at 4°C with the corresponding primary antibodies in blocking solution. Every antibody sample was followed by 3 washing steps à 15 min each with PBS-T. Immunodetection was carried out using rabbit-, mouse- or goat-specific secondary horse radish peroxidase (HRP)-conjugated antibodies or alkaline phosphatase (AP) antibodies in blocking solution (1 h at room temperature) and visualized with the assistance of the Pierce™ ECL Western Blotting Substrate (Thermo Scientific) or the SuperSignal™ West Dura Extended Duration Substrate (Thermo Scientific) on X-ray films. When secondary antibody was used that were coupled to alkaline phosphatase (AP) antibodies, visualization was accomplished with CDP Star (1:100 in Equilibration Buffer). X-ray films were scanned and using in the GIMP editing software.

4.3.1.6 Antibody removal from the PVDF-membranes

To eliminate bound antibodies from a PVDF or LF-PVDF membrane (Stripping), the β-mercaptoethanol is not long added to the stripping buffer and the membrane was incubated in 5mL of buffer for 30 min at 50°C. After that, the membrane was rinsed with water and scrupulously washed with PBS-T (3X 10 m), beforehand unspecific binding sites were blocked again by incubation with 5% dry milk in PBS-T (1h at room temperature) for a succeeding immunodetection.

4.3.2 Immunohistochemistry

Immunohistochemical staining (of each sample) of formalin-fixed paraffin-embedded (FFPE) specimen was made using specific antibodies for c-JUN(60A8) (Cell Signaling; 1:50 dilution) and phospho-$^{p44/42}$ERK (1/2) (Cell Signaling; 1:100 dilution) diluted in PBS containing 5% donkey serum. Initially, FFPE tissue sections were sliced of 5µm thickness and after incubated overnight at 60°C, deparaffinized in xylene and re-hydrated by passing over a decreasing alcohol row concluding in distilled water. After that, antigen retrieval was made in citrate buffer (10mM, pH 6.0) in a pressure cooker with 2 min under pressure, earlier the samples were left to cool down gradually in the hot buffer (30 min) and cold water was supplementary for a further incubation time of 10 min. Succeeding a 10 m-PBS wash, all the unspecific binding sites were obstructed with 5% donkey serum for 2 h. Finally, tissue sections were stained with the corresponding antibodies (Table 23, Table 24) diluted in 5% donkey serum through incubation at 4 °C overnight. Once three 10 m-PBS washes were performed, the Lab Vision™ UltraVision™ LP Detection System: AP Polymer, in addition to the Lab Vision™ Liquid Fast-Red Substrate-System were used rendering to the manufacturer's protocol. This process involved a 20 min incubation time with Primary Antibody Enhancer at 20-22 °C, followed through four 10 min PBS-washes, then a 30 min incubation with AP Polymer at 20-22 °C, another three 10 m PBS-washes, a 10 min incubation time in Liquid Fast Red Chromogen/Naphthol Phosphate Substrate (dependent on visual color change or development), and additionally three 5 min washes in ddH_2O. After countering with hematoxylin for 2 min and 15 min wash with ddH_2O, coverslip mounting was done using Kaiser's glycerol gelatin like an aqueous mounting medium.

4.3.3 Intracellular Cu uptake measurement

The amount of Cu that was shuttled into the intracellular compartment through the different treatments was measured. For this purpose, two million cells were seeded and 24 h later they were treated with their respective therapies. Monotherapy and combination therapy treatments were performed, where 125nM of Cu^{2+}, 125nM of ET and 125nM of CuET were used as monotherapy and the combination therapy was performed by the addition of 10nM of trametinib to the CuET. The cells were treated for 6 h and subsequently all cells were harvested via scraping. The cells were centrifuged at 800 rpm for 4 min and washed two times with PBS. The pellet was frozen at -20 °C. Then, the pellet was re-suspended in 1mL of 333nM HCl and incubated 3 h at 60 °C. 750µL were taken from the corresponding treated samples and placed in a new tube. 250µL of TCA (Table 36) was added, it was mixed properly by vortexing and

centrifuged at full speed for 5 min. After, 500µL of the supernatant was transferred into a new tube and 100µL of L-dihydroascorbate (DHA) was added and mixed by pipetting up and down. Finally, 400µL of solution C (Table 36) was added and mixed again by pipetting up and down. After 24 h of incubation at 37 °C the absorbance of the samples was measured with a photometer at λ=354nm and λ=560 nm. A Cu^{2+}- standard curve was made containing concentrations from 100µM to 0 µM in 333mM HCl.

Solution	Compound	Volume/Amount
Solution A	^{2,4,6}-Trichloroanisole (TCA)	30g
	ddH_2O	100 mL
Solution B	L-dihydroascorbate (DHA)	32.2mg
	ddH_2O	100 mL
Solution C	Bicinchoninic acid disodium	6 mg salt
	NaOH	3.6 g
	HEPES sodium salt	15.6g
	ddH_2O	100 mL

Table 37: Composition of the solutions used for the Cu uptake

4.3.4 Subcellular fractionation

A subcellular fractionation protocol for the melanoma was used in order to define which cell compartment had a higher amount of Cu^{2+} after the treatment. The cells were seeded and 24 h after treated during 6 h with the respective treatments. Once the cells were harvested, all the subsequent steps were performed at 4 °C. The cell pellets were re-suspended in 500µL fractionation buffer (Table 37) and incubated 15 min on ice. Using a 1mL syringe the cell suspension was forced 10 times through a 27-gauge needle in order to lyse all cells and thus break the cell membrane. After that, the cell suspension was left for 20 min at 4°C and then centrifuged 5 min at 3000 rpm. The pellet contained nuclei and the supernatant contained the rest of the cellular components (cytoplasm, membrane and mitochondria). The supernatant was transferred into a new tube. The nuclear pellet was re-suspended in 500µL fractionation buffer (Table 37), forced through a 25-gauge needle 10 times and finally centrifuged for 10 min at 3000 rpm. The pellet contained the pure nuclei and the supernatant was transfected into a new tube.

The supernatant containing membranes, mitochondria and cytoplasm, was subsequently centrifuged at 8000rpm for 5 min. The resulting pellet contained mitochondria and the supernatant the cytoplasm and membrane fractions. The mitochondrial pellet was following

washed in 500µL fractionation buffer and lastly centrifuged at 8000 rpm for 5 min. The supernatant was discarded. The mitochondrial and the nuclear pellets were re-suspended in 750µL of 333mM HCl. In order to homogenize the samples 250µL of 1M HCl was added to the cytoplasm plus membrane fractions. Once this process was completed, it was continued with the Cu^{2+}-uptake measurement protocol.

Substance	Molecular weight (g/mol)	Add per 1 l	Concentration
HEPES (pH 7.4)	238.30	4.77	20mM
KCL	74.55	0.75	10mM
$MgCl_2$	95.21	0.19	2mM
EDTA	380.35	0.38	1mM
DDT	1M	1mM	10µL

Table 38: Fractionation buffer

4.3.5 Lentiviral gene transfer (redox-sensitive GFPs)

Lentiviral particles were performed in HEK 293T cells (Biocat, Heidelberg, Germany) via the lentiviral vector pWPI (#12254, addgene) and a second-generation packaging system (pMD2.G and psPAX2).

GRX-roGFP2 (#64975, addgene) and *roGFP2-ORP-1* (#64991, addgene) were transfected into SKMEL23 melanoma cells by transduction via lentiviral particles. Thus, $5x10^4$ SKMEL23 per well were seeded onto a 24-well plate for 5 h. SKMEL23 melanoma cells were transduced in the presence of 8µg/mL polybrene using a multiplicity of infection (MOI) of 5. The transduction was performed in DMEM containing 10% FCS and 1% Penicillin/Streptomycin. After 48 h, the selection of successfully transduced SKMEL23 cells was performed with 0.5µg/mL *Puromycin.* The redox status of reduced glutathione (GSH/GSSG) and H_2O_2 levels in melanoma cells (SKMEL23) was accurately measured by flow cytometry through the fluorescence ratio Pacific Orange 405nm/Alexa Fluor 488nm.

A redox-sensitive specific GFP lentivirus transfection in SKMEL23 melanoma cells was conducted. Two different transgenic flies containing *roGFP2-GRX* or *roGFP2-ORP-1* targeted to either cytosol or mitochondria matrix were transfected by a lentivirus process into the melanoma cell line SKMEL23. RoGFP2 was linked to glutaredoxin (GRX) or thiol peroxidase (ORP-1) to measure glutathione redox state (GSH/GSSG ratio) or H_2O_2 levels, respectively[127]. RoGFP2 hold two cysteine residues on their surfaces, and its oxidation

determinates the fluorescence state of the protein. Increase in GSH/GSSG ratio or H_2O_2 levels oxidize the cysteine residues of GRX or ORP-1 respectively, resulting in disulfide bridge. Then, thiol-disulfide exchange is produced among GRX or ORP-1 and roGFP2 cysteines, resulting in roGFP2 disulfide bridge. The reduced roGFP2 holds an excitation around 405nm and 488nm. Therefore, the assay was measured by flow cytometry with Pacific Orange 405nm/Alexa Fluor 488nm channels. This assay was pH-insensitive[128].

4.4 *In vivo* methods

4.4.1 Melanoma Xenograft growth assay

Experiment 1: To assess melanoma growth *in vivo* under therapy with the MEK inhibitor (trametinib) as a monotherapy or in combination with CuET, 1×10^6 BRAF-WT melanoma cells in 100µl PBS/Matrigel (1:1) were subcutaneously injected into the right flank of NOD scid gamma (NOD.*Cg-Prkdc*^{scid} *Il2rg*^{tm1Wjl}/SzJ) mice. For the *in vivo* tumor growth assay evaluating the effect of the MEK inhibitor trametinib on BRAF WT melanoma cells (Four different TÜMEL melanoma BRAF-WT models from our biobank (TÜMEL62-1, TÜMEL110 and TÜMEL173), a total of 12 mice were used and randomized into three groups (n= 4). The study groups were a) control-1 (sham), b) control-2 (sham for 9 d, and at the last day one dose of DSF (50 mg/kg per os) in addition to trametinib at 0.3 mg/kg per os) and c) combination therapy with MEK inhibitor (trametinib at 0.3 mg/kg per os) with DSF (50 mg/kg per os) daily for 9 days. Since both drugs are orally bio-available they were applied by oral gavage. In order to guarantee the presence of enough copper ions to form the Cu^{2+}/diethyldithiocarbamate complex (CuET), the drinking water of the mice were supplied with additional copper gluconate (1.2µg/mL).

Using PET/MRT imaging in collaboration with the Werner Siemens Imaging Center (University of Tübingen), the copper uptake of the tumors was analyzed with the help of positron emitting copper-64. The copper-64 uptake was compared to melanoma-bearing animals that did not receive the treatment. This experiment was approved by the Regierungspräsidium Tübingen under the license number HT01/20G. The experiment 1 is illustrated as animal model-Part 1 in the Figure 17.

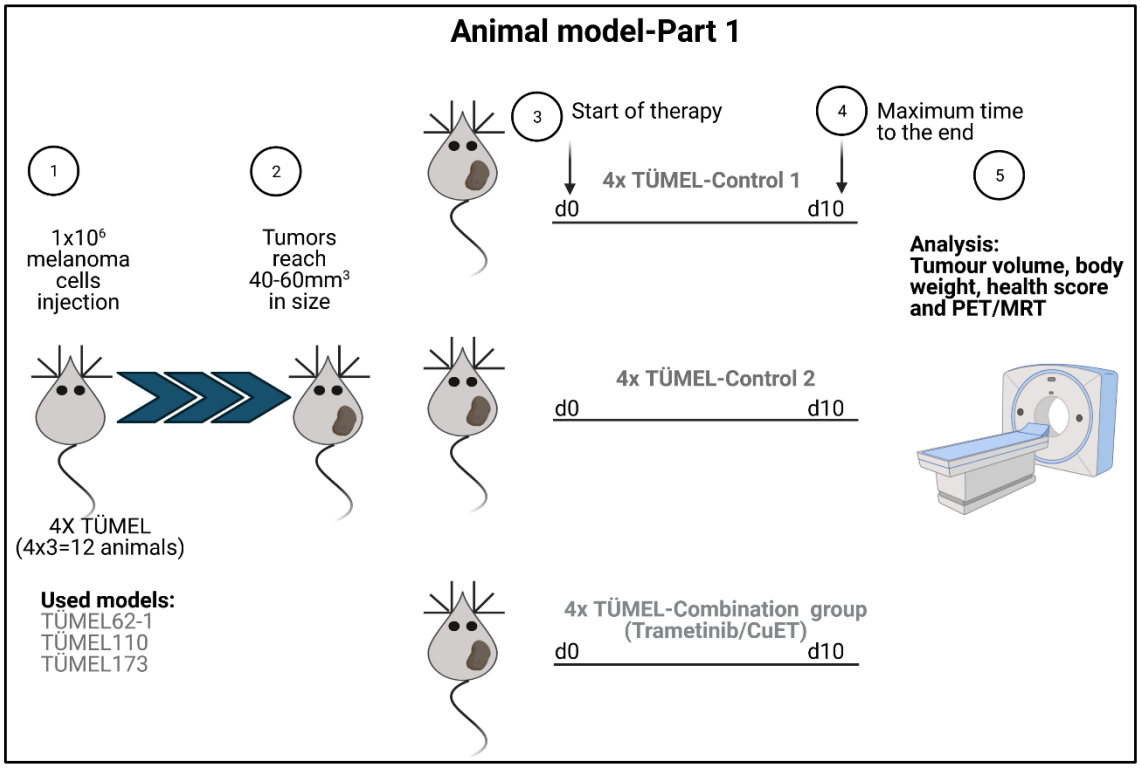

Figure 17: Animal Model-Part 1. The image shows the strategy for the realization of the first part of the in vivo experimentation where the expansion and preparation of the tumors of the different TÜMEL model (BRAF-WT), their respective treatments during 10 days and their final analysis were presented.

Experiment 2: To assess melanoma growth *in vivo* under therapy with the MEK inhibitor (trametinib) as a monotherapy or in combination with CuET, 1×10^6 BRAF-WT melanoma cells in 100 µL PBS/Matrigel (1:1) were subcutaneously injected into the right flank of NOD *scid* gamma (NOD.*Cg-Prkdc*^{scid} *Il2rg*^{tm1Wjl}/SzJ) mice. For the *in vivo* tumor growth assay evaluating the effect of the MEK inhibitor trametinib as a monotherapy or in combination with DSF on BRAF-WT melanoma cells (TÜMEL173), a total of 36 mice were used and randomized into four groups (n=6). The study groups were a) sham, b) MEK inhibitor (trametinib at 0.3 mg/kg per os), DSF (50 mg/kg per os) and combination (trametinib/DSF). Since both drugs are orally bio-available they will be applied by oral gavage. In order to guarantee the presence of enough copper ions to form the Cu^{2+}/diethyldithiocarbamate complex (CuET), the drinking water of the mice were supplied with additional copper gluconate (1.2µg/mL).

Treatment started as soon as the tumor volumes reached 5 mm^3 and lasted for 28 days or until tumors ulcerated or exceeded a volume of 1000 mm^3. The therapy was applied daily using oral gavage per os once a day for a maximum of 28 days, and the tumor growth was recorded by caliper measurements. At the end of the experiments the mice were euthanized and tumors

were isolated to perform protein analyses by immunohistochemistry and western blot in order to investigate the cell death mechanism and signaling pathways. Blood was drawn after evitus by heart puncture and plasma was isolated and stored at -80°C. The collected data comprising, tumor growth (volume), progression-free survival (increased diameter by >20% at two consecutive days), response and body weight were compared to determine the effect of the monotherapy and combination therapy. The experiment was approved by the Regierungspräsidium Tübingen under the license number HT01/20G. The experiment 2 is illustrated in the Figure 18.

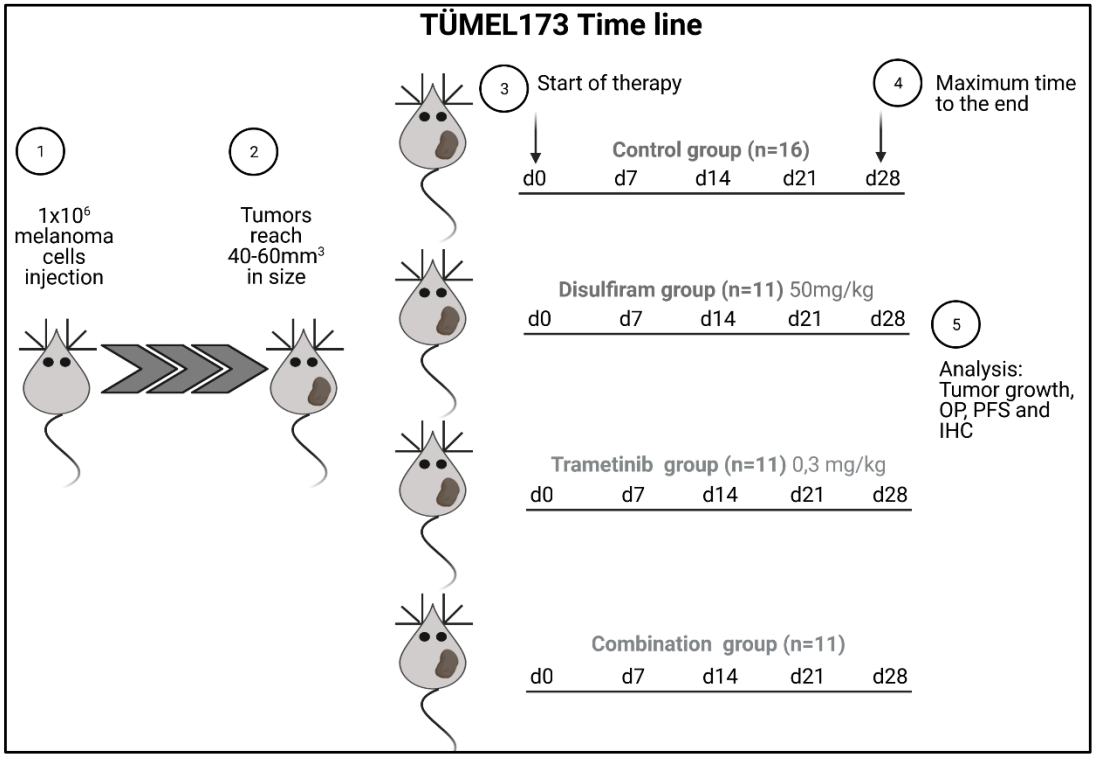

Figure 18: Animal model-Part2. The image shows the strategy for the realization of the second part of the *in vivo* experimentation where the expansion and preparation of the tumors of the TÜMEL176 melanoma model, their respective treatments during 28 days and their final analysis are presented

Tumor growth and health status were daily documented. The tumor volumes were calculated out of the daily caliper measurements with the formula: 0.5 x a (longer diameter) x b^2 (shorter diameter) and statistically compared at 7days, 14 days, 21 days and at maximum 28 days. Out of the tumor growth data, progression is determined by a confirmed increase of the tumor diameter >20% relative to the start of therapy. Similarly, response is determined as follows: Partial Response (PR)-reduction of the tumor diameter by >20%, complete response (CR) - disappearance of the tumor and SD - tumor diameter +/-20% of the initial value.

The four treatment groups sham (corresponding to a placebo group), trametinib, DSF and combination were statistically compared. Overall survival (in the time window of the 28-day *in vivo* experiment) and progression-free survival were analyzed and compared between the four groups. Using the tumor tissue of the mice experiments, Cu^{2+} content, c-JUN levels in addition to phospho-ERK1/2 levels were analyzed.

4.5 Statistical analysis

GraphPad Prism version 8.3.1. (GraphPad Software) was used for the statistical analysis of the data. Except mentioned otherwise, data were presented as mean values with its corresponding standard error of the mean (SEM) or standard deviation (SD). P-value design and significance determination were done with one-way ANOVA tracked by a Tukey's multiple comparisons test, with a two-tailed unpaired Student's t-test or with a two-tailed unpaired t-test with Welch's correction. The P-values which were in the scale of < 0.05 were considered statistically significant, with the corresponding reference:

* for $p < 0.05$

** for $p < 0.01$

*** for $p < 0.001$

**** for $p < 0.0001$.

Dose-response analysis was fixed with GraphPad Prism by means of mostly sigmoidal 4 parameter logistics regressions (performing x as log [concentration]).

5 Results

5.1 *In vitro* efficacy of the MEK inhibitor trametinib on BRAF- WT melanoma cells

5.1.1 Effects of MEK inhibitor trametinib on cell viability and growth on BRAF-WT melanoma under two-dimensional culture conditions

As initial approach the efficacy of the MEK inhibitor (trametinib) as single treatment on BRAF-WT melanoma cells was investigated. Therefore, viability assays (MUH assays) were conducted. One melanoma cell line belonging to the subgroup Triple-WT (SKMEL23), one melanoma cell line with NF1-*LoF* mutation (SKMEL113), two cell lines with a NRAS mutation (WM1366 and SKMEL119), four melanoma patient-derived short-term cultures cell lines with NRAS mutations (TÜMEL62-1, TÜMEL110, TÜMEL173 and TÜMEL176) and two Tubingen melanoma cell lines with a NRAS mutations (TÜMEL119 and TUMEL123-1) were chosen and treated with trametinib up to 2µM for 72 h. The effect of trametinib on viability reduction calculated from cell viability assays in both $BRAF^{mut}$ and BRAF-WT melanoma cell lines, with the aim of making an accurate comparison of inhibition in each of the two-melanoma subgroup. For this, a precise analysis of the response was done utilizing the IC_{50} of the MEK inhibitor trametinib of every cell line with its corresponding maximal inhibitory response, which is illustrated in Figure 19. Through this approach, a general overview of the response to the MEK inhibitors was evaluated. Most of the $BRAF^{mut}$ melanoma cells showed higher maximum effect rate to the MEK inhibitors although the IC_{50} were similar. Through this analysis it was found that BRAF-WT melanoma cell lines were higher sensitive to trametinib compared to $BRAF^{mut}$ cell lines where presented an inhibition of already 80-90% of cell growth. On the other hand, BRAF-WT melanoma cells showed around 50-60% inhibition of cell growth by trametinib, as illustrated in Figure 19.

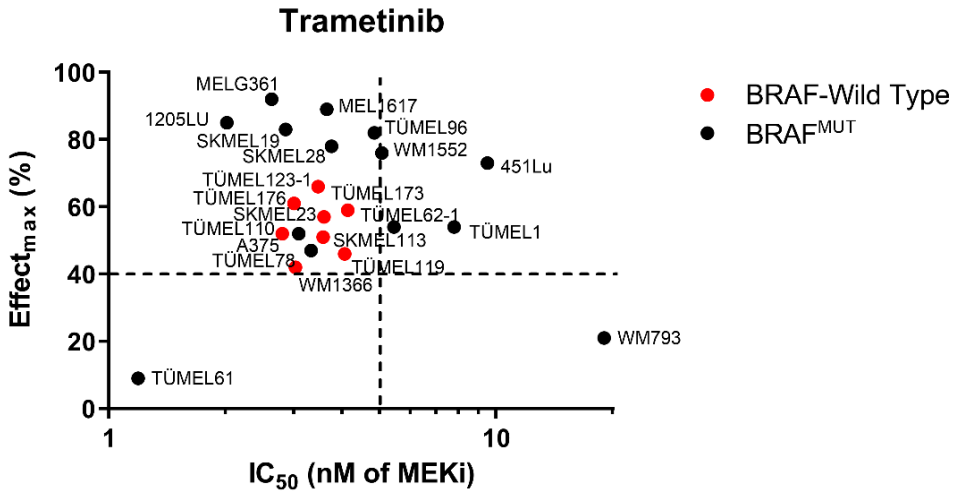

Figure 19: BRAF^{mut} and BRAF-WT melanoma cell viability to the MEK inhibitor trametinib. Schematic representation of the maximum *in vitro* therapeutic effect of MEK inhibitor trametinib (IC50). Cell viability (MUH assay) of BRAF^{mut} melanoma cell lines (A375, 451Lu, 1205LU, MELG361, MEL1617, SKMEL19, SKMEL28, TÜMEL1, TÜMEL61, TÜMEL78, TÜMEL96, WM793 and WM1552) and BRAF-WT melanoma cells (SKMEL23, SKMEL113, WM1366, TÜMEL119, TÜMEL123-1, TÜMEL110, TÜMEL62-1, TÜMEL173 and TÜMEL176) after treatment with the MEK inhibitor trametinib for 72 h. Values are means ± SEM of three replicates (n = 3; mean ± SD). Viability was normalized to untreated control cells.

As observed in the previous results, the MEK inhibitor trametinib as a monotherapy exhibited around 50% of cell growth inhibition already in the nanomolar range concentrations in BRAF-WT melanoma cells. MEK inhibitor trametinib as monotherapy exhibited similar anti-growth effect in all BRAF-WT melanoma cell lines tested. The maximum anti-growth effect was in the nanomolar range, and this effect did not increase in a dose-dependent manner. Therefore, the anti-growth effect of trametinib in all the BRAF-WT melanoma cell lines explored was maintained at around 50% of cell growth inhibition, even when the dose was increased up to 2 µM. To sum up, a similar detrimental effect was observed for all BRAF-WT melanoma cell lines. However around 50% of the viability remained even at high concentration of the MEK inhibitor, as is illustrated in Figure 20.

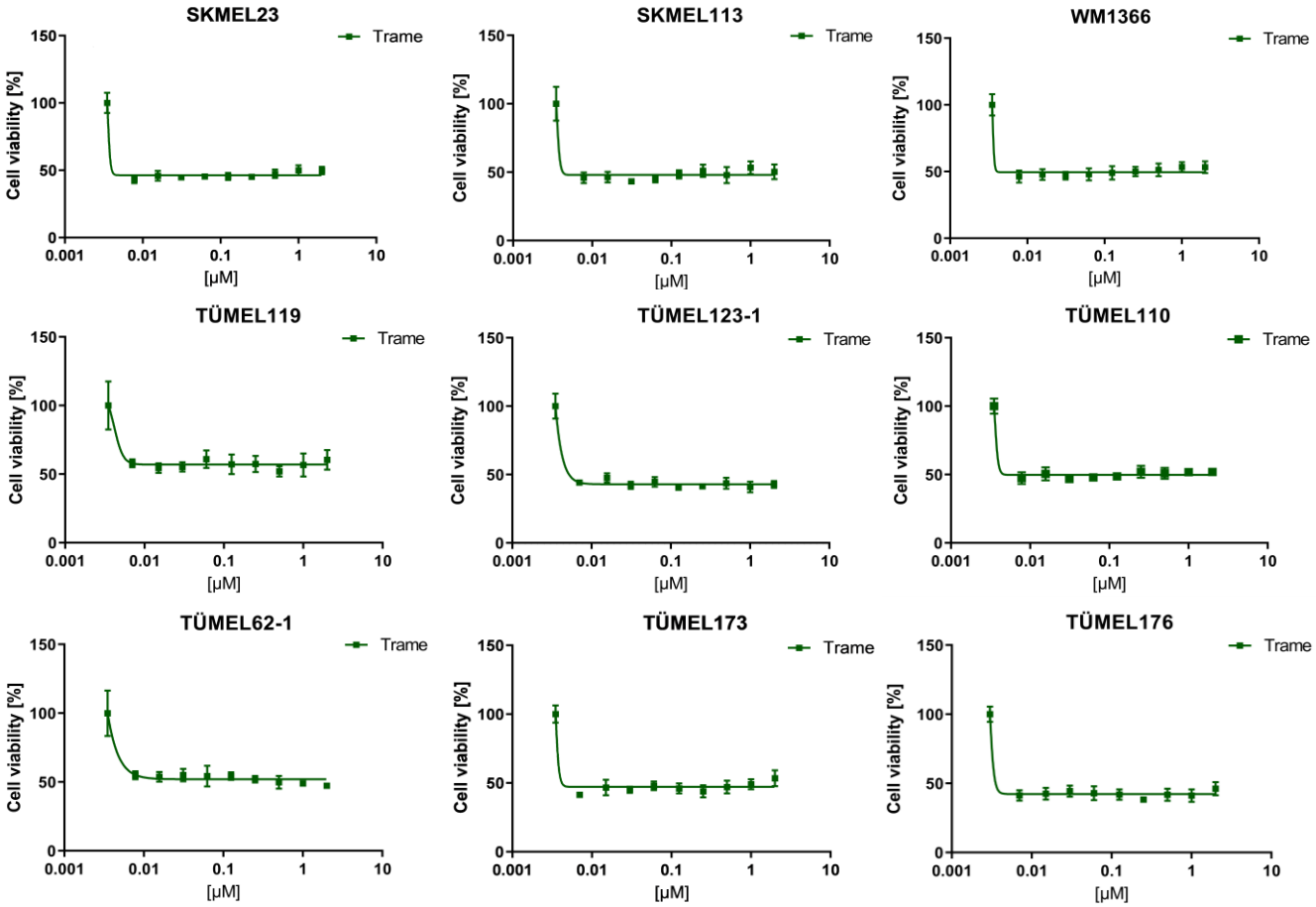

Figure 20: MEK inhibition mediated by trametinib impaired around 50% the viability of BRAF-WT melanoma cells under two-dimensional growth conditions *in vitro*. Cell viability assay (MUH assay) of BRAF-WT melanoma cell lines (SKMEL23, SKMEL113, WM1366, TÜMEL119, TÜMEL123-1, TÜMEL110, TÜMEL62-1, TÜMEL173 and TÜMEL176) after treatment with the MEK inhibitor trametinib (up 2 µM) for 72 h. Values are means ± SEM of three replicates (n = 3; mean ± SD). Viability was normalized to untreated control cells.

5.1.2 Targeted inhibition with the MEK inhibitor trametinib on protein level under two-dimensional culture conditions

Due to the fact that MEK inhibitors, such as trametinib, shored ensure a specific targeting of the MAPK signaling components (MEK1/2), key experiment was whether the phosphorylation status of the ERK1/2 changed upon MEK inhibitor. In addition, the analysis of the response and phosphorylation of different proteins of MAPK signaling pathway after treatment with trametinib was of particular interest. Therefore, treatment of the melanoma cell lines SKMEL23 and SKMEL113 with the MEK inhibitor trametinib in the nanomolar range for 3 h was conducted. It was observed at the protein level that trametinib effectively inhibited ERK phosphorylation, reflecting that trametinib was effective to block the MAPK pathway in BRAF-WT melanoma cells, as is illustrated in Figure 21.

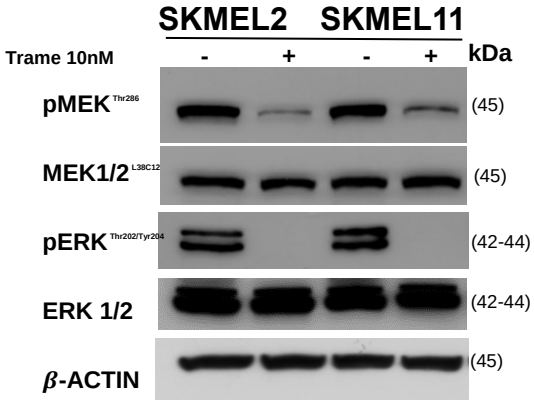

Figure 21: BRAF-WT melanoma cell lines showed efficient inhibition of ERK phosphorylation due to the MEK inhibitor trametinib after 3 h of treatment. Western blot analysis for pMEK, MEK, pERK and ERK of whole cell protein lysates of BRAF-WT melanoma cells (SKMEL23 and SKMEL113) after treatment with MEK inhibitor trametinib (10nM) for 3 h. β-ACTIN was used as loading control.

By the means of protein analysis by Western blot, the activity of the phosphorylated (p) MEK1/2 and total MEK1/2, pERK and total ERK, pRSK and total RSK, pAKT and total AKT and pS6 and total S6 were detected. pMEK and MEK were selected duo its direct target inhibitory activity of trametinib, however the rest of the MAPK pathway proteins (pERK, total ERK, pRSK and RSK) were explored due to their downstream position after the MAPKK MEK in the MAPK signaling pathway. In parallel, the PI3K pathway activity was additionally analyzed. AKT is triggered by PIP3, and AKT phosphorylation is totally dependent on PI3K pathway activation. AKT downstream proteins, such as S6 and mTOR, depend on pAKT. Activity and some modifications in phosphorylation can also be induced by MEK inhibitors, as described in chapter 1.3.3 of this work and as graphically summarized in Figure 3.

Time of treatment was 6 h since previous findings confirmed clear modification in the MAPK pathway even after 30 min of treatment, which are a sustained basis presented after 6 h without any damage after treatment morphological of the cells. This result indicates that after 6 h of treatment with trametinib in the nanomolar range, the MAPK pathway is affected. Additionally, the cells were treated with hydrogen peroxide (H_2O_2), as well as N-acetyl-cysteine (NAC), to try to observe whether the induction or inhibition of intracellular reactive oxygen species (ROS) plays a role in the activation of the MAPK and PI3K pathway. In addition, the same of the MAPK pathways were performed after serum starvation in the two melanoma cell lines. This screening was carried out because it has been previously described that growth factors and proteins included in fetal bovine serum (FCS) may play a significant role in MAPK and AKT phosphorylation and therefore could alter the results of the inhibitor trametinib. These

results described that trametinib at nanomolar range can affect MEK1/2 activity and consequently inhibited ERK phosphorylation, as is shown graphically in Figure 22.

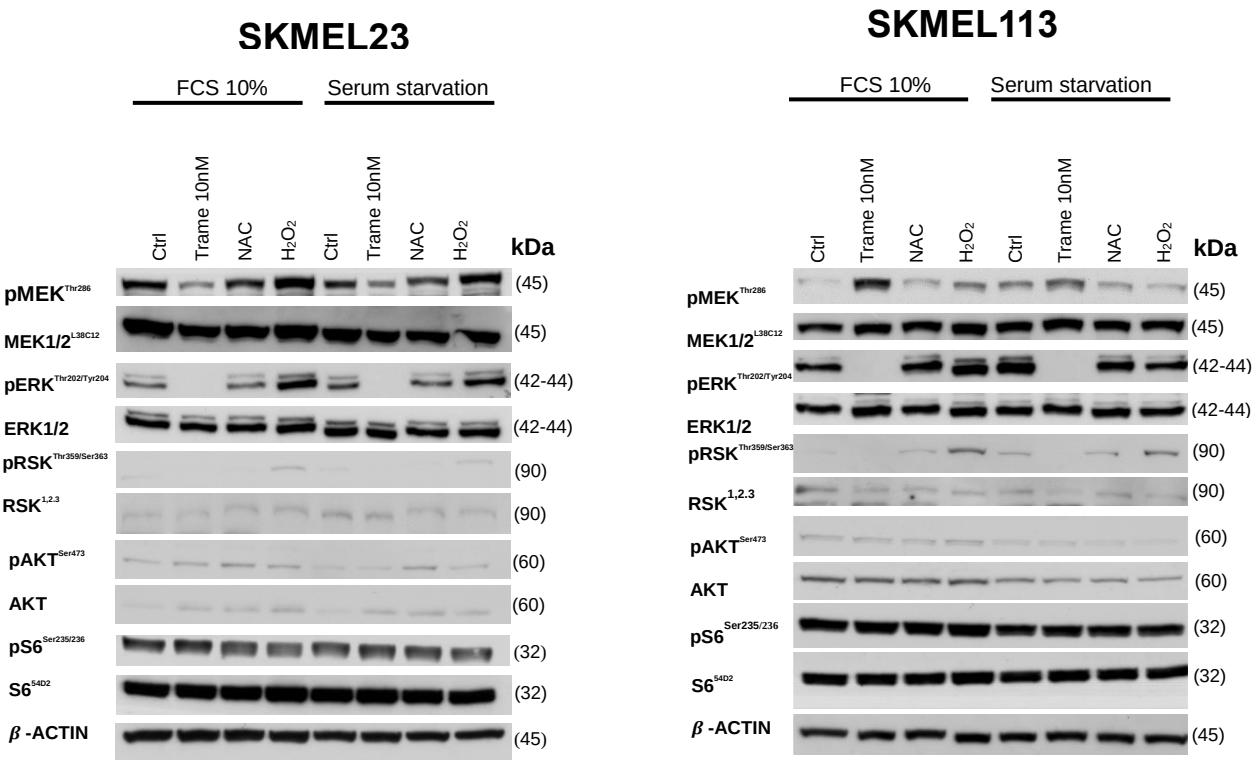

Figure 22: BRAF-WT melanoma cell lines showed reduced pERK and pRSK expression due to the MEK inhibitor trametinib treatment. The MAPK and the PI3K pathway were not modified by either NAC or H_2O_2 treatment. Western blot analysis for pMEK, MEK, pERK, ERK, pRSK, RSK, pAKT, AKT, pS6 and S6 of whole cell protein lysates of BRAF-WT melanoma cells (SKMEL23 and SKMEL113) after treatment with MEK inhibitor trametinib (10nM), NAC (1mM) and H_2O_2 (50µM) in 10% FCS medium or serum-starvations medium for 6 h. β-ACTIN was used as loading control.

By inhibiting MEK protein through trametinib it was estimated that proteins downstream of MEK in the MAPK pathway were inactive. Activation of each of the MAPK pathway proteins occurs by phosphorylation, so pERK and pRSK were compared to the total amount of ERK and RSK. As a result, it was totally clear that the phosphorylation status of the MAPK pathway downstream was finally dependent on the presence of the MEK inhibitor trametinib, while total MEK, ERK and RSK persisted stable. We also observed that both ROS inhibition via NAC and H_2O_2 mediated oxidative stress do not influence the activation or inhibition of the MAPK pathway.

Since PI3K is indirectly interconnected with the MAPK activity, it was expected that inhibition of ERK phosphorylation could increase AKT and P6 phosphorylation as an intracellular escape mechanism for protection and assimilation to ensure cellular survival.

However, when observing pAKT and pS6 levels in SKMEL23 and SKMEL113, no increase in PI3K pathway activity was observed after 6 h of treatment with the MAPK inhibitor trametinib. It should not be overlooked that MEK phosphorylation was increased in SKMEL113, at this time point, which was distinct from SKMEL23. Therefore, this increase in pMEK activity in SKMEL113 at 6 h of treatment could be associated with an immediate feedback response of the MAPK pathway to its inhibition by trametinib. However, this observed hyperactivity of pMEK did not affect downstream the inhibition of ERK phosphorylation in SKMEL113. These results suggest that the regulation of the MAPK pathways differs in each of the different BRAF-WT melanoma cells. NAC or H_2O_2 did not change the activity of the PI3K or MAPK pathway proteins. Due to the aim that the S6 protein is regulated by the AKT/PI3K pathway and indirectly thought the MAPK pathways, a fact of attention was to explore the modifications in phosphorylation of the S6 protein under the MEK inhibitor therapy. In brief, the S6 phosphorylation status gives the impression that was not dependent in all of the MEK inhibitor effect at time point of 6 h after treatment in BRAF-WT melanoma cell lines. Also, any impact of the NAC either H_2O_2 were observed on S6 activity and on PI3K activation as well in both of the BRAF-WT melanoma cell lines. Finally, in neither of the both melanoma cell lines were there any effect on ACTIN levels associated with the treatments, which expresses to a favorable control of the protein level between samples in this experiment.

5.2 The cytotoxic effect of trametinib is improved by the addition of CuET in BRAF-WT melanoma cells

To investigate the efficacy of trametinib in combination with bis-diethyldithiocarbamate (ET), which is the main active metabolite of disulfiram (DSF), cell viability assays (MUH assays) were performed. For this, the MEK inhibitor trametinib was mixed with the complex CuET (trametinib/CuET), and the antitumor activity as well as the monotherapies were analyzed after three days of treatment, as is illustrated in Figure 23. As previously observed trametinib at nanomolar concentrations exhibited about 50-60% inhibition of viability in BRAF-WT melanoma cells. However, when trametinib was combined with CuET this inhibitory effect was significantly increased. From this analysis, it was observed that the minimum effective dose to achieve complete inhibition of cell growth and a total reduction of the viability in BRAF-WT melanoma cells was 10nM of trametinib combined with 125nM of CuET.

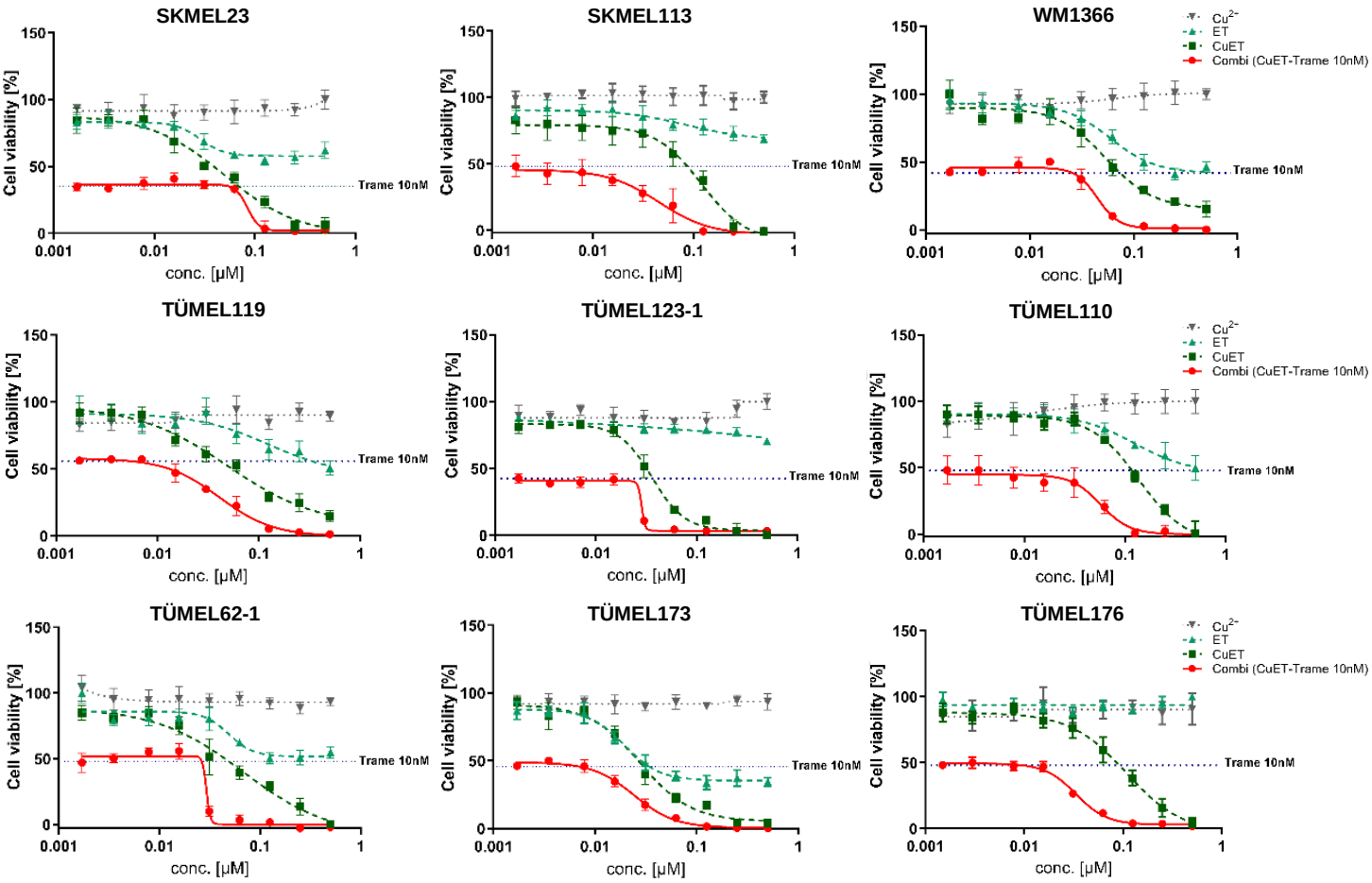

Figure 23: The cytotoxic effect of trametinib in BRAF-WT melanoma cells is improved by the addition of CuET under two-dimensional growth conditions *in vitro*. Cell viability assay (MUH assay) of BRAF-WT melanoma cell lines (SKMEL23, SKMEL113, WM1366, TÜMEL119, TÜMEL123-1, TÜMEL110, TÜMEL62-1, TÜMEL173 and TÜMEL176) after treatment with the MEK inhibitor trametinib (10nM), increasing doses of Cu^{2+} (up 500nM), ET (up 500nM), CUET (up 500nM), and trametinib (10nM) in combination with increasing doses of CuET (up 500nM) for 72 h. Values are means ± SEM of three replicates (n = 3; mean ± SD). Viability was normalized to untreated control cells.

Initially, all BRAF-WT melanoma cells tested showed a growth inhibition of about 50-60% when treated with the MEK inhibitor trametinib in the nanomolar range (10nM). Contrary, ET as monotherapy has a discrete anti-cancer effect, where the maximum inhibitory effect on cell growth exhibited was only about 40% in all BRAF-WT melanoma cells. It has been shown that ET, due its thiol bridges, chelates bivalent metal ions such as copper (Cu^{2+}), forming the ET-Cu^{2+} complex (CuET), which improves the antitumor activity of ET [101, 119]. As a result, the inhibitory effect of ET as monotherapy on BRAF-WT melanoma cells was further enhanced by the addition of Cu^{2+}. The inhibitory effect of CuET on BRAF-WT melanoma cell viability was dose-dependent as is illustrated in the Figure 23. In all melanoma cell lines tested, CuET as a monotherapy showed a dose-dependent relation between concentration and cell growth inhibition, which at the highest concentration (500nM) reached total inhibition. Contrary to the

anti-growth effect mediated by CuET as a monotherapy, its combination with 10nM of trametinib exhibited a complete inhibitory effect on cell growth in all BRAF-WT melanoma cell lines already at 125nM of CuET, as is illustrated in Figure 24. The minimum effective dose of the combination therapy with a complete reduction in viability was 10nM of trametinib mixed with 125nM CuET.

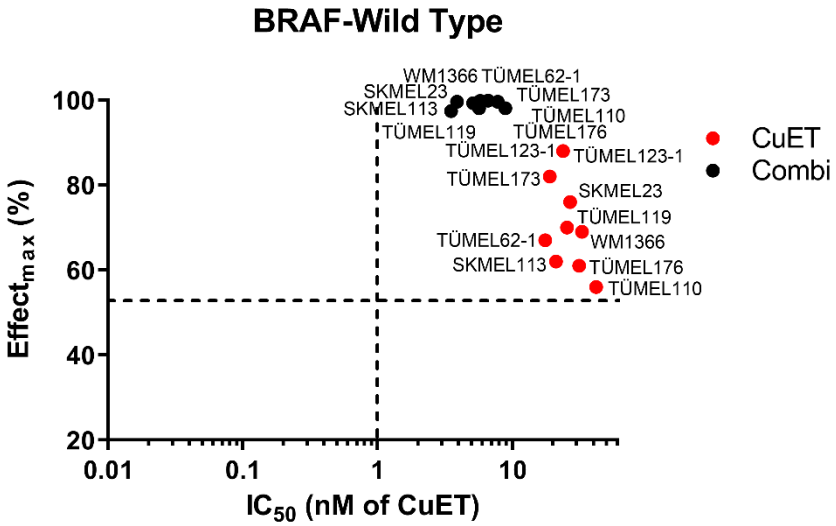

Figure 24: The cytotoxic effect of trametinib in BRAF-WT melanoma cells is improved by the addition of CuET under two-dimensional growth conditions in vitro. Schematic representation of the maximum therapeutic effect *(in vitro)* mediated by IC50 of CuET and combination of CuET with trametinib (10nM). Cell viability (MUH assay) of BRAF-WT melanoma cell lines (SKMEL23, SKMEL113, WM1366, TÜMEL119, TÜMEL123-1, TÜMEL110, TÜMEL62-1, TÜMEL173 and TÜMEL176) after treatment with CuET and the combination of MEK inhibitor trametinib (10nM) with CuET (up500nM) for 72 h. Values are means ± SEM of three replicates (n = 3; mean ± SD). Viability was normalized to untreated control cells.

Interestingly, treatment with the MEK inhibitor trametinib exhibited in all the BRAF-WT melanoma cells a distinct inhibition of cell growth, with TÜMEL123-1 and TÜMEL173 being the most sensitive melanoma cell lines to the MEK inhibitor therapy (60% cell growth inhibition). Due to the reason that in the NF1-*LoF*, NRAS^{mut} and Triple-WT melanoma cell lines, the cell types responded different to MEK inhibitor, as is illustrated in Figure 19 and Figure 20. However, the maximal cell growth inhibition due to the MEK inhibitor trametinib on the entire BRAF-WT melanoma cell lines were in the range around maximal 60% and additionally all of them exhibited a further significant enhances on the cell growth inhibition due to the addition of CuET, where they showed a complete inhibition of cell growth, as is illustrated in Figures 23 and 24.

The combination of the MEK inhibitor trametinib with CuET exhibited a substantial anti-cancer effect in all BRAF-WT melanoma cells. The inhibitory effect of by 125nM of CuET in combination of 10nM of trametinib was greater than that predicted by their individual effects. To sum up, the inhibitory effect of the combination therapy was significantly greater than the inhibitory effects of by each of the treatments as monotherapy in BRAF-WT melanoma cells. The cell viability experiments were conducted for a period of 72 h, which is considered as a short exposure time. Therefore, it was decided to explore the effects of the combination therapy over a longer period of time. For this, a clonogenic growth assay was conducted in four different BRAF-WT melanoma cells. This showed whether the combination therapy persistently inhibited the formation of colonies for a long period of time, as is illustrated in Figure 25.

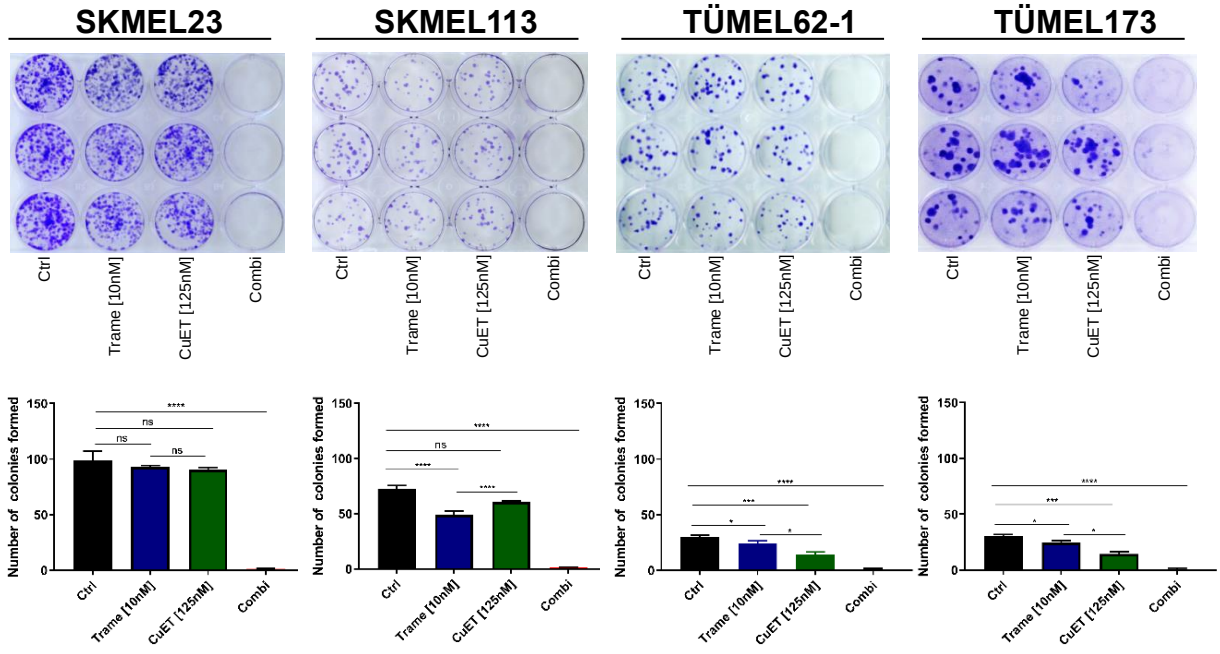

Figure 25: Trametinib in combination with CuET at nanomolar range persistently inhibited the cell growth in BRAF-WT melanoma cells, under two-dimensional growth conditions *in vitro*. Clonogenic growth assay of BRAF-WT melanoma cell lines (SKMEL23, SKMEL113, TÜMEL62-1 and TÜMEL173) after 14 d-treatment with MEK inhibitor trametinib (10nM), CuET (125nM) and combination. Cultures were stained with Coomassie Brilliant Blue. Representative images are shown (n = 3; mean ± SD). One-way ANOVA was used to identify the statistical significance associated to untreated (control) and it was followed by Tukey's multiple comparisons test. * $p < 0.05$; ** $p < 0.01$; *** $p < 0.001$; and **** $p < 0.0001$, ns (not significant).

In all four BRAF-WT melanoma cell lines, the inhibitory effect on colony formation due to individual therapy with trametinib as a monotherapy was marginal. Similarly, there was no general significant decrease in colony number after treatment with 125nM of CuET. To sum up, the antitumor effects of trametinib or CuET were small. However, there was a strong and significant reduction in the colony numbers with the combination of both. The inhibition of the

colony formation mediated by the combination therapy after the 14 d of therapy was greater than the sum of the individual therapy effects and can be considered synergistic. Specifically, the combination of 10nM of trametinib with 125nM of CuET was able to completely inhibit the formations of colonies on all BRAF-WT melanoma cells tested.

To test the treatment in a three-dimensional model a 3D spheroid model of BRAF-WT melanoma cells were generated and treated with the therapies of interest. To this purpose, spheroids from SKMEL23, SKMEL113, TÜMEL62-1 and TÜMEL173 melanoma cells were grown by the hanging drop method. Once the spheroids were formed, they were collected and embedded in a 96 well filter plate (0.5µm PVDF filter membrane) containing culture medium, with 2 spheroids in every. The spheroids were treated with the concentrations up to 500nM of Cu^{2+}, ET up to 500nM, CuET up to 500nM, 10nM of trametinib, and the combinations of 10nM of trametinib with CuET up to 500nM for 72 h. After the treatment for 72 h, the spheroids were washed twice with PBS and lastly, the cell viability was measured (MUH assay). This experiment confirmed, similar to the two previous 2D monolayer melanoma model, that the combination of trametinib with CuET induced a significantly greater anti-cancer effect than the one observed with the individual therapies, as is illustrated in the Figure 26.

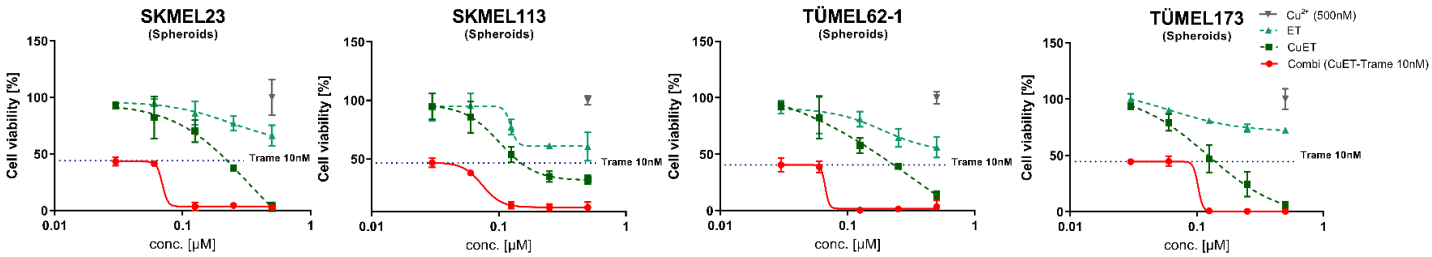

Figure 26: The cytotoxic effect of trametinib in BRAF-WT melanoma spheroids is enhanced by the addition of CuET, under three-dimensional (3D) growth conditions *in vitro*. Cell viability assay (MUH assay) of BRAF-WT melanoma spheroid models (SKMEL23, SKMEL113, TÜMEL62-1 and TÜMEL173) after treatment with MEK inhibitor trametinib (10nM), increasing doses of Cu^{2+} (500nM), ET (up to 500nM) and CuET (up to 500nM) and combination of trametinib (10nM) with CuET (up to 500nM) after 72 h. Spheroids were embedded in 10% FCS medium before treatment start. Values are means ± SEM of three replicates (n = 3; mean ± SD). Viability was normalized to untreated control cells.

The results of the 3D spheroid viability assay with the BRAF-WT melanoma cells confirmed that the combination therapy of MEK inhibitor trametinib with CuET further increased the anti-tumor effect mediated by trametinib in all the BRAF-WT melanoma models as a significant manner.

In addition, the 3D spheroid model of the BRAF-WT melanoma cells was carried out to explore the cell growth inhibition effect mediated by the MEK inhibitor trametinib as monotherapy or in combination with CuET in a collagen matrix. The viability of tumors cells in the spheroids after treatments was determined thought calcein-AM and propidium iodide. To perform this 3D spheroid models using the BRAF-WT melanoma cell lines SKMEL23, SKMEL113, TÜMEL62-1 and TÜMEL173 were formed. Again, spheroids were generated by the hanging drop method, collected and then embedded in culture medium containing 1.2mg/mL collagen I. Embedded spheroids were treated with 10nM of trametinib, 125nM of CuET, or a combination and thereof growth was observed microscopically over 6 days. Microphotographs of the spheroids were taken during the course of treatment and spheroid sizes were quantified and normalized to the initial spheroid size at baseline. On day 6, the spheroids were stained with calcein-AM and propidium iodide to accurately measure the viability of tumor cells in the spheroids (red = dead tumor cells, green = vital tumor cells). The results confirmed that the postulated effect of the combination of trametinib with CuET on BRAF-WT melanoma model was superior than the summation of the individual inhibitory effect in all four models. One of the most significant points that were confirmed through this model was that the inhibitory effect observed by the combination of trametinib with CuET could be archived in the nanomolar range also in the 3D models, although embedded in an appropriate matrix.

Highly significant data were obtained through the 3D model when doing morpho-metric analysis. It was observed that the spheroids treated with the combination of 10nM of trametinib with 125nM of CuET did not increase in diameter in all the BRAF-WT melanoma model tested. Spheroids treated with 10nM of trametinib exhibited a growth inhibition of 40-50% when compared to the control, confirming similar inhibitory effects as in the 2D models. This effect was further enhanced due to the addition of 125nM of CuET, confirming that the combination of trametinib with CuET at nanomolar range offered a significant higher inhibitory effect than the monotherapies, as show in Figure 27.

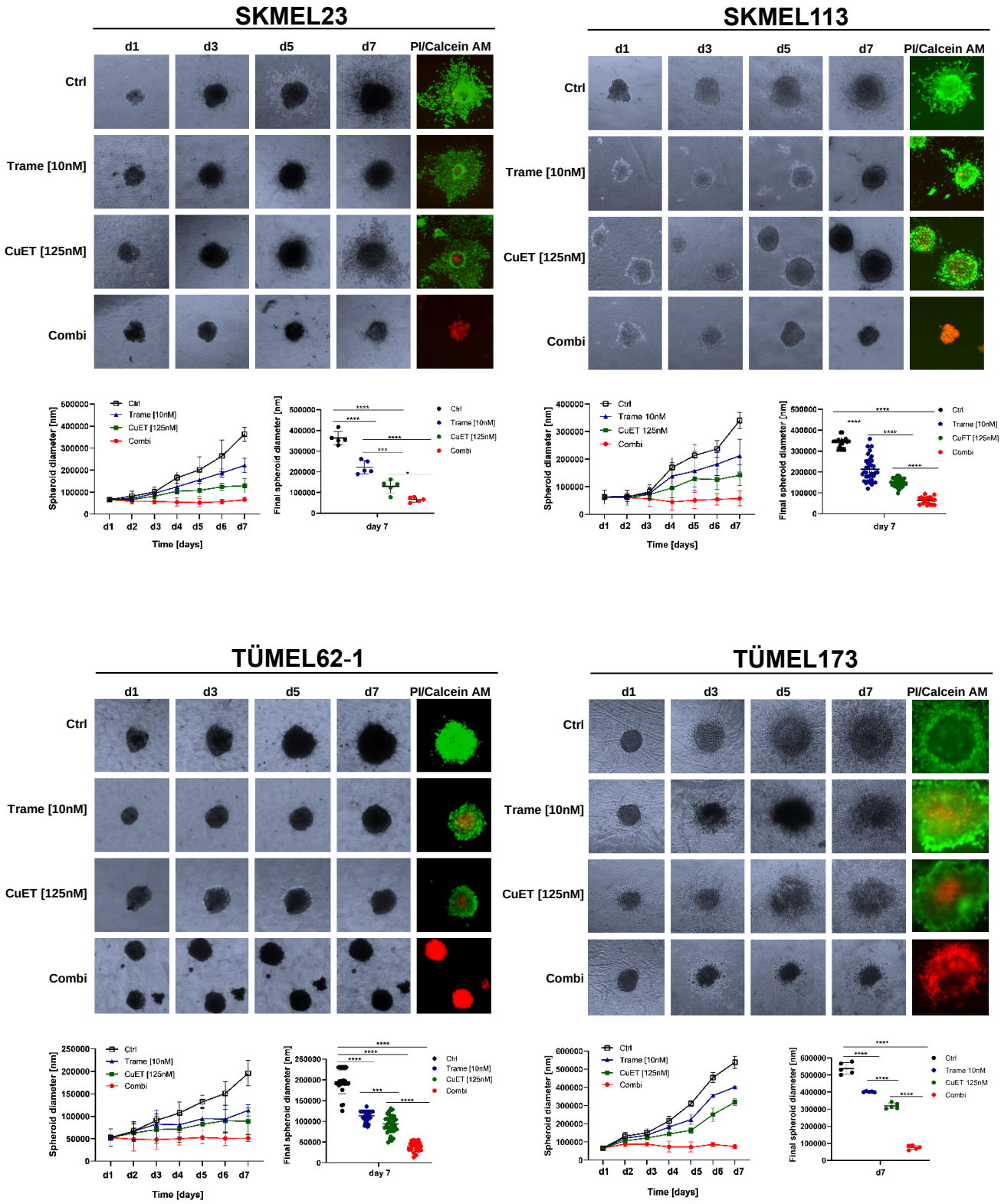

Figure 27: Effects of trametinib, CuET and combination therapy in BRAF-WT 3D tumor spheroid melanoma model. Growth of BRAF-WT melanoma spheroids (SKMEL23, SKMEL113, TÜMEL62-1 and TÜMEL173) embedded in soft collagen I under treatment with MEK inhibitor trametinib (10nM), CuET (125nM) and combination for 7 d. Microphotographs of the spheroids were taken over the course of treatment. Spheroid sizes quantified with ImageJ and normalized to the initial spheroid size at treatment start. At least three independent experiments with $n \geq 8$ were performed and representative data shown. On day seven, live-dead staining was done with calcein-AM and propidium iodide (upper graph, live (green) / dead (red) staining). The total end sizes of 5–10 spheroids per treatment group were quantified (lower graph, $n = 3$, mean ± SEM, Multiple t-test according to Holm Sidak method). * $p < 0.05$; ** $p < 0.01$; *** $p < 0.001$; and **** $p < 0.0001$, ns (not significant).

5.3 Induction of apoptosis through the combination of trametinib with CuET

5.3.1 Detection of apoptosis via cell-cycle analysis

To gain insight into the changes that occurs in BRAF-WT melanoma cells under combination therapy of the MEK inhibitor trametinib with CuET, cell-cycle analysis via flow cytometry was performed. The cell-cycle is divided into four interfaces, including G1 phase, S phase, G2 phase and lastly mitosis (M phase). The G1 phase lasts about 12 h and is the longest phase of proliferating human cells in an ordinary cell-cycle period of 24 h, followed by the S phase with 8 h, the G2 phase which lasts 3 h and finally the M phase, which is the shortest phase in a cell-cycle, with a duration of 1 h. Hence, under normal conditions, the following percentages of a cell population in each of the different phases result: 50 % G1-phase, 30 % S-phase, 15 % G2-phase and 5 % M-phase. These values may differ due to cell type [129]. Propidium iodide-based flow cytometric cell-cycle can be used to determine the amount of DNA and thus the relative number of cells in one of the phases. Cells undergoing apoptosis have lower amounts of DNA than living cells due to apoptotic DNA fragmentation; therefore, these cells are classified in the sub-G1 phase [130]. In healthy cells, less than 5% of cell populations are in the sub-G1 phase. However, melanoma-target therapy can to trigger apoptosis in tumor cells, so cell-cycle analysis was applied to identify the percentage of BRAF-WT melanoma cells in sub-G1 phase through combination therapy of the MEK inhibitor trametinib with CuET.

In all BRAF-WT melanoma cells tested a minor percentage of the control cells were detected in the sub-G1 phase, while the largest population of the untreated melanoma cells were detected in the G1 phase. This trend was exhibited by all BRAF-WT melanoma cells (SKMEL23 and SKMEL113), which was also seen over time (24 h, 48 h or 76 h). However, the BRAF-WT melanoma cells that were treated with 10nM of trametinib exhibited a strong G1 phase arrest, which appeared after 24 h of treatment and persisted until the last time point (72 h). The same trend was observed in both of the BRAF-WT melanoma cell lines analyzed (SKMEL23 and SKMEL113). Although trametinib at nanomolar concentrations (10nM) was capable to induce strong G1 arrest in all BRAF-WT melanoma cells, no induction of apoptosis was observed. This absence of sub-G1 fractions induction was observed at 24, 48 and 72 h in SKMEL23 and SKMEL113. Contrary to trametinib, 125nM of CuET induced a discrete accumulation of cells in sub-G1 (6-7%) at 72 h in both cell lines; however, it was not sufficient to induce vast apoptosis. In contrast to the monotherapies, 10nM of trametinib in combination

with 125nM of CuET strongly induced sub-G1 fractions, as an indicator for apoptosis, in both BRAF-WT melanoma cells. Induction of apoptosis due to combination therapy enhanced from 24 to 72 h in both BRAF-WT melanoma cell lines (40-50 % of sub-G1), as is illustrated in Figure 28.

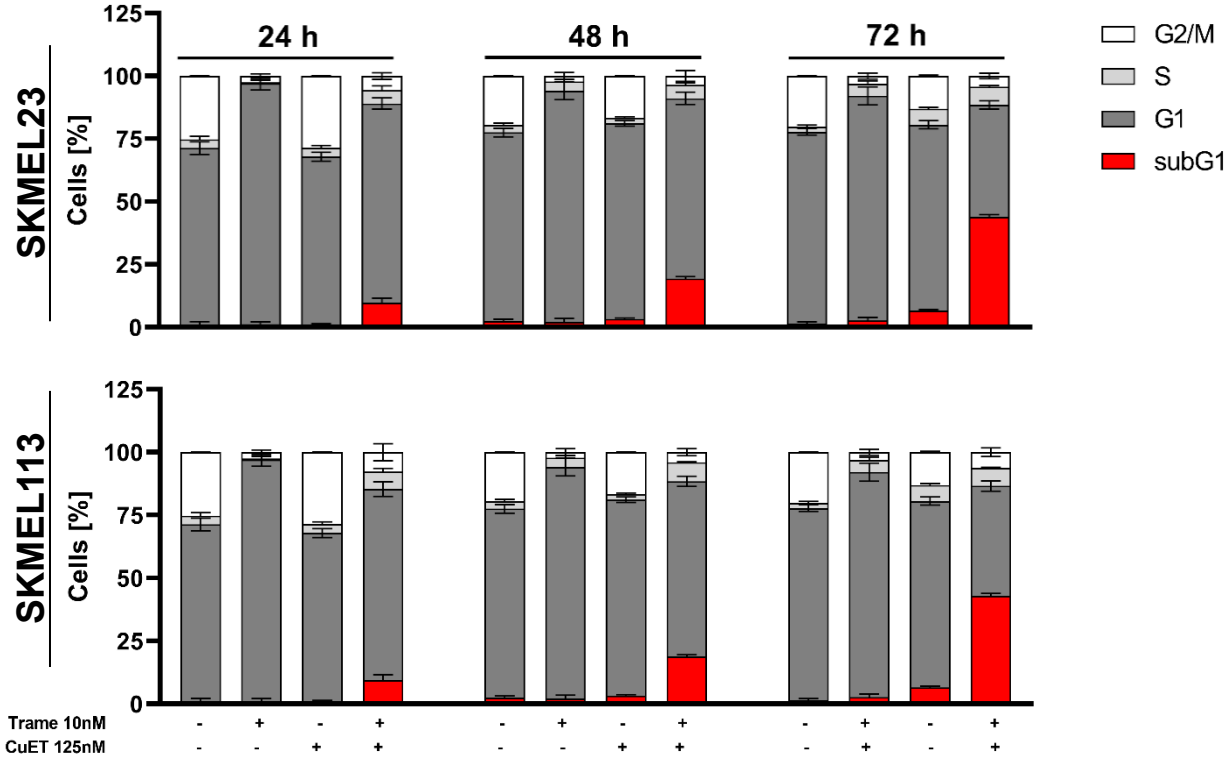

Figure 28: BRAF-WT melanoma cell lines showed a significant apoptosis induction through the combination of MEK inhibitor trametinib with CuET. Flow cytometric cell-cycle analyses of BRAF-WT melanoma cell lines (SKMEL23 and SKMEL113) after treatment with MEK inhibitor trametinib (10nM), CuET (125nM) and combination for 24, 48 and 72 h. Untreated melanoma cells were used as a control .The relative distribution in the different phases of the cell-cycle was quantified (n = 3, mean ± SD).

To sum up, the MEK inhibitor trametinib as monotherapy was not able to induce apoptosis in BRAF-WT melanoma cells, even after 72 h of exposure. Similarly, CuET at nanomolar concentrations (125nM) did not induce apoptosis in both melanoma cell lines. However, the combination of 10nM trametinib with 125nM CuET was able to strongly induce apoptosis in both BRAF-WT melanoma cell lines especially after 48 and 72h. The response rates and kinetics were completely similar in both BRAF-WT melanoma cell lines (SKMEL23 and SKMEL113). In summary the combination therapy resulted in a significant higher and synergistic apoptosis induction than the sum of the effects observed in the monotherapies. The results measured in the PI-based cell-cycle appeared to be similar to those observed in the 2D and 3D viability assays.

5.3.2 Detection of apoptosis via analysis of cleaved CASPASE-3 and PARP

Cysteine-dependent aspartate-specific proteases (CASPASES) are a large family pool of enzymes critical for starting and executing apoptosis. Several cellular factors trigger the beginning of the programmed cell death cascade mostly via proteolytic activation of CASPASES. One accurate effector is CASPASE-3, which is a protein that is cleaved and therefore activated during apoptosis. Cleaved CASPASES disseminate a strong apoptotic signal at specific downstream targets, comprising poly (ADP-ribose) polymerase (PARP). Thus, CASPASE-3 protein can be detected as activated or inactivated, where the cleaved CASPASE-3 is a sturdy indicator of apoptosis and cell death induction. As a result, a drastic decrease in inactive CASPASE-3 while activated CASPASE-3 shows a parallel increase is a significant indicator of apoptosis [131, 132].

In addition, PARP is a nuclear protein that is actively participates in diverse biological process particularly DNA repair and apoptosis. The cleavage of PARP by CASPASE-3 is one of the initial events in apoptosis. Once PARP is cleaved, fatal pathways are activated to induce programmed cell death. Similar to cleaved CASPASE-3, cleaved PARP is a specific marker of apoptosis induction, and both are commonly used to detect this cell death pathway [133, 134]. In order to confirm the apoptosis induction mediated by the combination of trametinib with CuET, the expression of cleaved CASPASE-3 and cleaved PARP proteins were analyzed. Combination therapy induced the cleaved of CASPASE-3 and PARP after 12 h of treatment in BRAF-WT, as is illustrated in Figure 29.

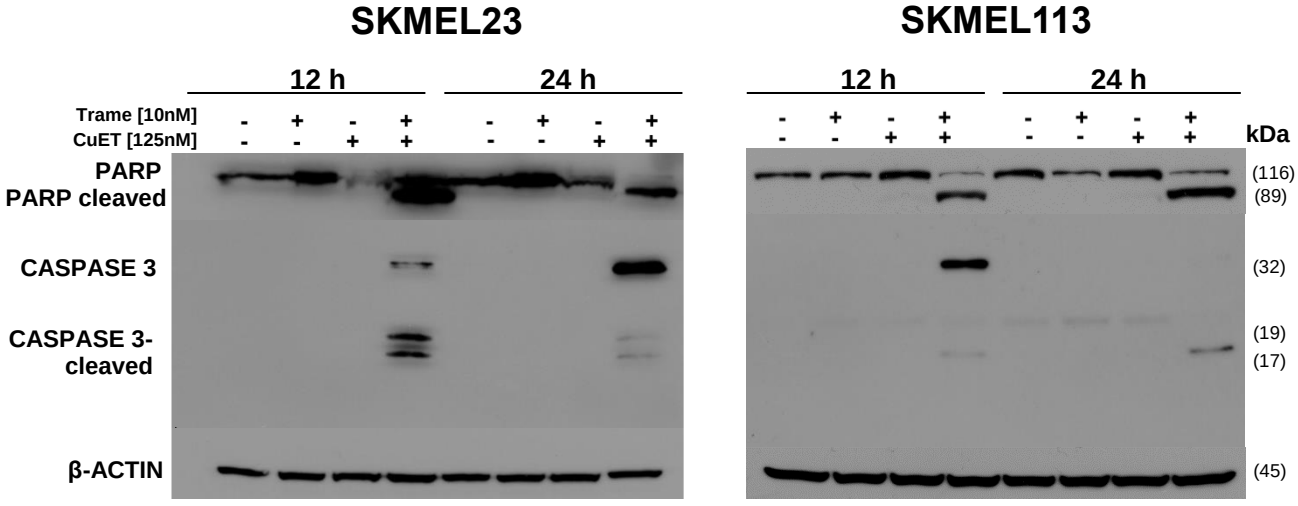

Figure 29: BRAF-WT melanoma cell lines SKMEL23 and SKMEL113 showed cleavage of the CASPASE-3 and PARP after treatment with combination of MEK inhibitors trametinib with CuET. Western blot analysis for PARP,PARP cleaved, CASPASE 3 and CASPASE 3-cleaved of whole cell protein lysates of BRAF-WT melanoma cells (SKMEL23 and SKMEL113) after treatment with MEK inhibitor trametinib (10nM), CuET (125nM) or combination for 12 and 24 h. β-ACTIN was used as loading control.

In both BRAF-WT melanoma cell lines (SKMEL23 and SKMEL113) the detection of cleaved PARP after treatment with the combination of 10nM of trametinib with 125nM of CuET for 12 h and 24 h was possible. PARP cleavage was observed after 12 h of treatment with the combination therapy only in both cell lines. PARP cleaved signal was drastically higher after 12h of treatment compared to 24 h in both cell lines but especially in SKMEL23. In contrast, untreated BRAF-WT melanoma cells did not express cleaved PARP. Monotherapy treatments, either 10nM of trametinib or 125nM of CuET, were not able to induce PARP cleavage in both BRAF-WT melanoma cell lines at 12 or 24 h. This trend follows the same pattern as the results observed in the PI-based cell-cycle, where the induction of apoptosis mediated by the combination therapy was greater than the sum of the apoptosis induction mediated by trametinib and CuET as monotherapy.

In addition, in both BRAF-WT melanoma cells explored, combination therapy of MEK inhibitor trametinib with CuET intensely induced cleaved CASPASE-3 (17,19 kDa). In contrast, monotherapies with trametinib or CuET were not able to induce CASPASE-3 cleavage after 12 and 24 h of treatment in both BRAF-WT melanoma cell lines. On the one hand, SKMEL23 melanoma cells showed a higher expression of cleaved CASPASE-3 due to the combination treatment at 12 h, which discretely decreased at 24 h. On the other hand, SKMEL113 cells showed greater expression of cleaved CASPASE-3 due to the combined therapy at 24 h compared to 12h. In both cell lines the expression levels of total CASPASE-3 decreased in parallel to the increase of the expression of the corresponding cleaved CASPASE-3. These results are closely related to the response of the cells to the combination therapy in the cell viability assays, where SKMEL113 melanoma cells have shown slightly higher resistance and late response to the combination of trametinib with CuET, in comparation with SKMEL23.

As a summary, the activity of the MEK inhibitor trametinib was again significantly enhanced by the addition of CuET. Furthermore, the combination therapy of trametinib and CuET appeared synergistic and more potent than the monotherapy with either trametinib or CuET. The Western blot analysis therefore confirmed the results of the PI- based cell-cycle analysis.

5.3.3 Detection of apoptosis induction by analysis of pro-apoptotic and anti-apoptotic proteins

In order to confirm the apoptosis induction mediated by combination therapy of trametinib with CuET in BRAF-WT melanoma cells, the exploration of the expression of B-cell lymphoma-2 (BCL-2) family of proteins was performed. The BCL-2 family is composed of several pro-apoptotic members as well as several anti-apoptotic proteins. Among the proteins which play a very relevant role as pro-apoptotic and regulate the programmed melanoma cell death are BIM, BID, BAX, BAK and Puma. On the contrary, the proteins that have relevant anti-apoptotic activity of the BCL-2 family are BCL-XL, BCL-2 and MCL-1. BCL-2 family members constantly interact with the BH3-only proteins, which act as a death sentinels and conduct the principal signal to persuade apoptosis directly to the core of the BCL-2 family proteins. To be specific, once the process of apoptosis has been initiated, the pro-apoptotic proteins BAX and BAK undergo severe conformational changes, which culminate in permeabilization of the mitochondrial outer membrane, giving access to multiple proteins. This process concludes in mitochondrial fractionation with release of cytochrome C, finally activating CASPASE proteases. This last step culminates in the effective dismantling of the dying cells. As a result, once the apoptosis pathway is onset, several apoptosis-driving steps are mediated by the activation of BCL-2 family proteins.

To investigate whether combination therapy of 10nM of trametinib with 125nM of CuET induced a modification in the expression levels of the BCL-2 family members, the expression of multiple players of this family were measured. The results exhibited that the combination therapy significantly enhanced the protein level of BAX (19 kDa) and the three corresponding BIM isoforms (BIM^{EL}, BIM^{L} and BIM^{S}; 22 kDa, 17 kDa and 14 kDa) after 12 h of treatment on SKMEL23 and SKMEL113. This relevant induction of all BIM isoforms probably contributed to apoptosis. Taken together, the combination therapy at nanomolar range significantly increased the expression of the pre-apoptotic proteins BIM and BAX in both cell lines with 12 h, as illustrated in the Figure 30.

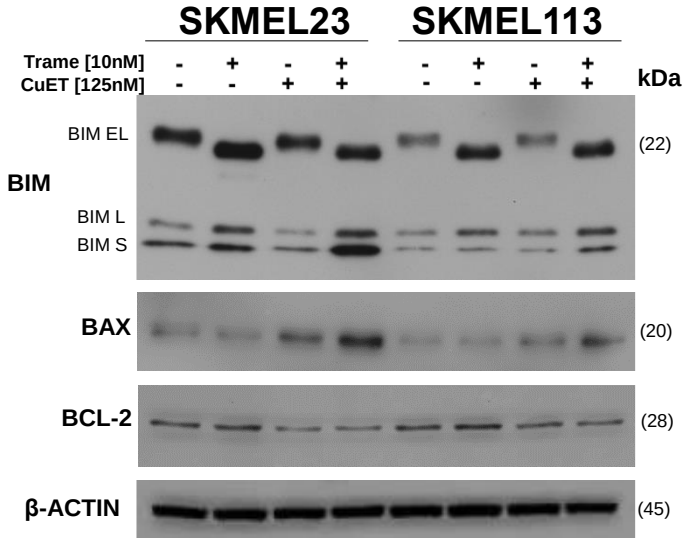

Figure 30: MEK inhibitor trametinib in combination with CuET induced high expression of pre-apoptotic proteins from the BCL-2 family on BRAF-WT melanoma cells. Western blot analysis for $BIM^{EL,L \text{ and } S}$, BAX and BCL-2 of whole cell protein lysates of BRAF-WT melanoma cells (SKMEL23 and SKMEL113) after treatment with MEK inhibitor trametinib (10nM), CuET (125nM) or combination for 12 h. β-ACTIN was used as loading control.

Additionally, other BCL-2 family members were analyzed. BCL-2 (27 kDa) is a protein that has a specific activity in the apoptosis cascade where it acts strongly as an anti-apoptotic protein. As a result, reduced BCL-2 expression is indicative of facilitated apoptosis induction. The combination therapy of 10nM of trametinib and 125nM of CuET induced a significant decrease in BCL-2 expression at 12 h in SKMEL23 and SKMEL113. Interestingly, MEK inhibitor trametinib did not induce a reduction in the BCL-2 expression after 12h of treatment in both of the explored melanoma cell lines. BCL-2 protein was discretely decreased after monotherapy treatment with 125nM of CuET at 12 h in both melanoma cell lines, compared with the control. Taken together, these results exhibited that the combination therapy at nanomolar range significantly decreased the anti-apoptotic protein BCL-2 expression in both BRAF-WT melanoma cell lines, as illustrated in Figure 30. To sum up, these data, in addition to the previous results, showing that in BRAF-WT melanoma cells the combination of MEK inhibitor trametinib with CuET mediated the induction of apoptosis, as well as a strong anti-tumor effect in 2D and 3D models.

5.3.4 CASPASE inhibition during combination therapy reduces cytotoxicity corroborating apoptosis induction

Apoptosis is an extremely advanced process in which several CASPASES, such as the effector CASPASE-3, play a relevant role. 14 CASPASES have been described, but from these only 8 members hat been implicated in the programmed cell death. The CASPASES associated with apoptosis are divided into two groups. The first group is the initiator CASPASES, which includes CASPASES-2, 8, 9 and 10. The second group is called effector CASPASES, which include CASPASES-3, 6 and 7. Several authors have described that the CASPASE-3 is the main effector apoptosis protease and its cleavage is the principal mechanism to activate apoptosis. However, other experiments with CASPASE-3 deletion propose that can be replaced by the effector CASPASE-7 [54]. Consequently, both effector CASPASES must be considered as the main effector for apoptosis.

Due to the critical role of CASPASES in the apoptosis induction, an experiment to test the role of activated CASPASES in the combination therapy was conducted. Therefore, the efficacy of the MEK inhibitor trametinib plus CuET was investigated in BRAF-WT melanoma cell lines when a pan-CASPASE inhibitor (Z-VAD-FMK) was added in parallel. Z-VAD-FMK is a well described pan-CASPASE inhibitor that does not influence the activity of the ubiquitin carboxy-terminal hydrolase L1, but inhibits the cleavage of CASPASE-3 and CASPASE-7 in order to suppress CASPASES activity. Viability assays (MUH assays) in the BRAF-WT melanoma cell lines were carried out in the presence of Z-VAD-FMK (10µM). In both cell lines, the addition of the pan-CASPASE inhibitor reduced the cytotoxic effect of the combination. This confirmed that the cell death mediated by the combination therapy was dependent on CASPASES activity and proved the induction of apoptosis by combined treatment with trametinib and CuET. The results of these co-treatments and its respective controls are illustrated in Figure 31.

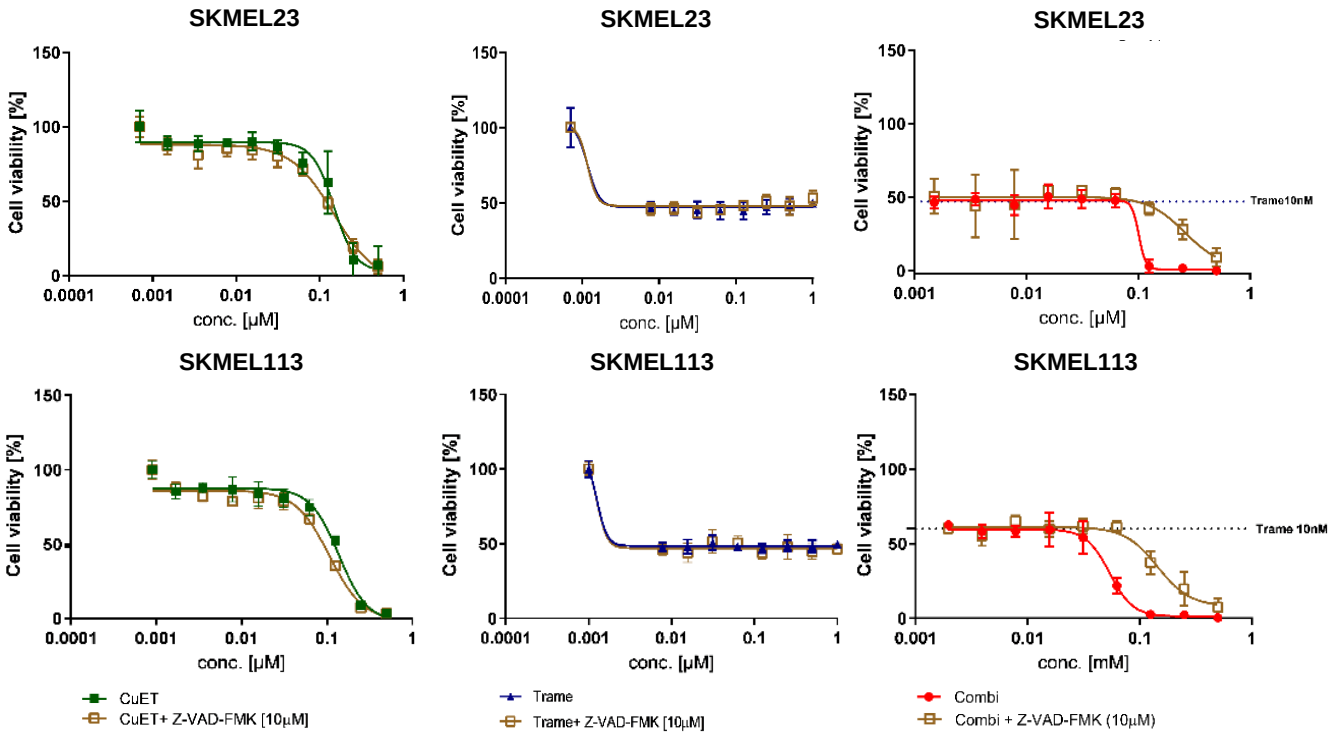

Figure 31: Pan-CASPASE inhibitor (Z-VAD-FMK) mitigates cytotoxic effects mediated by combination of trametinib with CuET in BRAF-WT melanoma cells under two-dimensional growth conditions *in vitro*. Cell viability assay (MUH assay) of BRAF-WT melanoma cell lines (SKMEL23 and SKMEL113) after treatment with the increasing dose of **(a)** CuET (up to 500nM), **(b)** trametinib (up 2µM) and **(c)** CuET (up 500nM) plus trametinib (10nM), or combination of treatments **(a-c)** with the pan-CASPASE inhibitor Z-VAD-FMK (10µM) for 72 h. Values are means ± SEM of three replicates (n = 3; mean ± SD). Viability was normalized to untreated control cells.

The results of the cell viability assays, it showed that inhibition of CASPASE activity reduced the cytotoxic effect of combination therapy of trametinib with CuET. It was further observed that the cytotoxic effect mediated by trametinib was not modified due to the addition of the CASPASE inhibitor. The resulting abolition of combination therapy-cell growth effect via CASPASE inhibitor was highly significant because the synergetic cytotoxic effect of both drugs was fully mitigated and only the pure effect of trametinib mediated growth inhibition remained. These results supported the postulated theory that the combination therapy-mediated cytotoxic effect on BRAF-WT melanoma cells was mediated by the induction of apoptosis.

Next the apoptosis induction mediated by combination therapy in addition to the CASPASE inhibitor Z-VAD-FMK was analyzed by cell-cycle analysis using flow cytometry, as illustrated in Figure 32. Combination therapy with 10nM of trametinib with 125nM CuET

induced apoptosis in BRAF-WT melanoma cells at 48 h and at higher level at 72 h of treatment. This postulated effect was mitigated by the CASPASE inhibitor at 24, 48 and 72h in both cell lines (SKMEL23 and SKMEL113). Thus, the CASPASE inhibitor Z-VAD-FMK complete abolished the apoptosis induction mediated by combined therapy in BRAF-WT melanoma cells.

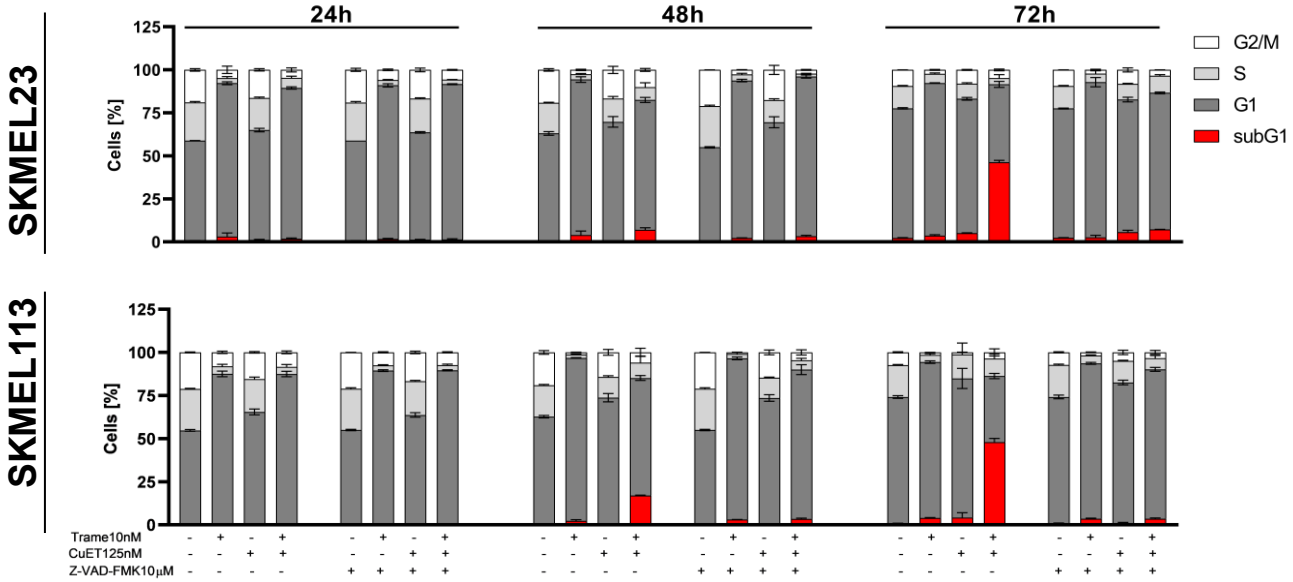

Figure 32: Pan-CASPASE inhibitor (Z-VAD-FMK) abolish the sub-G1 fraction accumulation (apoptosis induction) mediated by MEK inhibitor trametinib with CuET in BRAF-WT melanoma cells. Flow cytometric cell-cycle analyses on BRAF-WT melanoma cell lines (SKMEL23 and SKMEL113) after treatment with MEK inhibitor trametinib (10nM), CuET (125nM) and trametinib plus CuET, or combination of treatments with the pan-CASPASE inhibitor Z-VAD-FMK (10µM) for 24, 48 and 72 h. Untreated melanoma cells were used as a control. The relative distribution in the different phases of the cell-cycle was quantified (n = 3, mean ± SD).

The results of the cell-cycle analysis in both BRAF-WT melanoma cell lines confirmed the previous observation of the viability assays in the two BRAF-WT melanoma cell lines. The CASPASE inhibitor Z-VAD-FMK abolished the apoptosis induction (sub-G1 fraction accumulation) mediated by MEK inhibitor trametinib (10nM) in combination with 125nM CuET at 48 and 72h in BRAF-WT melanoma cells. Overall, the combined therapy induced a significant accumulation of sub-G1 phase after 48 and 72 h in both BRAF-WT melanoma cell lines, which is a specific marker of apoptosis. This significant induction of apoptosis mediated by combination therapy was abolished by the addition of a pan-CASPASE inhibitor. In contrast, monotherapy treatments (either MEK inhibitor trametinib 10nM or CuET 125nM), were nor modified by Z-VAD-FMK. Furthermore, it was observed that CuET as monotherapy did not induce G1 arrest in both BRAF-WT melanoma cell lines, however it induced some changes in the cell-cycle when compared to the control, characterized by a discrete increase in G1 phase combined with a decrease in S and G2/M phases. Taken together, inhibition of CASPASE activity reduces only the cytotoxic effect mediated by the combination of trametinib with CuET.

5.4 Induction of DNA damage through the combination of trametinib with CuET

5.4.1 Trametinib in combination with CuET induces high phospho-γH2AX expression on BRAF WT-melanoma cells

Due to the strong induction of apoptosis elicited by the combination of trametinib with CuET in BRAF-WT melanoma cells, analysis of putative DNA damage was analyzed. Since it has already been published that CuET mediates cell cytotoxicity by targeting NPL4 that concludes in DNA-damage, it was especially interesting to observe whether the MEK inhibitor trametinib enhanced the DNA-damage mediated by CuET [100, 135]. In addition, previous results exhibited that MEK inhibitors in combination with CuET displayed a strong antitumor effect in both 2D and 3D BRAF-WT melanoma models. It was interesting to identify whether the combination of the two drugs potentiated DNA damage. Accordingly, the next step was to investigate whether both BRAF-WT melanoma cells respond with trametinib, CuET or combination therapy to induction of phosphorylates form of the histone H2A family member (γH2AX), which is a specific marker of DNA double-strand breaks (DSBs). This phosphorylated protein, gamma-H2AX (P-γH2AX), is a representative of the initial phase in recruiting and containing DNA repair proteins. Exploration of the induction of phosphorylation of γ-H2AX (P-γH2AX) through monotherapy with 10nM of trametinib, 125nM and 250nM of CuET and combination therapy was carried out.

First, the induction of P-γH2AX by CuET (250nM) at 6, 24 and 48h in was explored in BRAF-WT melanoma cells. Additionally, 100µM H_2O_2 as a reactive oxygen species (ROS) positive control were added. Cisplatin (5µM) during 48 h was added as a positive control. Immunoblot detection with treated samples of SKMEL23 melanoma cells was carried out for 6, 24 and 48h, as illustrated in Figure 33. CuET at concentration of (250nM) induced high levels of P-γH2AX in a time-dependent manner in SKMEL23. This was particularly visible at 48 h, where P-γH2AX levels due to 250nM of CuET treatment was slightly higher than the positive control. In contrast, 100µM H_2O_2 was not able to induce P-γH2AX expression at the protein level at 6, 24 and 48 h in SKMEL23 melanoma cells. Since the main effect already described for CuET is the high intracellular production of ROS, the induction of DNA damage mediated to H_2O_2 was expected to be similar to 250nM of CuET [136]. However, considering the blot in Figure 33, this was not the case in this experiment. This strengthens the theory described by Skrott *et al*. in 2017, in which they described that the main mechanism mediating CuET cytotoxicity was the aggregation and thus immobilization and dysfunction of NPL4, which was

a crucial cofactor for the activity of the p97/VCP segregase; and the ROS production previously suggested as candidate, initially plays a secondary role [100].

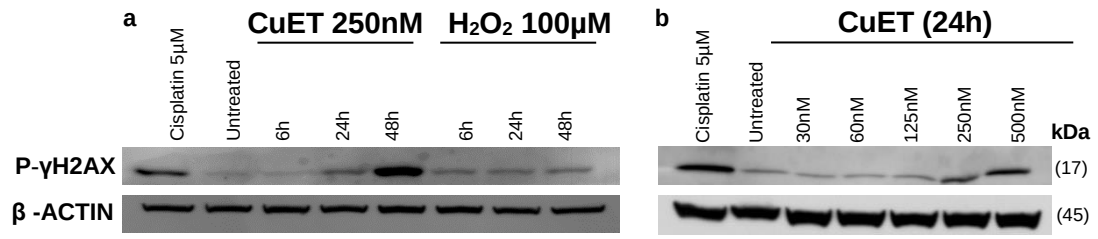

Figure 33: BRAF-WT melanoma cell line SKMEL23 exhibited high induction of γ-H2AX through CuET in a time and dose-dependent manner. a) Western blot analysis for P-γH2AX of whole cell protein lysates of BRAF-WT melanoma cells (SKMEL23) after treatment with CuET (250nM) and H_2O_2 (100µM) for 6, 24 and 48 h. **b)** Western blot analysis for P-γH2AX of whole cell protein lysates of BRAF-WT melanoma cells (SKMEL23) after treatment with increasing doses of CuET (30, 60, 125, 250 and 500nM) for 24 h. **a/b)** Cisplatin (5µM) for 48 h was used as positive control. β-ACTIN was used as loading control.

To determinate whether the induction of the P-γH2AX expression was dependent on the CuET dose, increasing CuET doses from 30nM up to 500nM on SKMEL23 melanoma cells were used, as illustrated in Figure 33. Because 250nM of CuET showed the earliest time-point of P-γH2AX induction at 24 h, this time-point was selected for the dose dependent test. Interesting, CuET induces strong phosphorylation of γH2AX in a dose-dependent manner in SKMEL23 melanoma cells. As expected, 250nM of CuET induced P-γH2AX, however stronger induction of P-γH2AX was observed with CuET500nM. CuET at 30nM, 60nM and 125nM were not able to induce P-γH2AX at 24h compared with the control.

Since the combination therapy of the MEK inhibitor trametinib with CuET exhibited a greater inhibitory effect than the sum of its monotherapies on BRAF-WT melanoma cells, further exploration of P-γH2AX induction due to combination therapy was conducted. For this, SKMEL23 melanoma cells were treated with 10nM of trametinib, 250nM of Cu^{2+} and 250nM of ET as monotherapy. BRAF-WT melanoma cells showed a discrete reduction in P-γH2AX expression compared to control following 48 h of trametinib treatment. Cu^{2+} and ET treatments showed also no induction of P-γH2AX at 48 h in BRAF-WT melanoma cells. Notably, combination therapy of trametinib and CuET evoked a strong increase in P-γH2AX levels, especially in the combination using 250nM CuET. However, the combination did not further increase P-γH2AXlevels compared to 250nM CuET alone, as illustrated in Figure 34.

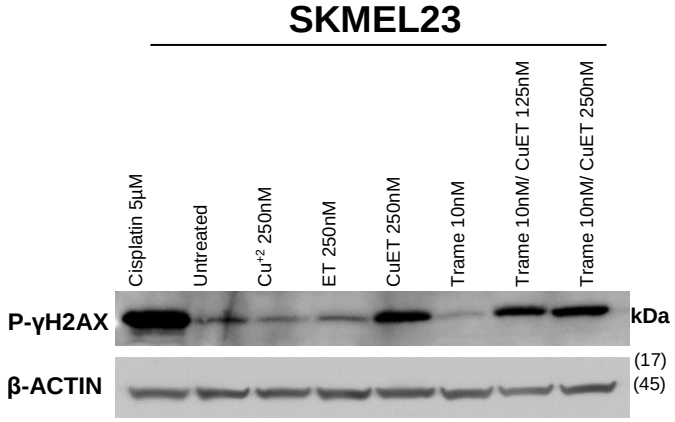

Figure 34: BRAF-WT melanoma cell line SKMEL23 showed high induction of P-γH2AX through combination of MEK inhibitor trametinib with CuET. Western blot analysis for P-γH2AX of whole cell protein lysates of BRAF-WT melanoma cells (SKMEL23) after treatment with Cu^{2+} (250nM), ET (250nM), CuET (250nM), MEK inhibitor trametinib (10nM) and combination of CuET (125nM or 250nM) plus trametinib (10nM) for 48 h. Cisplatin (5µM) for 48 h was used as positive control. β-ACTIN was used as loading control.

Taken together, these results clearly showed that the combination of the MEK inhibitor trametinib with CuET induced significant DNA damage in BRAF-WT melanoma cells. The effect observed through the combination therapy and CuET alone was greater than the effect induced by chemotherapy, which served as positive control. Thus, it became evident that the combination therapy induces significant DNA-DSBs in BRAF-WT melanoma cells.

5.4.2 Trametinib in combination with CuET activates P53/P21 signaling in BRAF WT-melanoma cells

The results so far showed that the anticancer activity of the combination therapy concluded in cell death and apoptosis including the induction of DNA damage. This includes early phosphorylation of γH2AX protein at positions bordering double-strand breaks (DSBs). To this end several DSB repair proteins (MRN Mre11, Rad50, Nbs1, and cohesins) are recruited to keep the DNA ends as close as possible during the repair process [133, 137]. This process provides the ability to further activate the ataxia telangiectasia mutated protein (ATM), which is responsible for the phosphorylation of several target proteins such as P53 and P21, in order to facilitate cell death and apoptosis. Since combination therapy of trametinib with CuET showed high induction of P-γH2AX foci in BRAF-WT melanoma cells, exploration of other DNA damage-associated target proteins was performed. For this purpose, induction of P53/P21 signaling due to DNA damage on BRAF-WT was measured. This experiment demonstrated that 10nM of trametinib in combination with 125nM of CuET induced high expression of P53 and P21 at 12h in SKMEL23 and SKMEL113 melanoma cells. Consequently, the combination therapy caused DNA-damage resulting in significant activation of P53 and P21 in both BRAF-

WT melanoma cells. 125nM of CuET induced discrete expression of P21 and P53 at 12h in both cell lines compared to control. However, combination of 10nM trametinib with 125nM CuET induced significantly higher expression of P21 and P53 at 12 h than monotherapy treatments in both BRAF-WT melanoma cell lines, as illustrated in Figure 35.

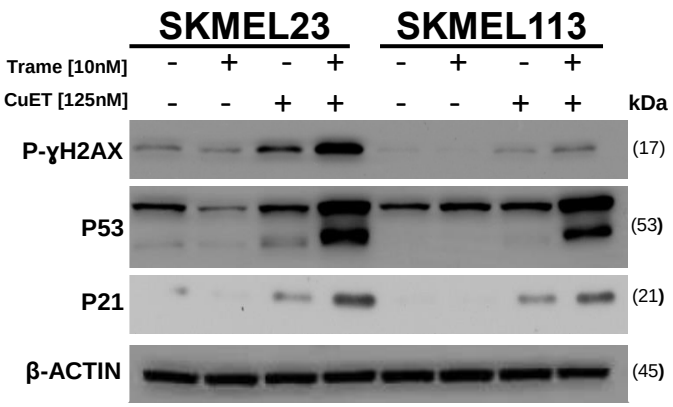

Figure 35: BRAF-WT melanoma cell lines SKMEL23 and SKMEL113 showed high induction of P53 and P21 proteins through combination of MEK inhibitor trametinib with CuET at 12h. Western blot analysis for P-γH2AX, P53 and P21 of whole cell protein lysates of BRAF-WT melanoma cells (SKMEL23 and SKMEL113) after treatment with MEK inhibitor trametinib (10nM), CuET (125nM) or combination for 12 h. β-ACTIN was used as loading control.

In addition, CuET at 125nM induced a discrete expression of P53 and P21 in both melanoma cell lines after 12 h of treatment. Contrary to the effect observed by CuET, 10nM of trametinib was not able to induce P53 or P21 expression after 12 h of treatment neither in SKMEL23 nor in SKMEL113. On the other hand, the significant response of P53 and P21 due to the combination therapy of 10nM of trametinib with 125nM of CuET was uniformly evident in both cell lines. Taken together, both cell lines displayed a high activation of the P53/P21 pathway after 12 h of combination treatment.

There was a coincidence of P53/P21 with P-γH2AX. It was detected that the response of each of the BRAF-WT melanoma cell lines explored was slightly different. SKMEL113 exhibited a discrete induction of P-γH2AX after 12 h of treatment with the combination of trametinib with CuET. SKMEL23 showed an intense P-γH2AX induction at 12 h of treatment with the combination therapy, confirming the data previously observed.

5.5 Trametinib combined with CuET induces intracellular reactive oxygen species (ROS)

To understand the mechanisms of action of the combination of the MEK inhibitor trametinib with CuET, several *signaling* pathways were investigated. Previous studies indicate that CuET induces cellular cytotoxicity in several cancer cell lines via reactive oxygen species (ROS) formation [111]. Due to the reason that CuET induced a high production of ROS in acute myeloid leukemia (CD34+/CD38+ leukemia stem-like cells) and breast cancer cells (MCF7, MDA-MB-231 and T47D), ROS induction by CuET in BRAF-WT melanoma cells was explored. Besides, CuET has been reported to overcome resistance to anticancer drugs, to promote damage DNA and to induce apoptosis through its ROS formation. Therefore, its combination with the MEK inhibitor trametinib was postulated as a potential ROS dependent alternative for the treatment of BRAF-WT melanoma [101, 102, 104].

As initial approach to investigate whether activation of ROS involved in was the mechanism responsible for cytotoxicity induced by CuET as monotherapy in BRAF-WT melanoma cells, cell viability assays (MUH assays) were performed with the addition of a potent ROS scavenger (N-acetyl-cysteine, NAC), to evaluate whether the cytotoxic effect mediated by DSF persists after inhibition of ROS formation, as shown in Figure 36. For the BRAF WT cell lines SKMEL23 and SKMEL113 CuET significantly induced cytotoxicity in a dose-dependent manner, which was completely reversed by addition of the ROS scavenger NAC. NAC mitigated the cytotoxic effects mediated by CuET in both cell lines explored. The cells were pre-incubated for 24 h with 1mM NAC, and subsequently treated with CuET up to 500nM for 72 h. Due to these results, CuET exhibited a strong reduction in cellular viability in a dose and ROS dependent manner. To confirm the effect of ROS on CuET-induced cellular cytotoxicity, a viability assay was performed with glutathione (GSH), another inhibitor of ROS. As illustrated in Figure 36, CuET-induced cytotoxicity was also mitigated by the addition of GSH in the BRAF-WT melanoma cells. However, this reduction of the CuET-cytotoxicity mediated by GSH was discretely minor at CuET 250nM and minimal at CuET 500nM. The sequence of biological intracellular events associated with apoptosis is mainly characterized by a 95% decrease in total GSH and consequently a partial preservation (25%) of mitochondrial GSH, without an increase in ROS production in the first 24 h [136]. When this process is not limited, the intracellular production of ROS is not restricted, leading inevitably to cell death. This phenomenon probably occurred in the BRAF-WT melanoma cells, when they were exposed to the CuET therapy for 72 h.

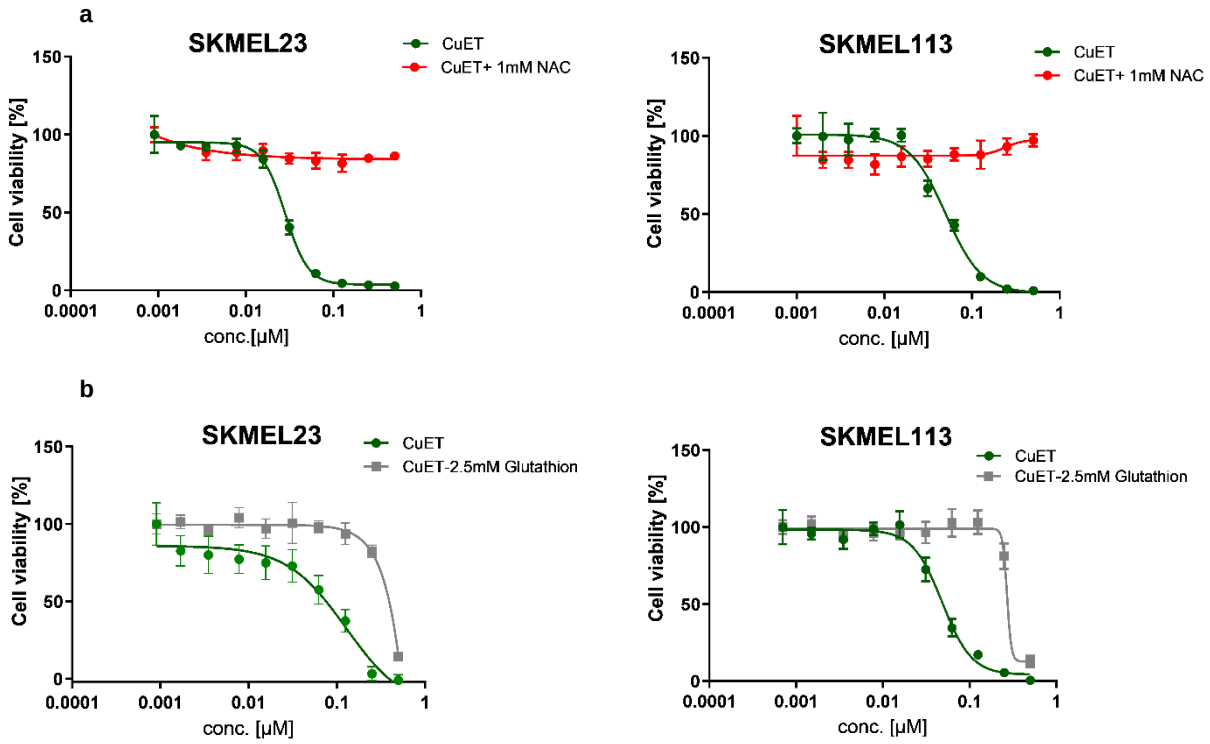

Figure 36: Intracellular ROS production was mainly responsible for CuET-induced cytotoxicity in BRAF-WT melanoma cells under two-dimensional growth conditions *in vitro*. a) Cell viability assay (MUH assay) of BRAF-WT melanoma cell lines (SKMEL23 and SKMEL113) after treatment with the increasing dose of CuET (up to 500nM), or combination of CuET (up to 500nM) with NAC (1mM) for 72 h. **b)** Cell viability assay (MUH assay) of BRAF-WT melanoma cell lines (SKMEL23 and SKMEL113) after treatment with the increasing dose of CuET (up to 500nM), or combination of CuET with GSH (2.5mM) for 72h. **a/b)**Values are means ± SEM of three replicates (n = 3; mean ± SD). Viability was normalized to untreated control melanoma cells.

In summary, the viability assays involving ROS scavengers (NAC and GSH) supported that the cytotoxic effect of CuET on BRAF-WT melanoma cells was mediated by the induction of ROS. In addition, combination therapy of 10nM trametinib with 125nM CuET enhanced the antitumor activity on BRAF-WT melanoma cells, as it was already described. Accordingly, the next step was to analyze whether NAC reversed trametinib/CuET-induced cytotoxicity in BRAF-WT melanoma cells. To this end, the melanoma cell lines SKMEL23 and SKMEL113 were analyzed. NAC completely abolished the additive to synergetic effect mediated by the combination therapy in BRAF-WT melanoma cells. In particular, NAC completely blocked the additive to synergistic effect triggered by the combination therapy. However, it did not suppress the cytotoxic effect mediated by trametinib, as illustrated in Figure 37. Taken together, the protective effect observed by NAC completely mitigated the effect associated with CuET, however it did not significantly diminish the combinational effect of the two drugs, supporting that ROS actively participate in the additional cytotoxic effect mediated by the combined therapy.

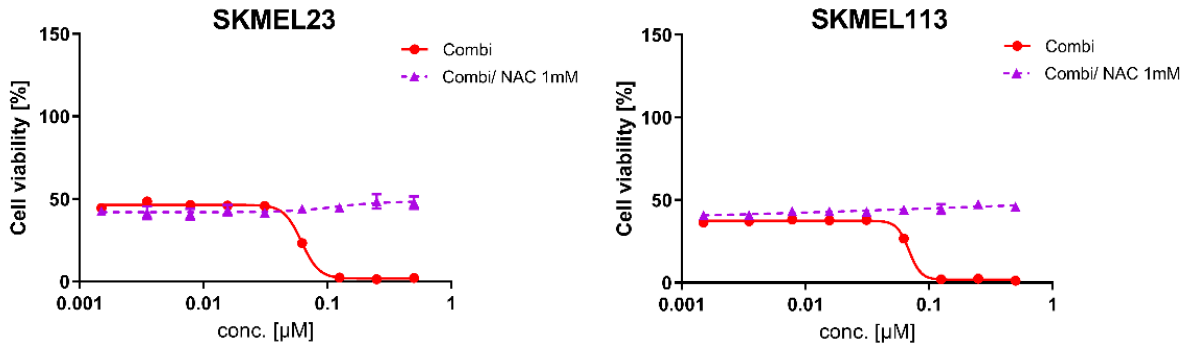

Figure 37: NAC strongly decreased the additive effect of the combination therapy of MEK inhibitor trametinib and CuET in BRAF-WT melanoma cells under two-dimensional growth conditions *in vitro*. Cell viability assay (MUH assay) of BRAF-WT melanoma cell lines (SKMEL23 and SKMEL113) after treatment with the MEK inhibitor trametinib (10nM) plus the increasing dose of CuET (up to 500nM), or combination of trametinib/CuET with NAC (1mM) for 72 h. Values are means ± SEM of three replicates (n = 3; mean ± SD). Viability was normalized to untreated control cells.

5.5.1 Measurement of ROS production by trametinib combined with CuET in BRAF-WT melanoma cells through redox-sensitive GFPs

In order to measure ROS production by CuET and the combination therapy in BRAF-WT melanoma, a redox-sensitive specific GFP lentivirus transfection in SKMEL23 melanoma cells was conducted. Two different transgenic flies containing *roGFP2-GRX* or *roGFP2-ORP-1* targeted to either cytosol or mitochondria matrix were transfected by a lentivirus process into the melanoma cell line SKMEL23. Due to the transfection, the redox status of GSH and H_2O_2 levels in BRAF-WT melanoma cells (SKMEL23) could be accurately measured by flow cytometry. Reduced glutathione (GSH) plays an important role as a scavenger of ROS, and the ratio of reduced (GSH) to oxidized glutathione (GSSG) inversely correlated with oxidative stress [127]. Thus, accurate measurements of the redox state of glutathione (GSH/GSSG ratio) were also obtained by flow cytometry. Concluding, targeted ROS production by CuET and combination therapy was carried out at 1, 6, 12, 24 and 48 h in BRAF-WT melanoma-bio sensor cells. Throughout all ROS experiments, CuET exhibited high ROS production, which was further increased by its combination with the MEK inhibitor trametinib. On contrast, trametinib alone did not induce ROS production in any of the explored models and, as already shown in Figure 36, its toxicity was not abrogated by ROS scavengers (NAC, GSH). Compared to both monotherapies, the combination of the MEK inhibitor trametinib with CuET significantly enhanced ROS production in ROS-sensor melanoma cells (SKMEL23 transfected with *roGFP2-GRX* or *roGFP2-ORP-1*). Taken together, the combination therapy then induced higher ROS production compared to both monotherapies, still, its mitigation through the ROS scavenger did not entirely abolish the cytotoxic effect mediated by the combination therapy, as illustrated in Figure 38.

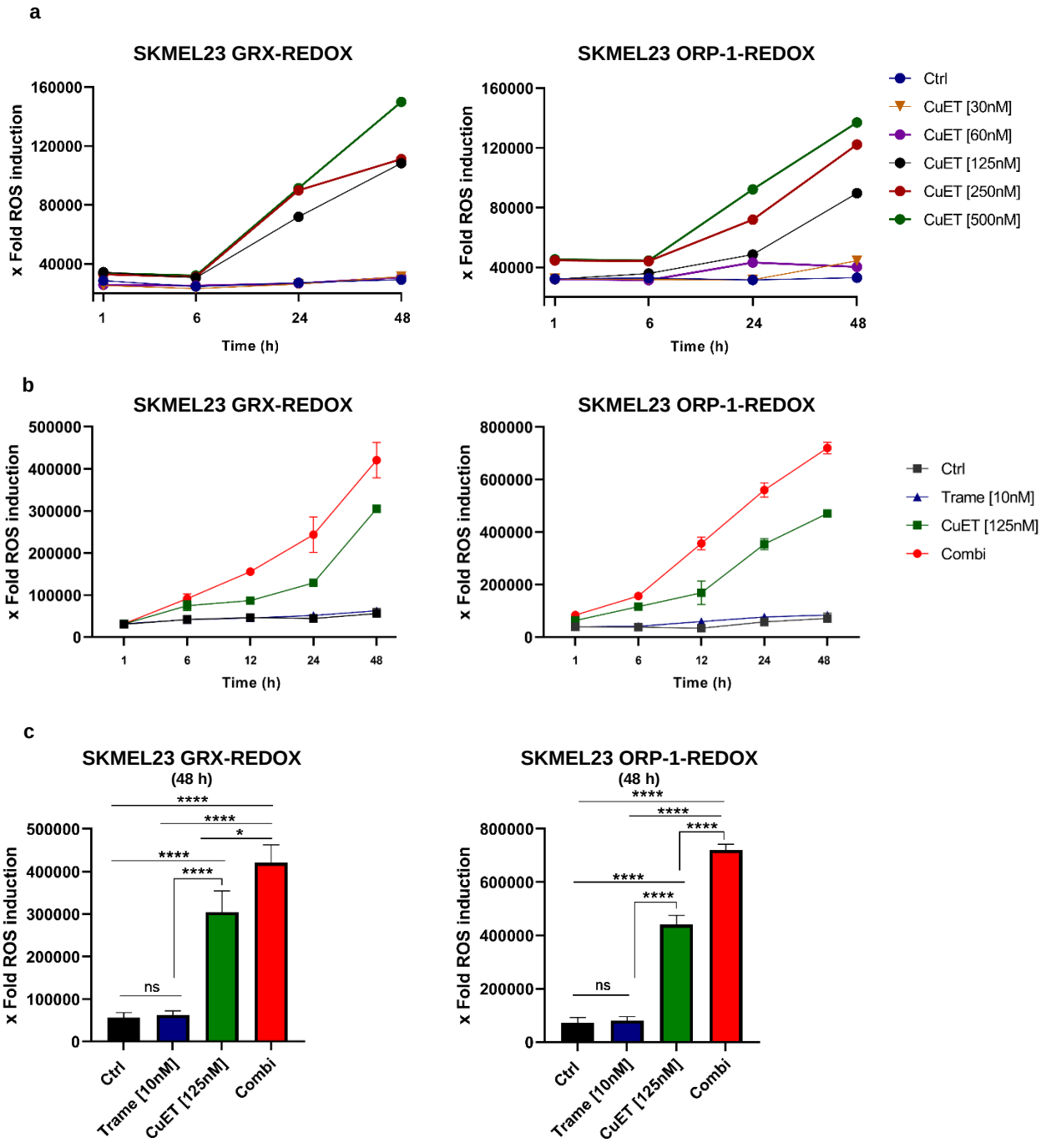

Figure 38: CuET+/- MEK inhibitor trametinib generated a high production of ROS on SKMEL23 GRX and ORP-1 biosensor melanoma cells. Flow cytometry measurement of the ratio Pacific Orange 405 nm/Alexa Fluor 488 nm, which resembles the amount of produced H_2O_2 (ORP-1) and redox state of glutathione GSH/GSSG ratio (GRX). **a)** SKMEL23 GRX and ORP-1 reporter cells were treated with increasing doses of CuET (30, 60, 125, 250 and 500nM) for 1, 6, 24 and 48 h. **b)** SKMEL23 GRX and ORP-1 reporter cells were treated with MEK inhibitor trametinib (10nM), CuET (125nM) and combination for 1, 6, 12, 24 and 48 h. **a/b)** Shown are the mean values with standard deviations of three independent experiments, each measured in quadruplicates and normalized to the untreated control. **c)** SKMEL23 GRX and ORP-1 reporter cells were treated with MEK inhibitor trametinib (10nM), CuET (125nM) and combination for 48 h. One-way ANOVA was used to identify the statistical significance associated to untreated (control) and it was followed by Tukey's multiple comparisons test. * $p < 0.05$; ** $p < 0.01$; *** $p < 0.001$; and **** $p < 0.0001$, ns (not significant).

5.5.2 Induction of ROS associated gene expression through the combination of trametinib with CuET in BRAF-WT melanoma cells

Since increased ROS production was observed by the combination of MEK inhibitor with CuET, a point of interest was to determine whether genes associated with ROS production were induced of regulated of trametinib with CuET. Thus, RNA sequencing (RNA-Seq) of SKMEL23 melanoma cells after treatment with 10nM trametinib, 125nM CuET and combination therapy was conducted. This assay analyses the complexity of the transcriptome in order to identify genes affected by the combination therapy. It was observed that 798 genes were exclusively upregulated by the combination therapy (>=4fold). Additionally, RNA-seq revealed the upregulation of several ROS associated genes as response to the combination of CuET with trametinib, such as a heme oxygenase (*HMOX1*), heat shock proteins family member 1A (*HSPA1*) and heat shock protein family member *1B (HSPA1B*), which specific indicate to a response to oxidative stress. Interestingly, CuET as monotherapy up-regulated the expression of several ROS-associated genes. For instance, CuET induced the expression of *SOD1* gene by 6-fold and that of other ROS-associated genes by more than 8-fold (*HMOX1*, *HSPA1A, HSPA1B*). This emphasized and confirmed the previous results, where 125nM CuET induced ROS production. However, the upregulation of ROS-associated genes was further enhanced by the combination of 10nM trametinib and 125nM CuET. The combination of 10nM trametinib with 125nM CuET induced a 15-fold higher expression of *SOD1* and at least 26-fold higher expression of genes with increased association with ROS (*HMOX1*, *HSPA1A, HSPA1B*). Similar upregulations due to the combination therapy compared to control were found for *HSPA1B* with 46-fold, *HMOX1* with 53-fold and *HSPA1* with 56-fold. Taken together, combination therapy of 10nM trametinib with 125nM CuET produced a significant upregulation of ROS-associated genes in SKMEL23 melanoma cells. In contrast, trametinib as monotherapy did not upregulate any of the ROS-associated genes. These results confirm the observations made previously, where ROS induction was observed to be one of the main mechanisms mediating cytotoxicity associated with combination therapy. These results are summarized in Figure 39.

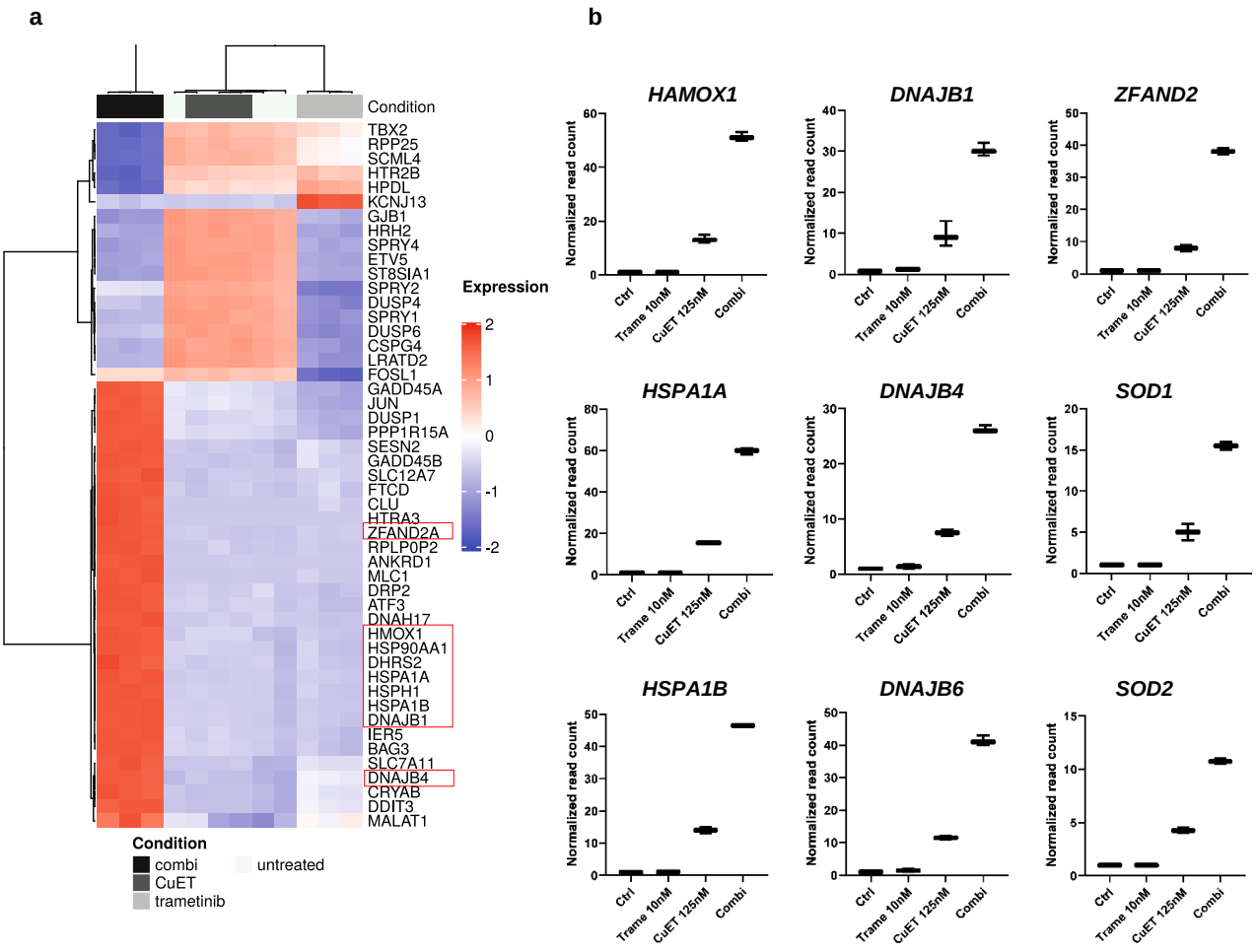

Figure 39. RNA-sequencing reveled induction of ROS-related genes by CuET, which were further induced by combined therapy in BRAF-WT melanoma cells. a) Supervised hierarchical collecting of differentially expressed genes on RNA-sequencing analysis by response of BRAF-WT melanoma cells (SKMEL23) at baseline and after treatment with MEK inhibitor trametinib (10nM), CuET (125nM) and combination for 12 h. A cut-off of gene expression fold change of ≥ 2 or ≤ 2 was applied. The relative high gene expression of ROS-related genes is shown ordered by the mean expression on BRAF-WT melanoma cells (SKMEL23) after treatment with trametinib (10nM), CuET (125nM) and the combination for 12h. The region of origin of each of the ROS-related genes **(b)** was indicated in Figure **(a)**.

The above results demonstrated that intracellular ROS was involved cellular cytotoxicity mediated by combination therapy. In addition, the fact that NAC prevented the increased cytotoxicity of the combination with trametinib and CuET proofed the role of ROS. Next, it was addressed whether the ROS scavenger NAC mitigated the induction of apoptosis mediated by the combination therapy. To this end, a propidium iodide-based cell-cycle flow cytometry analysis was performed. BRAF-WT melanoma cells were treated with the combination of 10 nM of trametinib with 125nM of CuET in addition to 1mM NAC. Therefore, cells were pretreated with NAC for 24 h and then the combined therapy was started. NAC significantly reduced the sub-G1 accumulation by the combination therapy group, at 24, 48 and 72 h, as illustrated in Figure 40. Accordingly, it was interpreted that ROS production mediated by the combination therapy plays an essential role in the activation of apoptosis These results are shown in Figure 40.

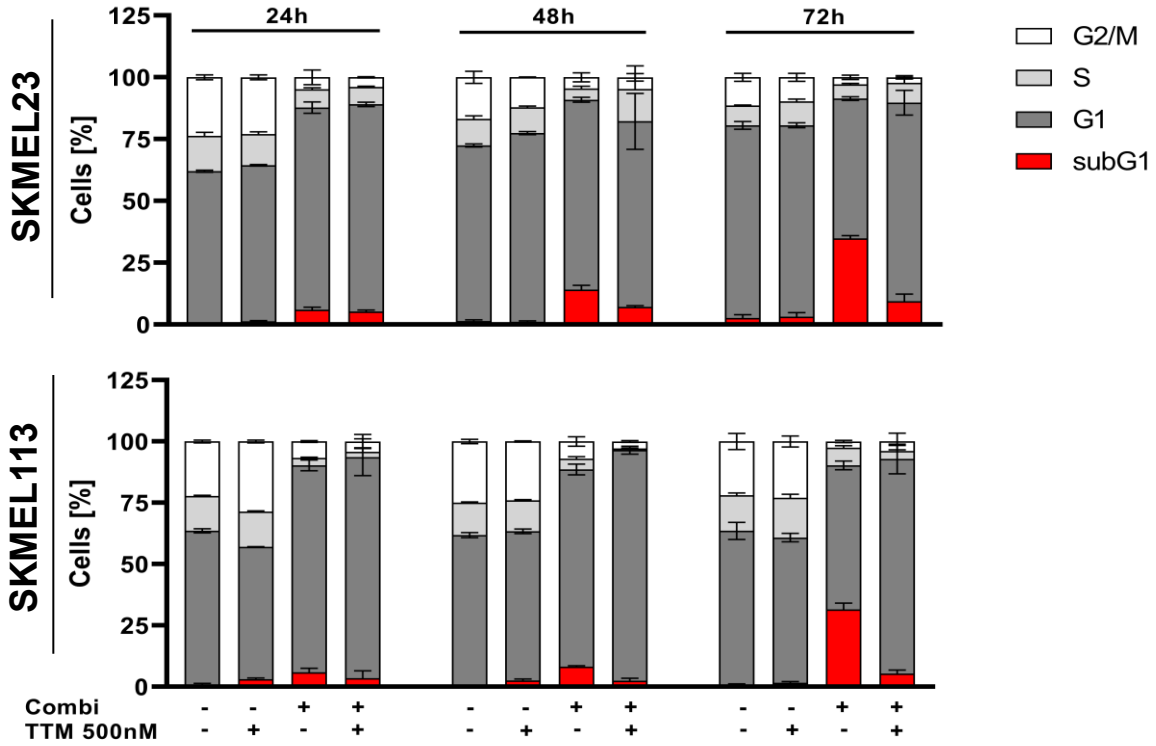

Figure 40: NAC significantly reduced the sub-G1 accumulation (apoptosis induction) mediated by MEK inhibitor trametinib with CuET in in BRAF-WT melanoma cells. Flow cytometric cell-cycle analyses of BRAF-WT melanoma cell lines (SKMEL23 and SKMEL113) after treatment with MEK inhibitor trametinib (10nM) plus CuET (125nM), or combination of trametinib/CuET (10nM/125nM) with the clinical Cu chelator ammonium tetrathiomolybdate (TTM 500nM) for 24, 48 and 72 h. Untreated melanoma cells were used as a control. The relative distribution in the different phases of the cell-cycle was quantified (n = 3, mean ± SD).

5.6 CuET induced protein stress in BRAF-WT melanoma cells

To better understand the effects of CuET on BRAF-WT melanoma cell biology, further experiments were performed. One of the suggested mechanisms of the antitumor effects exhibited by CuET was its interaction with the protein degradation machinery, as Skrott *et al.* already described. In MDA-MB-231 breast cancer cells, CuET induced accumulation of poly-ubiquitylated proteins (POLY-UB) [100]. In addition, CuET also resulted in the deubiquitylation of histone H2A (uH2A) and, finally, the increase of ubiquitylated proteins. This biological process is similar to that observed through proteasome inhibitors, such as Bortezomib and MG132. Therefore, it was of interest to know whether CuET induces the same effects in BRAF-WT melanoma cells. Therefore, further analysis on protein stress or other intracellular stresses, such as endoplasmic reticulum stress (ER-Stress), was done. Several assays were conducted to investigate whether CuET affect proteasome activity. In order to

evaluate the influence of CuET on proteasome activity, SKMEL23 melanoma cells were treated with CuET for 6 h and then intentionally analyzed for polyubiquitinated proteins. The positive control was defined by 10µM of MG132, a specific proteasome inhibitor. Immunofluorescence staining reveled that 250nM of copper did not induce accumulation of poly-ubiquitinated (POLY-UB) proteins after 6h of treatment compared with the control. In contrast, 250nM CuET induced a rapid cytoplasmic accumulation of POLY-UB proteins in SKMEL23 melanoma cells which was similar to the effect induced by the proteasome inhibitor MG132, as illustrated in Figure 41.

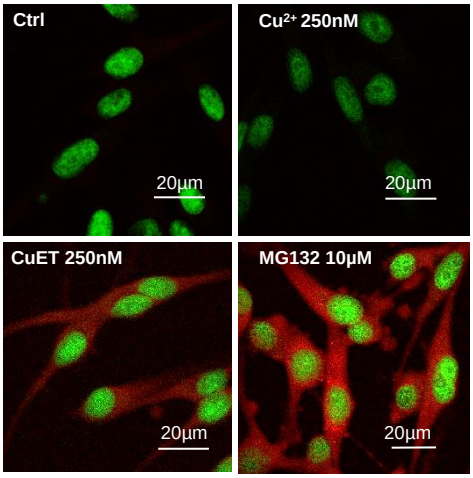

Figure 41: CuET treatment induces rapid cytoplasmic accumulation of POLY-UB proteins in BRAF-WT melanoma cells, similar to proteasome inhibitors. Immunofluorescence staining analysis for POLY-UB proteins on BRAF-WT melanoma cell lines (SKMEL23) after treatment with Cu^{2+} (250nM) and CuET (250nM) for 6 h. Proteasome inhibitor MG132 (10µM) for 6 h was used as a positive control. Untreated melanoma cells were used as a control. Scale bars represent 20µm.

To corroborate these results, a further assessment of proteasome activity was conducted. Therefore, the protein level of POLY-UB proteins was detected after the different treatments such as ET and CuET by Western blot. SKMEL23 melanoma cells were treated for 6 h. The results demonstrated an accumulation of POLY-UB proteins after 6 h of treatment with 125nM of CuET in SKMEL23 melanoma cells, which was significantly enhance with 250nM CuET. A similar response was observed in SKMEL23 melanoma cells treated with 10 µM of MG132. Thereby it was confirmed that CuET promoted the accumulation of POLY-UB proteins in SKMEL23 melanoma cells, as illustrated in Figure 42.

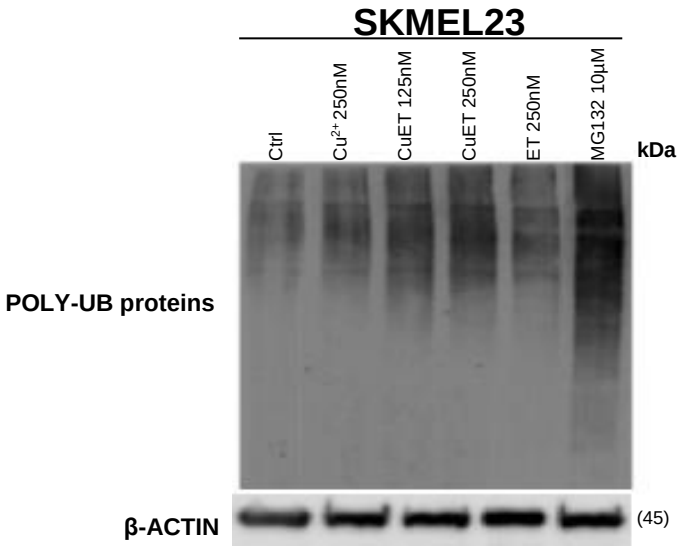

Figure 42: CuET treatment induced rapid cytoplasmic accumulation of POLY-UB proteins in BRAF-WT melanoma cells, similar to proteasome inhibitors. Western blot analysis for POLY-UBIQUITINATED proteins of whole cell protein lysates on BRAF-WT melanoma cells (SKMEL23) after treatment with Cu^{2+}(250nM), CuET (125 or 250nM) and ET (250nM) for 6 h. Proteasome inhibitor MG132 (10µM) for 6 h was used as a positive control. β-ACTIN was used as loading control.

These results underlined the concept that CuET induced different pathways stress in melanoma cells. Niessner *et al*. have shown that MEK inhibitors as monotherapy did not induce endoplasmic reticulum (ER) stress in melanoma cells, but their combination with BRAF inhibitors (BRAFi) caused significant upregulation of ER stress-related genes in NRAS melanoma cells [138]. Therefore, it was explored whether MEK inhibition in combination with CuET induced ER stress in BRAF-WT melanoma cells. Thus, the induction of ER stress-related genes in BRAF-WT melanoma cells by CuET as a single treatment, or in combination with trametinib were analyzed in the following.

5.7 Trametinib in combination with CuET upregulated ER stress-related genes in BRAF-WT melanoma cells

Several groups showed that the BRAFi (vemurafenib) induced ER stress in $BRAF^{mut}$ melanoma cells [57,58]. Several factors act as triggers for ER stress, such as disruption of protein glycosylation, hypoxia, nutrient imbalances or Ca^{2+} disproportion; which ends in increase amount of unfolded proteins in the ER and its subsequent unfolded protein response (UPR) [138, 139]. UPR pathway activation is mediated by three different mediators, activating transcription factor 6 (*ATF6*), PKR-like ER kinase (*PERK*) and lastly the inositol-requiring enzyme 1 (*IRE1*). Upon activation, these factors are detached from their main chaperone protein glucose-regulated protein 78 (*GRP78*) [140]. The UPR induces the transcription of UPR genes,

which results in the removal of the accumulated of unfolded proteins [141]. These modifications result stall the overall protein synthesis and subsequently result in the degradation of the ER-associated stimulatory protein in order to restore normal ER function. When the integral function of the ER fails to be restored, switches the UPR pathway from a pro-survival pathway to a pro-apoptotic pathway[142, 143].

Previous results revealed an induction of pro-apoptotic BCL-2 family members by the combination therapy with trametinib and CuET with accompanied. Therefor it was decided to explore the ER-stress induction by trametinib, CuET or the combination. The overall aim was to determine whether there is cooperation between ER-stress genes and pro-apoptotic BCL-2 proteins in apoptosis through the combination therapy. ER stress-related genes such as activating transcription factor 4 (*ATF4*), *P8* (*NUPR1* (nuclear protein-1), *NUPR1* (nuclear protein-1, *P8*) and DNA damage/growth arrest inducible transcription 3 (*DDIT3/CHOP*) were fully explored by quantitative real-time PCR and Western blot.

First, gene expression at the mRNA level was explored by quantitative real-time polymerase chain reaction (real-time qPCR). It was analyzed whether the expression of ER-related genes was regulated by monotherapies trametinib and CuET or their combination. BRAF-WT melanoma cells (SKMEL23 and SKMEL113) were treated with different concentrations of CuET in an ascending manner, with 30nM, 50nM, 125nM, 250nM and 500nM. To explore the effect of combination therapy to monotherapies, the same conditions with different CuET concentrations in combination with 10nM trametinib for 3 h were also tested. The ER-stress related genes selected were *ATF4, CHOP* and *P8 (NUPR1)*. In order to have an appropriate reference, the relative ratio ($2^{-\Delta Cq}$) of each ER-stress gene was compared to the housekeeping gene TATA-binding protein (*TBP*), which is a common transcription factor that binds to a DNA sequence named the TATA-box. Interestingly, CuET induced high expression of ER-stress related genes in a in a dose-dependent manner in SKMEL23 and SKMEL113 melanoma cells already after 3h of treatment. However, further upregulation of the ER-stress related genes was mediated by combination of trametinib with CuET, as illustrated in Figure 43.

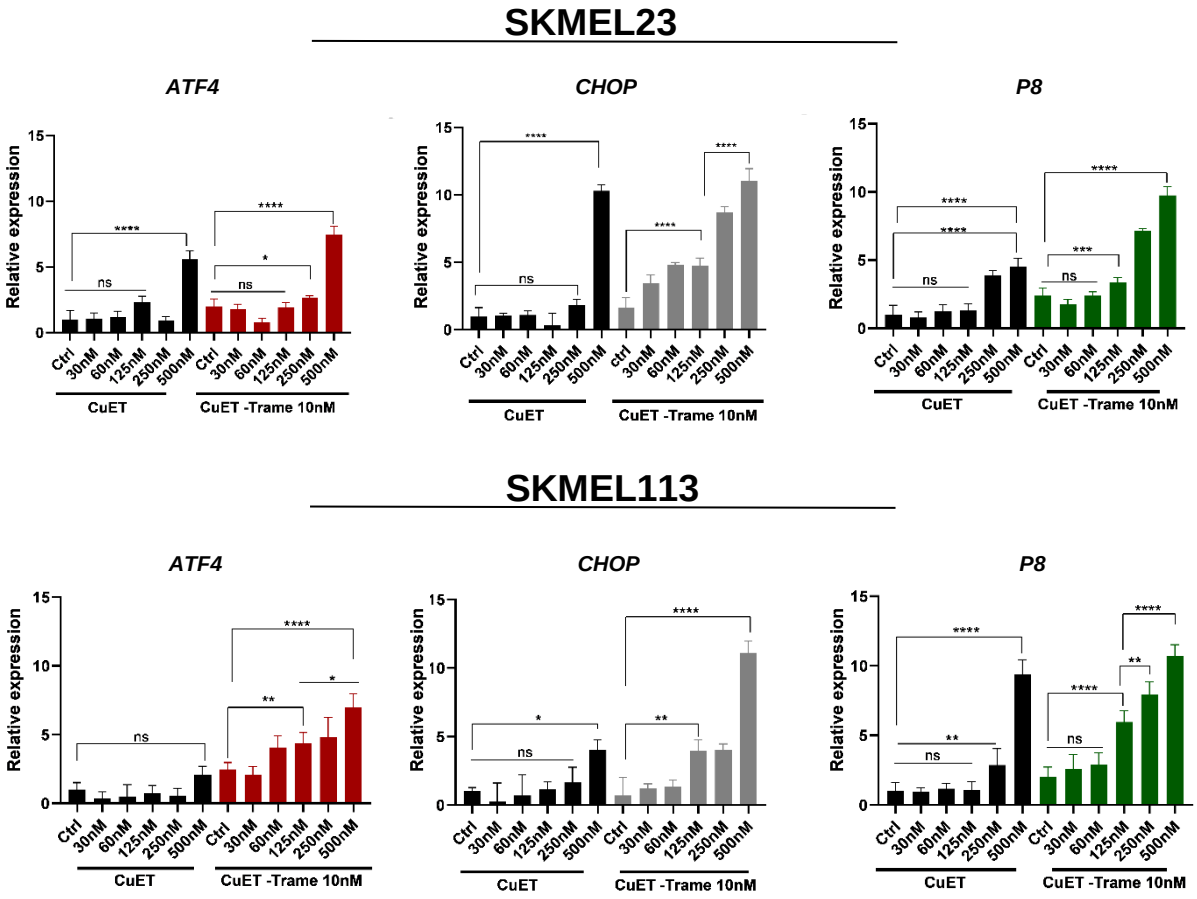

Figure 43: Combination of MEK inhibitor trametinib with CuET induced high expression of *ATF4, CHOP* and *NUPR1* (*P8*) in BRAF-WT melanoma cells. Transcript expression (real-time qPCR) of *ATF4*, *CHOP* and *NUPR1* (*P8*) on BRAF-WT melanoma cells (SKMEL23 and SKMEL113) after treatment with increasing doses of CuET (30, 60, 125, 250 and 500nM), or combination of CuET (30, 60, 125, 250 and 500nM) with trametinib (10nM) for 3 h. *TBP* was used as a reference gene. The relative ratio was calculated with the Light-Cycler® 96 software. Samples were measured in triplicates and the values are the means ± SD of three replicates.

The relative RNA expression of the target genes in the melanoma cells treated with CuET up to 500nM or in combination with the MEK inhibitor trametinib (10nM) was normalized to DMSO. Treatment with CuET as monotherapy discretely upregulated ER-stress related genes at its highest concentration, 500nM, however this upregulation was not significant for *ATF4* in SKMEL113. At lower concentrations, CuET did not induce expression of ER-stress related genes in both melanoma cell lines. Contrary, combination therapy caused significant upregulation of *ATF4, CHOP* and *P8* after 3h in both SKMEL23 and SKMEL113 melanoma cell lines. Due to these results, was clear that the combination of trametinib with CuET significantly upregulated ER stress -related genes in BRAF-WT melanoma cells.

The upregulation of ER-stress related genes by 500nM of CuET at 3 h, was further enhanced by the addition of 10nM trametinib. In SKMEL23, *ATF4* expression was increased (>5-fold) only with the highest concentration of CuET (500nM), and the subsequent increase in combination with 10nM trametinib was also observed with 500nM CuET (>7-fold). In SKMEL113, where CuET as single therapy did not induce a significant increase in *ATF4* expression. The combination of 125nM of CuET with 10nM trametinib exhibited a significant induction of *ATF4* expression (>5-fold) in SKMEL113. An additional significant increase in *ATF4* expression was observed with the combination of 500nM CuET with 10nM trametinib in SKMEL113 melanoma cells (>7-fold). *CHOP* expression in SKMEL23 treated with 500nM of CuET was significantly upregulated. This was already archived at lower CuET concentrations by the addition of 10nM trametinib. A similar trend in *CHOP* expression was observed in SKMEL113 melanoma cells. CuET up to 250nM did not induce an increase in *CHOP* expression after 3h of treatment in SKMEL23. Finally, SKMEL23 melanoma cells displayed upregulation of the *P8* gene by CuET at 250nM (>4-fold) and 500nM (>5-fold). Interestingly, the combination of only 125nM CuET with 10nM trametinib induced a significant increase in *P8* expression compared to control (>4-fold). Also, 500nM of CuET in combination with 10nM trametinib induced a significant increase in *P8* expression in SKMEL23. Similarly, 500nM of CuET induced a significant increase in *P8* gene expression in SKMEL113. Trametinib also enhanced this induction at lower concentrations of CuET. Taken together, the combination of trametinib with CuET induced upregulation of ER-stress related genes after 3h of treatment in both melanoma cell lines.

Since the combination of MEK inhibitor and CuET showed an upregulation of the expression of ER-stress related genes, was decided to explore this gene induction at different time points. Thus, the ER-stress related genes expression was explored at 3, 6, 12 and 24h. The combination of 125nM CuET plus 10nM trametinib, which induced significant apoptosis in BRAF-WT melanoma cells, was chosen in this experiment, in order to confirm the ER-stress induction as a main cytotoxic mechanism mediated by combination therapy. For this, SKMEL23 were treated with trametinib, CuET and combination therapy for 3, 6, 12 and 24 h. The expression of ER-stress related genes *ATF4*, *CHOP* and *P8* at this timepoints are illustrated in Figure 44.

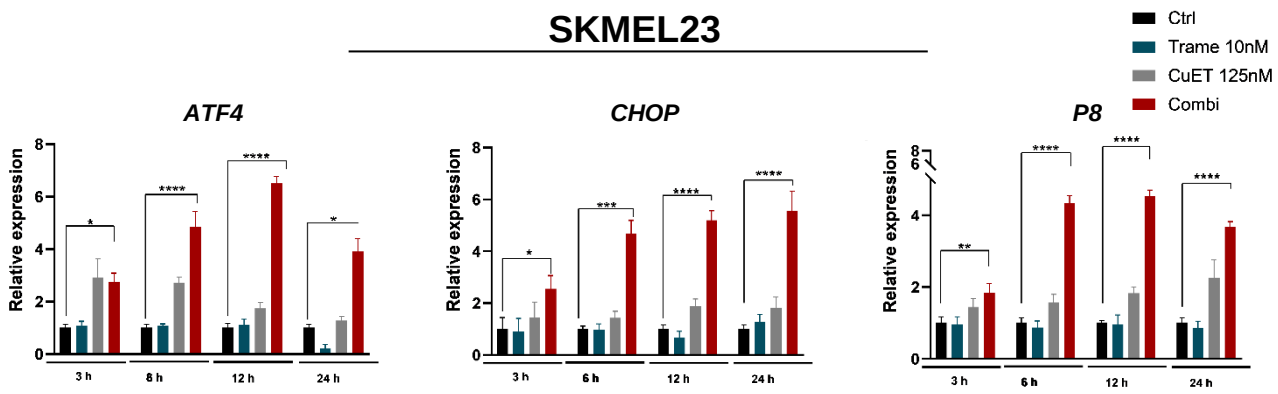

Figure 44: Combination of MEK inhibitor trametinib with CuET induced high expression of *ATF4*, *CHOP* and *NUPR1* (*P8*) in BRAF-WT melanoma cells. Transcript expression (real-time qPCR) of *ATF4*, *CHOP* and *NUPR1* (*P8*) on BRAF-WT melanoma cells (SKMEL23) after treatment with MEK inhibitor trametinib (10nM), CuET (125nM) and combination for 3, 6, 12 and 24 h. *TBP* was used as a reference gene. The relative ratio was calculated with the Light-Cycler® 96 software. Samples were measured in triplicates and the values are the means ± SD of four replicates. One-way ANOVA was used to identify the statistical significance associated to untreated (control) and it was followed by Tukey's multiple comparisons test. * $p < 0.05$; ** $p < 0.01$; *** $p < 0.001$; and **** $p < 0.0001$, ns (not significant).

The relative RNA expression of SKMEL23 melanoma cells treated with the MEK inhibitor trametinib (10nM), 125nM of CuET or the combination therapy was normalized to DMSO. Combination therapy induced a significant upregulation of *ATF4*, *CHOP* and *P8* genes in SKMEL23 melanoma cells at 3, 6, 12 and 24 h. To sum up, combination therapy of 10nM of trametinib with 125nM of CuET upregulated the expression of *ATF4*, *CHOP* and *P8* at 6 h in SKMEL23 melanoma cells (>5-fold). However, this effect was further enhanced at 12 h for all the ER-stress related genes (>6-fold). The upregulation of *CHOP* by combination therapy was maintained at 24 h (>6-fold), however the expression of *ATF4* and *P8* mediated by combination therapy discreetly decreased at 24 h. Taken together, the time point at which the highest significant upregulation of the three ER-stress related genes mediated by the combination therapy was observed was at 12 h.

In line with the results of Niessner *et al*., trametinib did not induce ER-stress related genes in SKMEL23 melanoma cells at 3, 6, 12 and 24h. In contrast, CuET induced an early *ATF4* upregulation (>3-fold) already at 3 h. But this upregulation decreased within 12 h and finally disappeared after 24 h. *CHOP* expression was not induced by 125nM CuET at 3, 6, 12 and 24 h in SKMEL23 melanoma cells. However, CuET was able to induce a discrete upregulation of *P8* at 24 h (>2-fold). To sum up, the effect of ER stress-related genes by 125nM CuET was similar to the previous observations, where no significant and sustained upregulation of any gene was produced with this concentration as monotherapy. In order to confirm the data, the experiment was repeated analyzing exclusively the time point that reflects the best

upregulation of the 3 genes, that was 12 h. For this, SKMEL23 and SKMEL113 melanoma cells were treated with the corresponding monotherapy as well as the combination therapy for 12 h. Combination therapy induced a significant upregulation of *ATF4*, *CHOP* and *P8* genes in SKMEL23 and SKMEL113 at 12 h compared to CuET. To sum up, combination therapy of 10nM of trametinib with 125nM of CuET significantly upregulated the expression of *ATF4*, *CHOP* and *P8* at 12 h in both BRAF-WT melanoma cells. The results confirm the data previously discussed and are illustrated in Figure 45.

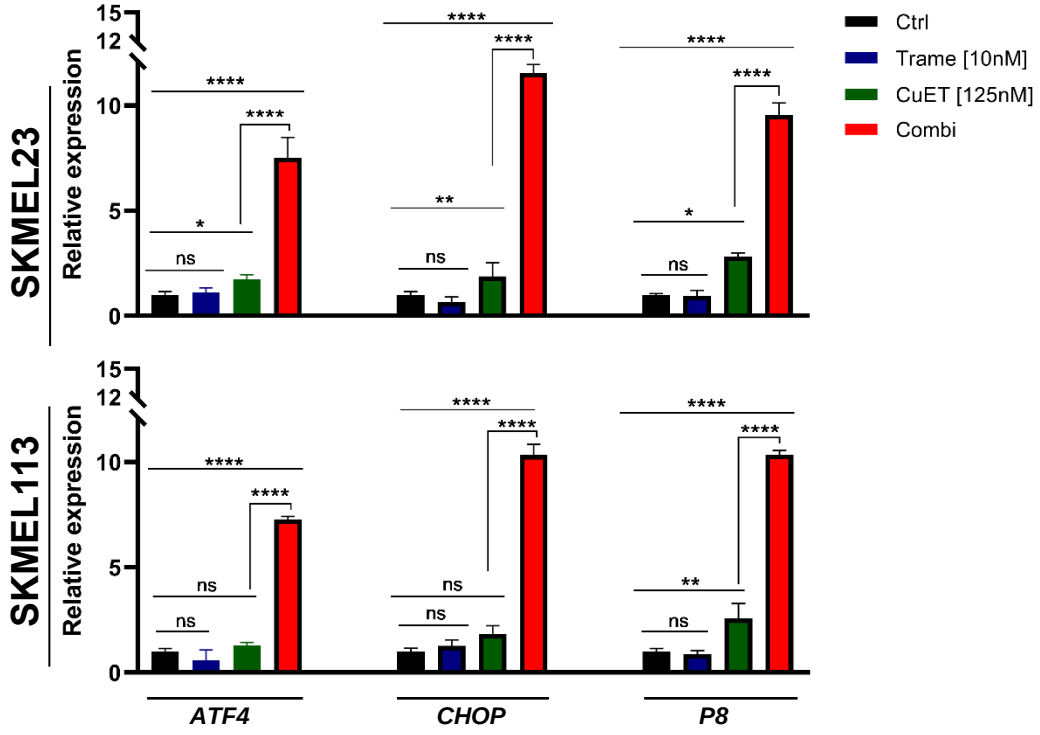

Figure 45: Combination of MEK inhibitor trametinib with CuET induced high expression of *ATF4, CHOP* and *NUPR1* (*P8*) after 12 h of treatment in both BRAF-WT melanoma cells. Transcript expression (real-time qPCR) of *ATF4*, *CHOP* and *NUPR1* (*P8*) on BRAF-WT melanoma cells (SKMEL23 and SKMEL113) after treatment with MEK inhibitor trametinib (10nM), CuET (125nM) and combination for 12. *TBP* was used as a reference gene. The relative ratio was calculated with the Light-Cycler® 96 software. Samples were measured in triplicates and the values are the means ± SD of four replicates. One-way ANOVA was used to identify the statistical significance associated to untreated (control) and it was followed by Tukey's multiple comparisons test. * $p < 0.05$; ** $p < 0.01$; *** $p < 0.001$; and **** $p < 0.0001$, ns (not significant).

ER-stress related genes were also analyzed in the transcriptome analysis done by RNA sequencing. The time of the highest induction of ER-stress related genes mediated by the combined therapy was at 12 h, as illustrated in Figure 45. This was exactly the treatment time in the RNA sequencing experiments using SKMEL23 cells. In line with the qPCR data, RNA sequencing revealed a significant increase in the expression of ER-stress related genes *ATF3*, *ATF4*, *CHOP* and *P8* by combination therapy in SKMEL23 melanoma cells. The MEK inhibitor trametinib (10nM) in combination with CuET (125nM) exhibited an increase in the expression of all ER-stress related genes analyzed, but especially *P8* which exhibited a greater

than 48-fold increase compared to the control. The same phenomenon was observed with the *CHOP* gene, which exhibited 36-fold increase duo to the combination therapy in SKMEL23 melanoma cells. Additionally, *ATF3* and *ATF4* also showed an upregulation (>22-fold and >16-fold respectively) by the combination therapy when compared with the untreated. Interestingly, *BIM* also showed a significant up-regulation (>10-fold), which confirms the induction of this pro-apoptotic player and apoptosis by the combination therapy. The induction of ER-stress related genes and the pre-apoptotic gene *BIM* confirmed that ER-stress induction acts as a main mechanism responsible for the apoptosis induction mediated by the combined therapy. The corroboration of ER-stress related genes induction due to combination therapy by RNA-seq is illustrated in Figure 46.

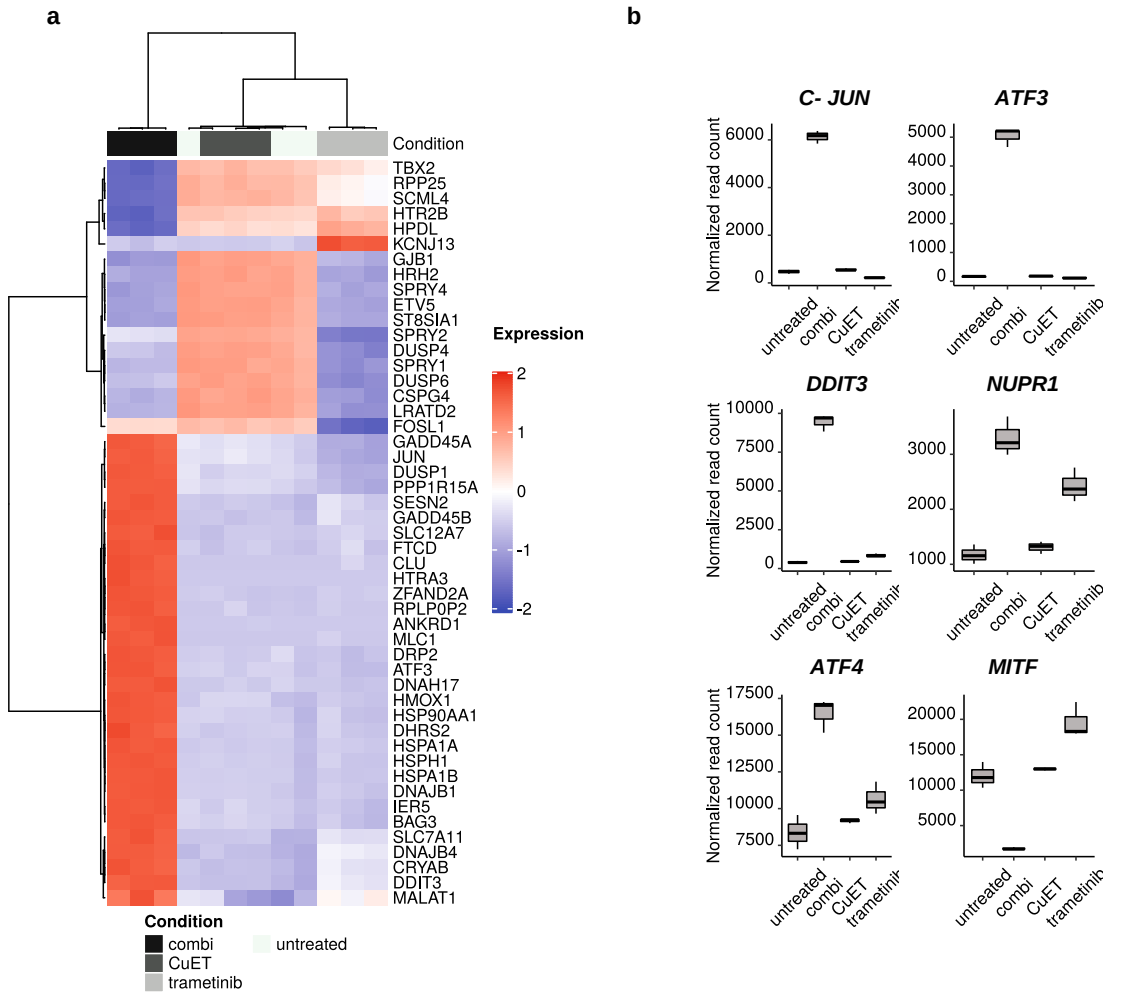

Figure 46. RNA-sequencing reveled induction of ER-stress related genes by combination of trametinib and CuET in BRAF-WT melanoma cells. RNA-sequencing exhibited 798 genes exclusively upregulated by the combined therapy (>=4fold) **a)** Supervised hierarchical collecting of differentially expressed genes on RNA-sequencing analysis by response of BRAF-WT melanoma cells (SKMEL23) at baseline and after treatment with MEK inhibitor trametinib (10nM), CuET (125nM) and combination for 12 h. A cut-off of gene expression fold change of ≥ 2 or ≤ 2 was applied. **b)** The relative high gene expression of ER-related genes is shown ordered by the mean expression on BRAF-WT melanoma cells (SKMEL23) after treatment with trametinib (10nM), CuET (125nM) and the combination for 12h. The region of origin of each of the ER-related genes **(b)** is indicated in Figure **a**. Values are means ± SEM of three replicates (n = 3; mean ± SD).

For a robust conclusion that the combination of trametinib plus CuET induces ER-stress, the expression of the previously investigated ER-stress related genes was analyzed at the protein level. This further confirmation was done via Western blot analysis. *ATF4*, *CHOP* and *P8* were analyzed after 12 h of treatment in SKMEL23 and SKMEL113 melanoma, as is shown in Figure 47.

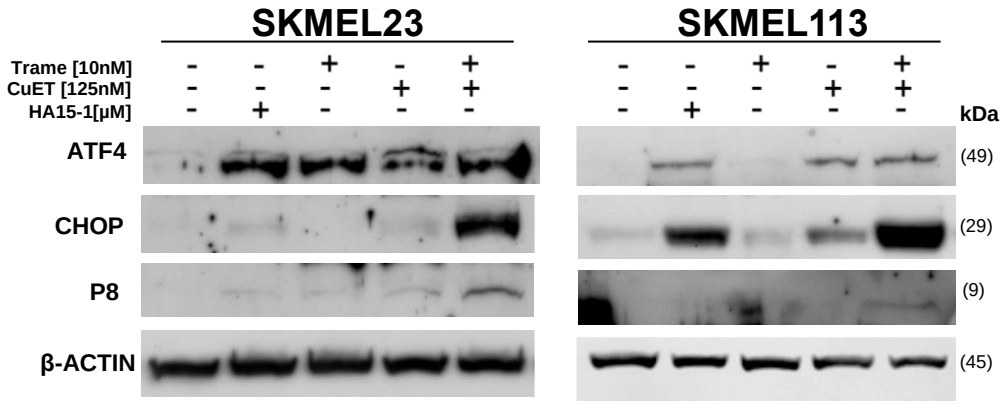

Figure 47: BRAF-WT melanoma cell lines SKMEL23 and SKMEL113 showed high induction of ER-stress related proteins through combination of MEK inhibitor trametinib with CuET at 12h. Western blot analysis for ATF4, CHOP and P8 of whole cell protein lysates of BRAF-WT melanoma cells (SKMEL23 and SKMEL113) after treatment with MEK inhibitor trametinib (10nM), CuET (125nM) and combination for 12 h. ER-stress inductor HA15-1 (1µM) for 12 h was used as a positive control. β-ACTIN was used as loading control.

The Western blot analysis showed a significant upregulation of ATF4 and CHOP at 12h after treatment with 125nM of CuET in both melanoma cell lines, which were further increased by combination therapy. In contrast, combination therapy induced a discrete upregulation of P8, which was not clearly detectable in SKMEL113. The ER stress inducer HA15 was used as a positive control. The induced expression by the combination therapy was similar to that of HA15 for ATF4 and higher for CHOP and P8. Although trametinib showed an induction of ATF4 in SKMEL23, it was not able to induce ATF4 in SKMEL113. Also, trametinib was not able to induce CHOP and P8 in both melanoma cell lines. Furthermore, these results confirmed that trametinib as a single therapy did not change the protein levels of ER-stress related genes in BRAF-WT melanoma cells.

5.8 JNK/c-JUN signaling plays an important role in apoptosis induction by the combination of trametinib with CuET

Since intracellular ROS levels, ER-stress related genes and pre-apoptotic protein expression were induced by the combination of the MEK inhibitor trametinib with CuET in BRAF-WT melanoma cells, a point of interest was whether these mechanisms were molecularly interconnected by the *JNK/c-JUN* signaling [138]. Initially, to explore the mechanisms responsible for these findings, upregulation of RNA by the combination therapy was observed. Additionally, RNA sequencing revealed that c-*JUN* stress was associated with the response of BRAF-WT cells to trametinib with CuET treatment, as was illustrated in Figure 46.

In order to confirm the postulated activation of the transcription factor c-JUN, the JNK/c-JUN pathway after combination therapy was explored. For this, the phosphorylation of JNK and the induction of c-JUN via Western blot analysis was analyzed (Figure 48). Interesting, combination therapy of 10nM of trametinib with 125nM of CuET induced a high phosphorylation of JNK and protein level of c-JUN in BRAF-WT melanoma cells after 12 h of treatment. Interestingly, the induction of JNK phosphorylation as well as c-JUN mediated by the combination therapy was completely abolished by the addition of a specific JNK inhibitor (SP600125). Thus, the induction of c-JUN was dependent on the JNK activation (Figure 48). Once the interaction of the MEK inhibitor and trametinib is initiated, a final phosphorylation of JNK and induction of c-JUN occurs, as exemplified in Figure 48. Taken together, these data suggest that the combination therapy of 10nM of trametinib with 125nM of CuET induced apoptosis in BRAF-WT melanoma cell lines via ROS/ER-stress-JNK-c-JUN pathway. These findings provided an enhanced understanding of the mechanisms underlying the cytotoxicity by combination therapy in BRAF-WT melanoma cells.

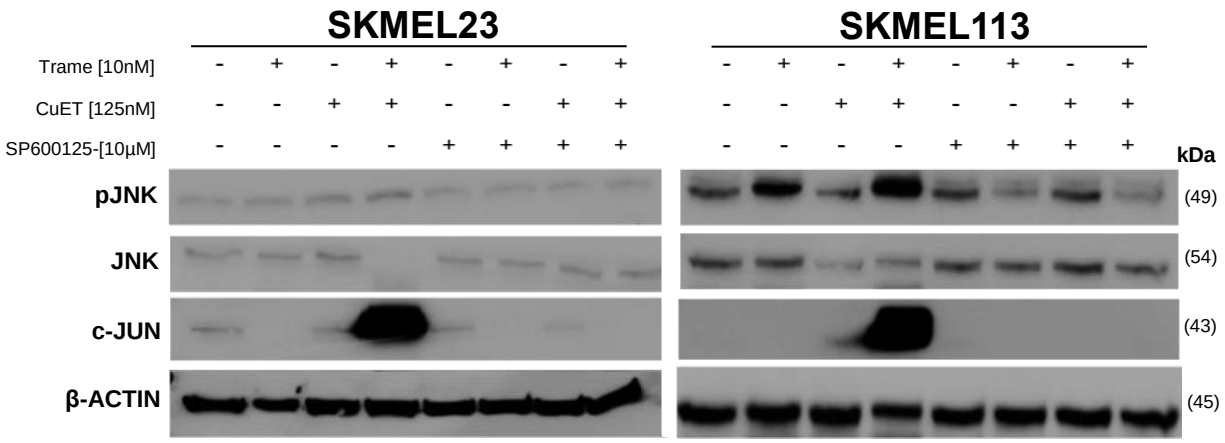

Figure 48: BRAF-WT melanoma cell lines SKMEL23 and SKMEL113 showed high induction of c-JUN and JNK phosphorylation by combination of MEK inhibitor trametinib with CuET at 12h. Western blot analysis for phosphorylated JNK (pJNK), JNK and c-JUN of whole cell protein lysates of BRAF-WT melanoma cells (SKMEL23 and SKMEL113) after treatment with MEK inhibitor trametinib (10nM), CuET (125nM) and trametinib plus CuET (10nM/125nM), or combination of treatments with the JNK inhibitor SP600125 (10µM) for 12 h. β-ACTIN was used as loading control.

ROS induction and ER-stress were postulated as a potential trigger for activation of the JNK-c-JUN pathway. To this end, c-JUN induction mediated by combination therapy in addition to the ROS scavenger molecule (NAC) in SKMEL23 and SKMEL113 was explored. NAC abolished the induction of c-JUN by combination therapy in both cell lines, as illustrated in Figure 49. In addition, SKMEL23 and SKMEL113 cell lines were treated with combination therapy in addition to 10µM of the JNKi SP600125. Interestingly JNKi turned off the JNK activation and subsequent abolished the induction of c-JUN. These data demonstrated that the activation of ROS/JNK pathway triggered the activation of c-JUN by combination therapy and played a relevant role in the mechanism mediated by combined therapy. Additionally, pharmacological reduction of cellular copper import with the clinical Cu chelator ammonium tetrathiomolybdate (TTM) inhibited the ROS formation mediated by combination therapy. Because it became evident by the previous result that Cu^{2+} was essential for cytotoxicity and ROS formation the Cu chelator TTM. The administration of TTM inhibited the final c-JUN induction mediated by the combination therapy. This reaction was mechanistically mediated by decreased copper import into the intracellular space. Therefore, the formation of ROS, in which Cu plays an essential role, did not occur. These results are illustrated in Figure 49.

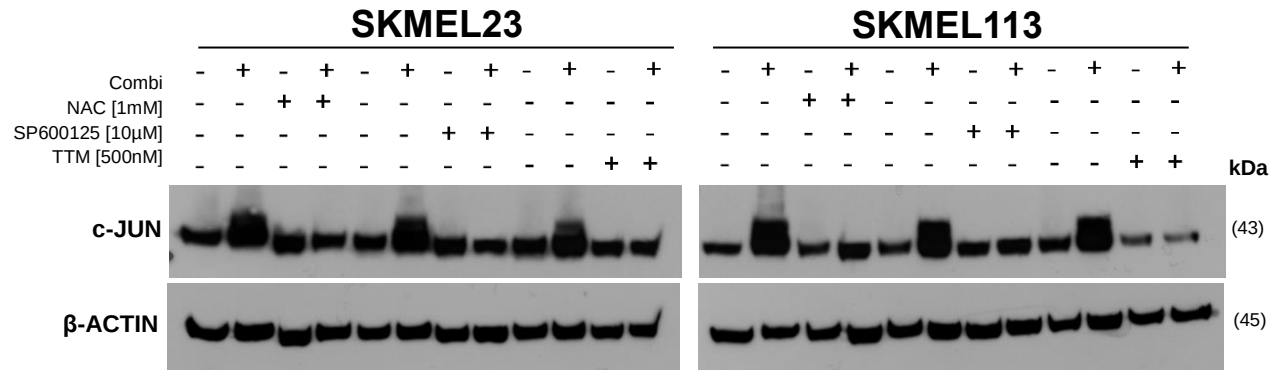

Figure 49: NAC and JNK inhibitor SP600125 abolished the c-JUN induction mediated by combined therapy in BRAF-WT melanoma cell lines. Western blot analysis for c-JUN of whole cell protein lysates of BRAF-WT melanoma cells (SKMEL23 and SKMEL113) after treatment with MEK inhibitor trametinib (10nM) plus CuET (125nM), or combination of trametinib/CuET either with NAC (1mM), the JNK inhibitor SP600125 (10µM) or TTM (500nM) for 12 h. β-ACTIN was used as loading control.

To determine whether JNK activation was also involved in the combination therapy-mediated apoptosis, cell-cycle analysis of combined therapy in addition to JNK inhibitor was conducted. SKMEL23 and SKMEL113 melanoma cells were treated with the combination of 10nM of trametinib with 125nM of CuET in addition to 10µM JNKi SP125 for 24, 48 and 72h. Interestingly, inhibition of the JNK activation by the SP600125 significantly reduced the sub-G1 accumulation in propidium iodide-based cell-cycle analysis to the baseline of control cells in BRAF-WT melanoma cells. Taken together, the current results indicated that JNK activation and thereby the JNK/c-JUN pathway is essential for the apoptosis induction through the combination of the MEK inhibitor trametinib with CuET. These results are illustrated in the Figure 50 demonstrating important role of JNK as a key regulator of apoptotic induction by combined treatment of trametinib with CuET.

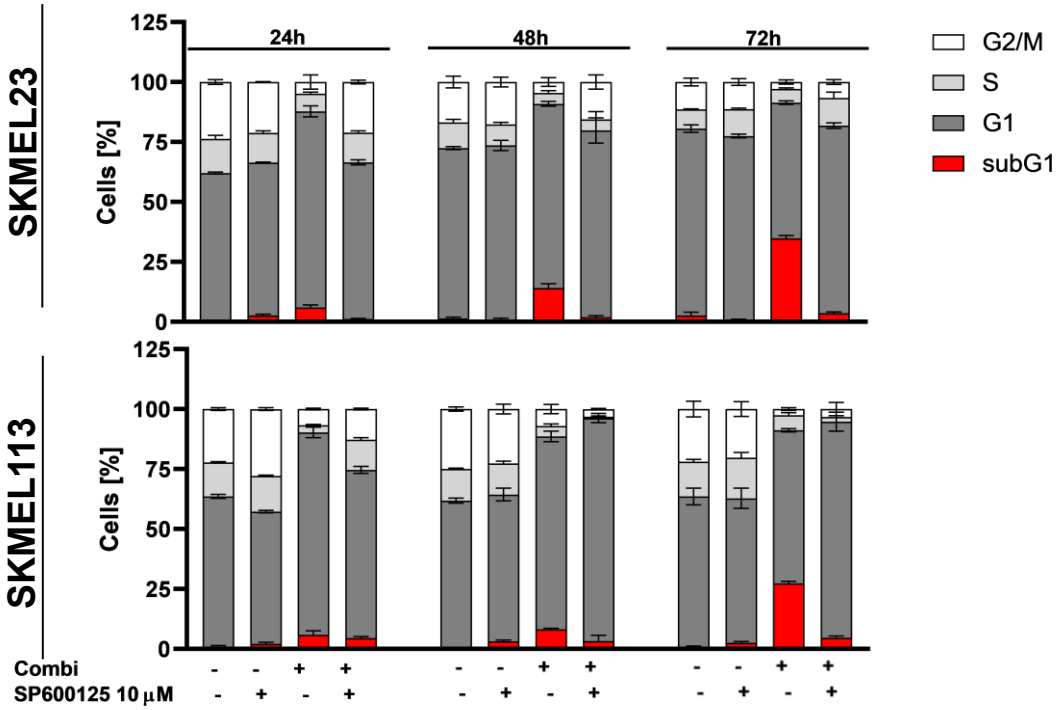

Figure 50: JNK inhibitor SP600125 significantly reduced the sub-G1 accumulation (apoptosis induction) mediated by MEK inhibitor trametinib in combination with CuET in in BRAF-WT melanoma cells. Flow cytometric cell-cycle analyses of BRAF-WT melanoma cell lines (SKMEL23 and SKMEL113) after treatment with MEK inhibitor trametinib (10nM), CuET (125nM) and trametinib plus CuET, or combination of treatments with the JNK inhibitor SP600125 (10µM) for 24, 48 and 72 h. Untreated melanoma cells were used as a control. The relative distribution in the different phases of the cell-cycle was quantified (n = 3, mean ± SD).

Next, the selective JNK inhibitor (JNKi) SP600125 was used to test whether of JNK activity plays a role in the cytotoxicity the combination therapy in BRAF-WT melanoma cells. For this, SKMEL23 and SKMEL113 cells were treated with the combination therapy in addition to the JNKi, before conducting cell viability assays. Through this, it was found that the inhibition of JNK activity mitigated the additional effect of trametinib combined with CuET, while preserving the cytotoxic effect mediated by the MEK inhibitor, as illustrated in Figure 51. In addition, it could be concluded that the cytotoxic effect mediated by the combination of MEK inhibitors and CuET was dependent on activity of JNK signaling and the activation of c-JUN resulted. Interaction of the two compounds in activation of c-JUN, which further activated pro-apoptotic proteins belonging to the BCL-2 family, ending in a significant apoptosis induction. Interestingly, the interaction between both therapies is not totally isolated to the interface of the high amounts of copper administered by ET with the inhibition of the MAPK pathway, but it has already been described that disulfiram molecularly interacts significantly with the MEK1 gene [144], so that a specific inhibition of MEK1 target inhibition leads to a significant synergism of CuET plus the MEK inhibitor trametinib. The viability data confirmed that both drugs potentiate the cytotoxicity in an JNK activation dependent manner.

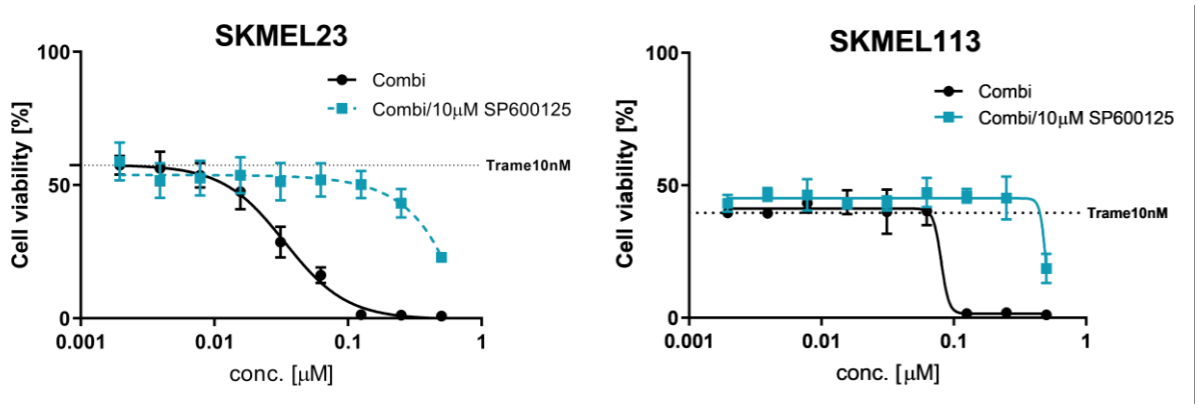

Figure 51: JNK inhibitor strongly decreased the additive effect of MEK inhibitor trametinib and CuET in BRAF-WT melanoma cells under two-dimensional growth conditions *in vitro*. Cell viability assay (MUH assay) of BRAF-WT melanoma cell lines (SKMEL23 and SKMEL113) after treatment with the MEK inhibitor trametinib (10nM) plus the increasing dose of CuET (up 500nM), or combination of trametinib/CuET with the JNK inhibitor SP600125 (10µM) for 72 h. Values are means ± SEM of three replicates (n = 3; mean ± SD). Viability was normalized to untreated control cells.

5.9 Cu^{2+} plays a critical role in the cytotoxicity mediated by the combination of trametinib with CuET

5.9.1 Role of Cu^{2+} in the activity of CuET treatments

Due to the reason that ET showed an inhibition of cell viability about 50% in BRAF-WT melanoma cell lines and this effect was significantly increased by the addition of Cu^{2+}, a point of interest was to confirm that Cu^{2+} plays a critical and substantial role in the cytotoxic activity of CuET, as previously described in the Figure 3. As described above, Cu^{2+} acts as an essential cofactor in melanoma cells for the phosphorylation of MEK. Cu^{2+} is needed by the melanoma cells. In consequence, several therapies using Cu^{2+} chelators for melanoma therapy, likewise ET. Thus, are of interest the role of Cu^{2+}, specially its transport and distribution after treatment with ET, CuET and combined therapy was further investigated.

To demonstrate that Cu^{2+} plays a relevant role in ET or CuET-mediated cytotoxicity, cell viability assays with a copper chelator were conducted. Interestingly, the inhibitory effect achieved by ET or CuET were completely reversed by the addition of a copper chelator (bathocuproindisulfonic acid/BTS). These results strengthened the essential role of copper in the observed cytotoxicity. When treated with ET only, the inhibitory effects were obviously mediated by the copper in the cell culture medium, which is present in fetal calf serum (FCS). Therefore, a second experiment was performed to confirm the effect of FCS by titration of the FCS. ET as monotherapy induced a cytotoxic effect on BRAF-WT melanoma cells when the medium contained 10% FCS, as previously described. Upon titration of the FCS, the cytotoxic

effect of ET was mitigated until completely abolished at 1% FCS. Taken together, this essential role of the Cu^{2+} in the cytotoxic effect mediated by ET and CuET are illustrated in Figure 52.

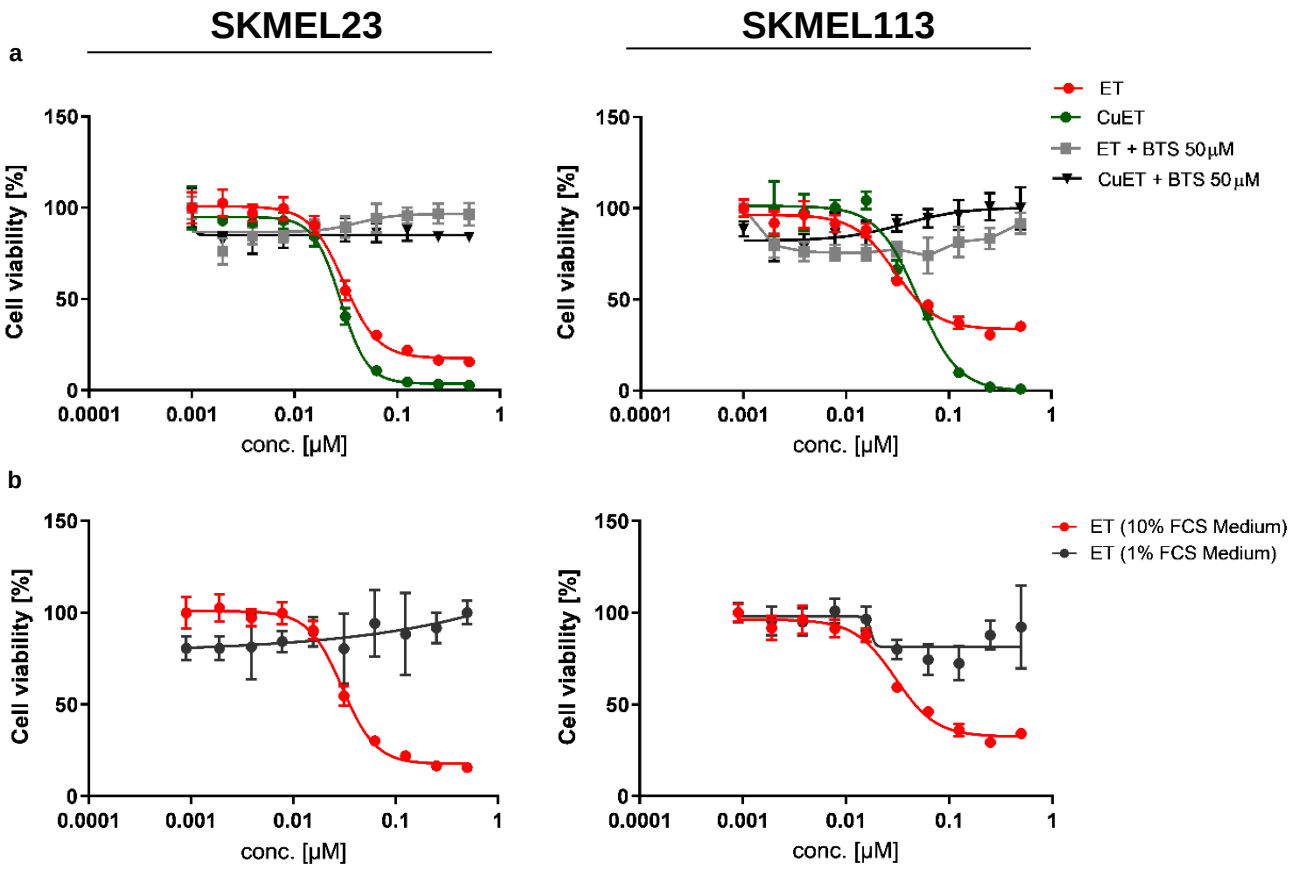

Figure 52: Chelation of copper abolishes the cytotoxic effect of CuET and the cytotoxic effect showed by ET is mediated due the titration of the FCS contained in the medium. a) Cell viability assay (MUH assay) of BRAF-WT melanoma cell lines (SKMEL23 and SKMEL113) after treatment with increasing doses of ET (up 500nM) and CuET (up 500nM), or combination of treatments with bathocuproindisulfonic acid BTS (50µM) for 72 h. **b)** Cell viability assay (MUH assay) of BRAF-WT melanoma cell lines (SKMEL23 and SKMEL113) after treatment with increasing concentrations of ET (up 500nM) in 1% or 10% FCS medium for 72 h. **a/b)** Values are means ± SEM of three replicates (n = 3; mean ± SD). Viability was normalized to untreated control cells.

To confirm the relevance of copper, treatments were combined with a selective intracellular Cu^{2+} chelator. BRAF-WT melanoma cells were treated with CuET up to 500nM in addition to the intracellular chelator ammonium tetrathiomolybdate (TTM) in a clonogenic growth assay. CuET at 250nM completely inhibited the growth of colonies within 14 days. The effects of CuET on BRAF-WT melanoma cells were completely reversed by the addition of the Cu^{2+} chelator ammonium tetrathiomolybdate (TTM) in SKMEL113 cells, proofing the essential role of Cu^{2+}. The results of this experiment are shown in the Figure 53.

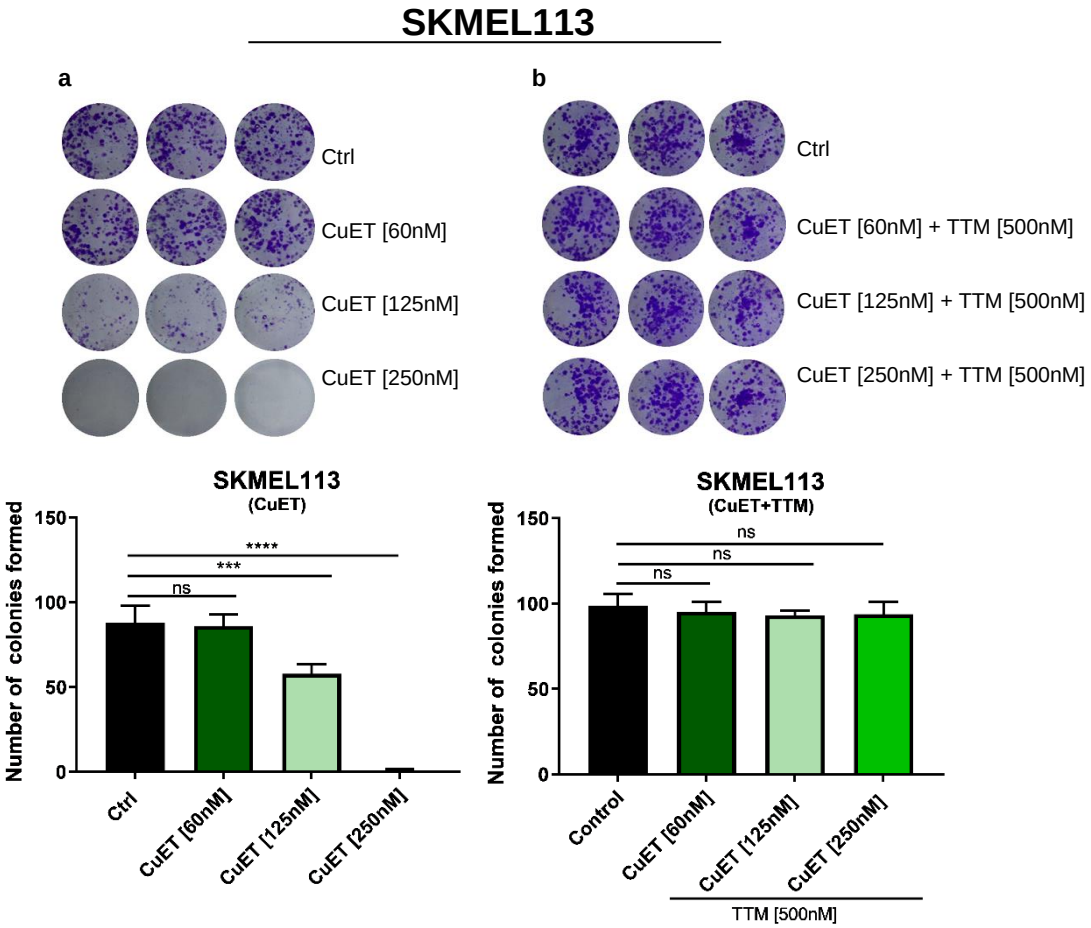

Figure 53: The persistently effects of CuET on BRAF-WT melanoma cells were complete inhibited by the selective Cu^{2+} chelation TTM. Clonogenic growth assay of BRAF-WT melanoma cell lines (SKMEL113) after 14 d-treatment with increasing concentrations of CuET (60, 125 and 250nM) alone **(a)** or in combination with copper chelator TTM (500nM) **(b)**. Cultures were stained with Coomassie Brilliant Blue. Representative images are shown (n = 3; mean ± SD). One-way ANOVA was used to identify the statistical significance associated to untreated (control) and it was followed by Tukey's multiple comparisons test. * $p < 0.05$; ** $p < 0.01$; *** $p < 0.001$; and **** $p < 0.0001$, ns (not significant).

To sum up, the cytotoxic effects mediated by CuET were completely reversible by the addition of different Cu^{2+} chelators, revealing the critical role of Cu^{2+}. However, the role of the trace metal Cu^{2+} on the combined therapy of trametinib with CuET was still unknow. As previously shown, the combination of 10nM of trametinib with CuET had the ability to induce significant cell growth inhibition in BRAF-WT melanoma cells. When SKMEL23 and SKMEL113 were treated additionally with 500nM of the Cu^{2+} chelator TTM to the trametinib/CuET therapy additive effect of CuET to the trametinib was completely abolished, as illustrated in Figure 54. Only, the effect mediated by the MEK inhibitor trametinib remained upon the addition of the copper chelator.

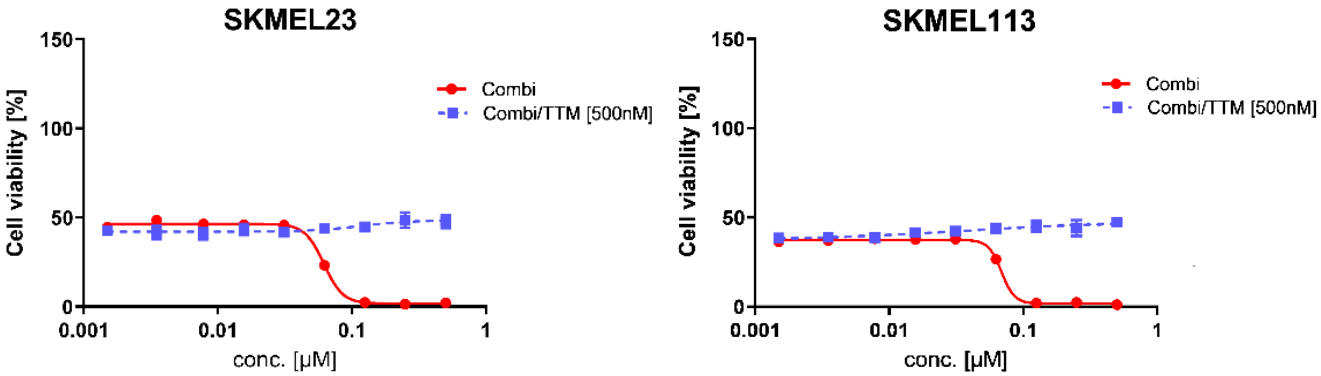

Figure 54: TTM completely abolished the additive effect of MEK inhibitor trametinib and CuET in BRAF-WT melanoma cells under two-dimensional growth conditions *in vitro*. Cell viability assay (MUH assay) of BRAF-WT melanoma cell lines (SKMEL23 and SKMEL113) after treatment with the MEK inhibitor trametinib (10nM) plus the increasing dose of CuET (up 500nM), or combination of trametinib/CuET with the coper chelator TTM (500nM) for 72 h. Values are means ± SEM of three replicates (n = 3; mean ± SD). Viability was normalized to untreated control cells.

Remarkable, these results reinforce the theory of a significant role of copper not only in CuET-mediated cytotoxicity, but also in the combinational effect of trametinib plus CuET. The model proposes that once copper has been transported into the intracellular space it generates severe reactions among which the generation of intracellular ROS and the interaction with MEK are key points concluding in the induction of cell death, probably mediated by apoptosis. Due to these results, it was decided to explore the apoptosis induction by the combination therapy in addition of TTM, as illustrated in Figure 55.

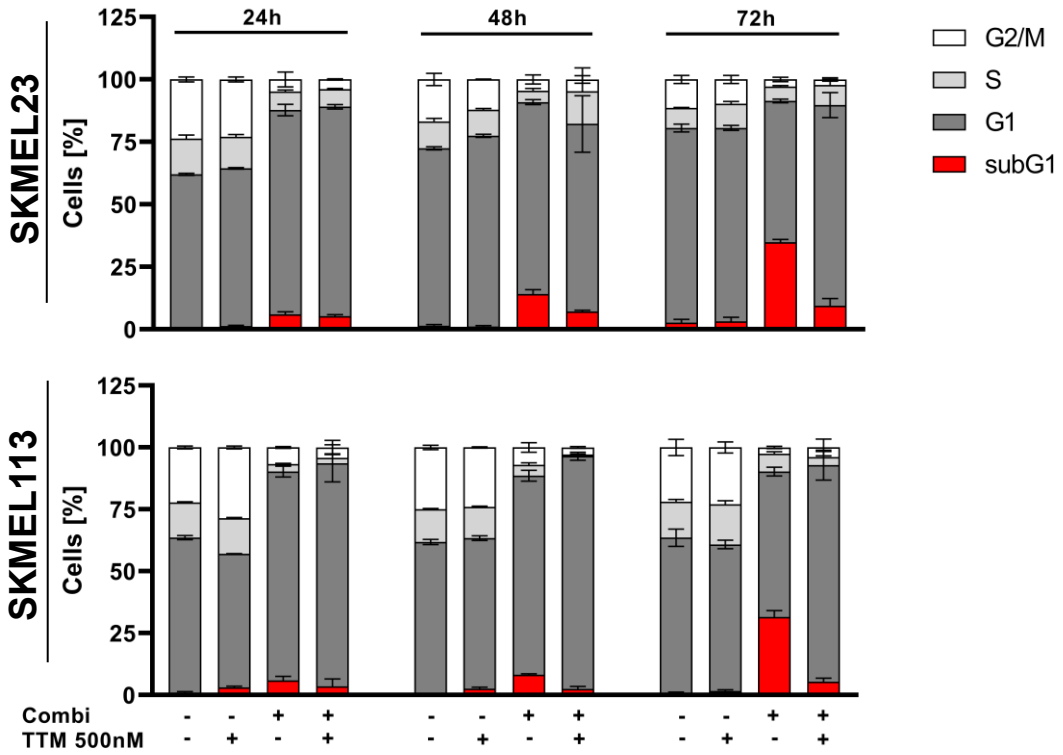

Figure 55: TTM significantly reduced the sub-G1 accumulation (apoptosis induction) mediated by MEK inhibitor trametinib with CuET in in BRAF-WT melanoma cells. Flow cytometric cell-cycle analyses of BRAF-WT melanoma cell lines (SKMEL23 and SKMEL113) after treatment with MEK inhibitor trametinib (10nM), CuET (125nM) and trametinib plus CuET (10nM/125nM) or combinations of treatments with the copper chelator TTM (500nM) for 24, 48 and 72 h. Untreated melanoma cells were used as a control. The relative distribution in the different phases of the cell-cycle was quantified (n = 3, mean ± SD).

For that, SKMEL23 and SKMEL113 cells were treated with the combined therapy with 500nM of TTM for 24, 48 and 72h. Interestingly, TTM completely abolished the apoptosis induction mediated by combination therapy in both BRAF-WT melanoma cell lines, as shown in Figure 55. Taken together, Cu^{2+} mechanistically mediated the cytotoxicity of CuET, and its absence prevented any additive effect to the trametinib-mediated cytotoxicity.

5.9.2 MEK inhibition with CuET enhanced the uptake of Cu^{2+} in BRAF-WT melanoma cells

As described above, Cu^{2+} is an essential trace metal also for melanoma cells, where it acts as a crucial cofactor for several enzymatic activities. Previous results showed that Cu^{2+} played a critical role in cytotoxicity and induction of the apoptosis by the combined therapy with trametinib and CuET in BRAF-WT melanoma cells. In particular the combination therapy exhibited a strong antitumor effect, which was abolished by a Cu^{2+} chelator. This phenomenon

emphasized that through combination therapy the Cu^{2+} triggers a mechanism that concludes in apoptosis. Others have described that once hCtr1-mediated Cu^{2+} transport into the cell occurs, copper is reduced to Cu^{+}, which is highly reactive. This, together with other data, proposed that intracellular copper accumulates in the intracellular space generating high concentrations of ROS, which is highly toxic to BRAF-WT melanoma cells. Intracellular ROS can be partially reduced to H_2O_2 through the cell's antioxidant system, led by glutathione and as an analog NAC. However, when ROS levels pass a threshold it is impossible for ROS-scavengers to mitigate the high toxic ROS levels. Such high intracellular ROS concentrations are only achieved by high intracellular Cu^{2+} accumulation, as it is hypothesized for CuET.

Therefore, intracellular Cu^{2+} levels after combination therapy were explored. The intracellular Cu^{2+} concentration was determined via a spectrophotometric assay in BRAF-WT melanoma. The cells were treated for 6 h in order to have sufficient time for the postulated Cu^{2+} uptake by the cell, but the membrane integrity of the cells was still preserved. This time-point was selected because until 24 h of treatment no toxicity data were observed in BRAF-WT melanoma cells by the combination therapy. As a result, the intracellular Cu^{2+} concentration could be determined. CuET as monotherapy induced high intracellular Cu^{2+} concentrations after 6 h treatment, however this was further significantly enhanced by the addition of trametinib, as shown in Figure 56.

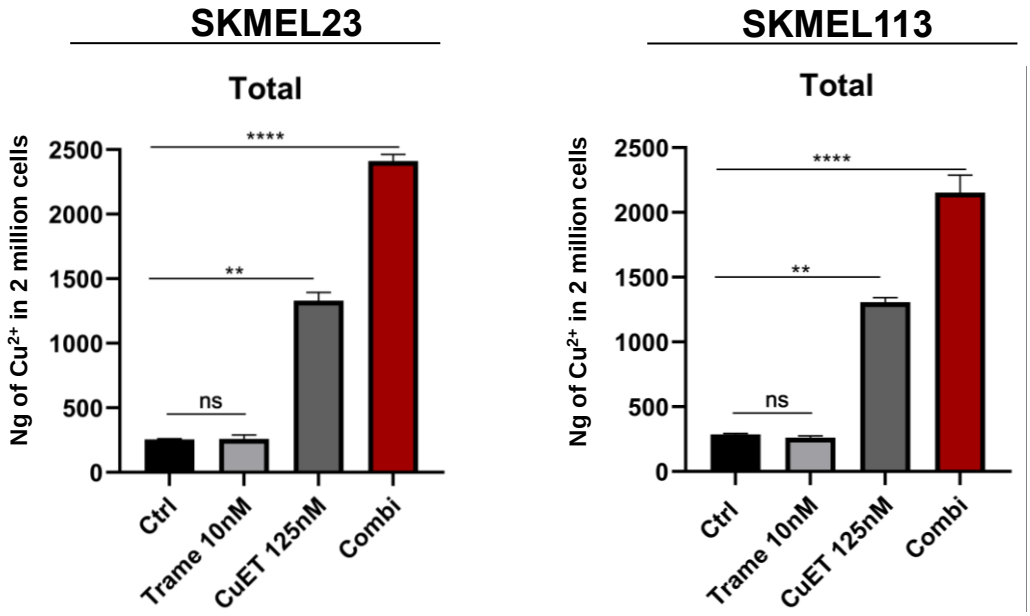

Figure 56: MEK inhibitor trametinib in combination with CuET induced a significant high accumulation of Cu in BRAF-WT melanoma cells. Spectrophotometry analysis at 354nm absorbance for intracellular Cu^{2+} concentration on BRAF-WT melanoma cell lines (SKMEL23 and SKMEL113) after treatment with MEK inhibitor trametinib (10nM), CuET (125nM) and combination for 6 h. Values are means ± SD of three replicates (n = 3, mean ± SD). One-way ANOVA was used to identify the statistical significance associated to untreated (control) and it was followed by Tukey's multiple comparisons test. * $p < 0.05$; ** $p < 0.01$; *** $p < 0.001$; and **** $p < 0.0001$, ns (not significant).

To visualize the intracellular copper after the treatments, the CooperGreen™ test was used. CooperGreen™ test is an ion detection probe, which is specific to detect Cu^+. The particular detection of Cu^+ through the CooperGreen™ probe is based on the fact that Cu^+ plays a major role in the balance of the intracellular redox state, as mentioned above. For this, SKMEL113 melanoma cells were treated for 6 h with CuET as a monotherapy and CuET in combination with trametinib in parallel with the CooperGreen™ substrate. Additionally, 4′,6-diamidino-2-phenylindole (DAPI) was added in order to stain the adenine–thymine-rich (AT) regions in dsDNA to identify the nuclei of the cells. In all cells the nuclei appeared in a healthy shape and cell integrity was preserved. Displaying nuclear integrity was one of the main objectives of limiting the exposure time of the combination therapy to 6 h, considering that this is a period that allows the ET to transfer copper to the intracellular space but no toxicity data had been observed yet. By confocal fluorescence microscopy it was confirmed that CuET as monotherapy caused an accumulation of intracellular Cu^+ compared to the control cells. However, this was significantly enhanced by the combination therapy, as illustrated in Figure 57. This phenomenon was quantified by measuring arbitrary units of fluorescence. This result is presented in Figure 57, where the significant increase in intracellular copper mediated by the combined therapy depicted.

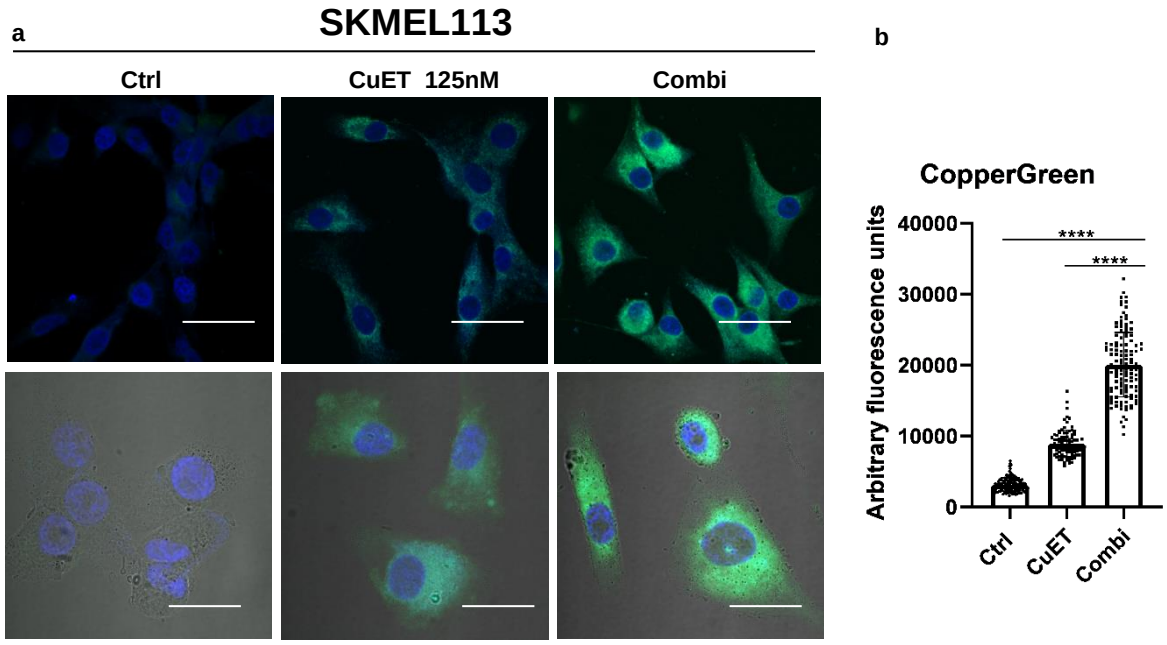

Figure 57: Combination of MEK inhibitor trametinib with CuET induced a significant high accumulation of Cu^+ in BRAF-WT melanoma cells. a) Confocal immunofluorescence analysis for Cu(I) (CooperGreen™) in BRAF-WT melanoma cells after treatment with CuET (125nM) or MEK inhibitor trametinib (10nM) plus CuET (125nM) for 6 h. Nuclei were stained with DAPI (blue). Scale bars represent 25µm. **b)** Quantification of Cu(I) fluorescence signal intensities following confocal immunofluorescence analysis in BRAF-WT melanoma cells after treatment with CuET (125nM) alone or in combination with MEK inhibitor trametinib (10nM). The signals in treated cells were normalized to untreated melanoma cells (n = 4). One-way ANOVA was used to identify the statistical significance associated to untreated (control) and it was followed by Tukey's multiple comparisons test. * $p < 0.05$; ** $p < 0.01$; *** $p < 0.001$; and **** $p < 0.0001$, ns (not significant).

Taken together, these data fully support the postulated shuttling of Cu^{2+} from the extracellular space to the intracellular space by ET, and that this process is significantly enhanced by trametinib. The fact that CuET as monotherapy was able to induce intracellular Cu^{2+} accumulation which was significantly increased by combination therapy strongly indicates that trametinib plays an important role in rendering BRAF-WT melanoma cells more susceptible to Cu^{2+} uptake to the intracellular space. This explains the putative synergism of the MEK inhibitor trametinib with CuET.

5.9.3 Subcellular localization of Cu^{2+} following treatment with combined therapy

Due to the reason that the combination therapy significantly induced intracellular Cu^{2+} accumulation, a point of interest was to identify whether the Cu^{2+} was transported in a specific compartment of the cell. Under normal conditions, following hCtr1-mediated cellular uptake, Cu^{2+} is transported to different intracellular compartments by so called Cu-chaperones. The main function of these chaperones is to prevent accumulation of free unbound copper and to transfer copper to different intracellular compartments, where Cu^{2+} acts as a cofactor for different cellular functions. Overall, this system provides a regulatory mechanism for the of intracellular homeostasis of copper and principally acts as an intracellular antioxidative structure. Thus, as already described, an imbalance of this system leads to significant cellular damage. Several authors have described that high intracellular Cu^{2+} accumulation concludes in ROS formation, which was also detected due to the combined therapy. In addition to the induction of ROS by the combination therapy, activation of P53/P21 signaling and expression of P-γH2AX was evident. All these effects postulated the nucleus as the site of intracellular copper accumulation. This is supported by visual analysis of copper accumulation through the CooperGreen™ assay where a high concentration of Cu^{+} was also observed in the perinuclear space. Therefore, it was extremely important to know about the precise localization of copper inside the cell after treatment with combination therapy. To accomplish that, subcellular fractionation of melanoma cells was performed. Thus, cells were treated for 6 h with the combination therapy and subsequently the intracellular compartments of the cell were separated into cytoplasm, nuclei and mitochondria. Combination therapy induced a significant nuclear Cu^{2+} accumulation, as illustrated in Figure 58.

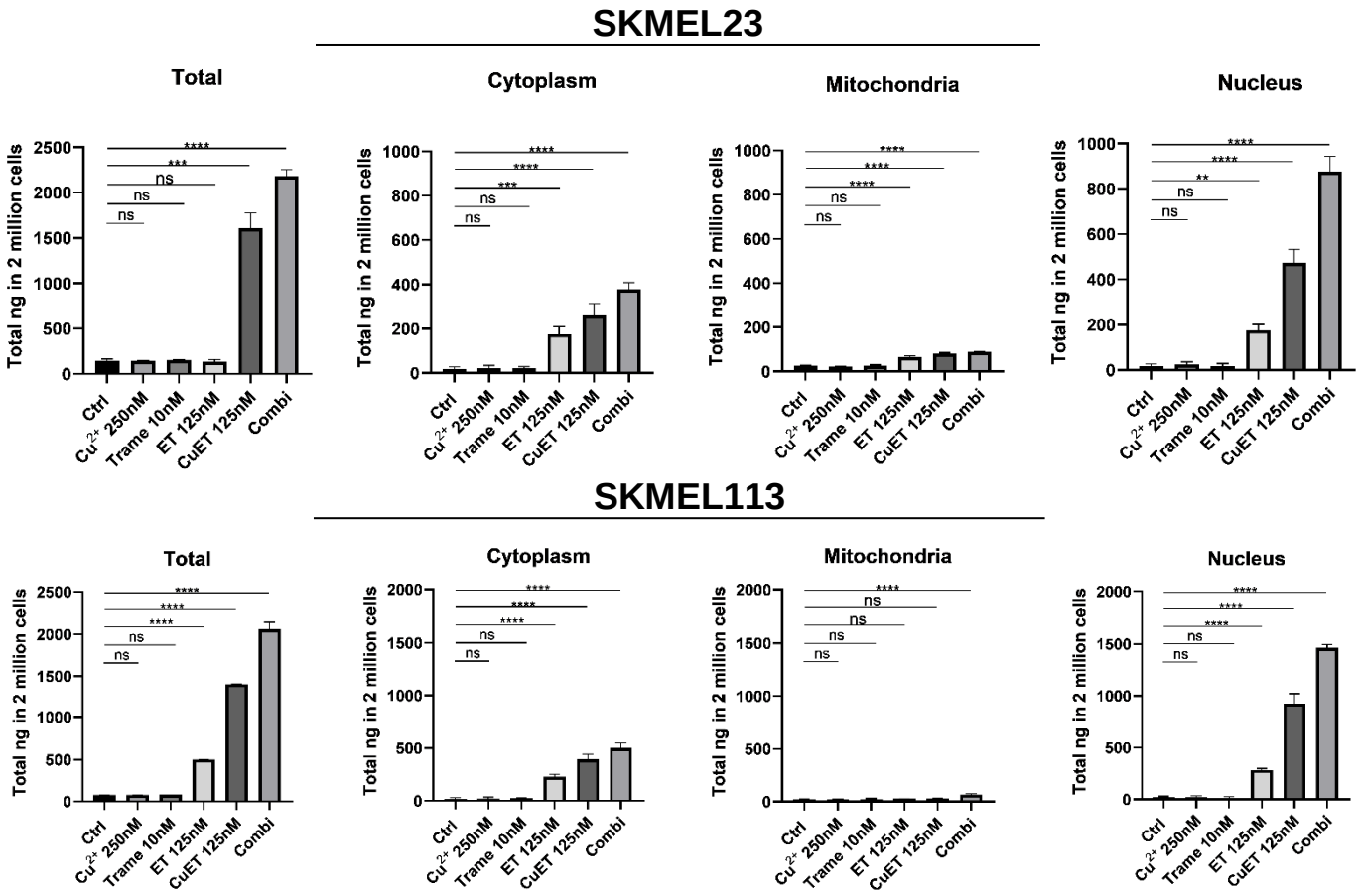

Figure 58: Combination of the MEK inhibitor trametinib with CuET induced an accumulation of copper in the nuclei in BRAF-WT melanoma cells. Spectrophotometry analysis at 354nM absorbance of on BRAF-WT melanoma cell lines (SKMEL23 and SKMEL113) after treatment with Cu^{2+} (500nM), ET (125nM), MEK inhibitor trametinib (10nM), CuET (125nM) and the combination of trametinib (10nM) plus CuET (125nM) for 6 h. After treatment all therapy groups were subsequently fractionated into corresponding subcellular compartments (cytoplasm, nuclei and mitochondria). Values are means ± SD of three replicates (n = 3, mean ± SD). One-way ANOVA was used to identify the statistical significance associated to untreated (control) and it was followed by Tukey's multiple comparisons test. * $p < 0.05$; ** $p < 0.01$; *** $p < 0.001$; and **** $p < 0.0001$, ns (not significant).

In order to corroborate that the subcellular fractionation was successful, a Western blot for the detection of specifically localized proteins was done. SKMEL113 melanoma subcellular fractions were blotted subsequently analyzed with a Lamin-B1 antibody, as shown in Figure 59. LAMIN-B1 is part of the nuclear lamina of the nucleus. Thus, the specific detection of LAMIN-B1 in the nuclear fraction confirmed the correct subcellular fractionation and confirmed the nuclear localization of Cu^{2+} mediated by combination therapy.

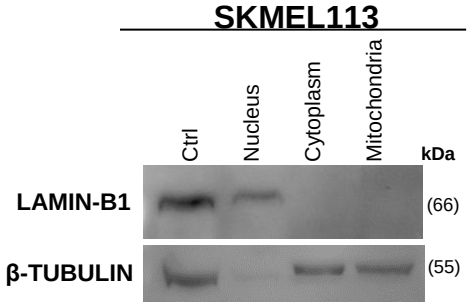

Figure 59: BRAF-WT melanoma cell line SKMEL113 showed high expression of LAMIN-B1 in the nuclear fraction after Subcellular fractionation. Western blot analysis for LAMIN-B1 and β-TUBULIN of whole cell protein lysates of BRAF-WT melanoma cells (SKMEL113) after subcellular fractionation in the intracellular compartments (cytoplasm, nuclei and mitochondria).

As a result, these data confirmed the intracellular Cu^{2+} accumulation by the combination therapy in the nucleus. This mechanism fully correlates with the previous results, where DNA double-strand breaks mediated by the combination therapy were observed by the detection of phospho- γH2AX. Once Cu^{2+} is in the nucleus, it generated high amounts of ROS causing DNA double-strand breaks. With the observation that the Cu^{2+} in the nucleus are significantly higher with combination therapy, it is assumed that there is an extra factor mediating this increase. Therefore, the copper transporters and chaperones were investigated in the following experiments.

5.9.4 Role of ATOX1 in the nuclear translocation of Cu^{2+} by the combination therapy

hCtr1-mediates the cellular Cu^{2+} uptake in melanoma cells under normal conditions. Once Cu^{2+} is in the intracellular compartment, it is transported to the P1B-type ATPases ATP7A and ATP7B, which are located in the Golgi network. The main cytoplasmic Cu-chaperone which is responsible for transporting Cu^{2+} to the Golgi network is ATOX1. ATOX1 is a small protein (68-aminoacids), with the function to bind Cu^{2+} by its conserved CXXC motif, as previously described. After binding the Cu, ATOX1 transports and delivers it to the Copper acceptors (ATP7A/B) by direct protein-protein interactions. No specific transcription factors have been reported to regulate the expression of human Cu^{2+} transporter proteins, particularly *ATOX1*. However, in the last years it has been suggested that *ATOX1* has a dual functionality, such that, additionally to its function as a cytoplasmic chaperone, it could act as transcription factor in the nucleus. This postulated dual mechanism for the function of *ATOX1* could represent a mechanism how Cu^{2+} is transported to and accumulates in the nucleus. To explore

the role of *ATOX1* as a putative Cu^{2+} transporter into the nucleus, down-regulation of the RNA expression of *ATOX1* in BRAF-WT melanoma cells was achieved by siRNA. First, the knock-down of the *ATOX1* gene expression by siRNA transfection in SKMEL23 and SKMEL113 was carried out. The relative expression of *ATOX1* was explored after 48h of the transfection in both cell lines, as by RT-PCR illustrated in Figure 60.

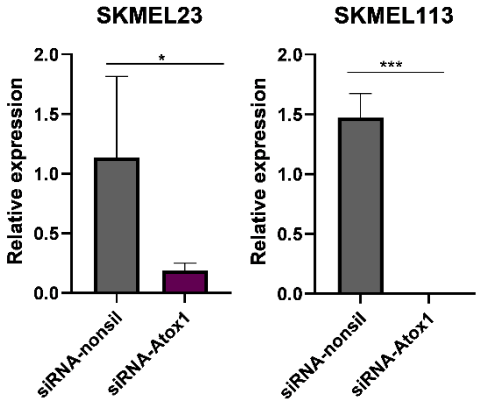

Figure 60: BRAF-WT melanoma cell lines showed a down-regulation of *ATOX1* expression via siRNA transfection. Transcript expression (real-time qPCR) of *ATOX1* on BRAF-WT melanoma cells (SKMEL23 and SKMEL113) transfected with control siRNA or siRNA directed against *ATOX1* 48 h after transfection. *TBP* was used as a reference gene. The relative ratio was calculated with the Light-Cycler® 96 software. Samples were measured in triplicates and the values are the means ± SD of four replicates. One-way ANOVA was used to identify the statistical significance associated to untreated (control) and it was followed by Tukey's multiple comparisons test. * $p < 0.05$; ** $p < 0.01$ and *** $p < 0.001$, ns (not significant).

Additionally, the knock-down of *ATOX1* after the siRNA transfection was confirmed by Western blot analyses. The relative expression of *ATOX1* and the protein level confirmed a down-regulation of the *ATOX1* after siRNA transfection, as is illustrated in Figure 61.

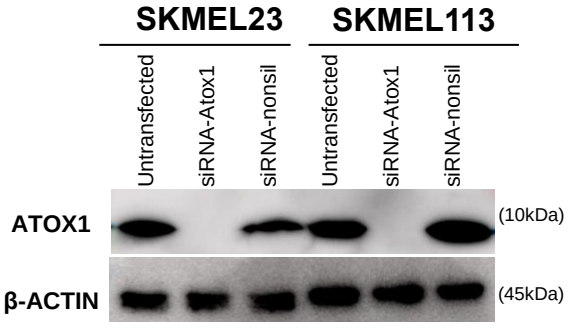

Figure 61: BRAF-WT melanoma cell lines showed a down-regulation of ATOX1 expression via siRNA transfection. Western blot analysis for ATOX1 of whole cell protein lysates of BRAF-WT melanoma cells (SKMEL23 and SKMEL113) 48 h after transfection with control siRNA or siRNA directed against ATOX1. β-ACTIN was used as loading control.

Due to the reason that ATOX1 was postulated to be the main regulator of intracellular Cu^{2+} transport into the nucleus, the nuclear Cu^{2+} levels in ATOX1 down-regulated-melanoma cells after combination therapy were explored. Particularly it was of interest whether down-regulation of ATOX1 decreased the Cu^{2+} accumulation in the nucleus. To this, siRNA transfected-melanoma cells were treated with combination therapy and then fractionated and the Cu^{2+} concentrations in each intracellular compartment were measured. Interestingly, down-regulation of the ATOX1 protein abolished the transport of Cu^{2+} into the nucleus after 6 h of treatment with the combination therapy in both BRAF-WT melanoma cell lines, as illustrated Figure 62. These data confirmed the proposed mechanism that the intracellular transport of Cu^{2+} into the nucleus is mediated via the cytoplasmic Cu-chaperone ATOX1.

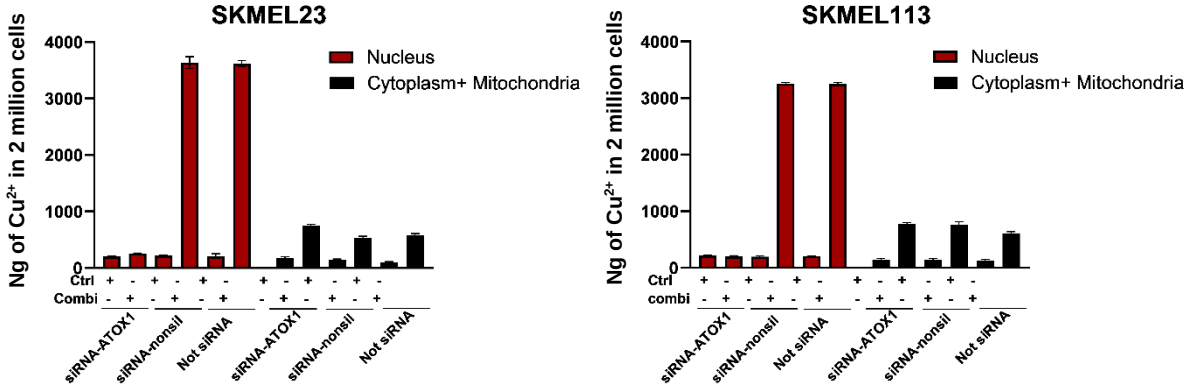

Figure 62: Down-regulation of ATOX1 abolished the Cu^{2+} transport into the nucleus mediated by combination therapy in BRAF-WT melanoma cells. Spectrophotometry analysis at 354nM absorbance for intracellular Cu^{2+} concentration on nuclear and cytoplasmatic cellular subfractions of BRAF-WT melanoma cell lines (SKMEL23 and SKMEL113) transfected with control siRNA or siRNA directed against ATOX1 after treatment with the combination of MEK inhibitor trametinib (10nM) plus CuET (125nM) for 6 h. Samples were measured in triplicates and the values are the means ± SD of three replicates.

To summarize, these data confirmed that ATOX1 plays a main role in the intracellular transport of Cu^{2+} into the nucleus, concluding in high nuclear Cu^{2+} levels. It seems that ATOX1 was the key mechanisms linking copper uptake with therapy effects of the combination therapy. Thus, as initial approach to investigate the efficacy of combination therapy in ATOX1 knockdown BRAF-WT melanoma cells, viability assays (MUH assay) were conducted. SKMEL23 and SKMEL113 melanoma cells with *ATOX1*-knockdown were treated with combined therapy and viability was measured after 72 h as illustrated in Figure 63. The *ATOX1* knockdown reduced sensitivity to the combination therapy of BRAF-WT melanoma cells and *ATOX1* knockdown decreased the cytotoxic effect mediated by combination therapy. This demonstrates the importance of ATOX1 in the cell death mechanism induced by combination therapy.

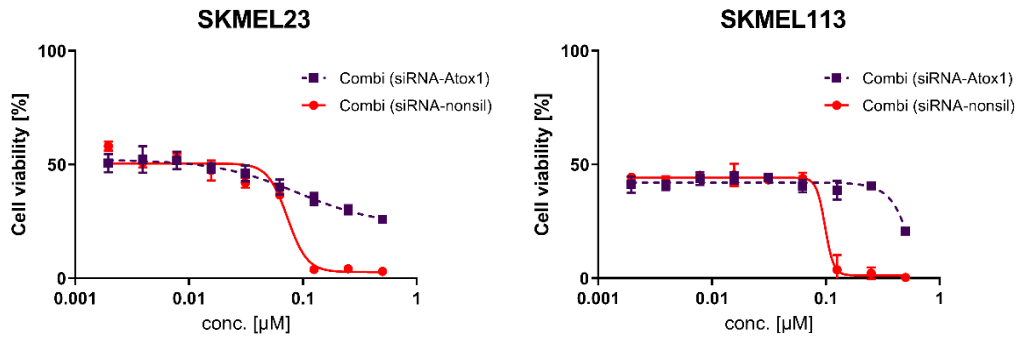

Figure 63: ***ATOX1*** **down-regulated BRAF-WT melanoma cells showed lower sensibility to the treatment with combination of trametinib and CuET under two-dimensional growth conditions** ***in vitro***. Cell viability assay (MUH assay) of BRAF-WT melanoma cell lines (SKMEL23 and SKMEL113) transfected with control siRNA or siRNA directed against *ATOX1* after treatment with the MEK inhibitor trametinib (10nM) plus the increasing dose of CuET (up 500nM) for 72 h. The treatment started after 24 h of the transfection. Values are means ± SEM of three replicates (n = 3; mean ± SD). Viability was normalized to untreated control cells.

5.10 *In vivo* efficacy of the MEK inhibitor trametinib in combination with CuET in BRAF-WT melanoma model

Based on the profound inhibitory effects of the combination of the MEK inhibitor trametinib with CuET on tumor growth in 2D and 3D BRAF-WT melanoma models, the *in vivo* application was tested in the following steps. To this end, the growth of subcutaneous BRAF-WT xenografts in immunocompromised mice was measured in response to the combination of trametinib and CuET and compared to vehicle treated controls. The BRAF-WT melanoma cell lines TÜMEL62-1, TÜMEL110 and TÜMEL173 were injected in NOD scid gamma (NSG) mice and treated with the combination therapy. PET/MRT imaging scan was carried out in order to analyses the tumor copper uptake after the treatment with the help of positron emitting copper-64. This imaging analysis was done in collaboration with the Werner Siemens Imaging Center from the University of Tübingen. Copper-64 uptake was compared to melanoma-bearing animals that did not receive therapy. This experiment was approved by the Regierungspräsidium Tübingen under the license number HT01/20G.

The mice in the experiment were divided into two groups: vehicle control group (sham) and combination group that received MEK inhibitor trametinib (at 0.3 mg/kg per os) with DSF (50 mg/kg per os). Since both drugs are orally bio-available they were applied by oral gavage. The MEK inhibitor trametinib was applied once a day (0.3 mg/kg per os) dissolved in an emulsion containing 0.5% CremophorEL and 0.2% DMSO as vehicle. In order to guarantee the presence of enough copper ions to form the Cu^{2+}/diethyldithiocarbamate complex (CuET), the drinking water of the mice was supplemented with additional copper gluconate (1.2µg/mL). To

this end, the growth of the BRAF-WT melanoma xenografts (TÜMEL62-1, TÜMEL110 and TÜMEL173) was observed in response MEK inhibitor trametinib with CuET therapy in the immunocompromised mice and compared to the vehicle treated controls. This is graphically illustrated in Figure 64 and 65.

Therapy started as soon as the tumors that formed subcutaneous injection of the TÜMEL melanoma models were palpable and reached a volume of 40-60 mm^3. Then, mice were randomized into combination therapy and vehicle control group (sham). Both study groups, combination group (trametinib/DSF) and vehicle control group were treated for 14 d and subsequently the PET/MRT scan was achieved. According to the ethical guidelines, the experiment was terminated before the tumor volume exceeded 1,000 mm^3, which did not occur during this experiment. The characteristic of the combination therapy group and vehicle control group are completely illustrated in the table 38.

TÜMEL model		**Group size (n)**	**Mean weight at the therapy start (g)**	**Mean weight at the therapy end (g)**
TÜMEL62-1	Control	***2***	***22.6***	***22.5***
	Treated	***2***	***23.9***	***23.3***
TÜMEL110	Control	***2***	***35.2***	***35.9***
	Treated	***2***	***36.9***	***36.6***
TÜMEL173	Control	***2***	***30.0***	***30.5***
	Treated	***2***	***30.4***	***30.0***

Table 38: Characteristics of the Therapy Groups in the TÜMEL Xenograft melanoma models.

Accordingly, the tumor growth curves representing the tumor volumes measured at the indicated time points are illustrated in Figure 64. These results revealed a significant deceleration of tumor growth during the first six days after initiation of the combination therapy in TÜMEL110, and, the tumor volumes remained stable the following four days. Contrary, the TÜMEL62-1 and TÜMEL173 melanoma models displayed a rapid stop of tumor growth once the combination therapy was initiated. These models (TÜMEL62-1 and TÜMEL173) exhibited a big difference when the treated group was compared to the control group. However, the tumor sizes remained stable once the therapy with the combination therapy was started, and it did not exhibit a reduction or shrinkage of the tumors in all three models during the ten days of treatment. The results of these experiments are summarized in Figure 64.

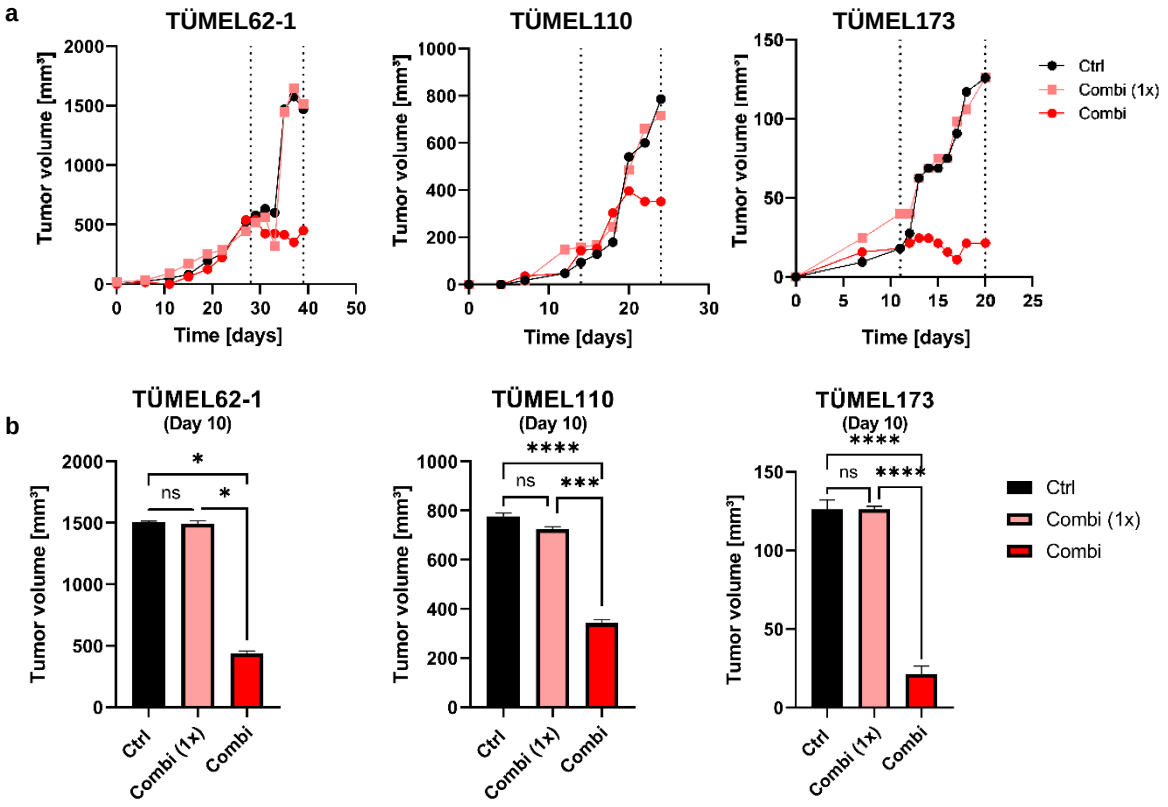

Figure 64. ***In vivo*** **effect of the combination of MEK inhibitor trametinib and CuET on BRAF-WT melanoma models. a)** Subcutaneous xenograft growth of the BRAF-WT melanoma cell line (TÜMEL62-1, TÜMEL110 and TÜMEL173) in NOD scid gamma (NSG) mice under combination therapy of MEK inhibitor trametinib with DSF. The combination of trametinib with DSF negatively affects tumor growth of BRAF-WT melanoma tumor model *in vivo*. Subcutaneous xenograft growth of the BRAF-WT melanoma model (TÜMEL62-1, TÜMEL110, TÜMEL173) in NOD scid gamma (NSG) mice under combined therapy (trametinib/DSF). The dotted lines indicate the therapeutic time window from star of treatment to conclusion of treatment. Mean tumor growth (±SEM, n = 2;) for the combination therapy of trametinib with DSF and the controls are exhibited. The mice were treated along 10 days. **b) S**tatistical analysis of the observed differences in tumor growth of BRAF-WT melanoma tumors in NSG mice in the following therapeutics groups after treatment for 10 d. One-way ANOVA was used to identify the statistical significance associated to untreated (control) and it was followed by Tukey's multiple comparisons test. * $p < 0.05$; ** $p < 0.01$; *** $p < 0.001$; and **** $p < 0.0001$, ns (not significant).

When comparing the terminal sizes of the tumors in all three melanoma models at the end of the experiment after 10 days treatment there was a significant difference in the tumor volumes of the mice receiving the combination therapy when compared with the control group. However, no reduction in the tumor volume at the end of combination therapy was observed in any of the models compared to tumor volume at the start of therapy. Therefore, similar to the 3D spheroid model, no tumor shrinkage was observed in any of the models PDX. Although the treated tumors did not significantly reduce their sizes, they did not grow at all. It shows the impact of the therapy based on the combination of the MEK inhibitor trametinib and DSF or CuET in BRAF-WT melanoma models.

The analysis of the tumor sizes at the end day of the experiment of each of the BRAF-WT melanoma tumor models of TÜMEL62-1, TÜMEL110 and TÜMEL173 was performed.

This analysis specifically confirmed a statistically significant difference between the control group and the group receiving the combination therapy. Furthermore, the combination therapy group also showed a statistically significant difference against the second group which received only one dose of the combination therapy. Similarly, as previously mentioned, magnetic resonance imaging (MRI) of the tumors was performed in each of the models studied. It is graphically depicted here that the combined therapy significantly decreased the tumor size in each of the melanoma models, as it shows in Figure 65.

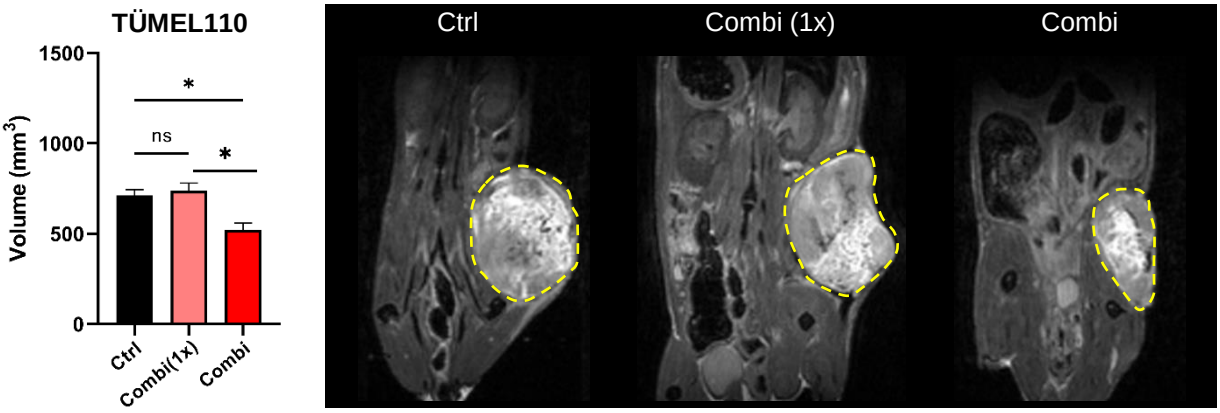

Figure 65. Conscious MEK inhibitor trametinib with DSF-treatment reduces TÜMEL110 tumor growth *in vivo*. Tumor volume of TÜMEL110 melanoma model from mice treated once (DSF(X)) or repeatedly with combination therapy or remained sham-treated (p.o.). Tumor volumes were determined by T2-weighted MR imaging. Representative anatomical T2-weighted MR images for visualization of the combination therapy (1x/rep) or sham-treated (Ctrl) subcutaneous TÜMEL110 tumors. Images were acquired at the end of the experiment. DSF (x) = one dose prior to the end of the experiment. Tumors are outlined with yellow dashed lines. Data are expressed as the mean ± SEM. Statistical significance was determined by Dunnett's multi comparison test. *p<0.05, ns (not significant versus untreated control).

To corroborate the inhibitory effect on the TÜMEL62-5 and TÜMEL173 melanoma models *in vivo*, we performed an analysis of tumor volume between the 3 study groups, finding that the combined therapy generated a significant negative effect on tumor growth in both models, which follows the same trend observed previously, as it shows in Figure 66.

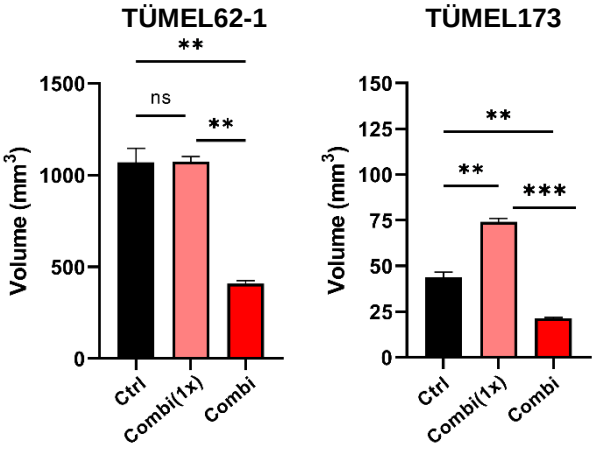

Figure 66. The MEK inhibitor trametinib in combination with CuET negatively affects tumor growth of BRAF-WT melanoma cells *in vivo*. Statistics analysis for Subcutaneous xenograft growth of the BRAF-WT melanoma cell line (TÜMEL62-1 and TÜMEL173) in NOD scid gamma (NSG) mice under combination therapy of MEK inhibitor trametinib with DSF. Mean tumor growth (±SEM, n = 2;) after 10-d of therapy of trametinib with DSF and combination one (combi1x). Statistical significance was determined by Dunnett's multi comparison test. *p<0.05, **p<0.01; and *** p < 0.001, ns (not significant).

At the conclusion of the experiment, all the tumors were excised and processed for analysis. To this end, mire received a final treatment with the respective therapy 24 h before the PET/MRT scan was performed. Following a correct and accurate well-fixed, a detailed observation of intranuclear detail was performed by hematoxylin and eosin staining (H&E). All the untreated BRAF-WT melanoma models (TÜMEL62-1, TÜMEL110 and TÜMEL173) exhibited a rounded and well-defined nucleus, with a well-distributed and intense central blue-purple condensation which is corresponding of a well highly condensed condensation of heterochromatin, referring to accelerated cell growth. It showed that in the control and combination therapy groups, the tumor areas were identified, including viable tumor cells in terms of morphological integrity.

The morphology of the nucleus in the combination therapy changed. It was observed that the combination therapy generated abnormalities in the nuclear shape, which started to be discretely oval with multiple nuclear membrane abnormalities including vacuolization of the nucleus, which it was observed in about 30% of the nuclei lacking heterochromatin. These data support the hypothesis previously demonstrated *in vitro*, where the combination therapy of MEK inhibitor trametinib plus CuET generates DNA damage. It illustrated in Figure 67-69.

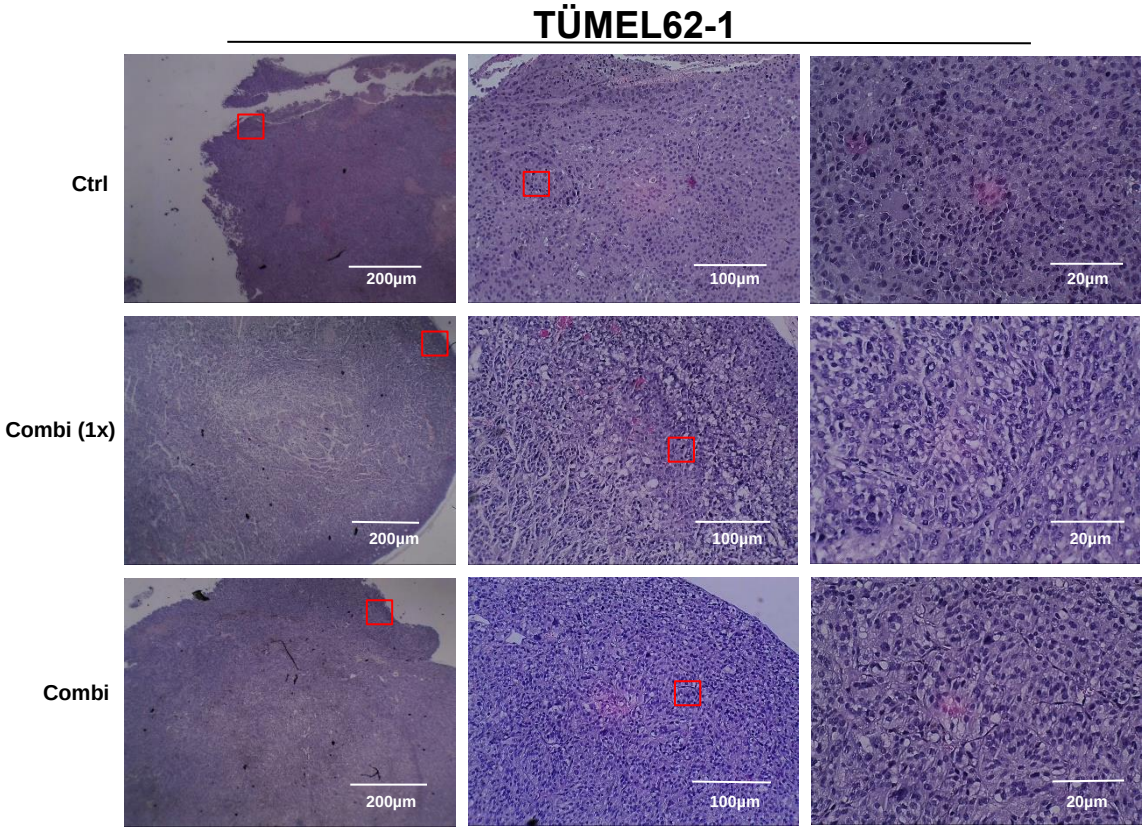

Figure 67. HE staining of the TÜMEL62-1 *in vivo* melanoma model under 10 days combination therapy. Hematoxylin und Eosin (HE) staining images of BRAF-WT melanoma model biopsies (TÜMEL62-1) were from NSG mice's after therapy with MEK inhibitor trametinib plus DSF for 10 d. Corresponding mouse ID and the respectively received *in vivo* therapy is indicated. Scaled to the figure to 200µm, 100µm, and 20µm are illustrated.

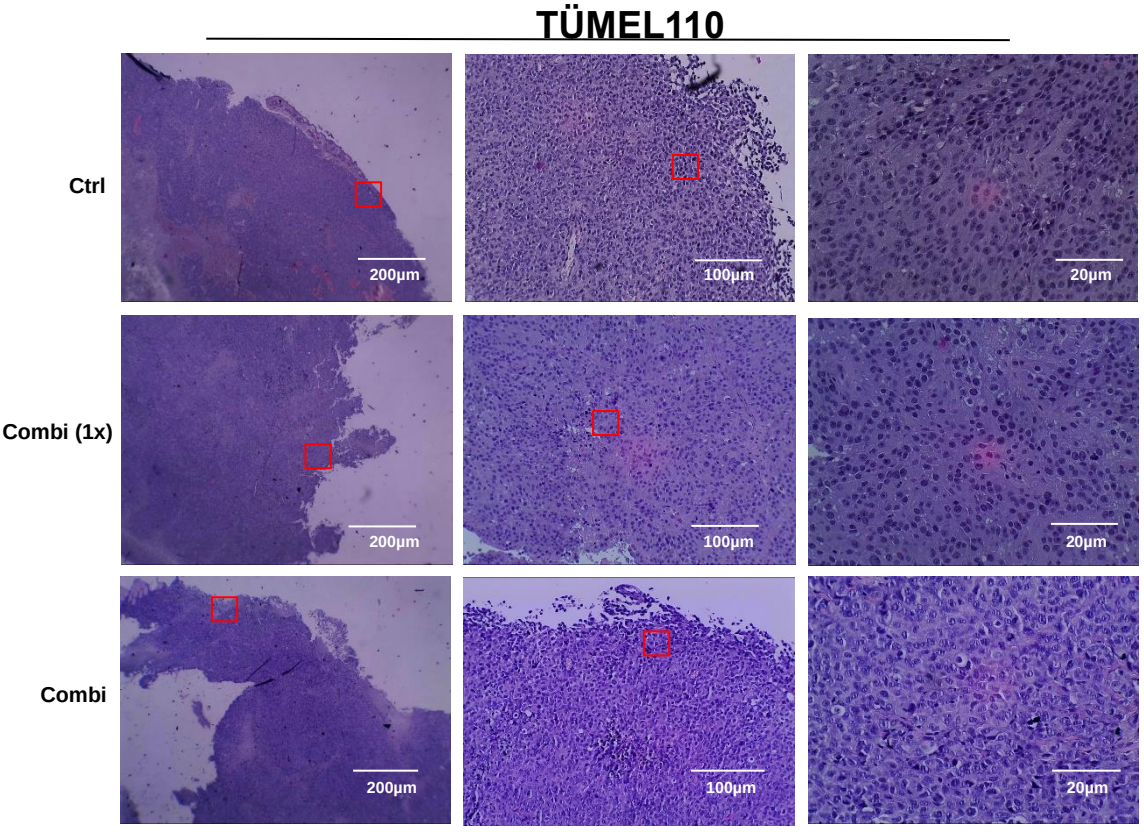

Figure 68. HE staining of the TÜMEL110 *in vivo* melanoma model under 10 days combination therapy. Hematoxylin und Eosin (HE) staining images of BRAF-WT melanoma model biopsies (TÜMEL62-1) were from NSG mice's after therapy with MEK inhibitor trametinib plus DSF for 10 d. Corresponding mouse ID and the respectively received *in vivo* therapy is indicated. Scaled to the figure to 200µm, 100µm, and 20µm are illustrated.

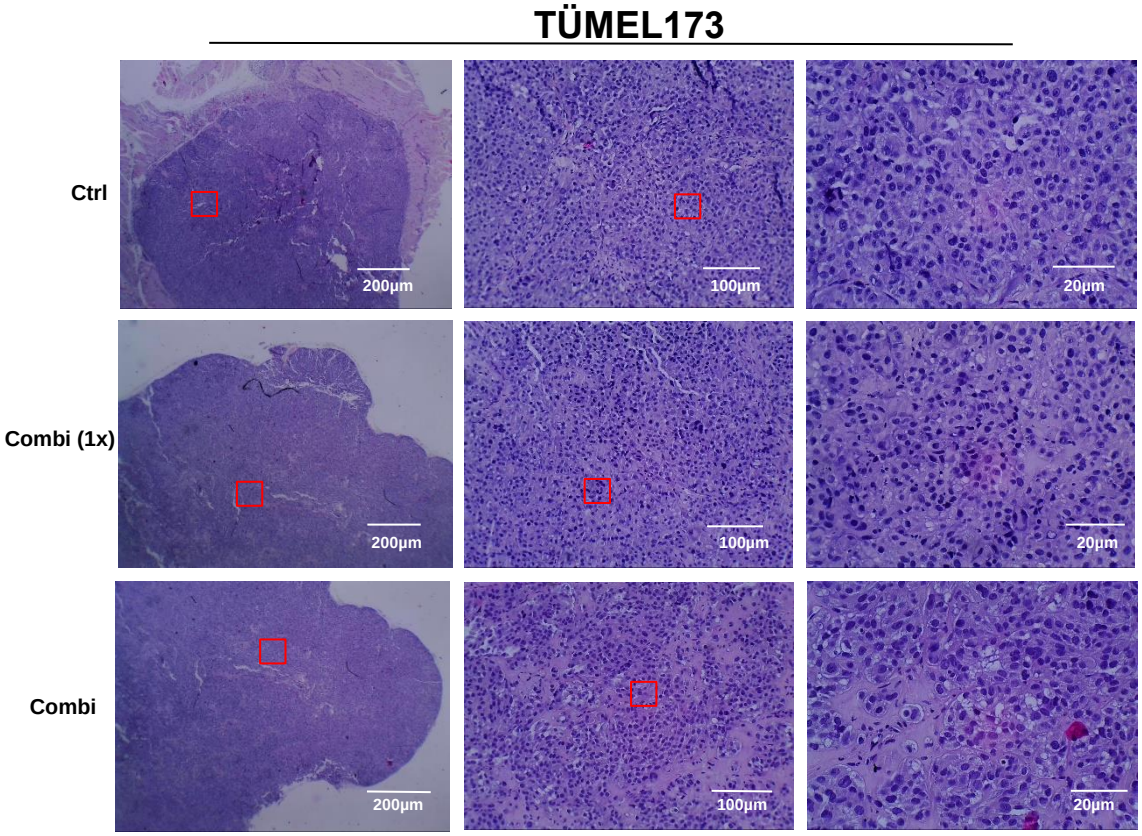

Figure 69. HE staining of the TÜMEL62-1 *in vivo* melanoma model under 10 days combination therapy. Hematoxylin und Eosin (HE) staining images of BRAF-WT melanoma model biopsies (TÜMEL62-1) were from NSG mice's after therapy with MEK inhibitor trametinib plus DSF for 10 d. Corresponding mouse ID and the respectively received *in vivo* therapy is indicated. Scaled to the figure to 200µm, 100µm, and 20µm are illustrated.

As a correlate effective MEK inhibition in the combined therapy, ERK phosphorylation and c-JUN expression was assessed in the TÜMEL62-1, TÜMEL110 and TÜMEL173 tumors xenografts of the combination therapy and control groups by immunohistochemistry. Immunohistochemical staining's of the xenografts exhibited a significant reduction of phosphorylated ERK levels in the tumors of the combination therapy mice compared to the vehicle control. In addition, a significant induction of c-JUN by combination therapy was seen in all three TÜMEL models. These data indicated that the tumor cytotoxicity mediated by the combination of trametinib plus CuET is dependent on c-JUN activation. For the above-mentioned reasons, it was decided to carry out the stain for phosphorylated ERK using a specific antibody. A significant difference between each of the groups was clearly observed, and these results are illustrated in Figures 70, 71 and 72.

In the first melanoma model (TÜMEL62-1) the control group showed a high expression of phosphorylated ERK which is mainly present at the tumor margin. This emphasized that MAPK activation plays a critical role in the growth and development of malignant melanoma. Interestingly, it was observed that the already group that received the combination therapy only once showed a decrease in the expression of ERK phosphorylation in this model. This effect was more pronounced in the group that received the combination therapy for 10 days, confirming the theory that the combination of the MEK inhibitor trametinib with CuET persistently inhibits ERK activation, as illustrated in the Figures 70, 71 and 72.

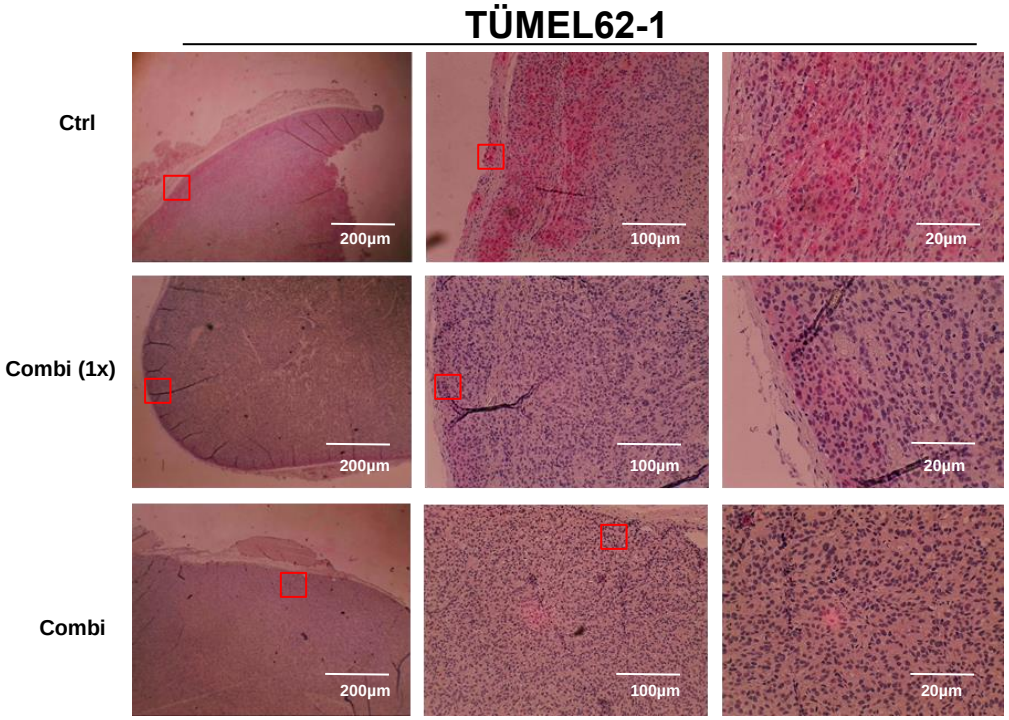

Figure 70. Phospho-ERK staining of the TÜMEL62-1 melanoma model under 10 days of combination therapy. Immunohistochemical staining of phosphorylated ERK (pERK) on BRAF-WT melanoma biopsies (TÜMEL62-1) obtained after treatment with MEK inhibitor trametinib plus CuET in NOD scid gamma (NSG) mice for 10 days. Corresponding mouse ID and the respectively received *in vivo* therapy is indicated. pERK levels are shown in red (Fast Red substrate) with a hematoxylin counter staining. Thickness of the tissue slices are 10 µm. Scaled to the figure to 200µm, 100µm, and 20µm are illustrated.

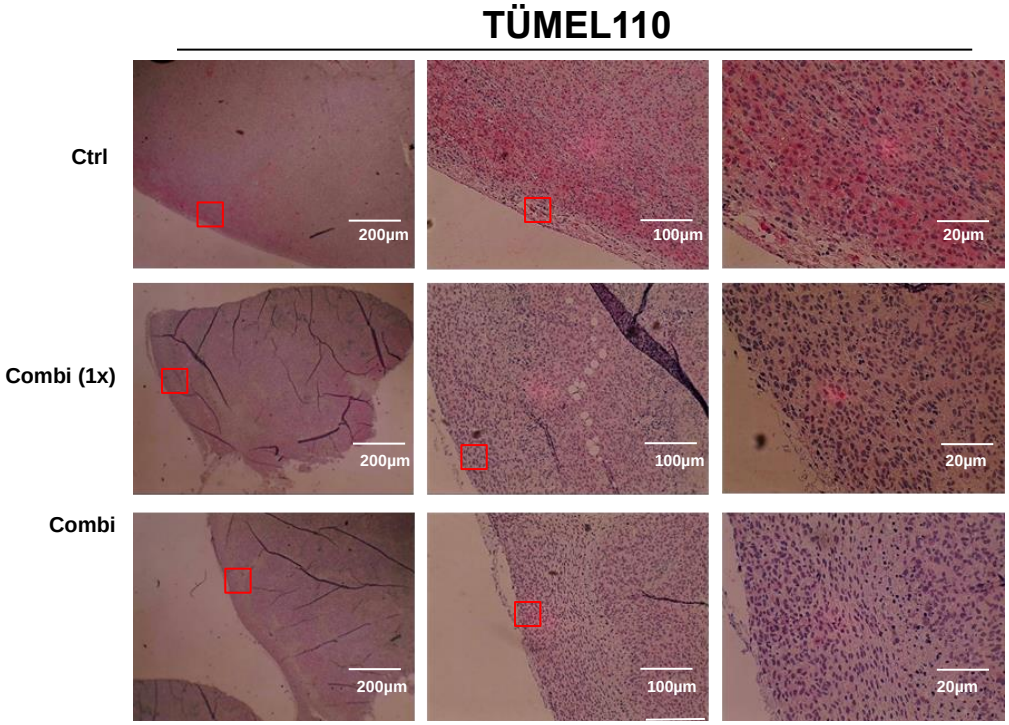

Figure 71. Phospho-ERK staining of the TÜMEL110 melanoma model under 10 days of combination therapy. Immunohistochemical staining of phosphorylated ERK (pERK) on BRAF-WT melanoma biopsies (TÜMEL62-1) obtained after treatment with MEK inhibitor trametinib plus CuET in NOD scid gamma (NSG) mice for 10 days. Corresponding mouse ID and the respectively received *in vivo* therapy is indicated. pERK levels are shown in red (Fast Red substrate) with a hematoxylin counter staining. Thickness of the tissue slices are 10 µm. Scaled to the figure to 200µm, 100µm, and 20µm are illustrated.

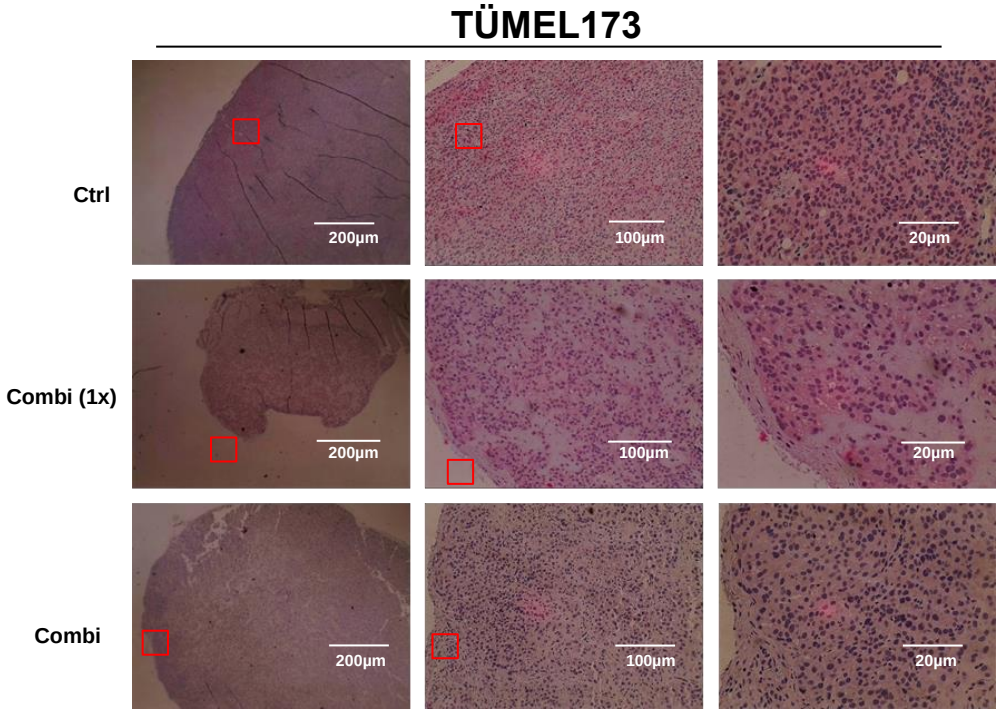

Figure 72. Phospho-ERK staining of the TÜMEL173 melanoma model under 10 days of combination therapy. Immunohistochemical staining of phosphorylated ERK (pERK) on BRAF-WT melanoma biopsies (TÜMEL62-1) obtained after treatment with MEK inhibitor trametinib plus CuET in NOD scid gamma (NSG) mice for 10 days. Corresponding mouse ID and the respectively received *in vivo* therapy is indicated. pERK levels are shown in red (Fast Red substrate) with a hematoxylin counter staining. Thickness of the tissue slices are 10 µm. Scaled to the figure to 200µm, 100µm, and 20µm are illustrated.

Through this technique, the results previously observed *in vitro* were fully confirmed. On the one hand, it was observed that all BRAF-WT melanoma models showed down-regulation of ERK phosphorylation (pERK) after a single application of the combination therapy to the melanoma bearing mice. This inhibition of ERK phosphorylation was significantly greater and persistent in the group that received the combination therapy for 10 days. No re-activation of ERK phosphorylation activity was observed even after 10 days of treatment, indicating that CuET could prevent BRAF-WT melanoma cells from developing resistance to MEK inhibitors. In addition, the untreated models showed different levels of pERK. However, all models studied had a significantly higher signal in the control groups than in the treated groups, strongly indicating that subsequent and persistent MAPK pathway activity is highly critical for their development and progression. For the detection of c-JUN in the tumors of the PDX models, immunofluorescence co-staining of pERK with c-JUN un were carried out in order to explore a putative up-regulation of c- JUN in association with the pERK inhibition mediated by the combination therapy. This is illustrated in the Figures 73, 74 and 75.

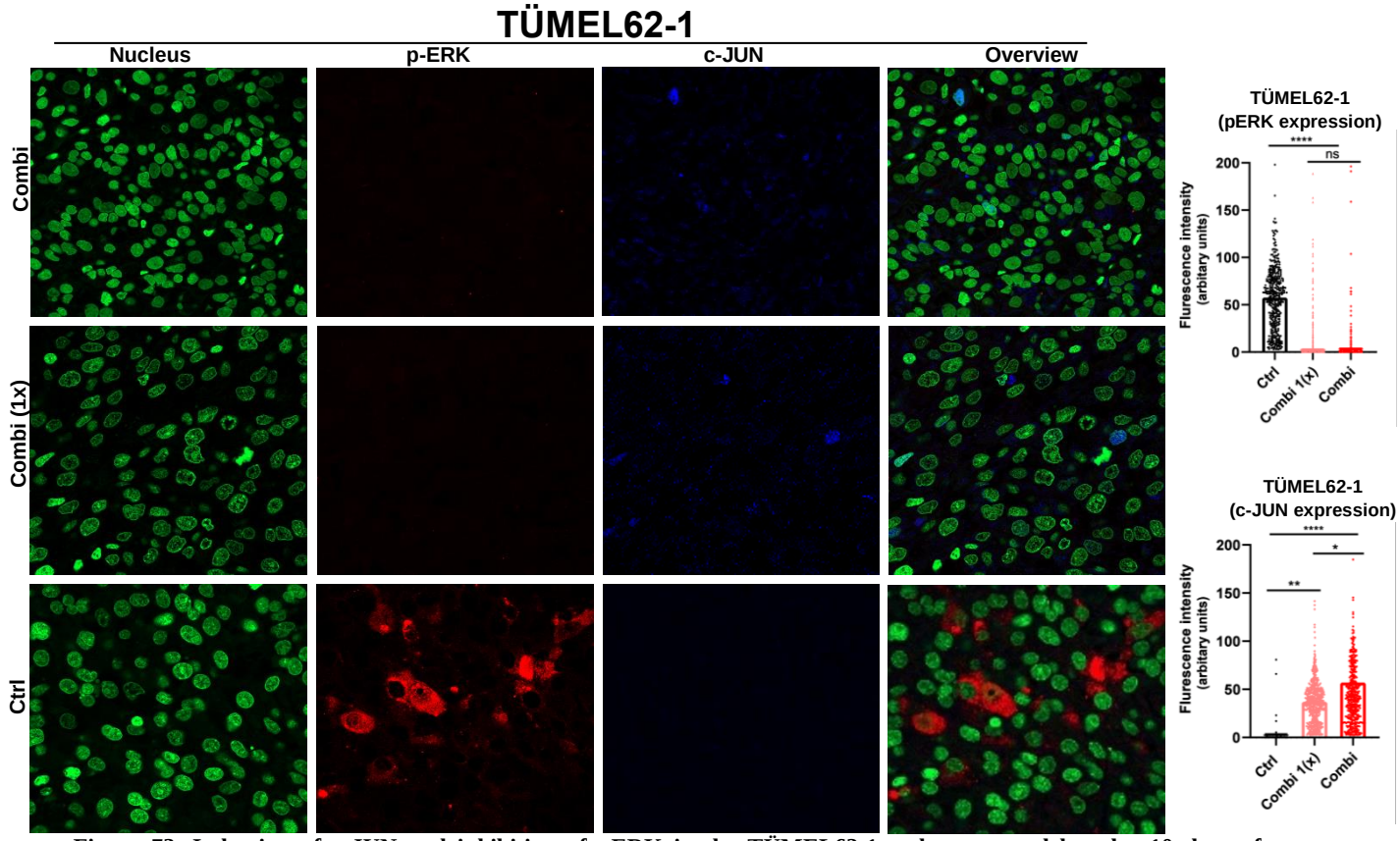

Figure 73. Induction of c-JUN and inhibition of pERK in the TÜMEL62-1 melanoma model under 10 days of combination therapy. Confocal immunofluorescence analysis of phosphorylation of ERK and c-JUN induction on BRAF-WT melanoma xenograft tissue after treatment with MEK inhibitor trametinib plus DSF for 10 d. ERK phosphorylation levels are shown in red (Cys-3) and c-JUN levels are illustrated in blue (Cys-5) (Immunofluorescence staining). Nuclei staining is green duo to the Yopro staining. Quantification fluorescence signal intensities of pERK and c-JUN following confocal immunofluorescence analysis in BRAF-WT melanoma slices after treatment. The signals in treated cells were normalized to untreated melanoma cells (n = 4). One-way ANOVA was used to identify the statistical significance associated to untreated (control) and it was followed by Tukey's multiple comparisons test. * $p < 0.05$; ** $p < 0.01$; *** $p < 0.001$; and **** $p < 0.0001$, ns (not significant).

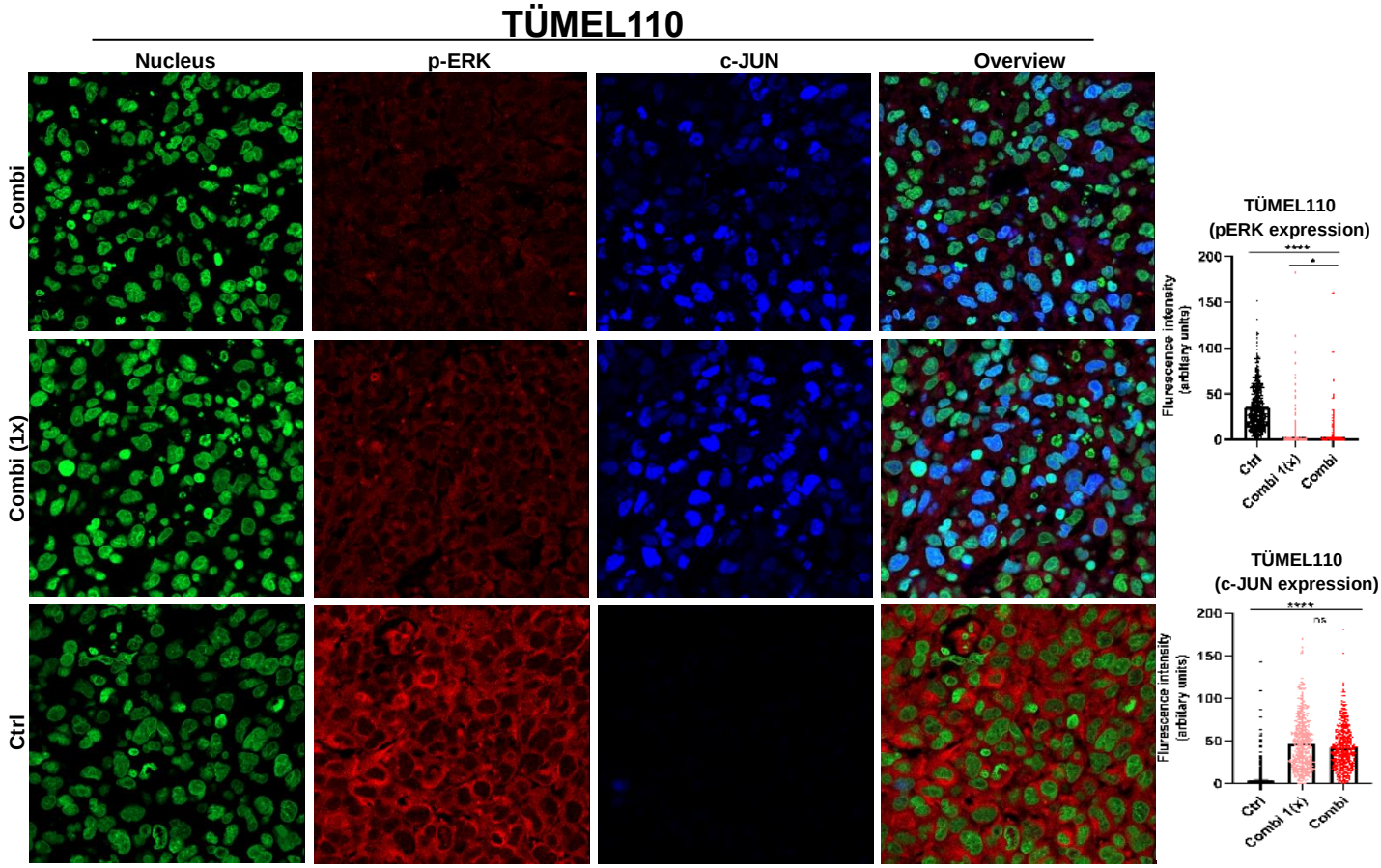

Figure 74. Induction of c-JUN and inhibition of pERK in the TÜMEL110 melanoma model under 10 days of combination therapy. Confocal immunofluorescence analysis of phosphorylation of ERK and c-JUN induction on BRAF-WT melanoma xenograft tissue after treatment with MEK inhibitor trametinib plus DSF for 10 d. ERK phosphorylation levels are shown in red (Cys-3) and c-JUN levels are illustrated in blue (Cys-5) (Immunofluorescence staining). Nuclei staining is green duo to the Yopro staining. Quantification fluorescence signal intensities of pERK and c-JUN following confocal immunofluorescence analysis in BRAF-WT melanoma slices after treatment. The signals in treated cells were normalized to untreated melanoma cells (n = 4). One-way ANOVA was used to identify the statistical significance associated to untreated (control) and it was followed by Tukey's multiple comparisons test. * $p < 0.05$; ** $p < 0.01$; *** $p < 0.001$; and **** $p < 0.0001$, ns (not significant).

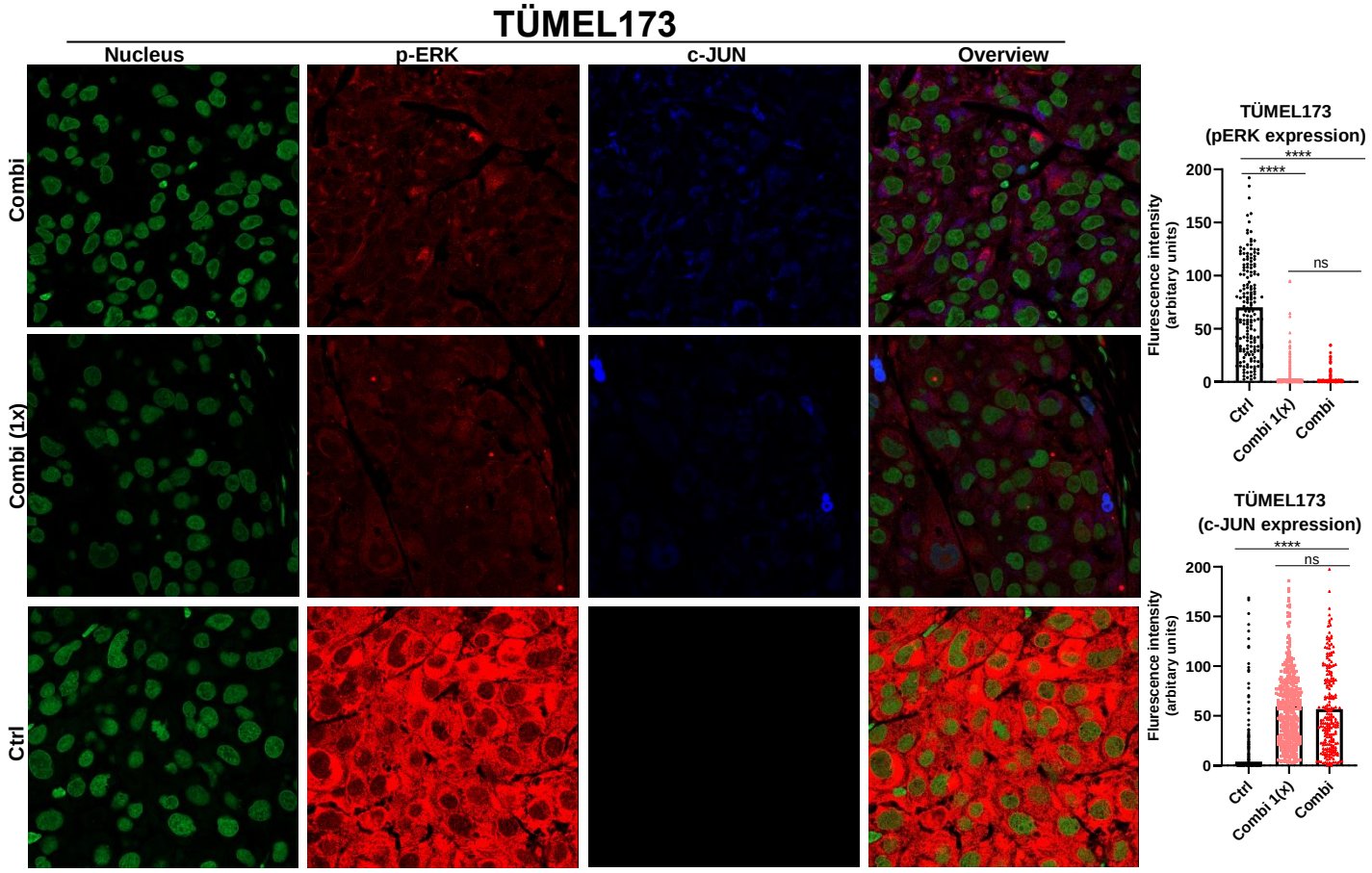

Figure 75. Induction of c-JUN and inhibition of pERK in the TÜMEL173 melanoma model under 10 days of combination therapy. Confocal immunofluorescence analysis of phosphorylation of ERK and c-JUN induction on BRAF-WT melanoma xenograft tissue after treatment with MEK inhibitor trametinib plus DSF for 10 d. ERK phosphorylation levels are shown in red (Cys-3) and c-JUN levels are illustrated in blue (Cys-5) (Immunofluorescence staining). Nuclei staining is green duo to the Yopro staining. Quantification fluorescence signal intensities of pERK and c-JUN following confocal immunofluorescence analysis in BRAF-WT melanoma slices after treatment. The signals in treated cells were normalized to untreated melanoma cells (n = 4). One-way ANOVA was used to identify the statistical significance associated to untreated (control) and it was followed by Tukey's multiple comparisons test. * $p < 0.05$; ** $p < 0.01$; *** $p < 0.001$; and **** $p < 0.0001$, ns (not significant).

It should be taken into consideration that based on the *in vitro* results, it was critical that the combination of trametinib with CuET interferes with several proteins belonging to the MAPK family. The activation of c-JUN by the combination therapy was completely dependent on the c-JUN NH_2-terminal kinase (JNK), an important member of the MAPK family. This encompassed the effects of combination therapy on the MAPK family, as well as the induction of apoptosis. This led us propose that induction of c-JUN is a critical point in the induction of apoptosis by the combination therapy. Taken together, immunofluorescence was performed in order to determine whether the anti-cancer effects shown in the *in vivo* experiments were also accompanied with the activation of c-JUN. It was observed a significative up-regulation of c-JUN mediated by the combined therapy compared with the control in the three-model tested, as was graphically in Figure 73-75.

The combination therapy was very effective *in vivo* as demonstrated in the first *in vivo* experiment, where the combined treatment group showed a significant inhibition of tumor growth in the three BRAF-WT melanoma models. Then was decided to perform a second experiment where the MEK inhibitor trametinib and CuET were administered not only in combination but also as monotherapies to investigate the effect of combination *in vivo.* Here, melanoma cells from TÜMEL173, were subcutaneous injected into the right flank of the mice (n=22). After the tumors have reached a volume of 20-60mm^3, the tumor-bearing mice were randomized and divided into four treatment groups:

1. control/sham treatment (n=6).
2. 50 mg/kg disulfiram (per os) (n=5)
3. 0.3 mg/kg trametinib (per os) (n=5)
4. combination of 2. and 3. (n=6)

Treatments were administered daily via gavage. The mice all receive drinking water containing copper drinking water to promote complexation of disulfiram to disulfiram-Cu^{2+}. The drinking water of the mice were supplied with additional copper gluconate (1.2µg/mL). Every two days, the tumors are measured (in length and width in millimeters) and the animals' weight (in grams) is determined. During the treatment period, tumor size is determined daily, and the body weight of the body weight of the animals. After a maximum of 28 days or when the discontinuation criteria were reached, all animals were killed at the same time by CO_2 into the cage. The criteria for discontinuation were that the tumor volume exceeded 1000 mm^3, that a drastic weight loss occurred, or that the mouse died.

Tumor growth curves of the TÜMEL173 model representing the mean tumor volumes in each of the different therapy groups throughout the 28 days are shown in Figure 76. A significant inhibition in tumor growth mediated by combination therapy was revealed. This decrease in tumor growth during the 28 days of treatment was significantly greater in the combination therapy when compared to both monotherapies, the MEK inhibitor and disulfiram. The combined therapy group stopped tumor growth for the first 20 days of treatment and at day 20 a discrete reduction in tumor size was observed, which was not observed in any of the other study groups. Additionally, the tumor growth curves for every mouse in the respective therapy group further shows the benefit associated to treatment with MEK inhibitor trametinib with CuET for that BRAF-WT melanoma model. Interestingly, the effect of the MEK inhibitor trametinib on BRAF-WT melanoma model (TÜMEL173) tumor growth was significantly greater than observed *in vitro* via 2D and 3D models. The trametinib-mediated tumor growth

inhibition was highly significant where it showed disease stability for about 20 days, after which tumor growth was measurable. There was a marked and significative suppression of xenograft tumor growth by combination therapy *in vivo,* associated to a complete prevention of the tumor growth. Contrary, the group receiving DSF presented a completely different trend, where tumor growth did not significantly differ to that observed in the control group, as shown in Figure 76.

Interestingly, the MEK inhibitor had a significant efficacy in slowing tumor growth *in vivo*. This effectiveness of trametinib corresponds to the clinical efficacy observed for MEK inhibitors against melanoma. But, MEK inhibitors (binimetinib) were not sufficient to increase the overall survival of $NRAS^{mut}$ melanoma or stop progression when compared to chemotherapy thought dacarbazine, as was previously described in the NEMO trial [124]. Trametinib displayed a significant reduction in tumor growth when compared to the control group, mainly during the first 15 days of treatment. Thereafter, the tumors in the group receiving the MEK inhibitor showed a discrete increase in tumor volume in the last 10 days of treatment. Finally, statistically significant differences were observed between the group treated with trametinib and the group treated with the combined therapy at day 28 on therapy, confirming the synergism between both therapies. The reoccurring tumor growth of tumors treated with the MEK inhibitor after 2 weeks of treatment is an adaptation mechanism that ends in resistance, which is also observed clinically in patients within a few months. Contrary, the combination therapy group did not show a reactivation of tumor growth, which can be interpreted as prevention or delay the adaptive resistance to MEK inhibitors due to CuET or disulfiram. Taken together, according to the results obtained in the second *in vivo* experiment, a synergistic inhibition of tumor growth was confirmed by the combination of trametinib with disulfiram.

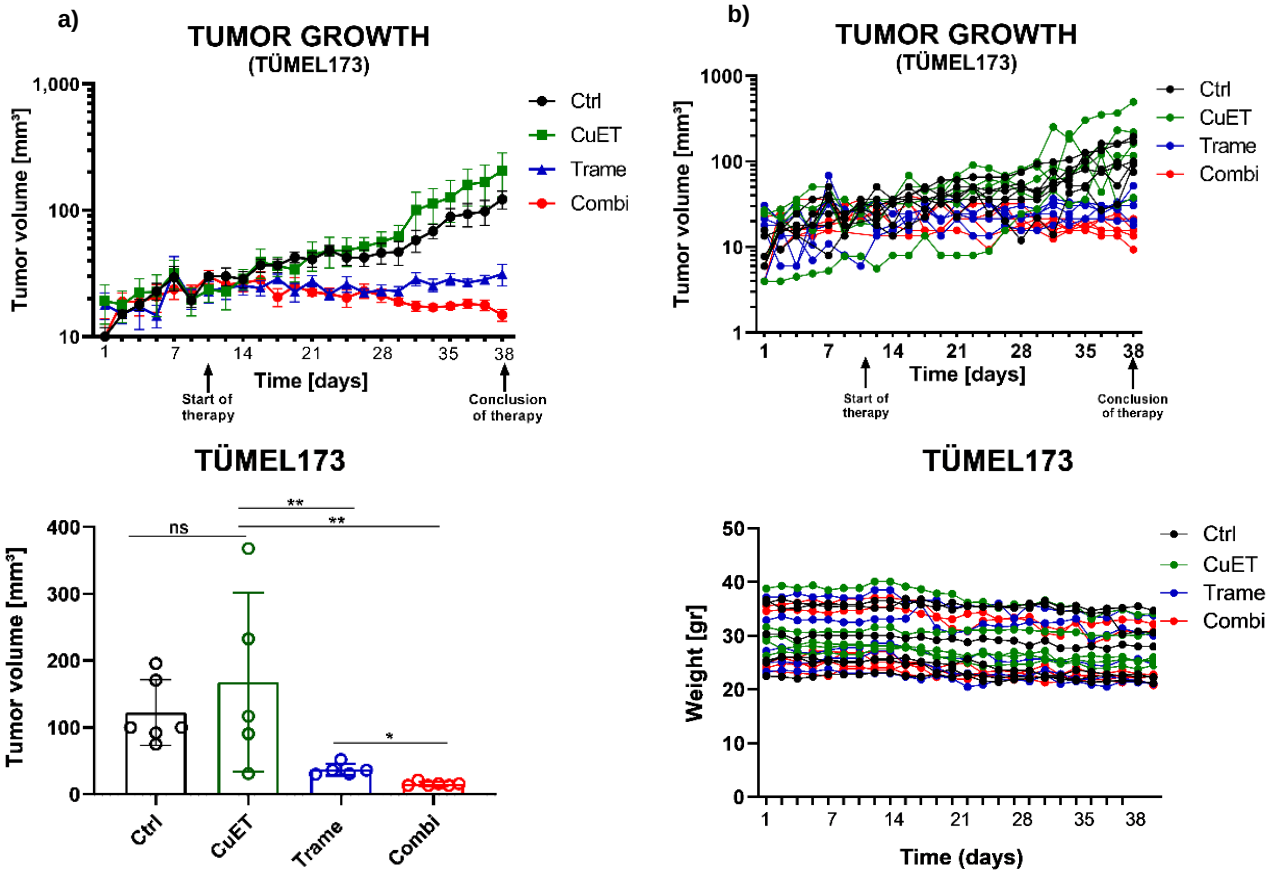

Figure 76. ***In vivo*** **tumor growth of BRAF-WT melanoma model can be significantly impaired by combination of MEK inhibitor trametinib with disulfiram**. a) Subcutaneous xenograft growth of the TÜMEL173 melanoma cell line in NOD scid gamma (NSG) mice under treatment with the MEK inhibitor trametinib, disulfiram and combination thereof (±SEM). b) Spider plots of individual tumor growth of subcutaneous xenograft growth of the TÜMEL173 melanoma cell line in NOD scid gamma. c) Tumor end volumes (±SEM) for all the respective therapy groups (control, trametinib, disulfiram and combination therapy) are shown (control n=6, CuET n=5, trametinib n=5, Combi n=6). d) Change in the weight of the animals during the experiment from the application of the cells until the end of the experiment. Mice were treated during 28d with sham as a control group, trametinib (at 0.3 mg/kg per os), disulfiram (50 mg/kg per os) and combination therapy (trametinib at 0.3 mg/kg per os plus disulfiram 50 mg/kg per os). The drinking water of the mice were supplied with additional copper gluconate. Significance was determined by one-way ANOVA with subsequent Tukey's multiple comparisons test. * $p < 0.05$; ** $p < 0.01$; *** $p < 0.001$; and **** $p < 0.0001$, ns (not significant). In the graphs (**a** and **b**) the data are fitted to log 10.

In order to confirm the persistent inhibition of ERK phosphorylation by the combination therapy, immunofluorescence tests were analyzed on tumor tissues. Through this technique, the results previously observed in Western blot were fully confirmed. On the one hand, it was observed that the combination therapy group showed a significant down-regulation of ERK phosphorylation (pERK) compared with the control. This inhibition of ERK phosphorylation was significantly greater in the group that received the combination therapy than the trametinib group, as shown in Figure 77. No re-activation of ERK phosphorylation activity was observed even after 28 days of treatment, indicating that CuET could prevent BRAF-WT melanoma cells from developing resistance to MEK inhibitors. Additionally, control and disulfiram groups had a significantly higher pERK signal than in the trametinib and combination groups, strongly indicating that subsequent and persistent MAPK pathway activity is highly critical for their

development and progression. For the detection of c-JUN in the tumors of the TÜMEL173 model, immunofluorescence with c-JUN were performed in order to explore a putative up-regulation of c-JUN in association with the pERK inhibition mediated by the combination therapy. It was observed a significative up-regulation of c-JUN mediated by the combination therapy compared with the trametinib and control groups. Taken together, the anti-cancer effects observed in the *in vivo* experiments were also accompanied with the activation of c-JUN, as show in Figure 77.

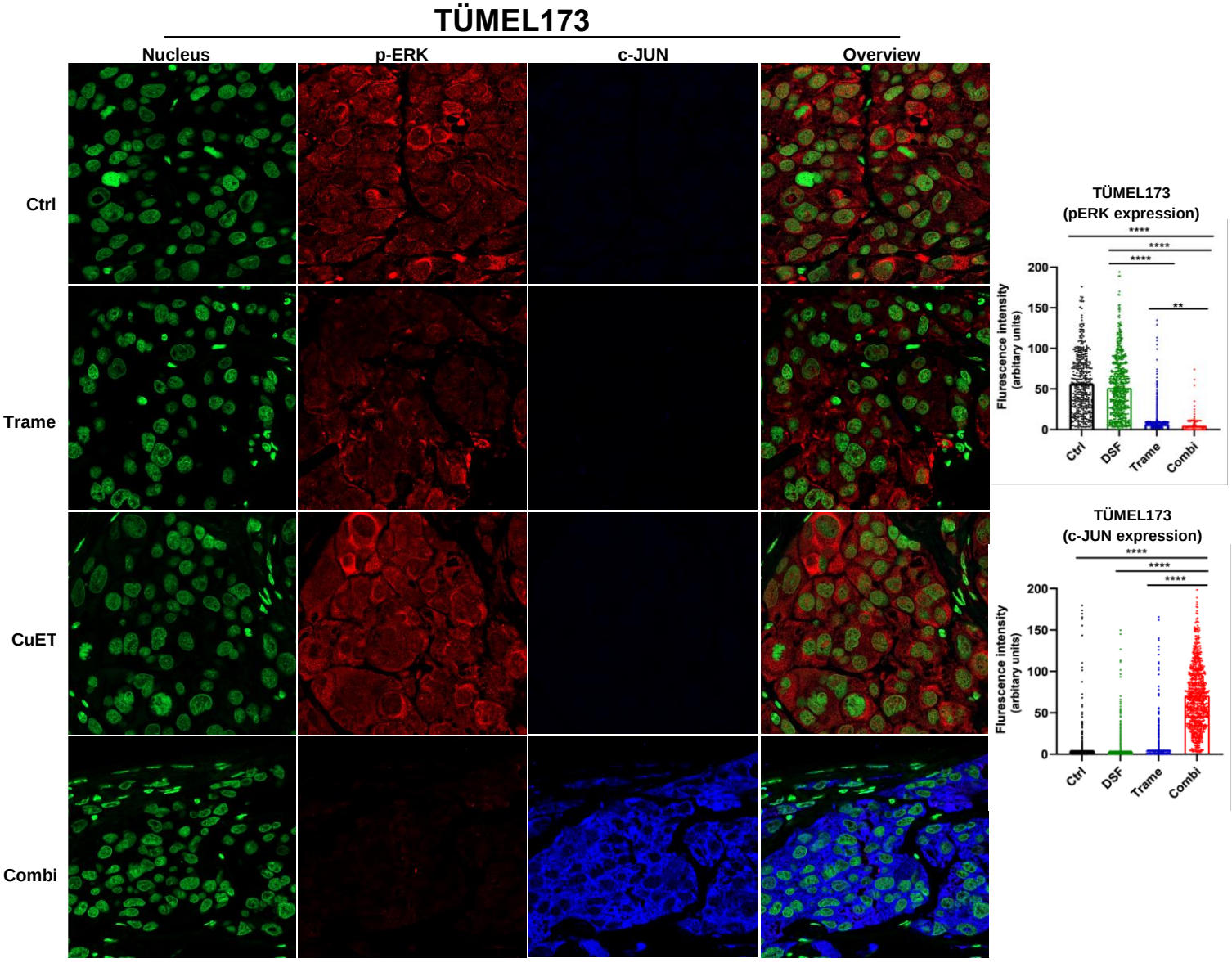

Figure 77. Induction of c-JUN and inhibition of pERK in the TÜMEL173 melanoma model after 28 days of combination therapy. Confocal immunofluorescence analysis of phosphorylation of ERK and c-JUN induction on BRAF-WT melanoma xenograft tissue after treatment with MEK inhibitor trametinib plus DSF for 28 d. ERK phosphorylation levels are shown in red (Cys-3) and c-JUN levels are illustrated in blue (Cys-5) (Immunofluorescence staining). Nuclei staining is green duo to the Yopro staining. Quantification fluorescence signal intensities of pERK and c-JUN following confocal immunofluorescence analysis in BRAF-WT melanoma slices after treatment. The signals in treated cells were normalized to untreated melanoma cells (n = 4). One-way ANOVA was used to identify the statistical significance associated to untreated (control) and it was followed by Tukey's multiple comparisons test. * $p < 0.05$; ** $p < 0.01$; *** $p < 0.001$; and **** $p < 0.0001$, ns (not significant).

As previously described, DSF and not CuET was used directly as monotherapy and in combination therapy in the two animal experiments. It was because DSF orally administrated exhibits a high absorption rate and an efficient biodistribution to tissues [126]. However, in order to bind to the available copper, DSF needed to be metabolized to bis-ET by glutathione reductase. If the DSF could not be metabolized by erythrocyte glutathione reductase, the bis-ET molecules were not generated. If this were to occur, there would definitely be no possibility of generating the CuET complex, however this was ruled out because the activation of DSF was studied after one h of exposure in whole blood from different donors and after its cytotoxicity was explored *in vitro* via cell viability assays in BRAF-WT melanoma cells, as shown in Figure 78. These experiments were performed to establish the role of glutathione reductase in the metabolic conversion of DSF to ET. DSF and ET alone or in combination with Cu^{2+} were administrated in heparinized whole blood and after 1 h exposition, serum was obtained. This serum was used to treat SKMEL23 and SKMEL113 melanoma cells during 72h. It confirmed that glutathione reductase induced a rapid metabolization of DSF to ET, which shortly bonded to the available copper, formed the CuET complex. DSF plus copper exhibited a cytotoxicity on BRAF-WT melanoma cells similar to that observed by direct administration of CuET.

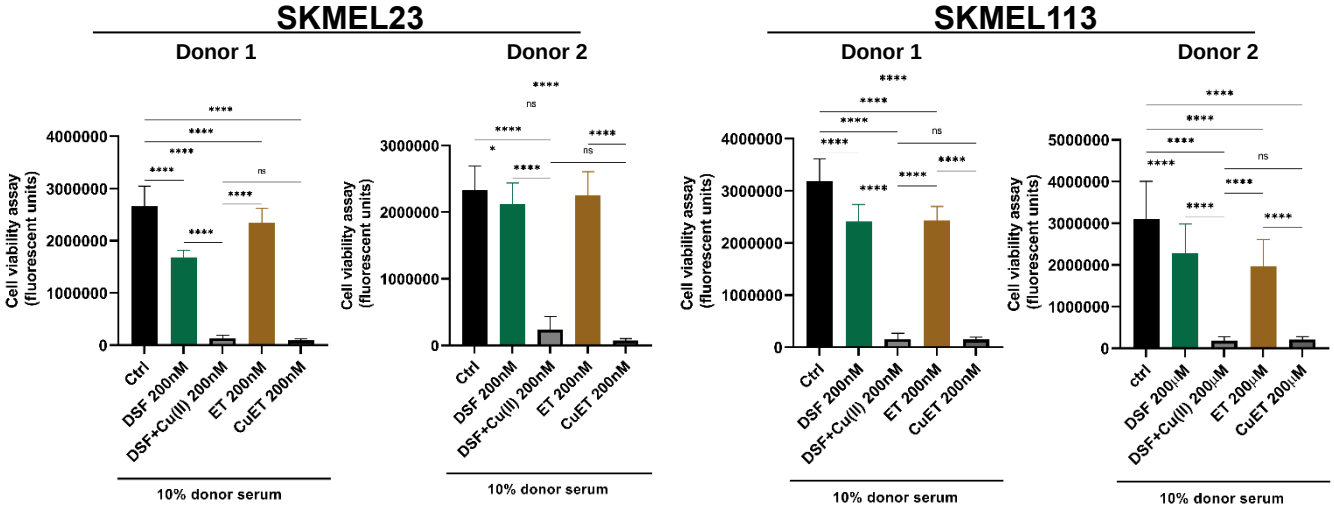

Figure 78: Activation of DSF through exposure to whole blood, mediated cytotoxicity on BRAF-WT melanoma cells. Cell viability assay (MUH assay) of BRAF-WT melanoma cell lines (SKMEL23 and SKMEL113) after treatment with DSF (200nM), DSF plus Cu^{2+} (200nM/200nM), ET (200nM) and CuET (200nM) for 72 h. The treatments were incubated in whole blood from 2 different donors for 1 h before serum was extracted and used for treatment of the melanoma cells (10% serum). Values are means ± SEM of three replicates (n = 3; mean ± SD). Viability was normalized to untreated control cells. One-way ANOVA was used to identify the statistical significance associated to untreated (control) and it was followed by Tukey's multiple comparisons test. * $p < 0.05$; ** $p < 0.01$; *** $p < 0.001$; and **** $p < 0.0001$, ns (not significant).

6 Discussion

In recent years, new therapies represented by approaches such as immunotherapy-based therapy and targeted therapy with BRAF or MEK inhibitors have been shown to significantly improve the overall survival of melanoma patients. However, the incidence of melanoma is increasing, which is compounded by tumor resistance to available drugs [40]. To underscore this, about 20% of melanoma patients treated with target therapy and about 50% of patients treated with immunotherapy do not respond to the first line of treatment or rapidly produce resistance to the administered therapy [8, 145]. In addition, no target therapy has been approved for certain subgroups, such as BRAF-WT melanomas, although these subgroups often express aggressive cell biology with an unfavorable prognosis [124]. A promising strategy for this unmet need to improve the efficacy of BRAF-WT melanoma treatment was the proposal of an approved target therapy in combination with repurposing of already approved therapies, with the aim of intensifying the potential efficacy of the target therapy. A promising strategy for this unmet need to improve the efficacy of BRAF-WT melanoma treatment was the proposal of an approved target therapy in combination with the repurposing of already approved therapies.

In addition to mutations in BRAFV600, which lead to hyperactivation of the MAPK pathway in approximately 40% of all cutaneous melanomas, other mutations in genes such as *NRAS* and *NF1* (BRAF-WT melanoma subgroup) result in constitutive activation of MEK1/2 and ERK1/2 in approximately 30-35% of cases [23]. Therefore, a targeted therapy with MEKi such as trametinib appears to be a rational consequence for BRAF-WT melanomas with hyperactivation of MAPK signaling. The clinical efficacy of MEKi as monotherapy in BRAF-WT melanoma has been further investigated in clinical trials, in particular in the phase 3 NEMO clinical trial [124]. However, although the NEMO study provided evidence that MEKi improved progression-free survival over dacarbazine (2.8 vs. 1.5 months), the overall response rate of MEKi was significantly poor, only 15%, but still higher than the 7% achieved in the dacarbazine group [124]. Therefore, combinations with other drugs that were able to improve BRAF-WT melanoma response rates to MEKi were needed. A promising strategy for this unmet need for improved treatment of BRAF-WT melanoma is the use of a target therapy in combination with repurposing of already approved therapies, with the aim of intensifying the efficacy of the target therapy.

The phosphorylation of MEK1/2 was a critical and substantial point of MAPK pathway signaling activation that concluded with the activation of subsequent nuclear transcription factors and ultimately the progression and development of melanoma [23, 30, 38, 58]. Therefore, inhibition of MEK1/2 phosphorylation played a significant role in inhibiting melanoma cell growth [156]. Trametinib played a relevant role as a therapeutic agent when combined with CuET. A similar inhibition of MEK1/2 and ERK1/2 phosphorylation was observed in all BRAF-WT melanoma cells explored, regardless of the mutation status, such as $NRAS^{mut}$, NF1-*LoF* and Triple-WT. This inhibition supported the idea of starting to combine the MEK1/2 inhibitor in this case because the inhibition offered by this therapy was completely accurate at the specific phosphorylation site, Ser286, which served as a docking site for the *PDK1* gene [157-159]. As a docking site for the *PDK1* gene and therefore facilitated activation of the NTKD, which was required to attain full kinase activity [160]. The phosphorylation status provided a critical readout on this BRAF-WT melanoma issue. As a result, it was a basis to include an upfront MEK1/2 inhibitor as one of the drugs to be combined for the treatment of BRAF-WT melanoma. However, since MEKi did not offer a remarkably significant difference against standard therapy for $NRAS^{mut}$ melanoma, the postulation of a combination therapy as in this research work was necessary [124].

Inhibition MAPK signaling pathway in combination with a second drug is an alternative to target the BRAF-WT melanoma [124]. An option was to combine MEKi with a molecule that also chemically interacts with MEK1/2. Small molecules interacted with multiple targets, concluding in a chain of subsequent genotype-specific effects [144, 172]. Marco Breinig *et al.* performed a multiparametric analysis of the molecular interaction of MEKi with DSF. Several phenotypes from the interaction of MEKi with DSF were analyzed. It showed that the MEKi amplified the cytotoxic effect of DSF on colon cancer cells [144]. The cytotoxic effect mediated by DSF on colon cancer cell line (HCT116 and DLD-1) was significantly enhanced MEKi U0126 or PD98059. DSF exerted multiple chemical-genetic interactions on colon cancer cells that concluded in an inhibition of cell viability. It was significantly enhanced in HCT116-MEK knock out colon cancer cells [144]. Thus, a hypothetical synergism between DSF and MEKi was postulated. It was confirmed in this work, where a synergism between the MEKi trametinib and DSF in BRAF-WT melanoma cells was observed. However, it is not clear whether the observed synergism was strictly mediated by precise MEK1 inhibition or whether it was observed with the unchallenged inhibition of the MAPK pathway, with the use of e.g. BRAF inhibitors or RSK inhibitors.

Using a novel MEKi, GSK1120212 (trametinib), which is a second-generation MEK1/2 inhibitor approved by the FDA in 2013 for the treatment of malignant melanoma effectively blocked MAPK signaling in all BRAF-WT melanoma cells [56]. Research on repurposing Disulfiram (DSF), a former FDA approved alcohol-aversion drug, which has been described to achieve anticancer effects on several tumors in preclinical studies, including melanoma, was such a drug candidate. Trametinib was combined with DSF (Antabuse® or Antabus®), also approved by the FDA in 1952 [104]. Trametinib plus CuET encouraged an up-regulation of ER stress related genes that drives activation of the *JNK/c-JUN* signaling pathway, concluding in apoptosis induction.

DSF is metabolized into bis-diethyldithiocarbamate by glutathione reductase activity in vivo, which has a strong chelating capacity and a high affinity for Cu(II), leading the bis-diethyldithiocarbamate-Cu complex (CuET) [104, 146]. Cu^{2+} as monotherapy had no influence on cell viability. In contrast, treatment with ET, in particular, the combination with Cu^{2+} (CuET), showed a significant cell growth inhibition. The minimal effective dose of CuET was 125nM. For these reasons, combining CuET with an approved melanoma therapy, as MEKi, was considered. The main purpose of this project was to evaluate whether the addition of CuET to the MEKi increase the effectiveness of the MEKi trametinib in BRAF-WT melanoma.

Marco Breinig *et al*. described that the cytotoxic synergism mediated by DSF plus MEKi was through proteasome inhibition [144]. The inhibition of proteasome activity was proposed as the main cytotoxic mechanisms mediated by DSF plus MEKi. However, in this work it was demonstrated that inhibition of proteasome activity did not play the main role as anticancer mechanism mediated by DSF plus MEKi. The main mechanism mediated by DSF plus MEKi was the induction of ER-stress genes and the activation of the *JNK/c-JUN* signaling pathway. The proteasome inhibition was a secondary cytotoxicity mechanism. Although the description made by Marco Breinig *et al*. was highly accurate, the mechanism behind the combined therapy was mostly mediated by the induction of ER-stress and not by the inhibition of proteasome activity.

As it has been suggested, the anticancer effect of DSF is copper-dependent [66, 118, 119]. It was confirmed that the therapeutic effect of DSF on melanoma cells was mediated by Cu. DSF up-tacked Cu into the intracellular space. The Antioxidant 1 Cu Chaperone (*ATOX1*) gene encodes a Cu^{2+} chaperone, which played a relevant role in the intracellular Cu transport. ATOX1 binds Cu and transport it into the ATPase proteins in the trans-Golgi network, where it was incorporated to the ceruloplasmin [65, 71, 86, 88]. Once Cu is in the intracellular spaces

a further gene expression induction is started, as the ATOX1 up-regulation [97]. Additionally, Shinichi Itoh and et.al. described by electrophoretic mobility shift assays and promoter analysis that the intracellular Cu^{2+} stimulates the binding of ATOX1 to a cis-sequence in the cyclin D1 promoter. The functional role of the nuclear Cu transport by ATOX1 was mainly activated through the massive intracellular concentrations of Cu [81, 84].

In contrast to $BRAF^{mut}$ melanoma cells, BRAF-WT melanoma cells carry different mutations that offer the tumors different proliferation and growth characteristics [15, 23]. These different mutations such as NF1-*LoF* and $NRAS^{mut}$ mainly modulate their responsiveness and resistance to MAPK target inhibitors such as BRAF and MEK inhibitors. To illustrate these data, Trousil *et al*., 2017; Koelblinger and Dummer, 2017 demonstrated that NF1-*LoF* and NRAS melanoma cells were highly difficult to treat with targeted therapy options [124, 148, 149]. However, in the development of this work, the usefulness of MEKi in combination with a ROS inducer such as CuET in BRAF-WT melanoma cells was already demonstrated.

Melanoma cells maintained a higher level of oxidative stress than the benign cells [161]. During the last years different new research has been postulated the induction of intracellular oxidation as an anticancer therapy [136, 162, 163]. The aim of this therapy was to overcome the cellular ROS threshold inducing apoptosis [116]. Consistent with this notion, appeared the ability of DSF to induced intracellular ROS formation and thereby inhibited BRAF-WT melanoma cell growth. [113]. ROS production by DSF was performed in a copper-dependent manner, where compressed either the interactions between Cu^{+} with H_2O_2, or of Cu^{2+} with hydroxide molecules (^{-}OH) [119, 156]. Both intracellular reactions concluded in a ROS production [146]. A complementary ROS production by DSF was described by its interaction with the mitochondrial membrane, generating superoxide (O_2^{-}). [114]. Even that the O_2^{-} was not a high robust oxidant, this interacted with the previously ROS produced, concluding in damage of several cellular organelles. After the initial damage induced by DSF, the mitochondrial O_2^{-} was transported to the cytoplasm. There, the interaction of the mitochondrial membrane with the outer ER membrane was in the near proximity. Therefore, the initial up-regulation of the ER stress by DSF or combination therapy was potentially performed due direct damage of the nascent polypeptides [20, 136, 164].

CuET induced intracellular ROS formation [114, 116]. The addition of a ROS scavenger NAC abolished the cell cytotoxicity mediated by CuET. The ROS formation mediated by CuET were measured by GRX/ORP-1 biosensor melanoma cells [128]. CuET induced an intracellular production of hydrogen peroxide (H_2O_2). H_2O_2 is converted to water by catalase, peroxiredoxins and mainly by glutathione peroxidases (GPXs). Glutathione peroxidases reduce accumulated H_2O_2 to water by the oxidizing of Glutathione (GSH) to Glutathione disulfide (GSSG). However, NADPH is used by glutathione reductase to translate GSSG to GSH in a continuous cycle, known as glutathione redox state [96, 128]. Thus, CuET induced formation of H_2O_2 and glutathione redox state. Trametinib significantly enhanced the ROS production mediated by CuET on BRAF-WT melanoma cells.

Cellular stress induced by DSF concluded in cell death if they cellular homeostasis is not restored [164]. This stress induction were mainly ROS formation and protein stress. DSF induced an abrupt accumulation of unfolded proteins in the endoplasmic reticulum, concluding in an up-regulation of the ER stress. It trigged into unfolded protein response (UPR). [120, 136]. The main target of UPR activation was a restoration of cellular functions through a specific suppression of its own translational processes. For this purpose, first a degradation of misfolded proteins occurred and then several signaling pathways were activated. Finally, it increased the synthesis of chaperones that were required for appropriate protein folding. UPR decreased the accumulation of mainly unfolded proteins thought the reduction of the synthesis of global proteins, induction of the UPR gene transcription and provoking ER-association protein degradation. When this process was not properly performed or the level of intracellular stress overcomes the threshold, the UPR activates a new signaling pathway which induced a programmed cell death [165]. Interestingly, the Protein Kinase RNA-like Endoplasmic Reticulum Kinase (*PERK*), Inositol-requiring Enzyme 1 (*IRE1*) and the Activating Transcription Factor 6 (*ATF6*) were a critical part and checkpoint in the regulation of the UPR. These proteins played a role as intracellular sensors, which detected ER stress by faulty protein folding and induce a response to the UPR control cascade [164]. In this work was observed that trametinib enhanced the ER stress induced by DSF. As a result, ER function was not completely restored and the UPR switched approach from pro-survival to proapoptotic in the BRAF-WT melanoma model.

In 2017 Niessner H. *et al.* described that the BRAF inhibitors (BRAFi) dabrafenib, vemurafenib and encorafenib induced significant ER stress features in $NRAS^{mut}$ melanoma cells [138]. The main ER stress features by BRAFi were morphological modifications of the

ER structure, mainly ER dilation [138, 168]. An analogous effect was observed between the combination of a BRAF inhibitor (encorafenib) with a MEKi (binimetinib), however the administration of MEKi alone did not generate these effects. In addition to these structural effects, the encorafenib as a monotherapy or in combination with MEKi binimetinib activated the sensor PERK, which leaded the phosphorylation of the elF2α on $NRAS^{mut}$ melanoma cells [168]. These data support the hypothetical theory that MEKi played a relevant role in the induction of ER stress in BRAF-WT melanoma based into their positive response in $NRAS^{mut}$ melanoma cells.

Along with a distinct activity of MAPK signaling in these cells due that the BRAF-WT melanoma cells hold a different genomic mutation ($NRAS^{mut}$, NF1-*LoF*, Triple WT), which provided a strong rationale for MEK inhibition in combination to the intracellular effects mediated by CuET throughout the different genomic melanoma subgroups associated with a hyperactivation of the MAPK signaling pathway [15]. In early work was already exhibited, that the combination of MEK with BRAF inhibitors induced a significant pro-apoptotic activity due to significant induction of ER stress on $NRAS^{mut}$ melanoma cells (Niessner 2017), which also belong to the BRAF-WT melanoma group [138]. This lays the groundwork to explore whether MEKi in combination with a second therapy generate ER stress induction in BRAF-WT melanoma cells [138, 143, 147]. This aspect was extremely relevant to open the panorama to combine MEKi with diverse therapies, because it was previously proved that the combination of MEK and BRAF inhibitors amplified the induction of apoptosis through the induction of ER stress, specifically in $NRAS^{mut}$ melanoma cells. In addition, several other relevant studies have emphasized and focused on ER stress induction as a direct driver of apoptosis induction in melanoma[136, 138, 140-142, 147]. Therefore, a novel therapy thought the combination of the MEKi trametinib with CuET on BRAF-WT melanoma cells was conducted.

Trametinib plus CuET up-regulated ER stress-related genes on BRAF-WT melanoma cells. Trametinib induced an inhibition of the entire MAPK pathway, including ERK. Inhibition of ERK hyperactivation resulted in high 78-kDa glucose-regulated protein (GRP78) accumulation since ERK is the main active inhibitor of GRP78, which is located mainly in the endoplasmic reticulum (ER) [138, 147]. The hypothetical interaction between the high concentrations of GRP78 with the massive intracellular accumulation of Cu^{2+} and the intracellular ROS concluded in the potential subsequent phosphorylation of the alpha subunit of polypeptide chain initiation factor (elF2α) in the ER as a response to cellular stresses.

Therefore, this constant intracellular interaction was a possible trigger of ER stress up-regulation.

Consider the data reported in this work, *CHOP* was up-regulated by CuET (500nM). It was unexpected that the MEKi trametinib further increased this induction. *CHOP* was well-known as a substantial mediator of the apoptosis induction mediated by ER stress [166]. As postulated in this work, inhibition of the MAPK kinase pathway exacerbated CuET-mediated UPR activity. It induced apoptosis in all these cells which expressed an up-regulation of *CHOP*. In contrast, cells that had minimal ER stress induction, such as benign cells, did not elicit toxicity by trametinib plus CuET. Combination of trametinib plus CuET up-regulated *CHOP*, *NURP1* (P8) and *ATF4* in BRAF-WT melanoma cells. Interesting, melanoma cells were higher sensitive to ER stress than benign cells. It was due that the melanoma cells had high levels of intrinsic stress that performed their requirement for aberrant growth [165, 167].

BRAFi encorafenib plus MEKi binimetinib up-regulated the ER stress related transcription factor genes *NUPR1, ATF4* and *CHOP*. These transcription factors were critical downstream features of elF2α phosphorylation [138]. Similar trend was observed by combining dabrafenib plus trametinib on $NRAS^{mut}$ melanoma cells. Encorafenib plus binimetinib up-regulated the expression of *CHOP, NUPR1 (P8)* and *ATF* in $NRAS^{mut}$ melanoma cells. It strengthened the MEKi as the basis of therapy for BRAF-WT melanoma cells. Therefore, in this work was combined a MEKi with the DSF on BRAF-WT melanoma cells. Trametinib plus CuET performed similar ER stress induction on BRAF-WT melanoma *in vitro* as was done by BRAFi plus MEKi on $NRAS^{mut}$ melanoma.

Trametinib plus CuET induced an inhibition of phosphorylation of known MEK1/2 targets, accumulation of pro-apoptotic BCL-2 family proteins and inhibition of anti-apoptotic proteins of the BCL-2 family. In this line, trametinib plus CuET induced a phosphorylation of BAX at serine 184 (Ser^{184}) residues, which mechanistically occurs in an AKT-dependent manner. Once BAX protein is phosphorylated by the combination therapy, the BAX protein is strongly retained in the cytoplasm, without performing its main regulation on mitochondrial activity and finally performs a heterodimerization with serine 70 (Ser^{70}) of the BCL-2 protein, concluding in a decrease of the anti-apoptotic activity of the BCL-2 protein [130, 150]. This mechanism of counter-regulation between BAX and BCL-2 in an AKT-dependent manner was already presented and illustrated by Gardai *et al.*, 2004 [151]. In parallel to BAX activation, phosphorylation of all three BIM isoforms (BIM^{EL}, BIM^{L} and BIM^{S}) by the combination therapy was observed, especially at serine residues 93, 94 and 98 ($Ser^{93,}$ $Ser^{94,}$ Ser^{98}) of BIM^{EL},

which strongly facilitates its proteasomal degradation and upon further stabilization of BIM^{EL} after MEK1/2 inhibition [152-154]. Therefore, this event reinforces the fact that an inhibition of the MAPK signaling axis in addition to the ER stress production abrogated the complete BIM phosphorylation on BRAF-WT melanoma cells. Taken together, the combined therapy induced substantial modifications in the behavior of intranuclear proteins which resulted in an increase in the signaling of the pro-apoptotic protein group of the BCL-2 family and a down-regulation on the expression of anti-apoptotic proteins. To sum up, it was observed a significant apoptosis induction through trametinib plus on BRAF-WT melanoma cells.

Hersey *et al*. reported that MEKi induced significant up-regulation of *BIM* in melanoma. Thus, was investigated whether BIM or another BCL-2 family protein was induced by trametinib plus CuET in BRAF-WT melanoma cells [147]. Trametinib plus CuET induced significant up-regulation of the ER stress-related genes *CHOP*, *ATF4* and *NUPR1*. *ATF4* and *CHOP* acted as a transcription factors which try to restore intracellular homeostasis. If is not archived, an up-regulation of *BCL-2* pro-apoptosis family proteins, such *BIM, BID, BAX, BAK* and *Puma* is started [169]. This activation concluded into the activation of the mitochondrial apoptosis pathway [170]. The further up-regulation of *CHOP* was related to a consequent activation of the *BIM* and down regulation of anti-apoptotic protein *BCL-2* [171]. The data reported in this work confirmed that trametinib plus CuET induced a significant up-regulation of the ER stress-related genes in association to the enhance of proapoptotic proteins expression, concluding mitochondrial apoptosis pathway. Confirmation of apoptosis activation was supported by the cleaved of the CASPASE-3 and PARP by trametinib plus CuET. The apoptotic activity trametinib was enhanced by CuET due the enhanced of expression of pro-apoptosis proteins BAX and BIM. To sum up, CuET significantly potentiated the intracellular effects mediated by the MEKi trametinib by promoting apoptosis. These data offered bases to understand that the CuET augmented the antitumor activity of trametinib. This effect was mediated mainly by the up-regulation of ER stress-related genes. Trametinib plus CuET provided a new and novel initiative in treatment of BRAF-WT melanoma.

Combination therapy of the MEK inhibitor (MEKi) trametinib plus CuET presented a significant prevention of tumor growth *in vivo* in the TÜMEL173 model, however this effect was visibly lower than what was observed in vitro. During 2D and 3D in vitro experiments, the combination therapy exhibited a clear synergism with high effectiveness in inhibiting cell growth of BRAF-WT melanoma cells. This effect was mediated by the intracellular interaction of Cu already transported by ET with trametinib, which up-regulated ER-stress related genes

as well as activation of the *JNK/c-JUN* pathway. Trametinib plus CuET induced a strong anticancer effect in a synergistic way. However, this effect was not completely similar *in vivo*. Although the combination therapy showed a significant prevention of tumor growth in vitro, a complete and total elimination of tumors was not observed. By observing that tumor growth of the CuET group was higher than the control group, it is postulated that there was a difficulty in the formation of CuET in the mice, and that the intracellular co Cupper released did not generate intracellular cytotoxic effects (such as ROS induction). Hypothetically, this limited amount of Cu in the intracellular space performed the hyperactivation of the MAPK pathway signaling due to MEK phosphorylation, as was previously described by Brady D.C. *et al.* in 2014 [2]. Taken together, as the limitation in the *in vivo* efficacy of combination therapy in the TÜMEL173 xenograft model was based on a possible delivery problem of the Cu. A second theory stipulates that the amount of Cu offered was extremely limited and because it does not have a significant affinity for tumor cells it was distributed to various benign cells, so the final amount localized in the intracellular space of tumor cells was significantly less than that required to generate cytotoxicity. The third theory is that ET bonded to another blood minerals with which it shares an affinity similar to that of copper, as Zinc (Zn^{2+}) or Silver (Ag^{2+}) [2, 85, 95]. If this were to occur, there would definitely be no possibility of generating the CuET complex.

Finding an effective treatment for aggressive BRAF-WT melanoma was one of the main aims of dermato-oncology research. The development of a target therapy for BRAF-WT melanoma patients is imperative. Dummer *et al.* demonstrated in a phase III clinical trial that the MEKi binimetinib was superior to chemotherapy (dacarbazine), but did not achieve a significant overall survival benefit [124]. However, it was demonstrated that MEKi provide strong tumor-specific antitumor activity in $NRAS^{mut}$ melanoma, which belongs to the BRAF-WT melanoma group[104]. The data presented in this work showed that CuET significantly potentiated the anticancer effects of the trametinib. MEKi trametinib plus CuET induced a synergistic cytotoxic effect on BRAF-WT melanoma cells. It was mediated by the interaction between high amount of nuclear Cu with the MAPK signaling pathway inhibition. This intracellular interaction induced several intracellular modifications, among which the significant up-regulation of ER stress-related genes and activation of *JNK/c-JUN* pathway, initiating the mitochondrial apoptosis pathway. In summary, this work provided a novel and effective therapy for the treatment of BRAF-WT melanoma.

7 Conclusion

MEKi therapy effectively inhibited the MEK1/2 phosphorylation in BRAF-WT melanoma. However, trametinib did not induce complete cell growth *in vitro*. Its effect was significantly enhanced by the addition of DSF in its active form (ET) plus Cu (CuET). In addition to the inhibitory effect on MEK1 and MEK2 kinases mediated by the MEKi trametinib, its combination with CuET did not influence the inhibition of phosphorylation of MEK1/2 serine's 217 and 221. Although, a significant decrease in MEK1/MEK2 activity was observed by trametinib and combination therapy, neither of them exhibited a complete inhibition of MEK1/2 phosphorylation on BRAF-WT melanoma cells, as was presented in Figure 21 and 22. Contrary to MEK1/2 activity, complete inhibition of ERK phosphorylation at the protein level was mediated by trametinib and combination therapy. However, emphasis was placed on not overlooked that this analysis was performed after 3 and 6 h of treatment, but no protein level analysis was made after 24, 48 and 72 h, during which time several modifications of MAPK signaling pathway activity occur. To supplement it, it was considered the response in the cell viability of BRAF-WT melanoma cells after 72 h of trametinib treatment, where was observed a maximal cell growth inhibition of about 50%.

As a potential antitumor therapy, trametinib combined with CuET exhibited significant apoptosis induction as well as important cell death. In order to confirm the significant therapeutic effects observed in 2D and 3D models of BRAF-WT melanoma, the exploration of the combination therapy was carried out in a in vivo model. Through this in vivo experiment, was found that CuET significantly enhanced the antitumor efficacy of trametinib in additive mode in a mice BRAF-WT melanoma model. Taken together, combination therapy between trametinib with CuET exhibited much better antitumor effectiveness that each of the monotherapies in vivo. Furthermore, trametinib in combination with CuET was found to induce an anticancer response mainly due to significant activation of the JNK/c-JUN pathway, leading to up-regulation of c-JUN expression. In addition, was observed a positive association in the inhibition of the ERK phosphorylation between trametinib and CuET in vivo. Thus, the combination therapy between trametinib with CuET protrudes as a novel reproducing therapy for the BRAF-WT melanoma treatment. Surprisingly, in vivo, CuET as a monotherapy did not induce a reduction in tumor size in vivo, probably due an insufficient tumoral up-take of copper. This concluded into an absence of intracellular ROS formation or a microenvironment conferred protective effect.

CuET plus trametinib induced a formation of intrinsic pro-apoptotic proteins of BCL-2 family such BIM und BAX as a decreased the level of anti-apoptotic proteins (BCL-2). Taken together, the marked production of pro-apoptotic proteins associated with the decrease of anti-apoptotic proteins of the BLC-2 family mediated by trametinib plus CuET concluded in a significant apoptosis induction in BRAF-WT melanoma. Interestingly, trametinib plus CuET induced CASPASE-3 activation, indicating that the CASPASE-dependent pathways were involved in the apoptosis induction mediated by trametinib plus CuET.

ATOX1 mediated the transport of Cu into the nuclei in BRAF-WT melanoma. It was significantly higher when CuET was combined with the MEKi trametinib. These emphasized that trametinib played a critical role in the intracellular transport of Cu from the cytoplasm into the nuclei. An aggregate effect was generated when the 2 drugs were co-administered, enhancing the intracellular Cu accumulation. The nuclear Cu accumulation mediated by CuET was significantly enhanced by trametinib. CuET plus trametinib was not able to induce nuclear Cu accumulation in ATOX1 down-regulation melanoma cells. These ATOX1 down-regulated cells exhibited lower sensitivity to the combination therapy. Mechanistically, trametinib plus CuET induced a nuclear Cu accumulation and then generated the activation of several intracellular cytotoxic mechanisms. Finally, the interaction that copper had with the rest of the organs as soon as it was in the bloodstream from the mice should be adjusted and studied. Its biodistribution, its need for vital functions and the absence of a single and continuous administration are issues that should be studied in the future to improve the therapeutic spectrum of copper.

Cellular cytotoxicity mediated by trametinib plus CuET was dependent on JNK/c- JUN. Trametinib plus CuET induced a JNK/c- JUN up-regulation in BRAF-WT melanoma cells, which might be the potential trigger for the activation of the apoptosis pathway. Up-regulation of the JNK/c-JUN signaling pathway was significantly higher in the combination therapy that both of the monotherapies. The protein analysis confirmed that trametinib plus CuET induced up-regulation of JNK/c-JUN pathway in parallel to the BIM und BAX, which cleaved the CASPASE-3 in BRAF-WT melanoma cells. The apoptosis induction produced by trametinib plus CuET were completely mitigated through a cell-selective JNK inhibitor (SP600125).

Trametinib plus CuET laded to even smaller tumor end volumes that trametinib as monotherapy, suggesting additional benefit from CuET. This indicated that the potentially microenvironment tumoral protective effect mediated by CuET was rescued through trametinib. Although the difference between trametinib and the combination treatment was not clear during

the first 20 days of the treatment, this reached significance difference at the end of the study. In addition, while not a total MEKi resistant was observed, a longer observation period is needed to adequately evaluate this matter.

In the framework of this Ph.D. thesis was presented that trametinib plus CuET encouraged a significant apoptosis induction on BRAF-WT melanoma. Trametinib plus CuET induced a significant *in vitro* and *in vivo* anti-cancer activity. MEKi trametinib plus DSF represented a valid method to effectively target BRAF-WT melanoma. To sum up, trametinib plus CuET emerged as a novel therapy for BRAF-WT melanoma patients.

8 Summary

The MAPK signaling pathway is commonly hyperactivated in melanoma and plays a critical role in the development, proliferation and survival of tumor cells. Thus, in melanoma cells without a BRAF mutations (BRAF-WT), hyperactivation of the MAPK pathway occurs in approximately 40% of cases. The clinical efficacy of MEK inhibitors as monotherapy in $NRAS^{mut}$ melanoma has been further investigated, particularly in the phase 3 NEMO clinical trial. The overall response rate of the MEK inhibitor was significantly poor (15%) and progression-free survival improved only marginally (2.8 vs. 1.5 months) over dacarbazine. Therefore, investigations on combinations of MEK inhibitors with additional effective drugs, which are able to improve the response rates of the BRAF-WT melanoma to the MEK inhibitors, are urgently needed.

Disulfiram (DSF), a former FDA approved alcohol-aversion drug, is such a drug candidate. DSF is metabolized into bis-diethyldithiocarbamate (ET) by glutathione reductase activity in vivo. ET has a strong chelating capacity and a high affinity for copper II (Cu^{2+}), forming the bis-diethyldithiocarbamate-copper complex (CuET). CuET has a strong anti-tumor effect, which is complete copper-dependent. For these reasons combining CuET with the MEK inhibitor trametinib was tested as novel anticancer therapy in this work. The combination treatment showed enhanced cytotoxicity compared to the monotherapies. It was demonstrated that trametinib/CuET induced a significant nuclear accumulation of copper in BRAF-WT melanoma cells. Copper was transported into the melanoma cells and further translocated to the nucleus by the copper chaperone ATOX1. Interestingly, the copper accumulation in the nucleus was associated with the cellular cytotoxicity mediated by combination therapy. It was further confirmed that melanoma cells with an ATOX1 gene down-regulation was induced were not able to generate nuclear copper accumulation and showed a lower sensitivity to the combination therapy, confirming the major role of ATOX1.

Mechanistically trametinib plus CuET induced high levels of reactive oxygen species (ROS) and a significant up-regulation of endoplasmic reticulum (ER) stress-related genes in BRAF-WT melanoma cells. Consistently, this significant up-regulation of ER stress-related genes such as ATF4, CHOP, and NUPR1 leaded to induction of apoptosis. Furthermore, trametinib plus CuET induced high levels of pro-apoptotic proteins of the BCL-2 family such as BIM and BAX, and reduced the anti-apoptotic BCL-2. Additionally, it was demonstrated that the apoptosis mediated by trametinib plus CuET was dependent on c-JUN N-Terminal Kinase (JNK/c-JUN) signaling. Cytotoxicity and apoptosis of the combination were completely mitigated through a selective JNK inhibitor, confirming its crucial role in apoptosis induction.

The co-administration of trametinib with CuET affected all melanoma cells tested. Specifically, the growth and survival of melanoma cells with $NRAS^{mut}$, NF1-LoF or Triple-WT were significantly impaired by the treatment and caused significant synergistic cytotoxicity. Trametinib/CuET was very effective in two and three-dimensional model systems. Most importantly, trametinib/CuET suppressed the in vivo growth of BRAF-WT melanoma xenografts. Taken together, these data suggest the combination of trametinib with CuET as a novel targeted therapy for BRAF-WT melanoma.

9 Zusammenfassung

Der MAPK-Signalweg ist bei Melanomen häufig hyperaktiviert und spielt eine entscheidende Rolle bei der Entwicklung, der Zellteilung und dem Überleben von Tumorzellen. So kommt es bei Melanomzellen ohne BRAF-Mutation (BRAF-WT) in etwa 40 % der Fälle zu einer Hyperaktivierung des MAPK-Signalwegs. Die klinische Wirksamkeit von MEK-Inhibitoren als Monotherapie bei $NRAS^{mut}$ Melanomen wurde weiter untersucht, insbesondere in der klinischen Phase-3-Studie NEMO. Die Gesamtansprechrate auf den MEK-Inhibitor war signifikant niedrig (15 %), und das progressionsfreie Überleben verbesserte sich nur geringfügig (2,8 vs. 1,5 Monate) gegenüber Dacarbazin. Daher sind Untersuchungen zu Kombinationen von MEK-Inhibitoren mit weiteren wirksamen Medikamenten, die die Ansprechraten des BRAF-WT-Melanoms auf die MEK-Inhibitoren verbessern können, dringend erforderlich.

Disulfiram (DSF), ein früher von der FDA zugelassenes Medikament zur Alkoholentwöhnung, ist ein solcher Medikamentenkandidat. DSF wird in vivo durch Glutathion-Reduktase-Aktivität zu Bis-Diethyldithiocarbamat (ET) metabolisiert. ET hat ein starkes Chelatbildungsvermögen und eine hohe Affinität für Kupfer II (Cu^{2+}), wodurch der Bis-Diethyldithiocarbamat-Kupfer-Komplex (CuET) gebildet wird. CuET hat eine starke Antitumorwirkung, die vollständig kupferabhängig ist. Aus diesen Gründen wurde in dieser Arbeit die Kombination von CuET mit dem MEK-Inhibitor Trametinib als neuartige Krebstherapie getestet. Die Kombinationsbehandlung zeigte im Vergleich zu den Monotherapien eine erhöhte Zytotoxizität. Es konnte gezeigt werden, dass Trametinib/CuET eine signifikante Anreicherung von Kupfer im Zellkern von BRAF-WT-Melanomzellen bewirkte. Das Kupfer wurde in die Melanomzellen transportiert und durch das Kupfer-Chaperon ATOX1 weiter in den Zellkern verlagert. Interessanterweise stand die Kupferakkumulation im Zellkern in Zusammenhang mit der durch die Kombinationstherapie vermittelten zellulären Zytotoxizität. Es wurde ferner bestätigt, dass Melanomzellen, bei denen das ATOX1-Gen herunterreguliert wurde, nicht in der Lage waren, eine Kupferakkumulation im Zellkern zu erzeugen, und eine geringere Empfindlichkeit gegenüber der Kombinationstherapie zeigten, was die wichtige Rolle von ATOX1 bestätigt.

Mechanistisch gesehen induzierte Trametinib plus CuET hohe Mengen reaktiver Sauerstoffspezies (ROS) und eine signifikante Hochregulierung von Genen, die mit dem endoplasmatischen Retikulum (ER) in Verbindung stehen, in BRAF-WT-Melanomzellen. Diese signifikante Hochregulierung von mit ER-Stress verbundenen Genen wie ATF4, CHOP und NUPR1 führte folgerichtig zur Induktion von Apoptose. Darüber hinaus induzierte Trametinib plus CuET hohe Konzentrationen von pro-apoptotischen Proteinen der BCL-2-Familie wie BIM und BAX und reduzierte das anti-apoptotische BCL-2. Darüber hinaus wurde nachgewiesen, dass die durch Trametinib plus CuET vermittelte Apoptose von der c-JUN N-Terminal Kinase (JNK/c-JUN) abhängig ist. Die Zytotoxizität und Apoptose der Kombination wurden durch einen selektiven JNK-Inhibitor vollständig abgeschwächt, was seine entscheidende Rolle bei der Apoptoseinduktion bestätigt.

Die gleichzeitige Verabreichung von Trametinib mit CuET beeinträchtigte alle getesteten Melanomzellen. Insbesondere das Wachstum und das Überleben von Melanomzellen mit $NRAS^{mut}$, NF1-LoF oder Triple-WT wurden durch die Behandlung erheblich beeinträchtigt und verursachten eine signifikante synergistische Zytotoxizität. Trametinib/CuET war in zwei- und dreidimensionalen Modellsystemen sehr wirksam. Vor allem aber unterdrückte Trametinib/CuET das In-vivo-Wachstum von BRAF-WT-Melanom-Xenografts. Zusammengenommen legen diese Daten die Kombination von Trametinib mit CuET als neuartigen Ansatz für eine zielgerichtete Therapie für BRAF-WT-Melanome nahe.

10 List of tables

11 List of Figures

12 References

1. Siegel, R.L., K.D. Miller, and A. Jemal, *Cancer statistics, 2016.* CA Cancer J Clin, 2016. **66**(1): p. 7-30.

2. Brady, D.C., et al., *Copper is required for oncogenic BRAF signalling and tumorigenesis.* Nature, 2014. **509**(7501): p. 492-6.

3. Garbe, C., et al., *Histopathological diagnostics of malignant melanoma in accordance with the recent AJCC classification 2009: Review of the literature and recommendations for general practice.* J Dtsch Dermatol Ges, 2011. **9**(9): p. 690-9.

4. Ferlay, J., et al., *Estimating the global cancer incidence and mortality in 2018: GLOBOCAN sources and methods.* Int J Cancer, 2019. **144**(8): p. 1941-1953.

5. Cabrera, R. and F. Recule, *Unusual Clinical Presentations of Malignant Melanoma: A Review of Clinical and Histologic Features with Special Emphasis on Dermatoscopic Findings.* Am J Clin Dermatol, 2018. **19**(Suppl 1): p. 15-23.

6. Miller, K.D., et al., *Cancer treatment and survivorship statistics, 2019.* CA Cancer J Clin, 2019. **69**(5): p. 363-385.

7. Hao, M.Z., et al., *Novel anti-melanoma treatment: focus on immunotherapy.* Chin J Cancer, 2014. **33**(9): p. 458-65.

8. Yu, Z. and L. Si, *Immunotherapy of patients with metastatic melanoma.* Chin Clin Oncol, 2017. **6**(2): p. 20.

9. Gershenwald, J.E., et al., *Melanoma staging: Evidence-based changes in the American Joint Committee on Cancer eighth edition cancer staging manual.* CA Cancer J Clin, 2017. **67**(6): p. 472-492.

10. Postow, M.A., et al., *Nivolumab and ipilimumab versus ipilimumab in untreated melanoma.* N Engl J Med, 2015. **372**(21): p. 2006-17.

11. Hodi, F.S., et al., *Nivolumab plus ipilimumab or nivolumab alone versus ipilimumab alone in advanced melanoma (CheckMate 067): 4-year outcomes of a multicentre, randomised, phase 3 trial.* Lancet Oncol, 2018. **19**(11): p. 1480-1492.

12. Balch, C.M., et al., *Final version of 2009 AJCC melanoma staging and classification.* J Clin Oncol, 2009. **27**(36): p. 6199-206.

13. Davies, H., et al., *Mutations of the BRAF gene in human cancer.* Nature, 2002. **417**(6892): p. 949-54.

14. Forschner, A., et al., *Improvement of overall survival in stage IV melanoma patients during 2011-2014: analysis of real-world data in 441 patients of the German Central Malignant Melanoma Registry (CMMR).* J Cancer Res Clin Oncol, 2017. **143**(3): p. 533-540.

15. *Genomic Classification of Cutaneous Melanoma.* Cell, 2015. **161**(7): p. 1681-96.

16. Dickson, P.V. and J.E. Gershenwald, *Staging and prognosis of cutaneous melanoma.* Surg Oncol Clin N Am, 2011. **20**(1): p. 1-17.

17. Fujisawa, Y., et al., *Nation-wide survey of advanced non-melanoma skin cancers treated at dermatology departments in Japan.* J Dermatol Sci, 2018. **92**(3): p. 230-236.

18. Philpott, C., et al., *The NF1 somatic mutational landscape in sporadic human cancers.* Hum Genomics, 2017. **11**(1): p. 13.

19. Hayward, N.K., et al., *Whole-genome landscapes of major melanoma subtypes.* Nature, 2017. **545**(7653): p. 175-180.

20. Shain, A.H. and B.C. Bastian, *Filling the gaps in the genomic catalogue of melanoma subtypes.* Pigment Cell Melanoma Res, 2017. **30**(6): p. 508-509.

21. Amann, V.C., et al., *Developments in targeted therapy in melanoma.* Eur J Surg Oncol, 2017. **43**(3): p. 581-593.

22. Wellbrock, C. and I. Arozarena, *The Complexity of the ERK/MAP-Kinase Pathway and the Treatment of Melanoma Skin Cancer.* Front Cell Dev Biol, 2016. **4**: p. 33.

23. Burotto, M., et al., *The MAPK pathway across different malignancies: a new perspective.* Cancer, 2014. **120**(22): p. 3446-56.

24. Turski, M.L., et al., *A novel role for copper in Ras/mitogen-activated protein kinase signaling.* Mol Cell Biol, 2012. **32**(7): p. 1284-95.

25. Brady, D.C., et al., *Copper Chelation Inhibits BRAF(V600E)-Driven Melanomagenesis and Counters Resistance to BRAF(V600E) and MEK1/2 Inhibitors.* Cancer Res, 2017. **77**(22): p. 6240-6252.

26. Thomas, N.E., et al., *Association Between NRAS and BRAF Mutational Status and Melanoma-Specific Survival Among Patients With Higher-Risk Primary Melanoma.* JAMA Oncol, 2015. **1**(3): p. 359-68.

27. Kiuru, M. and K.J. Busam, *The NF1 gene in tumor syndromes and melanoma.* Lab Invest, 2017. **97**(2): p. 146-157.

28. Krauthammer, M., et al., *Exome sequencing identifies recurrent mutations in NF1 and RASopathy genes in sun-exposed melanomas.* Nat Genet, 2015. **47**(9): p. 996-1002.

29. Vanhaesebroeck, B., M.A. Whitehead, and R. Piñeiro, *Molecules in medicine mini-review: isoforms of PI3K in biology and disease.* J Mol Med (Berl), 2016. **94**(1): p. 5-11.

30. Chang, L. and M. Karin, *Mammalian MAP kinase signalling cascades.* Nature, 2001. **410**(6824): p. 37-40.

31. Neale, B.M., et al., *Meta-analysis of genome-wide association studies of attention-deficit/hyperactivity disorder.* J Am Acad Child Adolesc Psychiatry, 2010. **49**(9): p. 884-97.

32. Chamcheu, J.C., et al., *Role and Therapeutic Targeting of the PI3K/Akt/mTOR Signaling Pathway in Skin Cancer: A Review of Current Status and Future Trends on Natural and Synthetic Agents Therapy.* Cells, 2019. **8**(8).

33. Wang, J., et al., *PTEN regulates IGF-1R-mediated therapy resistance in melanoma.* Pigment Cell Melanoma Res, 2015. **28**(5): p. 572-89.

34. Madhunapantula, S.V., P.J. Mosca, and G.P. Robertson, *The Akt signaling pathway: an emerging therapeutic target in malignant melanoma.* Cancer Biol Ther, 2011. **12**(12): p. 1032-49.

35. Li, J., et al., *Uncoupling protein 2 is upregulated in melanoma cells and contributes to the activation of Akt/mTOR and ERK signaling.* Int J Oncol, 2020. **56**(5): p. 1252-1261.

36. Liang, F., et al., *The crosstalk between STAT3 and p53/RAS signaling controls cancer cell metastasis and cisplatin resistance via the Slug/MAPK/PI3K/AKT-mediated regulation of EMT and autophagy.* Oncogenesis, 2019. **8**(10): p. 59.

37. Pollock, P.M. and J.M. Trent, *The genetics of cutaneous melanoma.* Clin Lab Med, 2000. **20**(4): p. 667-90.

38. Lee, E.R., et al., *Interplay between PI3K/Akt and MAPK signaling pathways in DNA-damaging drug-induced apoptosis.* Biochim Biophys Acta, 2006. **1763**(9): p. 958-68.

39. Zheng, C.F. and K.L. Guan, *Activation of MEK family kinases requires phosphorylation of two conserved Ser/Thr residues.* Embo j, 1994. **13**(5): p. 1123-31.

40. Maverakis, E., et al., *Metastatic melanoma - a review of current and future treatment options.* Acta Derm Venereol, 2015. **95**(5): p. 516-24.

41. Coit, D.G., et al., *Cutaneous Melanoma, Version 2.2019, NCCN Clinical Practice Guidelines in Oncology.* J Natl Compr Canc Netw, 2019. **17**(4): p. 367-402.

42. Coit, D.G., et al., *Melanoma, version 2.2013: featured updates to the NCCN guidelines.* J Natl Compr Canc Netw, 2013. **11**(4): p. 395-407.

43. Guillot, B., et al., *[Guidelines for stage I to III melanoma]*. Bull Cancer, 2016. **103**(9): p. 743-52.

44. Michielin, O., et al., *Cutaneous melanoma: ESMO Clinical Practice Guidelines for diagnosis, treatment and follow-up†.* Ann Oncol, 2019. **30**(12): p. 1884-1901.

45. Coit, D.G., et al., *NCCN Guidelines Insights: Melanoma, Version 3.2016.* J Natl Compr Canc Netw, 2016. **14**(8): p. 945-58.

46. Wada-Ohno, M., T. Ito, and M. Furue, *Adjuvant Therapy for Melanoma.* Curr Treat Options Oncol, 2019. **20**(8): p. 63.

47. Degirmenci, U., M. Wang, and J. Hu, *Targeting Aberrant RAS/RAF/MEK/ERK Signaling for Cancer Therapy.* Cells, 2020. **9**(1).

48. Mahoney, K.M., G.J. Freeman, and D.F. McDermott, *The Next Immune-Checkpoint Inhibitors: PD-1/PD-L1 Blockade in Melanoma.* Clin Ther, 2015. **37**(4): p. 764-82.

49. Davey, R.J., A. van der Westhuizen, and N.A. Bowden, *Metastatic melanoma treatment: Combining old and new therapies.* Crit Rev Oncol Hematol, 2016. **98**: p. 242-53.

50. Amaral, T., F. Meraz-Torres, and C. Garbe, *Immunotherapy in managing metastatic melanoma: which treatment when?* Expert Opin Biol Ther, 2017. **17**(12): p. 1523-1538.

51. Thompson, N. and J. Lyons, *Recent progress in targeting the Raf/MEK/ERK pathway with inhibitors in cancer drug discovery.* Curr Opin Pharmacol, 2005. **5**(4): p. 350-6.

52. Flaherty, K.T., et al., *Combined BRAF and MEK inhibition in melanoma with BRAF V600 mutations.* N Engl J Med, 2012. **367**(18): p. 1694-703.

53. Long, G.V., et al., *Combined BRAF and MEK inhibition versus BRAF inhibition alone in melanoma.* N Engl J Med, 2014. **371**(20): p. 1877-88.

54. Long, G.V., et al., *Dabrafenib and trametinib versus dabrafenib and placebo for Val600 BRAF-mutant melanoma: a multicentre, double-blind, phase 3 randomised controlled trial.* Lancet, 2015. **386**(9992): p. 444-51.

55. Solit, D.B., et al., *BRAF mutation predicts sensitivity to MEK inhibition.* Nature, 2006. **439**(7074): p. 358-62.

56. Gilmartin, A.G., et al., *GSK1120212 (JTP-74057) is an inhibitor of MEK activity and activation with favorable pharmacokinetic properties for sustained in vivo pathway inhibition.* Clin Cancer Res, 2011. **17**(5): p. 989-1000.

57. Abe, H., et al., *Discovery of a Highly Potent and Selective MEK Inhibitor: GSK1120212 (JTP-74057 DMSO Solvate).* ACS Med Chem Lett, 2011. **2**(4): p. 320-4.

58. Yamaguchi, T., et al., *Antitumor activities of JTP-74057 (GSK1120212), a novel MEK1/2 inhibitor, on colorectal cancer cell lines in vitro and in vivo.* Int J Oncol, 2011. **39**(1): p. 23-31.

59. Salama, A.K. and K.B. Kim, *Trametinib (GSK1120212) in the treatment of melanoma.* Expert Opin Pharmacother, 2013. **14**(5): p. 619-27.

60. Zeiser, R., H. Andrlová, and F. Meiss, *Trametinib (GSK1120212).* Recent Results Cancer Res, 2018. **211**: p. 91-100.

61. Zeiser, R., *Trametinib.* Recent Results Cancer Res, 2014. **201**: p. 241-8.

62. King, J.W. and P.D. Nathan, *Role of the MEK inhibitor trametinib in the treatment of metastatic melanoma.* Future Oncol, 2014. **10**(9): p. 1559-70.

63. Chapman, P.B., et al., *Improved survival with vemurafenib in melanoma with BRAF V600E mutation.* N Engl J Med, 2011. **364**(26): p. 2507-16.

64. Nesbit, C.E., J.M. Tersak, and E.V. Prochownik, *MYC oncogenes and human neoplastic disease.* Oncogene, 1999. **18**(19): p. 3004-16.

65. Bompiani, K.M., et al., *Copper transporters and chaperones CTR1, CTR2, ATOX1, and CCS as determinants of cisplatin sensitivity.* Metallomics, 2016. **8**(9): p. 951-62.

66. Molloy, S.A. and J.H. Kaplan, *Copper-dependent recycling of hCTR1, the human high affinity copper transporter.* J Biol Chem, 2009. **284**(43): p. 29704-13.

67. Elam, J.S., et al., *Copper chaperones.* Adv Protein Chem, 2002. **60**: p. 151-219.

68. Palumaa, P., *Copper chaperones. The concept of conformational control in the metabolism of copper.* FEBS Lett, 2013. **587**(13): p. 1902-10.

69. Markossian, K.A. and B.I. Kurganov, *Copper chaperones, intracellular copper trafficking proteins. Function, structure, and mechanism of action.* Biochemistry (Mosc), 2003. **68**(8): p. 827-37.

70. Skopp, A., et al., *Copper-zinc superoxide dismutase (Sod1) activation terminates interaction between its copper chaperone (Ccs) and the cytosolic metal-binding domain of the copper importer Ctr1.* Biometals, 2019. **32**(4): p. 695-705.

71. Levy, A.R., et al., *Ctr1 Intracellular Loop Is Involved in the Copper Transfer Mechanism to the Atox1 Metallochaperone.* J Phys Chem B, 2016. **120**(48): p. 12334-12345.

72. Ren, F., et al., *X-ray structures of the high-affinity copper transporter Ctr1.* Nat Commun, 2019. **10**(1): p. 1386.

73. Nose, Y., E.M. Rees, and D.J. Thiele, *Structure of the Ctr1 copper trans'PORE'ter reveals novel architecture.* Trends Biochem Sci, 2006. **31**(11): p. 604-7.

74. Schwab, S., et al., *Sequence proximity between Cu(II) and Cu(I) binding sites of human copper transporter 1 model peptides defines reactivity with ascorbate and O2.* J Inorg Biochem, 2016. **158**: p. 70-76.

75. Lee, J., et al., *Biochemical characterization of the human copper transporter Ctr1.* J Biol Chem, 2002. **277**(6): p. 4380-7.

76. Öhrvik, H. and D.J. Thiele, *The role of Ctr1 and Ctr2 in mammalian copper homeostasis and platinum-based chemotherapy.* J Trace Elem Med Biol, 2015. **31**: p. 178-82.

77. Hartwig, C., et al., *Trafficking mechanisms of P-type ATPase copper transporters.* Curr Opin Cell Biol, 2019. **59**: p. 24-33.

78. Yanatori, I. and F. Kishi, *DMT1 and iron transport.* Free Radic Biol Med, 2019. **133**: p. 55-63.

79. Xiao, S., et al., *Identification of an "alpha-helix-extended segment-alpha-helix" conformation of the sixth transmembrane domain in DMT1.* Biochim Biophys Acta, 2010. **1798**(8): p. 1556-64.

80. Ilyechova, E.Y., et al., *CRISP-R/Cas9 Mediated Deletion of Copper Transport Genes CTR1 and DMT1 in NSCLC Cell Line H1299. Biological and Pharmacological Consequences.* Cells, 2019. **8**(4).

81. Kim, Y.J., et al., *Copper chaperone ATOX1 is required for MAPK signaling and growth in BRAF mutation-positive melanoma.* Metallomics, 2019. **11**(8): p. 1430-1440.

82. Lin, C., et al., *Copper uptake by DMT1: a compensatory mechanism for CTR1 deficiency in human umbilical vein endothelial cells.* Metallomics, 2015. **7**(8): p. 1285-9.

83. Field, L.S., E. Luk, and V.C. Culotta, *Copper chaperones: personal escorts for metal ions.* J Bioenerg Biomembr, 2002. **34**(5): p. 373-9.

84. Matson Dzebo, M., et al., *Copper Chaperone Atox1 Interacts with Cell Cycle Proteins.* Comput Struct Biotechnol J, 2018. **16**: p. 443-449.

85. Shanmugavel, K.P. and P. Wittung-Stafshede, *Copper relay path through the N-terminus of Wilson disease protein, ATP7B.* Metallomics, 2019. **11**(9): p. 1472-1480.

86. Moore, S.D., et al., *Tissue localization of the copper chaperone ATOX1 and its potential role in disease.* Mamm Genome, 2002. **13**(10): p. 563-8.

87. Yatsunyk, L.A. and A.C. Rosenzweig, *Cu(I) binding and transfer by the N terminus of the Wilson disease protein.* J Biol Chem, 2007. **282**(12): p. 8622-31.

88. Magistrato, A., et al., *Copper trafficking in eukaryotic systems: current knowledge from experimental and computational efforts.* Curr Opin Struct Biol, 2019. **58**: p. 26-33.

89. Qasem, Z., et al., *The pivotal role of MBD4-ATP7B in the human Cu(i) excretion path as revealed by EPR experiments and all-atom simulations.* Metallomics, 2019. **11**(7): p. 1288-1297.

90. Lutsenko, S., *Copper trafficking to the secretory pathway.* Metallomics, 2016. **8**(9): p. 840-52.

91. Yu, C.H., et al., *The metal chaperone Atox1 regulates the activity of the human copper transporter ATP7B by modulating domain dynamics.* J Biol Chem, 2017. **292**(44): p. 18169-18177.

92. Jouybari, L., et al., *Copper Concentrations in Breast Cancer: A Systematic Review and Meta-Analysis.* Curr Med Chem, 2020. **27**(37): p. 6373-6383.

93. Zhang, Y., et al., *Roles and mechanisms of copper transporting ATPases in cancer pathogenesis.* Med Sci Monit, 2009. **15**(1): p. Ra1-5.

94. Atakul, T., et al., *Serum Copper and Zinc Levels in Patients with Endometrial Cancer.* Biol Trace Elem Res, 2020. **195**(1): p. 46-54.

95. Ackerman, C.M. and C.J. Chang, *Copper signaling in the brain and beyond.* J Biol Chem, 2018. **293**(13): p. 4628-4635.

96. Li, Y., et al., *Copper Chaperone for Superoxide Dismutase Promotes Breast Cancer Cell Proliferation and Migration via ROS-Mediated MAPK/ERK Signaling.* Front Pharmacol, 2019. **10**: p. 356.

97. Inkol, J.M., A.C. Poon, and A.J. Mutsaers, *Inhibition of copper chaperones sensitizes human and canine osteosarcoma cells to carboplatin chemotherapy.* Vet Comp Oncol, 2020. **18**(4): p. 559-569.

98. Cirenajwis, H., et al., *Molecular stratification of metastatic melanoma using gene expression profiling: Prediction of survival outcome and benefit from molecular targeted therapy.* Oncotarget, 2015. **6**(14): p. 12297-309.

99. Karginova, O., et al., *Inhibition of Copper Transport Induces Apoptosis in Triple-Negative Breast Cancer Cells and Suppresses Tumor Angiogenesis.* Mol Cancer Ther, 2019. **18**(5): p. 873-885.

100. Skrott, Z., et al., *Alcohol-abuse drug disulfiram targets cancer via p97 segregase adaptor NPL4.* Nature, 2017. **552**(7684): p. 194-199.

101. Xu, B., et al., *Disulfiram/copper selectively eradicates AML leukemia stem cells in vitro and in vivo by simultaneous induction of ROS-JNK and inhibition of NF-κB and Nrf2.* Cell Death Dis, 2017. **8**(5): p. e2797.

102. Morrison, B.W., et al., *Disulfiram induces copper-dependent stimulation of reactive oxygen species and activation of the extrinsic apoptotic pathway in melanoma.* Melanoma Res, 2010. **20**(1): p. 11-20.

103. Mutschler, J., et al., *Current Findings and Mechanisms of Action of Disulfiram in the Treatment of Alcohol Dependence.* Pharmacopsychiatry, 2016. **49**(4): p. 137-41.

104. Meraz-Torres, F., et al., *Disulfiram as a Therapeutic Agent for Metastatic Malignant Melanoma-Old Myth or New Logos?* Cancers (Basel), 2020. **12**(12).

105. Lu, C., et al., *Disulfiram: a novel repurposed drug for cancer therapy.* Cancer Chemother Pharmacol, 2021. **87**(2): p. 159-172.

106. McMahon, A., W. Chen, and F. Li, *Old wine in new bottles: Advanced drug delivery systems for disulfiram-based cancer therapy.* J Control Release, 2020. **319**: p. 352-359.

107. Ekinci, E., et al., *Repurposing Disulfiram as An Anti-Cancer Agent: Updated Review on Literature and Patents.* Recent Pat Anticancer Drug Discov, 2019. **14**(2): p. 113-132.

108. Viola-Rhenals, M., et al., *Recent Advances in Antabuse (Disulfiram): The Importance of its Metal-binding Ability to its Anticancer Activity.* Curr Med Chem, 2018. **25**(4): p. 506-524.

109. Farooq, M.A., et al., *Recent advances in the delivery of disulfiram: a critical analysis of promising approaches to improve its pharmacokinetic profile and anticancer efficacy.* Daru, 2019. **27**(2): p. 853-862.

110. Zuhra, K., et al., *Mechanism of cystathionine-β-synthase inhibition by disulfiram: The role of bis(N,N-diethyldithiocarbamate)-copper(II).* Biochem Pharmacol, 2020. **182**: p. 114267.

111. Zha, J., et al., *Disulfiram targeting lymphoid malignant cell lines via ROS-JNK activation as well as Nrf2 and NF-kB pathway inhibition.* J Transl Med, 2014. **12**: p. 163.

112. Li, Y., et al., *Disulfiram/Copper Induces Antitumor Activity against Both Nasopharyngeal Cancer Cells and Cancer-Associated Fibroblasts through ROS/MAPK and Ferroptosis Pathways.* Cancers (Basel), 2020. **12**(1).

113. Majera, D., et al., *Targeting the NPL4 Adaptor of p97/VCP Segregase by Disulfiram as an Emerging Cancer Vulnerability Evokes Replication Stress and DNA Damage while Silencing the ATR Pathway.* Cells, 2020. **9**(2).

114. Yang, Z., et al., *Disulfiram modulates ROS accumulation and overcomes synergistically cisplatin resistance in breast cancer cell lines.* Biomed Pharmacother, 2019. **113**: p. 108727.

115. Mah, L.J., A. El-Osta, and T.C. Karagiannis, *gammaH2AX: a sensitive molecular marker of DNA damage and repair.* Leukemia, 2010. **24**(4): p. 679-86.

116. Yip, N.C., et al., *Disulfiram modulated ROS-MAPK and NFκB pathways and targeted breast cancer cells with cancer stem cell-like properties.* Br J Cancer, 2011. **104**(10): p. 1564-74.

117. Brar, S.S., et al., *Disulfiram inhibits activating transcription factor/cyclic AMP-responsive element binding protein and human melanoma growth in a metal-dependent manner in vitro, in mice and in a patient with metastatic disease.* Mol Cancer Ther, 2004. **3**(9): p. 1049-60.

118. Cen, D., et al., *Disulfiram facilitates intracellular Cu uptake and induces apoptosis in human melanoma cells.* J Med Chem, 2004. **47**(27): p. 6914-20.

119. Li, H., et al., *The combination of disulfiram and copper for cancer treatment.* Drug Discov Today, 2020. **25**(6): p. 1099-1108.

120. Schweizer, M.T., et al., *Pharmacodynamic study of disulfiram in men with non-metastatic recurrent prostate cancer.* Prostate Cancer Prostatic Dis, 2013. **16**(4): p. 357-61.

121. Nechushtan, H., et al., *A phase IIb trial assessing the addition of disulfiram to chemotherapy for the treatment of metastatic non-small cell lung cancer.* Oncologist, 2015. **20**(4): p. 366-7.

122. Huang, J., et al., *Final results of a phase I dose-escalation, dose-expansion study of adding disulfiram with or without copper to adjuvant temozolomide for newly diagnosed glioblastoma.* J Neurooncol, 2018. **138**(1): p. 105-111.

123. Huang, J., et al., *A multicenter phase II study of temozolomide plus disulfiram and copper for recurrent temozolomide-resistant glioblastoma.* J Neurooncol, 2019. **142**(3): p. 537-544.

124. Dummer, R., et al., *Binimetinib versus dacarbazine in patients with advanced NRAS-mutant melanoma (NEMO): a multicentre, open-label, randomised, phase 3 trial.* Lancet Oncol, 2017. **18**(4): p. 435-445.

125. Wu, L., et al., *Disulfiram and BKM120 in Combination with Chemotherapy Impede Tumor Progression and Delay Tumor Recurrence in Tumor Initiating Cell-Rich TNBC.* Sci Rep, 2019. **9**(1): p. 236.

126. Askgaard, G., et al., *Use of disulfiram and risk of cancer: a population-based case-control study.* Eur J Cancer Prev, 2014. **23**(3): p. 225-32.

127. Albrecht, S.C., et al., *In vivo mapping of hydrogen peroxide and oxidized glutathione reveals chemical and regional specificity of redox homeostasis.* Cell Metab, 2011. **14**(6): p. 819-29.

128. Tormos, K.V. and N.S. Chandel, *Seeing the light: probing ROS in vivo using redox GFP*. Cell Metab, 2011. **14**(6): p. 720-1.

129. Vermeulen, K., Z.N. Berneman, and D.R. Van Bockstaele, *Cell cycle and apoptosis.* Cell Prolif, 2003. **36**(3): p. 165-75.

130. Jacotot, E., K.F. Ferri, and G. Kroemer, *Apoptosis and cell cycle: distinct checkpoints with overlapping upstream control.* Pathol Biol (Paris), 2000. **48**(3): p. 271-9.

131. Crowley, L.C. and N.J. Waterhouse, *Detecting Cleaved Caspase-3 in Apoptotic Cells by Flow Cytometry*. Cold Spring Harb Protoc, 2016. **2016**(11).

132. Fox, R. and M. Aubert, *Flow cytometric detection of activated caspase-3.* Methods Mol Biol, 2008. **414**: p. 47-56.

133. Schiewer, M.J., et al., *PARP-1 regulates DNA repair factor availability.* EMBO Mol Med, 2018. **10**(12).

134. Pascal, J.M., *The comings and goings of PARP-1 in response to DNA damage.* DNA Repair (Amst), 2018. **71**: p. 177-182.

135. Kuo, L.J. and L.X. Yang, *Gamma-H2AX - a novel biomarker for DNA double-strand breaks.* In Vivo, 2008. **22**(3): p. 305-9.

136. Shah O'Brien, P., et al., *Disulfiram (Antabuse) Activates ROS-Dependent ER Stress and Apoptosis in Oral Cavity Squamous Cell Carcinoma.* J Clin Med, 2019. **8**(5).

137. Skirnisdottir, I. and T. Seidal, *Association of p21, p21 p27 and p21 p53 status to histological subtypes and prognosis in low-stage epithelial ovarian cancer*. Cancer Genomics Proteomics, 2013. **10**(1): p. 27-34.

138. Niessner, H., et al., *BRAF Inhibitors Amplify the Proapoptotic Activity of MEK Inhibitors by Inducing ER Stress in NRAS-Mutant Melanoma.* Clin Cancer Res, 2017. **23**(20): p. 6203-6214.

139. Zhang, X., et al., *Redox signals at the ER-mitochondria interface control melanoma progression.* Embo j, 2019. **38**(15): p. e100871.

140. Lee, W.S., W.H. Yoo, and H.J. Chae, *ER Stress and Autophagy.* Curr Mol Med, 2015. **15**(8): p. 735-45.

141. Song, S., et al., *Crosstalk of ER stress-mediated autophagy and ER-phagy: Involvement of UPR and the core autophagy machinery.* J Cell Physiol, 2018. **233**(5): p. 3867-3874.

142. Xu, W. and L. Neckers, *Gr(i)p the ER to Stress Out Melanoma.* Cancer Cell, 2016. **29**(6): p. 769-771.

143. Cerezo, M., et al., *Compounds Triggering ER Stress Exert Anti-Melanoma Effects and Overcome BRAF Inhibitor Resistance.* Cancer Cell, 2016. **29**(6): p. 805-819.

144. Breinig, M., et al., *A chemical-genetic interaction map of small molecules using high-throughput imaging in cancer cells.* Mol Syst Biol, 2015. **11**(12): p. 846.

145. Echevarría-Vargas, I.M., et al., *Co-targeting BET and MEK as salvage therapy for MAPK and checkpoint inhibitor-resistant melanoma.* EMBO Mol Med, 2018. **10**(5).

146. Calderon-Aparicio, A., M. Strasberg-Rieber, and M. Rieber, *Disulfiram anti-cancer efficacy without copper overload is enhanced by extracellular H2O2 generation: antagonism by tetrathiomolybdate.* Oncotarget, 2015. **6**(30): p. 29771-81.

147. Hersey, P. and X.D. Zhang, *Adaptation to ER stress as a driver of malignancy and resistance to therapy in human melanoma.* Pigment Cell Melanoma Res, 2008. **21**(3): p. 358-67.

148. Trousil, S., et al., *Phenformin Enhances the Efficacy of ERK Inhibition in NF1-Mutant Melanoma.* J Invest Dermatol, 2017. **137**(5): p. 1135-1143.

149. Koelblinger, P., O. Thuerigen, and R. Dummer, *Development of encorafenib for BRAF-mutated advanced melanoma.* Curr Opin Oncol, 2018. **30**(2): p. 125-133.

150. Aggarwal, B.B. and Y. Takada, *Pro-apototic and anti-apoptotic effects of tumor necrosis factor in tumor cells. Role of nuclear transcription factor NF-kappaB.* Cancer Treat Res, 2005. **126**: p. 103-27.

151. Gardai, S.J., et al., *Phosphorylation of Bax Ser184 by Akt regulates its activity and apoptosis in neutrophils.* J Biol Chem, 2004. **279**(20): p. 21085-95.

152. Dehan, P., et al., *DNA methylation and cancer diagnosis: new methods and applications.* Expert Rev Mol Diagn, 2009. **9**(7): p. 651-7.

153. Khanzadeh, T., et al., *Investigation of BAX and BCL2 expression and apoptosis in a resveratrol- and prednisolone-treated human T-ALL cell line, CCRF-CEM.* Blood Res, 2018. **53**(1): p. 53-60.

154. Zadi Heydarabad, M., et al., *Apoptotic effect of resveratrol on human T-ALL cell line CCRF-CEM is unlikely exerted through alteration of BAX and BCL2 promoter methylation.* J Cell Biochem, 2018. **119**(12): p. 10033-10040.

155. Ley, K., *The role of selectins in inflammation and disease.* Trends Mol Med, 2003. **9**(6): p. 263-8.

156. Calderon-Aparicio, A., et al., *Anticancer response to disulfiram may be enhanced by co-treatment with MEK inhibitor or oxaliplatin: modulation by tetrathiomolybdate, KRAS/BRAF mutations and c-MYC/p53 status.* Ecancermedicalscience, 2019. **13**: p. 890.

157. Scortegagna, M., et al., *PDK1 and SGK3 Contribute to the Growth of BRAF-Mutant Melanomas and Are Potential Therapeutic Targets.* Cancer Res, 2015. **75**(7): p. 1399-412.

158. Stacpoole, P.W., *Therapeutic Targeting of the Pyruvate Dehydrogenase Complex/Pyruvate Dehydrogenase Kinase (PDC/PDK) Axis in Cancer.* J Natl Cancer Inst, 2017. **109**(11).

159. Emmanouilidi, A. and M. Falasca, *Targeting PDK1 for Chemosensitization of Cancer Cells.* Cancers (Basel), 2017. **9**(10).

160. Picco, M.E., et al., *STAT3 enhances the constitutive activity of AGC kinases in melanoma by transactivating PDK1.* Cell Biosci, 2019. **9**: p. 3.

161. Obrador, E., et al., *Oxidative stress and antioxidants in the pathophysiology of malignant melanoma.* Biol Chem, 2019. **400**(5): p. 589-612.

162. Yang, Y., et al., *Mitochondria and Mitochondrial ROS in Cancer: Novel Targets for Anticancer Therapy.* J Cell Physiol, 2016. **231**(12): p. 2570-81.

163. Zaidieh, T., et al., *ROS as a novel indicator to predict anticancer drug efficacy.* BMC Cancer, 2019. **19**(1): p. 1224.

164. Senft, D. and Z.A. Ronai, *UPR, autophagy, and mitochondria crosstalk underlies the ER stress response.* Trends Biochem Sci, 2015. **40**(3): p. 141-8.

165. Sidhu, A., et al., *Borrelidin Induces the Unfolded Protein Response in Oral Cancer Cells and Chop-Dependent Apoptosis.* ACS Med Chem Lett, 2015. **6**(11): p. 1122-7.

166. Fribley, A.M., et al., *Complementary cell-based high-throughput screens identify novel modulators of the unfolded protein response.* J Biomol Screen, 2011. **16**(8): p. 825-35.

167. Xi, Y., et al., *Cantharidins induce ER stress and a terminal unfolded protein response in OSCC.* J Dent Res, 2015. **94**(2): p. 320-9.

168. Beck, D., et al., *Vemurafenib potently induces endoplasmic reticulum stress-mediated apoptosis in BRAFV600E melanoma cells.* Sci Signal, 2013. **6**(260): p. ra7.

169. Lee, Y.S., et al., *Ferroptosis-Induced Endoplasmic Reticulum Stress: Cross-talk between Ferroptosis and Apoptosis.* Mol Cancer Res, 2018. **16**(7): p. 1073-1076.

170. Iurlaro, R. and C. Muñoz-Pinedo, *Cell death induced by endoplasmic reticulum stress.* Febs j, 2016. **283**(14): p. 2640-52.

171. Gong, J., et al., *Molecular signal networks and regulating mechanisms of the unfolded protein response.* J Zhejiang Univ Sci B, 2017. **18**(1): p. 1-14.

172. Nietzel, T., et al., *The fluorescent protein sensor roGFP2-Orp1 monitors in vivo H(2) O(2) and thiol redox integration and elucidates intracellular H(2) O(2) dynamics during elicitor-induced oxidative burst in Arabidopsis.* New Phytol, 2019. **221**(3): p. 1649-1664.

13 Declaration

I affirm that I have written the dissertation myself and have not used any sources and aids other than those indicated. The references are presented accorded to standard rules for publication and standard citation guidelines.

Tubingen, 2022

_____

Francisco Meraz Torres

14 Acknowledgment

I dedicate and deeply thank all my family, my brother Manuel, my sister Sofia, my nephew Iker and my siblings Pavel, Sandra and Ángeles, as well as all my wife family Héctor, Yolanda, David and Ingrid, for all the love and support during my doctoral studies. Without them, this would not have been possible.

Honestly, I would especially like to thank Dr.rer.nat. Heike Niessner and Dr.rer.nat Tobias Sinnberg for their outstanding supervision and friendship. During the conduct of the experiments for my doctoral's thesis, Heike and Tobias were always willing to discuss and advise on questions concerning the project

Additional I would like to thank Professor Claus Garbe and Professor Birgit Schittek for the provision of working space materials and facilities to develop my project. I would also like to acknowledge Professor Olaf Rieß and Professor Macek for reading my dissertation.

A warmly thank goes to all the lab members and old friends; and regular supervision meetings: Birgit Sauer, Jule Focken, Lisa Marie Fröhlich, Constanze Hirn, Kathrin Hofmeister, Jasmin Scheurer, Eftychia Chatziioannou and Matti Böcker for their help and the nice atmosphere. A lovingly thank goes to old friends: Corinna Kosnopfel and Elena Makino. Last but not least I would like to thank my friends and family for advising and supporting me.